EXPERIMENTAL INVESTIGATIONS OF THE MECHANICAL, WEAR AND BIO-COMPATIBLE PROPERTIES OF NICKEL TITANIUM ALLOY

THESIS

submitted in fulfillment of the requirement of the degree of

DOCTOR OF PHILOSOPHY

to

YMCA UNIVERSITY OF SCIENCE & TECHNOLOGY

by

NEERAJ SHARMA

Registration No: YMCAUST/Ph29/2012

Under the supervision of

DR. TILAK RAJ
PROFESSOR
Department of Mechanical Engineering

DR. KAMAL KUMAR
ASSISTANT PROFESSOR
Department of Mechanical Engineering

Department of Mechanical Engineering
Faculty of Engineering & Technology
YMCA University of Science & Technology
Sector-6, Mathura Road, Faridabad, Haryana, India

DECEMBER, 2016

EXPERIMENTAL INVESTIGATIONS OF THE MECHANICAL, WEAR AND BIO-COMPATIBLE PROPERTIES OF NICKEL TITANIUM ALLOY

THESIS

submitted in fulfillment of the requirement of the degree of

DOCTOR OF PHILOSOPHY

to

YMCA UNIVERSITY OF SCIENCE & TECHNOLOGY

by

NEERAJ SHARMA

Registration No: YMCAUST/Ph29/2012

Under the supervision of

DR. TILAK RAJ
PROFESSOR
Department of Mechanical Engineering

DR. KAMAL KUMAR
ASSISTANT PROFESSOR
Department of Mechanical Engineering

Department of Mechanical Engineering
Faculty of Engineering & Technology
YMCA University of Science & Technology
Sector-6, Mathura Road, Faridabad, Haryana, India

DECEMBER, 2016

DECLARATION

I hereby declare that this thesis entitled **EXPERIMENTAL INVESTIGATIONS OF THE MECHANICAL, WEAR AND BIO-COMPATIBLE PROPERTIES OF NICKEL TITANIUM ALLOY** by **NEERAJ SHARMA,** being submitted in fulfillment of the requirements for the Degree of Doctor of Philosophy in MECHANICAL ENGINEERING under Faculty of Engineering and Technology of YMCA University of Science & Technology Faridabad, during the academic year 2012-2016, is a bona fide record of my original work carried out under guidance and supervision of **DR. TILAK RAJ, PROFESSOR, MECHANICAL ENGINEERING, YMCA UNIVERSITY OF SCIENCE AND TECHNOLOGY, FARIDABAD** and **DR. KAMAL KUMAR JANGRA, ASSISTANT PROFESSOR, MECHANICAL ENGINEERING, PEC UNIVERSITY OF TECHNOLOGY, CHANDIGARH** and has not been presented elsewhere.

I further declare that the thesis does not contain any part of any work which has been submitted for the award of any degree either in this university or in any other university.

(Neeraj Sharma)
Registration No. YMCAUST/Ph29/2012

CERTIFICATE

This is to certify that this Thesis entitled **"EXPERIMENTAL INVESTIGATIONS OF THE MECHANICAL, WEAR AND BIO-COMPATIBLE PROPERTIES OF NICKEL TITANIUM ALLOY"** by **NEERAJ SHARMA** in fulfilment of the requirements for the Degree of Doctor of Philosophy in the **MECHANICAL ENGINEERING** under Faculty of Engineering and Technology of YMCA University of Science & Technology Faridabad, during the academic year 2012-2016, is a bona fide record of work carried out under our guidance and supervision

We further declare that to the best of our knowledge, the thesis does not contain any part of any work which has been submitted for the award of any degree either in this university or in any other university.

Dr. Kamal Kumar
ASSISTANT PROFESSOR
Mechanical Engineering Department
PEC University of Technology, Chandigarh

Dr. Tilak Raj
PROFESSOR
Department of Mechanical Engineering
Faculty of Engineering & Technology
YMCA University of Science and Technology, Faridabad

Dated:

ACKNOWLEDGEMENT

I take the opportunity to express my heartfelt respect and gratitude to my supervisors, Dr. Tilak Raj, Professor, Department of Mechanical Engineering, YMCA University of Science and Technology, Faridabad and Dr. Kamal Kumar, Assistant Professor, Mechanical Engineering Department, PEC University of Technology, Chandigarh for their unconditional help, constructive suggestions, thought provoking discussions and forward encouragement in nurturing this research work. It has been a blessing for me to spend many favorable moments under the guidance of the perfectionist at the zenith of professionalism. The present work is evidence to his promptness, encouragement and devoted personal interest, taken by them during the course of this research work.

I am grateful to Dr. M.L. Aggarwal Professor and Chairman, Department of Mechanical Engineering, YMCA University of Science and Technology, Faridabad for providing facilities to carry out the work. Thanks are also due to Dr. Sandeep Grover, Dean (Engineering and Technology), Professor and former Chairman, Department of Mechanical Engineering, YMCA University of Science and Technology, Faridabad to motivate me for my research work.

The author wishes to place on record his profound gratitude to Dr. Vinod Kumar, Assistant Professor, Chandigarh Group of Colleges, Landran for his timely guidance, support and encouragement during the course of my work.

I wish to thank Dr. Rajesh Khanna (M.E., D.A.V. University, Jalandhar), Dr. Vivek Jain (M.E., Thapar University, Patiala) and Sh. R D Gupta (M.E., M.M. University, Mullana) for providing valuable suggestions concerning this research work.

I am particularly thankful to Mr. Mohit, Labsaul –India for providing technical assistance during the experimental work.

The services and help of all faculty members, Department of Mechanical Engineering, YMCA University of Science and Technology, Faridabad are acknowledged with sincere thanks.

It is a pleasure to acknowledge the support and help extended by all my colleagues Sh. Ajit Singh, Sh. Sandeep Kumar Rawal, Sh. Neeraj Ahuja, Sh. Gurpreet

Singh, Sh. Vedraj Khullar, Sh. Mohit Prabhakar, Sh. Nater Singh, Ms. Bheeni Chaudhry and Sh. Rajat Gupta for their encouragement from time to time.

I cannot close these prefatory remarks without expressing my deep sense of gratitude and reverence to my father Sh. Narender Sharma, whose blessing always with me from the top of sky. My ultimate gratitude goes to my mother, Smt. Neeta Sharma for her blessings and endeavor to keep my moral high throughout the period of my work. The author feels extremely happy to express his sincere thanks to his wife Renu and lovely daughter Dhun for their understanding, care, support and encouragement.

I want to express my sincere thanks to all those who directly or indirectly helped me at various stages of this work.

Above all, I express my gratitude to the "**ALMIGHTY**" for all His blessing and kindness.

(Neeraj Sharma)

Registration No. YMCAUST/Ph29/2012

ABSTRACT

Nitinol exists in an equi-atomic phase of Ni and Ti. Nitinol has growing applications in engineering (i.e. aerospace industries, MEMS etc.) and bio-medical industries due to its unique properties of pseudo-elasticity, bio-compatibility and shape-memory effect. Behaviour of NiTi can be modified by altering the composition, modifying the porosity and applying external thermal and mechanical treatment. Due to high composition sensitivity, there are several impediments in fabrication of NiTi with conventional techniques which impel the use of additive manufacturing methods. But due to very high cost of equipments, these processes have not been commercialized till now. After the addition of Cu into NiTi SMA, compressive strength and corrosion behaviour increases at the cost of shape-memory effect. Cell density of NiTi SMA is increased upto certain limit then decreases. Wear rate is also decreased after copper addition, due to increase of micro-hardness of material.

There are some challenges involved in powder metallurgy process. First, effect of compaction pressure, sintering temperature and sintering time on strength and other responses can be considered by researchers. Second, influence of different binders may be another task for investigation. Researchers used different types of binders for the attachment of powder particles. An attempt can be made to study the influence of percentage composition of binders on the porosity. Third, some study can be carried on particle-shape, particle-size and inter-connection between different particles. In the present work, the Ni-Ti alloy has been processed with powder metallurgical technique. Copper with different percentage composition has been added to study its effect on different characteristics of NiTi alloy. More specifically the below mentioned work has been undertaken.

- ❖ Fabrication of homogeneous and porous structures of Ni-Ti: a titanium alloy, using conventional powder compaction technique.
- ❖ Experimentally determining the influence of process parameters on mechanical properties and shape memory effect of Ni-Ti. Input process parameters are:
    - Concentration of alloying elements
    - Compaction pressure

- Sintering temperature
- Sintering time

❖ The output responses are strength, modulus of elasticity, wear, corrosion, porosity, bio-compatibility and shape memory effect.

❖ Surface characterization and orientation of material is processed using scanning electron microscopy (SEM).

The following levels of process parameters are selected for the present work:

Process Parameters and their Levels

Factors	Parameters	Units	Levels		
			L1	L2	L3
A	Compaction Pressure	MPa	107	141	177
B	Sintering Temperature	°C	950	1050	1150
C	Sintering Time	Min	20	40	60

Powder compaction press of Kimaya Engineers (Mumbai) make of 15 kN was used in present work. Apart from the parameters mentioned in Table the following parameters were kept constant during the experiments:

❖ Work-Material : Ni, Ti and Cu Powders

❖ Compaction Press Capacity : 15kN

❖ Compaction Time : 10min

❖ Work-piece height : 12mm

❖ Work-piece diameter : 6mm

❖ Blending time : 10hrs

❖ Ball mill rotation Speed : 300R.P.M.

DIFFERENT STEPS OF EXPERIMENTATION

To accomplish the objectives, present work has been done in following five steps:

Step-I

❖ Prepare the homogeneous mixture of different powders. As different powders consist different densities, so it becomes necessary to make homogeneous mixture.

- ❖ Ball mill is used for the homogeneous mixing of different powders. Also optimum value of mixing time is evaluated.

Step -II

- ❖ To find the experimental set up of providing varying range of input parameters in powder metallurgy process.
- ❖ Investigation of the working ranges and the levels of the powder metallurgy process affecting the selected quality characteristics.

Step –III

- ❖ Investigation of the effects of process parameters on quality characteristics viz. Porosity, compressive strength and Young's modulus at different percentage of copper in NiTi alloys.
- ❖ Optimization of quality characteristics:
  - Prediction of optimal sets of process parameters
  - Prediction of optimal values of quality characteristics.
- ❖ Experimental verification of optimized individual quality characteristics.

The Taguchi's parameter design approach has been used to achieve the above objectives.

Step-IV

- ❖ Prepare the specimen for wear characteristics measurement considering lower Young's modulus value.
- ❖ Investigation of the wear behaviour at different combination of temperature and load.

Step –V

- ❖ In-vitro testing of fabricated $Ni_{50-x}Ti_{50}Cu_x$ (x=0, 5 and10) for corrosion behaviour, bioactivity and bio-compatibility.
- ❖ Determination of cell-density of living cells (L929 mouse fibroblast) on $Ni_{50-x}Ti_{50}Cu_x$ (x=0, 5 and10) at specified conditions.

TABLE OF CONTENTS

LIST OF TABLES

LIST OF FIGURES

LIST OF ABBREVIATIONS

Symbol	Description
A	Compaction Pressure
ANOVA	Analysis of variance
B	Sintering temperature
C	Sintering time
CI	Confidence interval
CS	Conventional Sintering
DF/DOF	Degree of freedom
EBM	Electron beam machining
$F_{\alpha}(1, f_e)$	The F ratio at a confidence level of $(1-\alpha)$ against DOF 1, and error degree of freedom f_e
HIP	Hot Isostatic Pressing
HV	Vicker's hardness
LENS	Laser Engineered Net Shaping
MIM	Metal Injection molding
MEMS	Micro-electromechanical Mechanical System
MS	Mean square
N	Sample size
OA	Orthogonal array
OFAT	One factor at a time
p	p value, Probability
p	Percentage Contribution
R	Sample size for confirmation experiment
S/N	Signal to Noise
SEM	Scanning electron microscopy
SHS	Self Propagating High Temperature Synthesis
SLM	Selective laser melting
SLS	Selective Laser Sintering
SMA	Shape Memory Alloy

SME	Shape memory effect
SMM	Shape memory Metal
SPS	Spark Plasma Sintering
SS	Sum of Square
$\overline{T}$	Overall mean of the response characteristics
V_e	Error of the variance
VAR	Vacuum Arc Remelting
VIM	Vacuum Inert melting
XRD	X-ray diffraction

CHAPTER 1
INTRODUCTION

1.1 NICKEL-TITANIUM ALLOY

Equi-atomic NiTi alloy is categorized as a smart material due to its distinctive characteristics viz., Shape memory effect, biocompatibility, osseo-integration and super elasticity, etc. This alloy has many applications in medical and engineering fields. Nitinol (Ni_{50}-Ti_{50}) is used in orthopaedic implants, cardio stents, orthodontic devices, etc. due to good biocompatibility and strain recovery **(Castleman et al., 1976)**. Biocompatibility is a property by which a material can be used in a bio-fluid environment for a long time without any reaction with the bio-media **(Catauro et al., 2004)**.

SME is the property by virtue of which a material can regain its original shape from permanent position after some thermal changes. Figure 1.1 represents the transformation temperature range for NiTi alloy, which varies from 143K-351K. Due to high composition sensitivity, precise control of NiTi composition is a major issue. Using conventional methods, the properties of NiTi are severely affected because of the contamination of material due to the presence of oxygen and carbon in the surrounding environment **(Frenzel et al., 2007)**. Additive manufacturing methods **(Elahinia and Ahmadian, 2005; Lee et al., 2006; Williams et al., 2010)** are advanced techniques used to fabricate net shape NiTi geometries with highly controlled composition. But these methods are highly expensive and still not commercialized. NiTi can be produced with appreciating properties using inert atmosphere in conventional casting or powder metallurgy processes. But some post processing of NiTi is further required to remove the excess material and to neglect any minor possibility of release of Ni^{+} ions in human bodies. This short discussion indicates that the fabrication of net shape NiTi implants and other devices are highly challenging.

1.2 APPLICATIONS OF NITI

NiTi has various applications in medical field viz. orthopedics, cardiovascular, stent technology, orthodontics, etc. and in different fields of engineering (viz. MEMS in

aerospace, aircrafts, electrical switches, actuators and vibration absorbers, etc.) as it shows good osseo-integration and biocompatibility **(Catauro et al., 2004).**

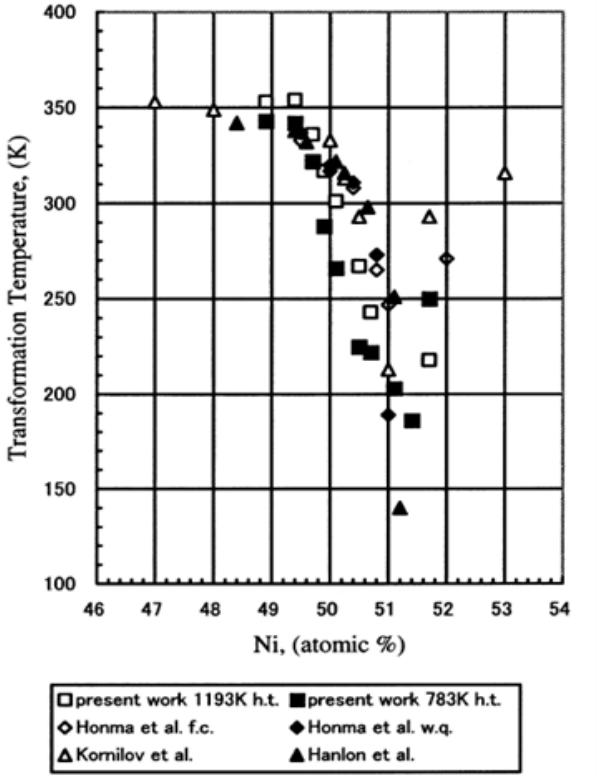

Figure 1.1: Transformation temperature against nickel contents in solution treated and quenched Nitinol (Kaieda, 2003)

SMA is a sub-group of SMM (Shape Memory Material). When the alloy is stretched and then released, it remains in the stretched form until temperature above transition temperature is not applied. NiTi is mostly utilized in surgical devices and coronary stents due to its self-expanding nature and anti-thrombosis property. Thrombosis is a property of material in contact with bio-fluid to clot the white/red thrombus on its surface.

Equi-atomic NiTi exhibit negligible thrombosis as compared to medical devices like stent made of stainless steel, wherein the later material, the probability of corrosion due to hostile electrolytic environment of the human body is very high **(Whitcher, 1997; Furie and Furie, 2008; Thierry et al., 2002).**

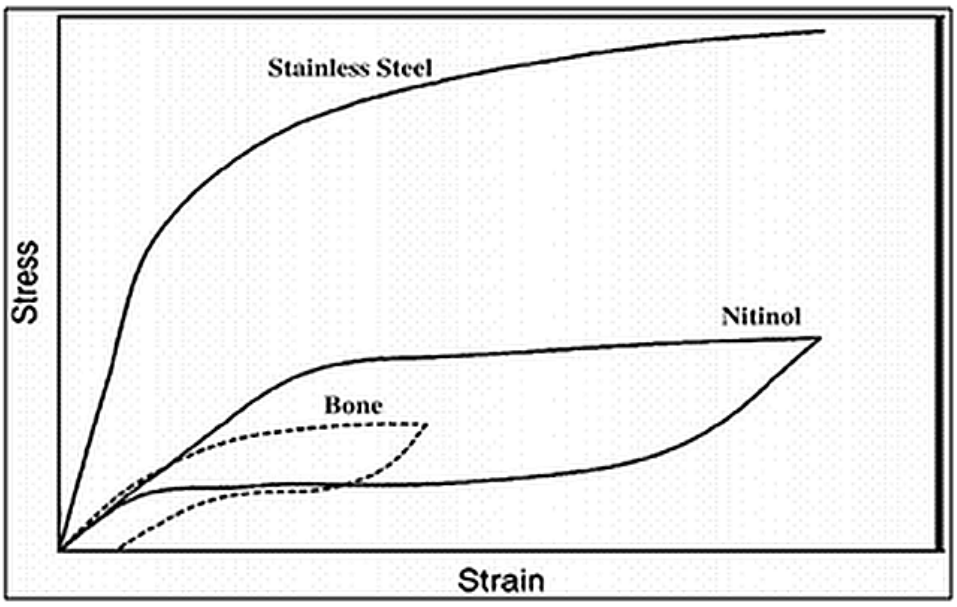

Figure 1.2: Stress–strain diagram of bone, NiTi, and stainless steel (Krishna et al., 2007)

In case of equi-atomic NiTi, a protective layer of TiO_2 is formed that prevents the release of Ni^+ ions and improves the corrosion, and hence shows good biocompatibility as verified by Es-Souni et al. **(2005)** through in-vitro cytotoxicity test. Stress shielding on human bones is a major problem for the medical implants made of steel alloy and Ti. Due to high value of young's modulus of these metallic materials, there is a mismatch between moduli of bone and steel alloy which causes implant loosening. Figure 1.2 shows the strain recovery behaviour of stainless steel, NiTi and bone. NiTi shows a high value of pseudo-elasticity and high damage of strain recovery. The Young's modulus of NiTi is also comparable with that of bone **(Krishna et al., 2007)**. Therefore, NiTi has replaced the steel alloys for medical implants.

Nowadays, porous implants of NiTi are gaining very high acceptance. Porosity influences the young's modulus and strain recovery of NiTi as shown in Figure 1.3, representing the stress-strain graph of loading and unloading compressive experiment, performed by Xiong et al. **(2008).** Also, porous structure favours high bone tissue ingrowth in pores of metallic implants **(Xiong et al., 2008).**

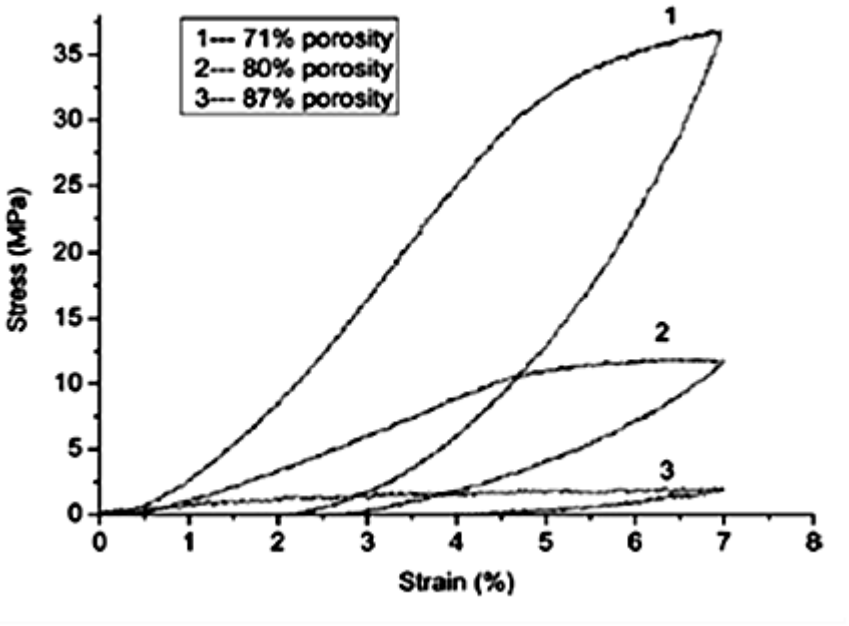

Figure 1.3: Stress–strain graph of loading–unloading compressive tests of NiTi alloy at various porosities (Xiong et al., 2008)

Due to the distinctive quality of SME, NiTi has gained wide acceptance as actuators in mechanical and aerospace industries. Micro-electromechanical systems (MEMS) are developed for micro-level instruments since Ni-Ti alloys have high damping properties along with high abrasion resistance. NiTi in the form of thin films has technological importance in the fabrication of MEMS. Film thickness has a great role in controlling the transformation behaviour of NiTi from the martensite to austenite phase **(Otsuka and Ren, 2005; Kumar et al., 2012).** Micro and nano-finishing plays an important role for NiTi to be used for the applications in μ-TAS (Total Analysis System), fluidic devices and medical instruments. Controlling the chemical reaction of NiTi with working environment is a quite challenging research opportunities. In case, highly smooth NiTi film is used as MEMS in laser operated devices, then energy loss may occur and response of NiTi may get affected. Therefore, some surface modification may be allowed for improving the SME.

Recently, NiTi alloys have been used in civil structures for vibration controls and for seismic isolations. Reinforcement and repair of damaged structure using SMAs is to be introduced in civil engineering **(Savi et al., 2011; Shahin et al., 2005; Burton et al.,**

2006; Guo and Kato, 2015; Wang and Mak, 2014; Damanpack et al., 2014; Asadi et al., 2013; Dieng et al., 2013; Freed and Aboudi, 2008; Files and Olson, 1997), might be founders in crack healing SMA and followed by many others **(Savi et al., 2011; Hamada et al., 2003; Kirkby et al., 2008)**. In almost all previous surveys, NiTi SMAs were embedded inside a matrix and have excellent corrosion resistance. NiTi is used in civil structures, because of high density, energy dissipation through hysteresis, corrosion resistance, shape recovery after large strain and high fatigue resistance high stress. High performance structures can be fabricated by SMA due to active vibration control **(Shahin et al., 2005)**. But still design guidelines are in a pending state to use SMA as seismic protective system **(Ozbulut et al., 2011).** The more detailed applications of Nitinol in different areas are summarized in **Table 1**.

Table 1.1: Applications of NiTi in different fields of Medical and Engineering

Broad Application	**Specified Field**	**Object**	**Description**
Medical Applications	**Cardiovascular**	Simon Filter **(Levi et al., 2008)**	It is used to filter the clots present in the bio-fluid
		Atrial Septal occlusion device **(Lagoudas et al., 1999)**	This device acts as an alternative to atrial hole surgery, which takes place when an hole is occurred in heart's right and left atrial (upper part of heart).
		Self-expanding Stent (Figure 1.4) **(Petrini and Migliavacca, 2011)**	It is used to maintain the diameter of blood vessel
		Aortic valve (Figure 1.5) **(Levi et al., 2008)**	These are used in the endovascular treatment and the membranes called "eNitinol". These are much flexible and have longer life than the mechanical valves. By the use of these membranes, size of the prosthesis reduces significantly
	Orthopedic	Spinal Vertebra spacer **(Duerig et al., 1990)**	This spacer is used in case of scoliosis.
		Orthopedic	It is used to heal the broken bone or

		Staples **(Dai et al., 1993)**	fracture.
		Shape memory plates and screw **(Mantovani, 2000)**	During the recovery of bone, when it is difficult to place a cast material then SMA plates and screws are used specially in nose, eye, facial area and jaw socket.
	Surgical Instruments	SMA Basket **(Kourambas et al., 2000)**	It is utilized to remove bladder, bile duct stone and kidney.
		Intra-aortic balloon Pump **(Duerig et al., 1999)**	This pump is used to un-lock blood vessels during angioplasty.
		Laparoscopy Tools **(Duerig et al., 1999)**	Grippers, tongs and scissors come under this category. These tools are utilized for the smooth movement of muscles. The complex regions can be accessed with the help of these tools.
	Neurosurgical Field	Micro-coil **(Hoh et al., 2009)**	Cerebral aneurysms (intracranial arteries localized dilation) can be treated with the help of coils.
		Micro-guide wire **(Hoh et al., 2009)**	These are utilized for the positioning of stent.
	Orthodontic	Wire **(Torrisi, 1999)**	These wires along with multi-bracket are used in orthodontic treatment. The dentist deform the wire (martensite phase) and place on teeth. This wire tries to recover its shape (austenite phase) due to SME. The position of teeth can be improved due to constant force.
		Palatal arches and orthodontic distractor **(Idelsohn et al., 2004)**	SMA wires are used in steel palatal arches to provide expanding, torquing and rotating force. Teeth overcrowding can also be resolved by pseudoelasticbehavior of orthodontic distractors.
		Endodontic File **(Sattapan et al., 2000)**	This file is used to study the issues with the tooth pulp and tissues near root of tooth. This file also performs cleaning action during root canal.
Space and Aero-space	**Aero-space**	Fixed Wing **(Sanders et al., 2004)**	It is the development of SMA wire tendon and torque tube under the roof of Smart wing program by Defence

			Advanced Research Projects Agency (DARPA). SMA torque tendon facilitates span-wise wing twisting while wire tendon actuate hingeless ailerons by SME and shape recovery.
		Inlet Cowl **(Kudva, 2004)**	It is used in the propulsion system to orient it in two different directions by SME (SAMPSON program by NASA).
		Chevrons **(Mabe et al., 2004)**	These are used to reduce the engine noise by using bending actuation at take-off and landing.
		Morphing of Wings **(Balta et al., 2001)**	The symmetry changed by the actuation of SMA wire to optimize the flight performance.
		MEMS **(Mani et al., 2003)**	MEMS placed under aero-dynamic surface of aero-space. These devices will help to energize boundary layer and decrease turbulent drag.
		Air-craft Structural Panel **(Tawfik et al., 2002)**	Due to SME it represents elastic stiffness after deformation.
		Rotor Craft **(Prahlad and Chopra, 2001)**	This is the torque tube to change the twist of rotor blade. Optimization of tiltrotor performance carried in both forward and hover flight.
	Space-craft	Shock-absorber **(Williams et al., 2000)**	SME is used for removing the low-shock release problem.
		Qwknut/Micro-step-nut **(Peffer et al., 2000)**	The component is de-twinned and deformed before installation, when this mechanism is repeated which is utilized in rotary latch.
		Stepper motor **(Godard et al., 2003)**	This is made by SMA wire for orientation of light-weight flexible solar flap. This is utilized in the space-craft antennae for its rotation.
		Antagonistic flexural unit cell **(Pitt et al., 2001)**	This is used for morphing the entire structure. In this system two, one-way SMA wire/ribbon are used by simple hinging mechanism.
		Solar panel dust cover **(Godard et al., 2003)**	The SMA material is used to cover the solar panel to protect them from dust particle, which makes a clean region.
		Sensors **(Birman, 1997)**	SMA's properties changes with the change in phase transformation by the

			effect of loading/heating. Each phase exhibit its unique electrical resistivity. This property utilized to measure the deformation of large span space structure.
		Vibration isolator/ damper **(Williams et al., 2000)**	Pseudo-elasticity of SMA makes them suitable for the desired application. Due to this property material can absorb high vibration load during launching of space-craft.
Industrial Applications		NiTi eye glass Frame **(Zider and Krumme, 1990)**	This material is utilized in eye-glass frame due to high resistance towards the permanent set on accidental damage and bending. Low temperature super-elasticity often enhanced by significant cold work.
		NiTi underwire **(Wu and Schetky, 2000)**	These consist of much lower elastic modulus than steel wires. These wire are resistant to permanent deformation and improve elongation.
		Solder **(Hahnlen et al., 2012)**	NiTi powder is used in SnPbAg solder to increase the resistance towards thermal fatigue. During the joining of electronics device on PCB create rupture and cracks, the main reason is the thermal expansion coefficient difference between the PCB and component. Copper coated NiTi powder reveals improvement in ductility and stiffness.
	Constrained Recovery Applications	Cryofit Coupling **(Wu and Ewing, 1994)**	These couplings are used in hydraulic system of aircraft, petro-chemical, petroleum and utility industries due to strong joint.
		Connector, Sealing and Clamping Component **(Schetky, 1994)**	NiTi-Nb alloys gives reliable work in the temperature range of -65°C to 300°C.
		Diesel Fuel injector **(Wu and Wu, 2000)**	Fuel passage, a plunger cylinder and solenoid valve are elements of diesel fuel injector. During manufacturing, one end kept open and other end sealed. If NiTi-Nb plug used as a seal, then it can be installed at low temperature than conventional steel plug. Tight seal made

			by constrained recovery, which is capable to bear extreme pressure.
	Actuator Applications	Compression wire and tension spring **(Busch, 2000)**	Thermal and electrical actuator utilized SMA in compression wire and tension spring.
		Self Cleaning oven **(Wu and Ewing, 1994)**	NiTi-Cu spring used in the device for the door opening of self-cleaning oven.
		Domestic safety device**(Wu and Ewing, 1994)**	Small cantilever of NiTiCu is used in antiscald valve, which is further utilized in hospitality building equipments like sink, tub and shower.
		Industrial safety valve **(Vu et al., 1999)**	NiTi-Cu spring used in semi-conductor industry to close the flow of gas (i.e. these gas may be highly flammable or toxic). Petrochemical and petroleum industries use safety valve to cope up with fire danger.
		NiTi bent disc actuator **(Johnson et al., 1997)**	SMA protect the high density (Li ion), when temperature rise upto un-controllable limit due to short-circuit if any
		MEMS **(Thorsen et al., 2000)**	These are developed for micro-level instruments becauseNi-Ti alloys have high damping properties.
		SMA actuator (Blade tab control - Helicopter) **(Busch, 1994)**	NiTi twin tubular torsion actuators are used to adjust the trailing edge tab by SMA tracking control.
		Lab on chip **(Janke et al., 2005)**	Full size lab shrinks to coin size by micro-channel/pump.
Civil Engineering Application	**Vibration Absorber**	Shape memory energy absorbers **(Janke et al., 2005; Isalgue et al., 2006)**	Due to super-elasticity property this material used in vibration absorber and insulators.
Electrical Applications		Electric power industry **(Duerig et al., 1990)**	Pre-heated NiTi SMA used in electrical circuit because it break the circuit during over-heating.

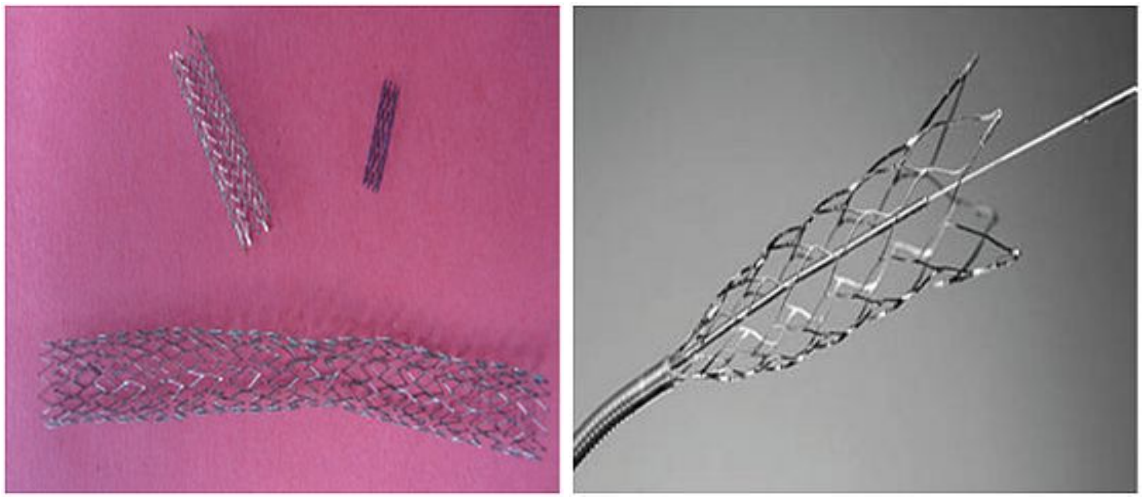

Figure 1.4: (a) Example of SMA stents: (top right) coronary stent, (top left) carotid stent, (bottom left) femoral stent. (Petrini and Migliavacca, 2011) (b) NiTi self-expandable neurosurgical stent

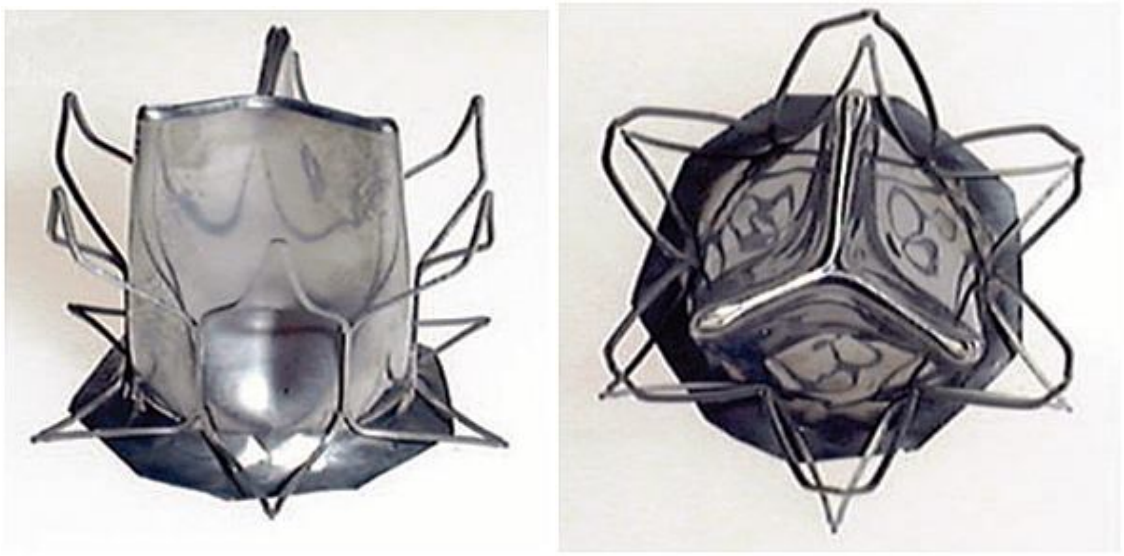

Figure 1.5: Percutaneous Aortic valve realized with eNiTinol membranes and NiTi alloy stent (Levi et al., 2008)

1.3 POROUS NITI

Porous NiTi is useful in tissue growth, medical devices and implants. These materials show voids formation either with the help of pore forming agent or by some other mean. The strength of porous material is always less than the dense material and also exhibit

lower value of young's modulus as desirable in implant. Uniform structure of particles (spherical particles), pore forming, and low temperature additives favours the formation of voids and finally porous structure. Porous NiTi alloys are gaining more importance in medical applications due to low Young's modulus that closely meets with human bone (Figure 1.2) and high bone tissue ingrowth in pores of metallic implants. Thus porous NiTi alloys are suggested biomaterials for hard tissue replacement. In porous implants for bone tissues, pore density and pore size are of great importance. Porosity depends upon the pore size and pore inter-connectivity. Using microwave sintering, porous structure can be obtained in minimum holding time at lower temperature. Porous NiTi alloys are explained in detail in section 2.2.

1.4 FABRICATION ROUTE OF NITI

After consideration of porous structure applications in MEMS and implants, the different methods of its fabrications are plasma spraying, space holder method, combustion synthesis, vapour deposition, rapid prototyping etc. and given in Figure 1.6. One of the foremost techniques for the production of porous structure is powder metallurgy. It is a technique for producing near net-shape objects using different metal powders. Section 1.4.1 describes powder metallurgy process and its steps in detail. There are two ways for generating porous structure during powder metallurgy. First method is use of pore forming agent like NH_4HCO_3 and in the second method is the use organic element. Initially organic element acts as a binder and during sintering it is evaporated and forms porous structure.

Nitinol can be produced by conventional casting processes by melting the material trailed by the hot working process **(Funakubo, 1987)**. Using conventional casting process, precise composition of nickel and titanium is very difficult to control which causes significant alterations in mechanical properties and transition temperature for NiTi **(Morgan and Broadley, 2003)**.

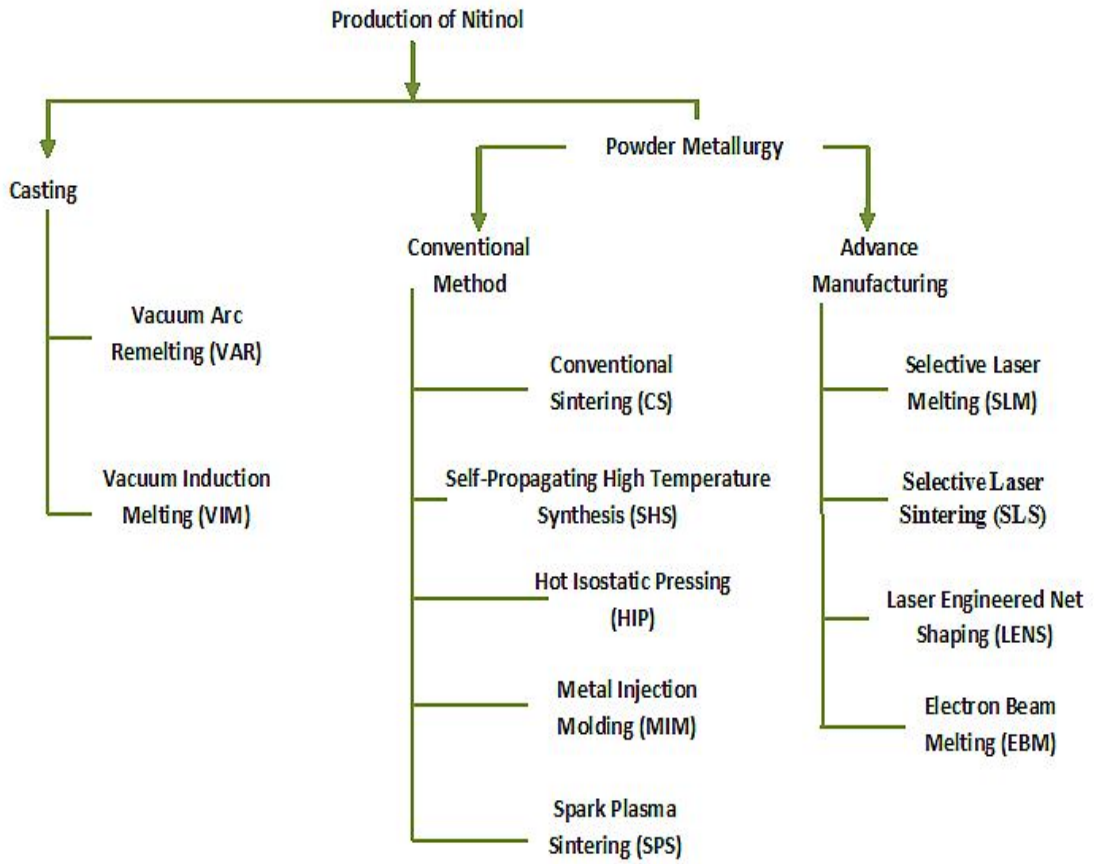

Figure 1.6: Different Fabrication route for the production of NiTi

According to Otsuka and Ren **(2005)**, a metastable equilibrium phase between Ti-Ni and Ti_3Ni_4 is helpful for regulating the transformation temperature and to enhance shape memory characteristics (SMC).

Nitinol can be produced by powder-metallurgy using either pure metal or alloy metal powder. In this process green compact of nickel and titanium powder is subjected to sintering (near about melting temperature) to encapsulate in binary NiTi.

Self-propagating high temperature synthesis starts by thermal explosion from one end, which then proliferates in the specimen by self-continuation manner. But in SHS, the inter-metallic phase cannot be controlled in this method **(Li et al., 2000a)**.

Hot isostatic pressing (HIP) is a sintering process in which uniform pressure is applied in all direction during sintering to produce dense products. In HIP the elemental

powder mixture is kept in an air-tight box with the application of temperature and isostatic pressure.

This process requires pre-alloyed NiTi powders and high temperature during the sintering process. The MIM process completes in four stages viz. feedstock, injection molding, debinding, and finally sintering **(Krone et al., 2004)**.

Three-dimensional solid objects in a multi-layer method through the selective photo initiated cure reaction of a polymer can be achieved by the Stereo-lithographic process **(Elahinia et al., 2005; Lee et al., 2006; Williams et al., 2010; Hadi et al., 2010).** Rapid manufacturing (RM) or rapid prototyping (RP) is the process of producing net shape parts by summation of successive layers of material. In these processes, a thin layer of material is added one over the other to generate definite geometry defined by 3D-computer aided design model. In this process, no post processing like machining is required. It is an energy efficient and eco-friendly process **(Gibson et al., 2010).** These fabrication routes are discussed in detail in section 2.3.

After the fabrication of NiTi alloy some post-processing is also required like machining, shape setting, heat treatment, coating etc. The major machining operation on NiTi includes drilling for joining with bones, finishing or burr removal operations, etc. Machining of NiTi with conventional machining methods (like turning, milling, drilling,etc) is very difficult because of hardening of machined surface, poor surface finish, high tool wear rate and burr formation at machined surface **(Lin et al., 2001)**. Also, the material removal rate is low. Lin et al. **(2000)**, Weinert and Petzoldt **(2004)** and Manjaiah et al. **(2014)** performed experiments to understand the machining characteristics of NiTi.

1.4.1 Powder metallurgy Process

Powder Metallurgy is a method of fabrication of net shaped components by mixing elemental or pre-alloyed powders together, compacting this blend in a die, and sintering or heating the pressed part in a controlled atmosphere furnace to bond the particles metallurgically.

The P/M process is a unique part fabrication method that is highly cost effective in producing simple or complex parts at, or close to, final dimensions.

Blending: Blending or mixing is a process to mix the different powders and make a homogeneous mixture. A rotary ball-mill is used in the present research work for homogeneous mixing of powders.

Compaction: Homogeneous mixture obtained after blending put in a die and punch set-up and compact them with the help of powder compaction press or compaction press at room temperature or elevated temperature as per requirement.

Sintering: During this process metal powder forms a solid below (60-70% of melting temperature) the melting temperature. The powder particles are bonded together by atomic transport mechanism or diffusion. The sintering process is governed by the following parameters:

- Temperature and time,
- Geometrical structure of the powder particles,
- Composition of the powder mix,
- Density of the powder compact,
- Composition of the protective atmosphere in the sintering furnace.

P/M processing provides the following advantages: Production of complex shapes to very close dimensional tolerances, with minimum scrap loss and fewer secondary machining operations. Physical and mechanical properties of components can be tailored through close control of starting materials and process parameters. Particular properties can be improved through secondary processing operations such as heat treating and cold/hot forming.

1.5 NITI BASED ALLOYS PRESENT AND FUTURE

In the field of tissue engineering, to accelerate the cell growth on NiTi, prevascularized microcapillary-like structure can be generated. The research on the performance of this system as a branch of circulatory organism is still underway. In orthodontics, speed of preparation of root canal using NiTi tool is much faster than steel instruments with no undue aberrations. But still there are some challenges in fabricating these small instruments regarding machining with high surface finish and geometrical

accuracy. Electro-chemical and electric discharge machining are the most important machining method used for NiTi **(Rajurkar et al., 2006)**. But some more optimal methods can be investigated for better machining of NiTi. The wear of these NiTi instruments during sterilization and usage is still to be investigated. The research on the less invasive medical procedure is the most promising area of NiTi applications.

NiTi based composites are also the researchers' interest. Aluminum alloy reinforced with NiTi exhibit excellent wear and mechanical properties. Good collaboration between the SMM community, material scientists, engineering designers and marketing personals for the utilization of information platform or database to share knowledge. Development of computational model and new design approaches are still in a pending state **(Pieczyska et al., 2014).**

1.6 OBJECTIVES

In the present work, the Ni-Ti alloy has been processed with powder metallurgical technique. Copper with different percentage composition has been added to study its effect on different characteristics of NiTi alloy. More specifically the below mentioned work has been undertaken.

- Fabrication of homogeneous and porous structures of Ni-Ti: a titanium alloy, using conventional powder compaction technique.
- Experimentally determining the influence of process parameters on mechanical properties and shape memory effect of Ni-Ti. Input process parameters are:
    - Concentration of alloying elements
    - Compaction pressure
    - Sintering temperature
    - Sintering time
- The output responses are strength, modulus of elasticity, wear, corrosion, porosity, bio-compatibility and shape memory effect.
- Surface characterization and orientation of material is processed using scanning electron microscopy (SEM).

1.8 ORGANIZATION OF THESIS

This thesis is sub-divided into seven chapters followed by references. **First chapter** is the introduction porous structure, powder metallurgy process, fabrication of porous structure by powder metallurgy process, introduction of NiTi alloy, its applications and objectives.

Second chapter gives a fundamental understanding of NiTi alloy its production methods by different routes. Also effect of different additives on the characteristics of NiTi alloy, NiTi composites and its post processing are also discussed. This post processing includes its machining, surface coating and heat treatment.

Third chapter provides the experimental set-up details, input and output parameters. Also work-material used in this research along with its processing is discussed.

Forth chapter deals with details of Taguchi experimental design technique. Also, the data analysis procedure has been described in this chapter.

Fifth chapter presents the processing of metal powder in a high energy ball mill. The mechanism of powder processing is discussed in detail.

Sixth Chapter describes the process variables and their selection using Taguchi methods. Different mechanical characteristics were measured at the optimized results provided by Taguchi Technique. Further discussions were made in this chapter.

Seventh chapter consists the wear characteristics of NiTi alloy. In this chapter, wear characteristics were computed at different range of temperature at pin-on-disc apparatus.

Eighth chapter investigates the in-vitro corrosion test, bio activity and bio-compatibility test to confirm the corrosion behaviour and cyto-toxicity of material. These tests were made in the presence of artificial saliva, stimulated body fluid and L929 mouse fibroblast cell at specified temperature and conditions.

Final Chapter contains the summary of the research conducted in this thesis. Also, at the end of this chapter, some suggestions for future work on the related topics have been enumerated.

CHAPTER 2

LITERATURE REVIEW

NiTi alloys present unique characteristics of SME and super-elasticity. Due to these characteristics nickel-titanium alloys are used in actuators, medical devices etc. A number of researchers are actively involved in its fabrication, porous structure, composites and post-processing of alloys. Their researches are described by category-wise as:

2.1 NITI PHASES

Ni-Ti exhibits equi-atomic intermetallic compound of nickel and titanium, which can undergo a reversible solid state phase transformation from ordered cubic crystal structure (B2), called austenite, to distorted monoclinic (B19) called martensite. Shape-memory behaviour is of two types:

- One way (1W)
- Two Way (2W)

When the parent phase regains its original position it is 1W shape memory effect, while in 2W SME regains its shape both in parent and product phase, and it can be accomplished by heating and cooling the specimen **(Elahinia et al., 2012; Huang et al., 2010).**

The unique characteristics of NiTi can be stabilized and improved by controlling the chemical composition and microstructure. Grain size that influences the martensitic start temperature and elasticity of NiTi alloys can be manipulated by controlling the chemical composition and with suitable heat treatment **(Wei et al., 1998)**. Figure 2.1 shows the influence of temperature on transformation for NiTi alloy**.**

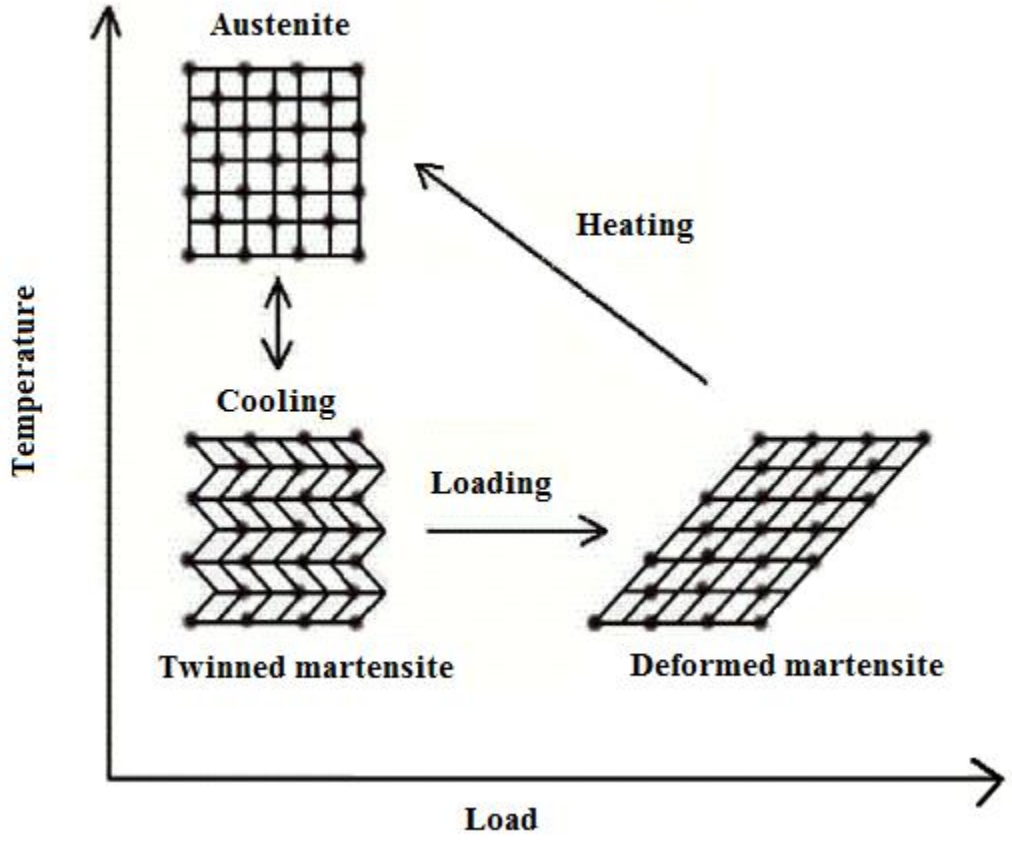

Figure 2.1: Shape memory effect (Ryhanen, 1999)

2.2. FABRICATION OF NITI ALLOY

Nitinol can be produced by different conventional and non-conventional manufacturing methods. Each method of fabrication consists of its own merits and demerits, which is explained in the respective section.

2.2.1. Casting

Nitinol can be produced by conventional casting processes by melting the material trailed by the hot working process **(Funakubo, 1987)**. Using conventional casting process, precise composition of nickel and titanium is very difficult to control which causes significant alterations in mechanical properties and transition temperature for NiTi **(Morgan and Broadley, 2003)**. Figure 2.2 represents the binary phase diagram of alloy

(NiTi). **Otsuka and Ren (2005)** emphasised the central portion of the phase diagram corresponding to 50% nickel percentage as the most reliable. According to Otsuka and Ren **(2005)**, a metastable equilibrium phase between Ti-Ni and Ti_3Ni_4 is helpful for regulating the transformation temperature and to enhance shape memory characteristics (SMC).

Contamination due to atmospheric air, carbon and oxygen in NiTi, alter the equilibrium phase between TiNi and Ti_3Ni, and therefore a small change in the composition significantly varies the properties of NiTi alloy. The carbon content in the ingot varies from 200 to 500 ppm. The percentage of carbon relies on the melting temperature of the furnaces. The shape memory composites are not affected much by this amount of carbon. At melt temperatures greater than 1723^0 K, graphite crucibles are commonly not in practice **(Frenzel et al., 2007; Frenzel et al., 2004; Mantovani, 2000)**. Martensite transformation depends on sample thickness. Reducing the thickness of the sample, transformation temperature also reduces. But at critical value (≈22nm - 50nm) no transformation is observed. Reducing the thickness, oxygen content decreases during oxidation **(Li et al., 2014)**.

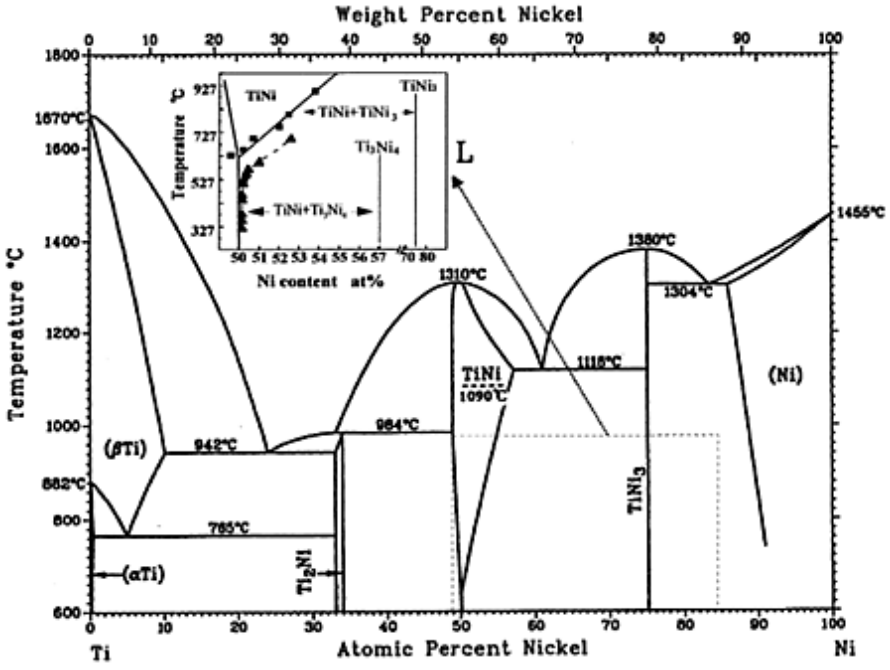

Figure 2.2: Phase diagram of NiTi alloy (Otsuka and Ren, 2005)

The O_2 is present in the TiC crystal lattice as an impurity **(Duerig et al., 1999).** The problem of contamination can be minimized by melting the Ni and Ti ingots in an inert environment **(Morgan and Broadley, 2003)**.Two commonly used methods of melting in inert environment are:

1. Vacuum arc re-melting (VAR)
2. Vacuum induction melting (VIM)

Both of these methods can fulfil the requirements of the materials for medical devices economically **(ASTM-F2063, 2000)**. These processes use 99.9% pure raw material. Main limitations in both VIM and VAR processes include higher reactivity of the molten material and segregation. The main reason of segregation may be the density difference in the reacting melt **(Reinoehl et al., 2000)**. Through the VAR process, cast samples of NiTi consist of dendritic and inhomogeneous micro-structures. The composition of $Ti_{58}Ni_{27}O_{15}$ supports the formation of Ti_4Ni_2O with a well-defined atomic ratio **(Toro et al., 2009).** The formation of Ti_2NiO_x occurs during VAR due to presence of O_2 in the re-melting stage. The homogeneous treatment eliminates the problem of micro-segregation while O_2 contents remain as it is in the VAR process **(Kabiri et al., 2012).**

The temperature ranges for VAR process are 825-875°C and 950-975°C. Highest strain rate is observed at 975°C. Grain refinement can be achieved by re-crystallization of melts at high temperature, but it results in very poor fatigue properties **(Yeom et al., 2014; Jiang S et al., 2013a).** NiTi samples produced by VIM followed by annealing at 300°C and 450°C of local canned compression specimen induce nano-crystallization of NiTi samples, which are unstable. At higher temperature upto 600°C, complete crystallization of the NiTi samples takes place. The presence of Ni_3Ti and Ni_4Ti_3 precipitates is also observed in the deformation bands **(Jiang S et al., 2013b; Jiang H et al., 2013; Bhagyaraj et al., 2013).** At high temperature, NiTi is sensitive to strain rate, but at low temperatures compressive test becomes insensitive to strain rate. This may be due to the changing of dendritic grains into equi-axed grains after plastic deformation in the martensite state at low temperatures **(Jiang and Zhang, 2012).**

In VIM, TiC compound were formed in nickel matrix when the carbon reacted with the Ti and results found a decrease in martensite transformation **(Morgan and Broadley, 2003)**. Reduction in contamination and carbon contents present in the molten pool is another thrust area for investigation **(Otubo et al., 2003).** The influence of oxygen content present during VAR process and improvement in the porosity during casting process can be a probable research interest for material scientist.

2.2.2. Powder Metallurgy

Nitinol can be produced by powder-metallurgy using either pure metal or alloy metal powder. In this process green compact of nickel and titanium powder is subjected to sintering (near about melting temperature) to encapsulate in binary NiTi. Success of this process (conventional sintering) depends on input parameters such as size of metal powder, compacting pressure, sintering temperature and time. In powder metallurgy, metal powders of fine size are generally prepared by milling the metal powder of large size in a planetary high energy ball mill for 5 to 60 hours. Milling time and milling speed greatly affect the powder size **(Sharma et al., 2016)**.

Hot isostatic pressing (HIP) is a sintering process in which uniform pressure is applied in all direction during sintering to produce dense products. In HIP the elemental powder mixture is kept in an air-tight box with the application of temperature and isostatic pressure. Inert gas atmosphere is provided with the air-tight chamber. Parts produced by this method had porosity of 5% approximately. The advantages of HIP processes consist of good control of pore size, ability to manipulate geometry and thermo-dynamic stability **(Hosseini et al., 2013).** During HIP complete diffusion of the elements occurs. Porosity upto 50% can be achieved at average pore size of 20 μm by reducing compaction pressure and sintering time **(Lagoudas and Vandygriff, 2002)**.

Metal injection molding (MIM) is another powder-based method for large production of small and complex net shape, high density NiTi **(Bram et al., 2002; Aust et al., 2006)**. This process requires pre-alloyed NiTi powders and high temperature during the sintering process. The MIM process completes in four stages viz. feedstock, injection molding, debinding, and finally sintering **(Krone et al., 2004)**. The optimization of process

parameters for each step is essential to get the best results. This optimization can be accomplished by considering the response variable (viz. Porosity, strength, fatigue strength, etc.). Some optimization techniques like Taguchi method, response surface methodology, Genetic algorithm etc. can be utilized by considering proper level of input parameters of MIM process. In the first step, the blending of powder takes place with binder in proper proportion. The second step consists of melting and injection of metal powder through a mold. The designing of the mold is an important criterion so that a uniform distribution of pressure and temperature takes place with a capability to remove the injected sample properly. After that the binder is vaporized in a chemical bath at an elevated temperature under vacuum. Finally sintering is performed at 1200^{O}C to get a green density equivalent to the material's theoretical density. The density of MIM product is 95% of theoretical density **(Aust et al., 2006)**. The powder metallurgy techniques are highly influenced by the high affinity of NiTi alloy to uptake carbon and oxygen, which increases the chance of the formation of Ti_2Ni and TiC phases with enriched oxygen in the nickel matrix. Precipitation of Ni_4Ti_3 also occurs when the material is cooled from sintering temperature. The existence of Ni_4Ti_3 reduces the mixture content which balances the O_2 and C uptake and results in decrease in ductility **(Bram et al., 2012)**.

Porous structure of NiTi can be produced by different sintering methods viz. spark plasma sintering, SHS and pulse electric current sintering. These processes are further discussed in detail in section 2.2 of porous NiTi. Different sintering or heating methods provide varying percentage of porosity. As already discussed, high porosity is required for matching the young's modulus of NiTi as with the moduli of bone. During SHS **(Li et al., 2000b)** porosity of above 50% can be obtained for NiTi. SHS starts by thermal explosion from one end, which then proliferates in the specimen by self-continuation manner. But in SHS, the inter-metallic phase cannot be controlled in this method **(Li et al., 2000a)**. In case of SPS, pre-alloyed powders are filled and compressed in a die followed by heating of the die using electric current. Finally, a joint is formed at low temperature and in less time as compared to HIP. The porosity obtained by this method is less (only 12%) (**Nasser et al., 2005; Ying et al., 2005; Sun et al., 2012).**

Recently microwave sintering attracts the researchers' interest due to energy saving, short processing time, improved mechanical properties, higher heating rate and eco-friendly. Porous NiTi can be produced without any pore-forming agent by the use of microwave sintering even at low temperature (850^0C) and short sintering time (15 min). The increase of holding time increases the porosity upto 48% **(Tang et al., 2011).** The elastic modulus and compressive strength of porous NiTi (in case of microwave Sintering) was 5.5GPa and 360MPa. After the micro-structural evaluation it has been found that the pores are inter-connected with pore size varying from 20-100μm. Also strain recovery and shape recovery decrease with the increase of pore size (from 97 μm to 294 μm) by 0.73% and 21.4% respectively by using pore forming agent like NH_4HCO_3. Corrosion resistance of porous NiTi decreases three times as compared to dense NiTi **(Xu et al., 2014; 2015a)**. The compressive strength of porous NiTi alloy also was found to be decreased from 880 to 62 MPa with increase of porosity from 22% to 62 %. The bending strength of alloy also decreased from 371.4MPa to 74 MPa with increase of porosity **(Xu et al., 2015b).**

2.2.3. Rapid Manufacturing

Rapid manufacturing (RM) or rapid prototyping (RP) is the process of producing net shape parts by summation of successive layers of material. In these processes, a thin layer of material is added one over the other to generate definite geometry defined by 3D-computer aided design model. In this process, no post processing like machining is required. It is an energy efficient and eco-friendly process **(Gibson et al., 2010).**

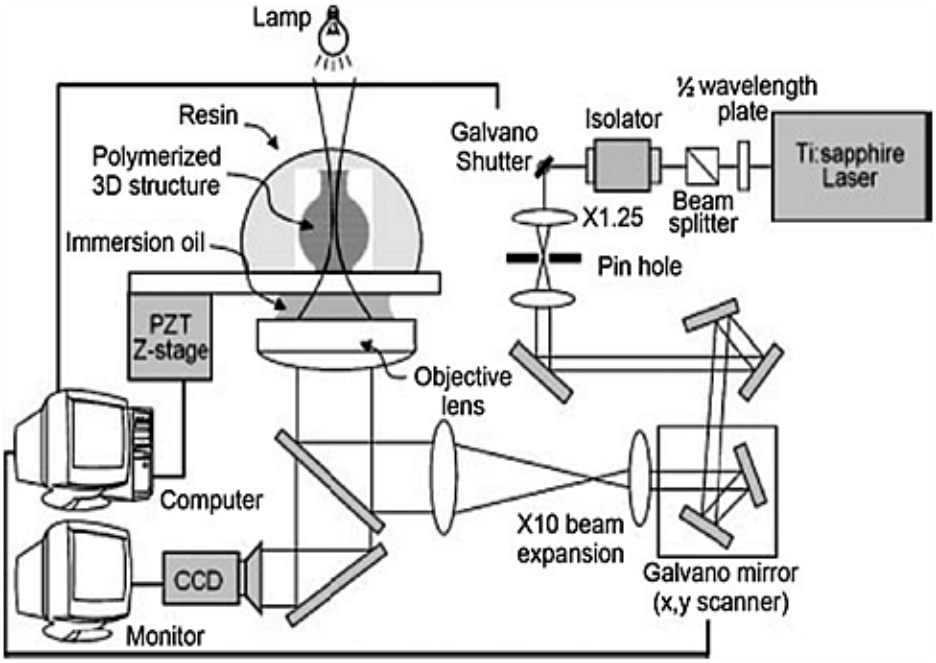

Figure 2.3: The Stereolithography System (Lee et al., 2006)

Three-dimensional solid objects in a multi-layer method through the selective photo initiated cure reaction of a polymer can be achieved by the Stereo-lithographic process **(Elahinia et al., 2005; Lee et al., 2006; Williams et al., 2010; Hadi et al., 2010).** These processes (Figure 2.3) apply two different methods of irradiation; first utilizing ultra-violet beam to solidify liquid resin, while in the second one, patterned mask is utilized by shifting the image to liquid polymer. These techniques are used in tissue engineering due to its ability to cure quickly for the production of scaffolds. Other applications are in the production of micro-needles for transdermal drug delivery, surgical guides for dental implants, hearing aids, temporary crowns, resin model for lost wax casting and bridges **(Noort, 2012; Ovsianikov et al., 2011).** Laser-based additive manufacturing processes such as selective laser melting (SLM) is another process for direct products of metallic parts with complex three-dimensional objects. This process has remarkable potential to develop shape memory objects of NiTi **(Yadroitsev, 2007).**

The specimens manufactured from SLM exhibit pseudo-elastic behaviour directly after manufacturing, i.e., without additional heat treatments. A shape recovery of up to 3% strain was demonstrated. An optimum parametric combination has been found by

Bormann et al. **(2012)**; Walker and Elahinia **(2013)** and found that the transformation temperature driving unique behaviour are very much sensitive to the relative concentration of nickel and titanium.

Laser Engineered Net Shaping (LENS) utilized for fabricating homogeneous nickel titanium alloy results in high micro-hardness as compared to conventionally made alloy. In this process a laser beam and metallic powder is used. A small melt pool is formed by the laser beam and 3-D CAD software is used to create the geometry. Once the geometry is completed, the head moves for the fabrication of product layer by layer. Metal powder is distributed around the circumference using either the gravitational force or pressurized carrier gas. Sometimes different but compatible material is used during injection (Figure 2.4). Oxidation of pool can be prevented by the use of inert gas **(Gibson et al., 2010).** Corrosion resistance of NiTi is found to be improved by laser surface treatment as verified in the Hank's solution and potentio-dynamic test by Krishna et al. **(2009).**

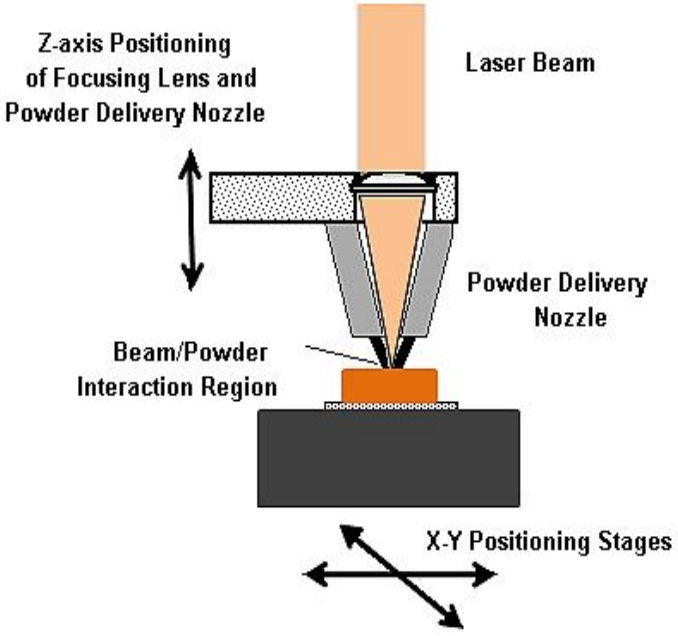

Figure 2.4: Schematic illustration of the LENS process

The major problems involved in the LENS process is high cost, it's intrinsically hazardous, quite a slow process and has poor surface finish. In LENS, argon consumption is another task to be maintained **(Bernard et al., 2009)**.

EBM (Electron Beam Melting) used electron beams for the fabrication of the melt pool by scrutinizing a layer of powder **(Hao and Harris, 2008; Koike et al., 2011)**. EBM process contains two sections viz. electron beam gun section and the specimen-fabrication section both kept in a high vacuum. Very high beam-material coupling efficiency, very small spot sizes and high scanning speed can be obtained with the help of EBM **(Hao and Harris, 2008)**. The accuracy range and surface roughness value of EBM is 0.3–0.4 mm and 25mm respectively **(Noort, 2012).**

2.3. FABRICATION OF POROUS NITI

Porous NiTi alloys are gaining more importance in medical applications due to low Young's modulus that closely meets with human bone and high bone tissue ingrowth in pores of metallic implants. Thus porous NiTi alloys are suggested biomaterials for hard tissue replacement. In porous implants for bone tissues, pore density and pore size are of great importance. Porosity depends upon the pore size and pore inter-connectivity. Using microwave sintering, porous structure can be obtained in minimum holding time at lower temperature **(Tang et al., 2011)**.

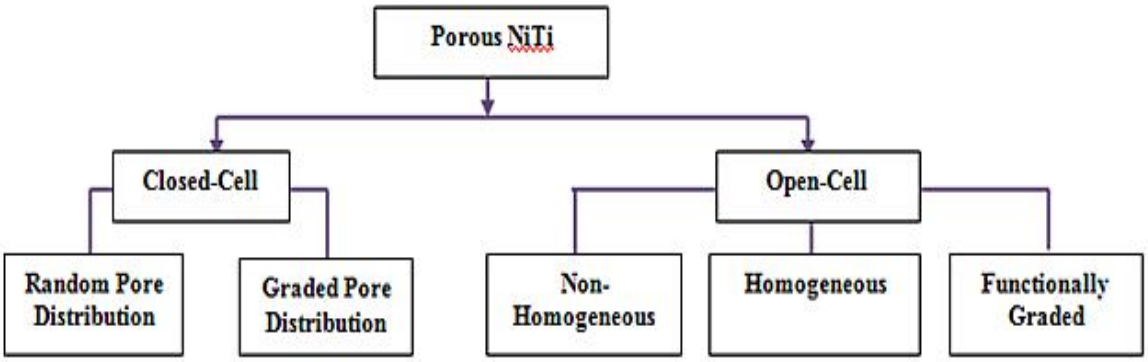

Figure 2.5: Classification of porous NiTi structures

Depending upon the distribution of pores and its inter-connectivity, porous NiTi can be further classified as shown in Figure 2.5. In closed-cell porous structures, every cell is covered by a thin film of metals and pore inter-connectivity is poor whereas in open-cell porous structures, the individual cells are interconnected, permitting tissue to permeate

the form (porous structure). The presence of voids decreases the bulk stiffness in closed cell structure which enables it to match the properties of bones and decreases the stress shielding problems. The closed-cell porous implants are preferred for high load bearing orthopaedic applications like artificial hip replacement, artificial human arms or legs, etc. Open cell porous implants are more preferred for low load applications where high cell ingrowth and proliferation are required **(Banhart, 2000).**

The mechanical and bio-properties of NiTi alloy can be changed by altering the pore-size and shape, porosity and density, **(Tosun and Tosun, 2012)** which depends on the fabrication method. To fabricate porous metallic implants, there are several techniques such as plasma spraying, space holder method, combustion synthesis, vapour deposition, rapid prototyping, etc. Two general routes for the generation of porosity in metals are melting and powder metallurgy **(Ryan et al., 2006)**. During the melting process there are two ways to manufacture porous structure either by gas forming or injection of gas into the melt **(Banhart, 2001).**

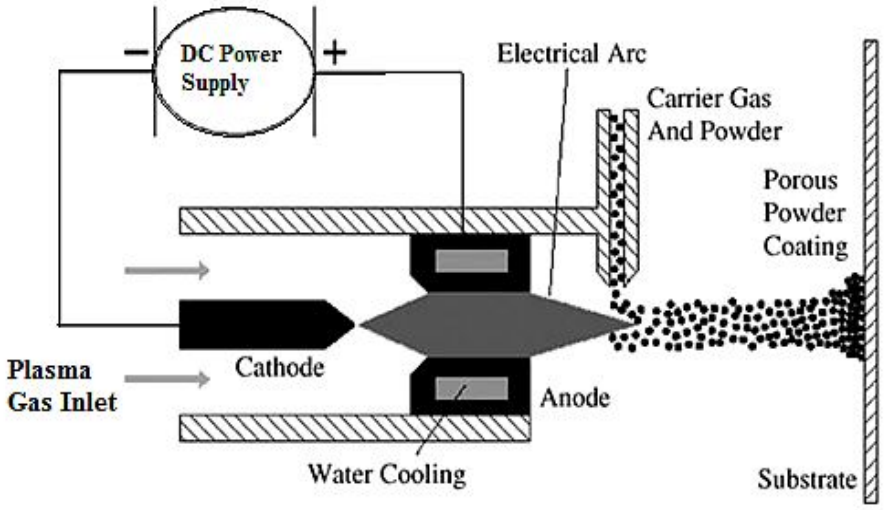

Figure 2.6: Schematic diagram of the plasma spraying process

While in powder metallurgy, binder or pore forming agents are appended in powder particle and the compacted part is placed in a high temperature atmosphere, which causes the powder particles to bond together. Using pore-forming agents (NH_4HCO_3) in NiTi,

50% porosity can be obtained with nearly uniform and large size pores (larger than 300 μm) **(Zhang et al., 2007)**. Pore size and density are significantly affected by the compaction pressure and sintering time. Aydogmus and Bor **(2012)** obtained the porosity in the range of 38-59% using low boiling point spherical magnesium powder as additive. Porous NiTi (35% porosity) that is fabricated by microwave sintering gives excellent corrosion resistance in Hank's solution. Pore size varies from 20-100μm and represents a good bone-tissue cell penetration. Compressive strength varies from 360MPa-5.5 GPa. Compressive strength, pore size and porosity can be controlled by sintering temperature and time. Increase in sintering time decreases irrecoverable strain **(Nikolay et al., 2014; Jani et al., 2014).** Porous structure in NiTi can be produced by plasma spraying. Using this technique, porous surface coating and solid surface textures can be created on solid cores **(Salito et al., 1998).**

Figure 2.6 shows the schematic representation of plasma spraying technique. In plasma spraying process, two water cooled electrodes are used to generate an electric arc which is utilized for the generation of high temperature in the range of 20000^0C to heat the gas and form a plasma jet. In this process, high pressure powder is injected with carrier gas by jet-shaped anode onto the plasma gas stream. It strikes the substrate at high velocity (i.e. high kinetic energy) which melts the powder and results in the coating. The degree of porosity can be changed by varying spraying parameters. Porous sample of NiTi with high porosity can be fabricated by the space holder method. In this process, appropriate space holder material having very low boiling point (like urea **(Bram, 2000)**, ammonium hydrogen carbonate **(Wen et al., 2001a)** and polymer binder **(Tuchinskiy and Loutfy, 2003)**) is mixed with metal powder followed by the compression of the mixture to form the green compact. Later this compact is subjected to high temperature which evaporates and results into the porous structure with porosity in the range of 60-78% (**Wen et al., 2001b).**

Combustion synthesis (CS) is another recognized technique to produce porous NiTi alloys. In this process particle fusion takes place by the heat released during the self-sustaining exothermic reaction. The specimens are situated in an inert atmosphere and ignition takes place by means of electrical heated coil or electric discharge. When

ignition takes place the reaction flows as combustion through the whole mixture without addition of extra energy. In combustion synthesis the morphology and porosity are affected by compaction pressure, particle size of powder and binder **(Yea and Sung, 2004).** Li et al. **(2000)** obtained the open porous structure with 60% porosity. Researchers found that the increase in preheat temperature increases the combustion temperature and inter-metallic NiTi compound melt above 450°C. Through this process, high purity and porosity of more than 50% can be obtained. The compression behaviour of both porous and dense NiTi is different. During loading and unloading of NiTi, the ductility decreases, while the probability of crack initiation increases by 10%.

Porous NiTi shows initial rapid strain accumulation which reaches a plateau value after a certain number of cycles. The research on biological study of porous NiTi is yet on its starting stage compared to dense NiTi **(Bansiddhi et al., 2008).** With increasing porosity, permanent deformation takes place at very low stress value.

2.4. NITI COMPOSITES

The developing era of research on materials had introduced numerous novel materials. Researchers work on the characteristic enhancement of material by introducing some metal, non-metal, reinforcement etc. in it through a proper technique. Today is the time of composites in every field of engineering to increase strength, wear resistance, corrosion resistance, weight reduction (or any one of above) of material. Now, NiTi composites are used for structural purposes, where strength is the main criterion. Shape memory and bio-compatibility of composite material is reduced. NiTi works as a good matrix material, so reinforcement of carbon nanotubes (CNT) utilized to enhance the mechanical strength **(Lee et al., 2014)**. NiTi/Al_2O_3 **(Farvizi et al., 2014)** and NiTi /TiC **(Yang et al., 2006)** based composites used to enhance the wear characteristics of the material.Now researchers also utilized NiTi as reinforcement to enhance the characteristics of low strength or low wear resistant material especially in case of Mg alloys **(Sankaranarayanan et al., 2015).**

Mechanical characteristics of nano-composite are found to be very low as per expectations. This is due to the phase formation, which cannot be completed by nano-

particle in metal matrix **(Hao et al., 2013).** NiTi matrix can be considered a better alternate to form nano-wires. Nano reinforcement of NbTi (~ 70% by % vol.) in NiTi matrix sustain high elastic strain of 2.72% along with 2.53 GPa stress **(Jiang et al., 2015)**. Al 1100 matrix embedded with NiTi particle exhibit better mechanical properties with no interfacial products. Shape memory characterstics of NiTi utilized to induce residual tensile and compressive stresses in AL 1100 matrix **(Dixit et al., 2007)**.

2.5 EFFECT OF ADDITIVES ON NITI

In past years many researchers have experimented on deliberate addition of alloying elements in NiTi with an objective to improve austenitic strength, alter the transformation temperature and increase corrosion resistance and radio-opacity. A little variation in stoichiometric ratio of binary NiTi, shows variation in transformation temperature and other properties. If care is not taken during melting or graphite crucibles are used at high temperature, carbon can exist in Nitinol, specifically as titanium carbide (TiC). This carbide reduces fatigue life and ductility **(Treppanier, 1995).** Addition of transition metals - Mn, Co, Cr, Fe and V- could all be surrogated in minute quantities for nickel without losing the SME, but they decrease the martensite temperature. NiTiCo with 2% cobalt added for nickel also became popular. Like the iron ternaries, NiTiCo is easily formed, worked and quite ductile and stable also. The effects of Cr, Mg and V are very similar to those of cobalt and iron.

To avoid self-actuation of SMA at low temperature, it was necessary to develop the alloy with M_S temperature up to 150^0C or above that would allow electrical actuation for desired applications. Therefore, platinum (Pt) and palladium (Pd) were added into NiTi. Pt and Pd are not added as a substitute for Ni or Ti, but forming the alloys TiPt-TiNi and TiPd-TiNi. Both Pt and Pd act as martensite repression ingredients at below 10%, but at larger quantities above 10% both are martensite stabilizers and provide high transformation temperature SMA **(Duerig et al., 1990; Benafan et al., 2015).**Transformation temperature range can be widened while retaining super-elasticity by addition of zirconium (Zr) and hafnium (Hf) **(Radu and Li, 2007).** The addition of zirconium retains the phase structure of nickel-titanium alloy, increasing the unit cell

volume of alloy and lattice constant. The addition of Zr reduces liquidus temperature and increases the transformation temperature to 200°C **(Vermaut et al., 2003).** The addition Hafnium (Hf) will result into fully recoverable SME upto 700MPa **(Karaca et al., 2011).** Hafnium based TiNi SMAs are potentially high temperature operating alloys up to 225 °C **(Firstov et al., 2004).**

Copper can also be substituted for nickel in small quantities without affecting the martensitic phase transformation and while completely retaining super-elasticity and shape memory **(Kang et al., 2008).** Addition of Cu in NiTi increases the hot ductility temperature by 50°C, while 20% reduction in the area observed during tensile test. The regeneration pattern also reduced after the generation of cracks and cavities with high volume fraction **(Morakabati et al., 2011)**. After 5% addition of Cu, the shape memory characteristics are measured with cooling/heating rate of 0.017K/s and tensile test with strain rate $10^{-3}s^{-1}$. Ti_2Ni ribbon at 1673K shows the partial shape memory characteristics, while increase in temperature during ribbon formation, perfect super-elasticity is observed in NiTiCu (Taguchi-Grey relational) **(Jiang H, 2013; Sadeghi et al., 2014; Gao et al., 2015).**

A little suppressive effect on transformation temperatures can be observed by Niobium (Nb). It was further observed that Nb raises the hysteresis of the alloy. Nb allows wider storage temperature range for medical devices due to large super-elastic temperature range, as well as being suitable for new non-medical applications. Nb is significantly more radio-opaque than Ni or Ti **(Luo et al., 2006).** The advantages of addition of these costly ternary elements are generally offset by losses in other specific properties of NiTi.

2.6 CHARACTERIZATION OF NITI ALLOY

NiTi alloys present excellent mechanical properties due to intermettalics i.e. Ni_3Ti and $NiTi_2$.

Nam et al. (2008) described the effect of Ti2Ni particle on microstructure, shape recovery and super-elasticity of NiTi alloy. During the melt spinning when the temperature increases from 1773K, the intermetallic particle size is approximately equal to 13nm. The presence of intermetallic in the NiTi alloy also exhibits a good

shape recovery even the stress is increased upto 160MPa. The absence of intermetallic in the NiTi alloy represents partial super-elasticity rather than a perfect elasticity.

Morakabati et al. (2011) found the optimum range of temperature for hot tensile strength of as cast NiTi SMA. It has been found that the hot tensile strength of NiTi alloy is maximum in the temperature range of 700-1000°C and is equal to 340MPa. Lowest value of ductility was found at 700°C due to cavitation effect in the structure. The softening mechanism behind this is the dynamic recrystallization. With the addition of copper content in the alloy the formation of cavities and cracks increased and lowers the value of hot ductility.

Shariat et al. (2013) investigated the hystoelastic deformation behavior of NiTi alloy (fabricated by geometrically grading). It was observed that at 370MPa, the phase transformation changes from austenite to martensite. The graded NiTi SMA exhibit ultimate tensile strength of 1150MPa. The graded NiTi alloy model was fabricated by finite element method.

Xu et al. (2014) investigated the mechanical characteristics of NiTi alloy fabricated by microwave sintering and is found that the material represents 360MPa compressive strength and 5.5 GPa Young's modulus. At 850°C, little amount of $NiTi_2$ phase was present. With the increase of sintering temperature the presence of Ni_3Ti also detected with the NiTi phase. These results were also verified by the XRD analysis. **Song et al. (2014a)** investigated the multi-axial transformation ratcheting of NiTi SMA. The experiments were performed on a combined tension-torsion loading conditions. The maximum value of stress found is equal to 400MPa which is greater than the shear stress (calculated from torsion test) of material. The energy dissipation is largest at the very first cycle of ratcheting and after that it decreases rapidly and attains a stable value.

Kucharski et al. (2014) studied the effect of nitrogen ion implantation on the mechanical properties of NiTi SMA. It was found that the after ion implantation, strain was increased from 0.045 to 0.05 while a little improvement in the tensile strength also observed. The properties of NiTi alloy changes on the surface as well as in bulk material. Same can be verified by penetration tests and load-penetration curve.

Song et al. (2014b) compared the properties of NiTi-Al composite reinforced with Nb and Mo and fabricated by as-cast method and forged iso-thermally. As-cast NiTi alloy contain $(TiNb)_2Ni$, NiTi, $(NbTi)_{ss}$ phases while in forged NiTi-Al, the grains are perpendicularly elongated in the direction of forging. Nb solubility in the NiTi matrix decreases after the addition of Mo and many nano-scale precipitates are observed.

Tan et al. (2003) investigated the corrosion and wear rate for plasma source ion implanted (oxygen) NiTi alloy. Potentiodynamic polarization curve has been used to evaluate the wear rate. It was observed that wear-corrosion and pitting corrosion rate decreased after the oxygen implantation. The best value of pitting corrosion resistant value has been observed at austenite finish temperature of 21°C. Wear corrosion rate found to be improved after oxygen implantation due to $Ti_{11}Ni_{14}$ precipitates.

Gialanella et al. (2008) performed the wear calculations of NiTi SMA of two phases i.e. austenitic NiTi alloy and martensitic NiTi alloy. The couterfaces during the experimental work are WC-Co and AISI M2 high speed steel. At lower value of load on pin-on disc apparatus, oxidation layer has been formed, so oxidation wear overcomes other wears. Due to frictional heat martensitic alloys get converted into austenitic alloy and debris formation with delamination takes place at higher value of load. Wear rate of NiTi alloy with WC-Co counterface is more than the NiTi/M2 steel couple.

Yan et al. (2013) performed the ball-on-disk wear test on martensitic NiTi alloy using alumina balls. The coefficient of friction and wear characteristics were evaluated during ball-on-disk apparatus. Three stages of wear are found in these experimentations. In the first stage wear rate is zero and coefficient of friction is very low i.e. <0.1. Second stage of wear is the transition state, where the wear rate increases rapidly and coefficient of friction also increases. Last stage of wear is abrasive wear and in this debris is found with the increase in coefficient of friction.

Abedini et al. (2012) calculated the wear rate of NiTi SMA against the steel by differing the normal load from 20N to 80N. During the wear test when the load is varying from 20N to 40N, there will be no oxide layer observed in this load range during wear test. When the load is increased from 40N to 80N, then the oxide layer

was observed which acts as a barrier to wear and wear rate decreased with increase of sliding speed.

Yan and Liu (2014) studied the deformation mechanism of NiTi SMA at different temperature. Below the martensite temperature the coefficient of friction decreased upto 0.8 from 1. Coefficient of friction decreases from 0.8 to 0.4, when the wear test was performed in between the martensite finish and austenite finish temperature. The austenite NiTi alloy represents better wear resistance as compared to martensitic NiTi alloy.

Yan and Liu (2015) worked on austenitic NiTi alloy to investigate the wear rate using ball-on-disc. After the calculation of coefficient of friction and surface wear, the deformation mechanism has been evaluated. Two modes of wear behavior have been observed for austenitic NiTi alloy. In the first mode the temperature of alloy lies in between the austenitic finish and martensitic start temperature. Wear is significant due to the presence of interplay of contact stress, shape recovery and temperature. If the temperature is increased beyond the martensitic start temperature, then the NiTi alloy lost its super-elasticity and shape recovery.

Huang et al. (2003) performed the Ni ion release test of NiTi alloy orthodontic wire in the atmosphere of artificial saliva. Atomic adsorption spectrophotometer is utilized for the study of Ni and Ti release. Orthodontic wire has been placed in artificial saliva at 37°C (pH value = 2.5 to 6.25) for 1-28days. If the solution pH ≥ 3.75, then no Ti ion release has been found. The main reason is the formation of TiO_2 layer on the NiTi wire.

Shabalovskaya et al. (2009) studied the effect to oxide on the Ni ion release. The thickest surface oxide layer thickness found to be equal to 720nm, which prevent the leaching of Ni ion.

2.7 RESEARCH GAPS

The literature review has revealed a number of gaps in NiTi alloys processing and characterization. Few of them are described below

There are some challenges involved in powder metallurgy process. First, effect of compaction pressure, sintering temperature and sintering time on strength and other responses can be considered by researchers. Second, influence of different binders may be another task for investigation. Researchers used different types of binders for the attachment of powder particles. An attempt can be made to study the influence of percentage composition of binders on the porosity. Third, some study can be carried on particle-shape, particle-size and inter-connection between different particles.

Some critical points come into picture during the review of production methods for NiTi. The production method has a significant influence on mechanical and biocompatible behaviour of NiTi. A little change in the composition significantly alters the response behaviour of NiTi. Although influence of ternary elements in NiTi has been studied by many researchers, still some research gap is pending in development of new NiTi alloys, that should be economical to produce and highly acceptable for different applications.

The major problem associated with porous NiTi alloy is its high sensitivity towards crack propagation. Although porous structure highly favours the tissue ingrowth and reduces the probability of implant loosening but large size pores act as stress risers and results into decrease in strength at repeated loading. Hence, development of porous NiTi alloy with controlled pore size and interconnectivity is quite challenging task. Some more methods should be investigated over above mentioned methods to produce structures with good capillary action.

The effect of different additives like Nb, Hf, Pd, Zr, Pt, Mn, Co, Cr, Fe and V on NiTi has been presented for transformation temperature and shape recovery. But still there is lack of database for the researchers to understand the complete characteristics of ternary alloy over a large variation of additives. The behavior of additional additives in porous structures is still missing.

CHAPTER 3
EXPERIMENTATIONS

3.1 PREPARATION OF WORK SAMPLES

Experiments are performed using powder metallurgy process. Cylindrical and rectangular samples are prepared for NiTi alloy.

3.1.1 Work Material

The work material selected in the study is NiTi alloy which is an equi-atomic alloy of nickel and titanium. Because of its good wear resistance, shape-memory effect, super-elasticity and high hardness, it can be used in applications of space and aero-space, medical, civil structure, micro-electromechanical systems etc. The effect of additives can alter its properties. For the present study, the copper (purity > 99.9%) is added into different proportion to study its effect on the characteristics of NiTi alloys. Figure 3.1 shows the different specimens after sintering. The mechanical and physical properties of NiTi material are given in Table 3.1. The chemical composition of Ni and Ti powders as envisaged from Spectro test is given in Table 3.2.

Table 3.1: Mechanical and Physical Properties of NiTi alloys

Properties	**Ni-Ti**
Recovered Elongation	8%
Bio-compatibility	Excellent
Elastic modulus (GPa)	48 (Approx.)
Density (g/cm^3)	6.45
Magnetic	No
Ultimate tensile Strength	1240 MPa (Approx.)
Coefficient of Thermal Expansion	Martensite – 6.6×10^{-6} ($cm/cm/^oC$) Austenite – 11.0×10^{-6} ($cm/cm/^oC$)
Resistivity	80-100 ($\mu\Omega$ cm)

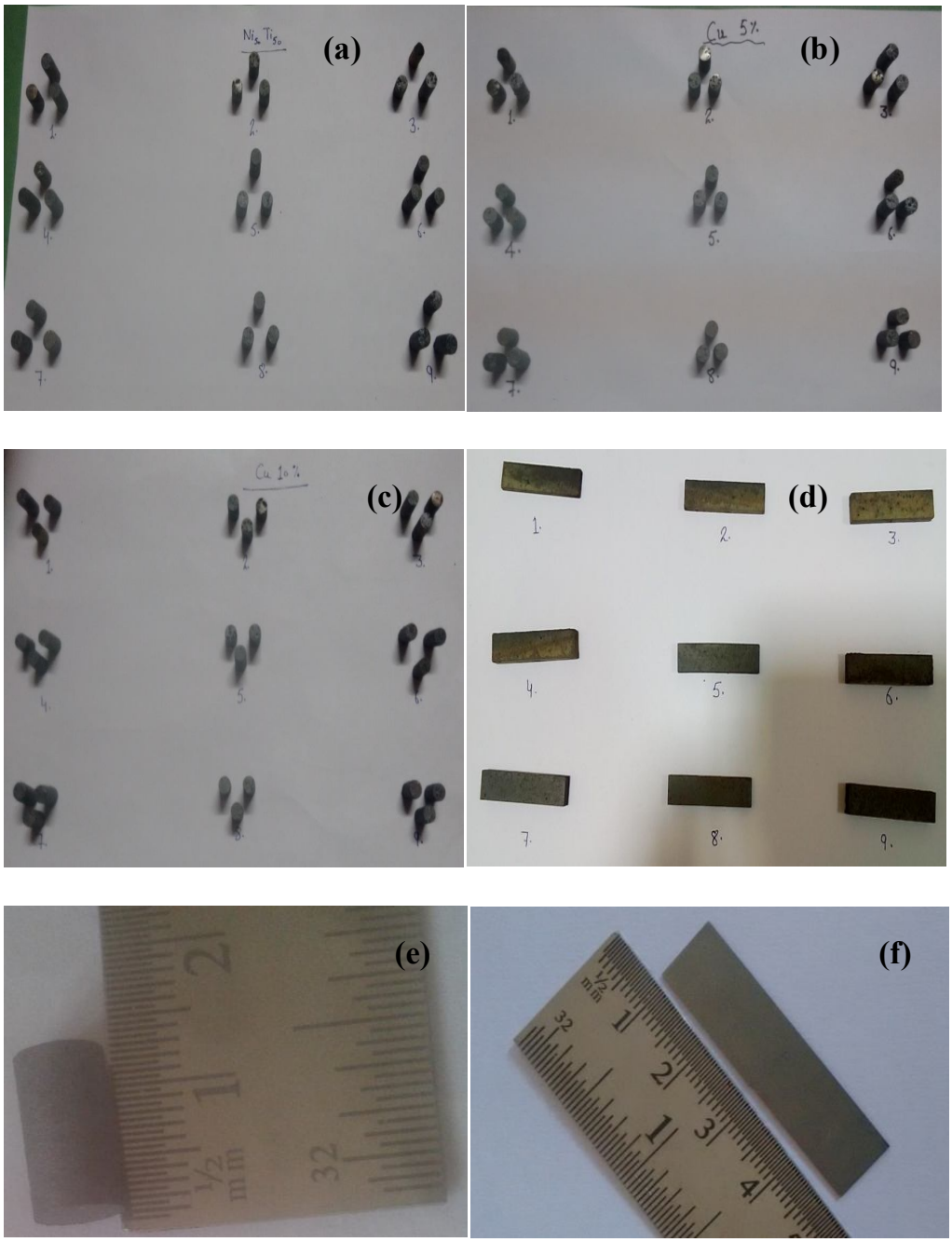

Figure 3.1: Specimens after compaction and Sintering

3.1.2 Rotary Ball Mill for Blending

High-energy ball mill (Rotary) was used for the mechanical alloying (300 R.P.M.) of elemental powders as shown in Figure 3.2. Steatite ceramic balls (25 no. of 15mm diameter each) were used for mechanical alloying. Steatite is a silicate based ceramic and contains zirconium oxide to increase the mechanical stability. A ball to powder

ratio (BPR) 10:1 was maintained during the milling of elemental powder. This is a mandatory step for the homogeneous mixing of elemental powders. The process flow diagram of homogeneous mixing is shown in Figure 3.2. Initially elemental powders were selected for the homogeneous mixing. A proper weight of powders was measured by precise weighing balance. In the second step these are placed into the rotary ball mill for proper mixing using steatite ceramic ball. Here ceramic balls were selected instead of steel ball considering its wear characteristics.

Table 3.2: Chemical Composition of Titanium and Nickel Powder

Sr. No.	**Titanium Powder**		**Nickel Powder**	
Sr. No.	**Element**	**% Composition**	**Element**	**% Composition**
1	Ni	0.086	Fe	0.031
2	Fe	0.930	Cr	0.024
3	V	0.341	Co	0.090
4	Mo	0.050	Ni	99.84
5	Ti	98.590		

As steel ball disintegrates, Fe particles mix in the powder, which may change the characteristics of SMA. After 8-10 hrs mixing the homogeneous mixture can be used for powder compaction.

3.1.3 Powder Compaction Press

The experiments were carried out on a Powder compaction press (Kimaya Engineers, Mumbai) installed at PEC University of Technology, Chandigarh, India. The Powder compaction press (Figure 3.3) has the following specifications:

Working Area

Over all Dimension	:	300 mm× 270mm ×425mm
Overall Weight	:	50 Kg
Max Permissible Pressure	:	15kN
Max Permissible Ram Stroke	:	15mm

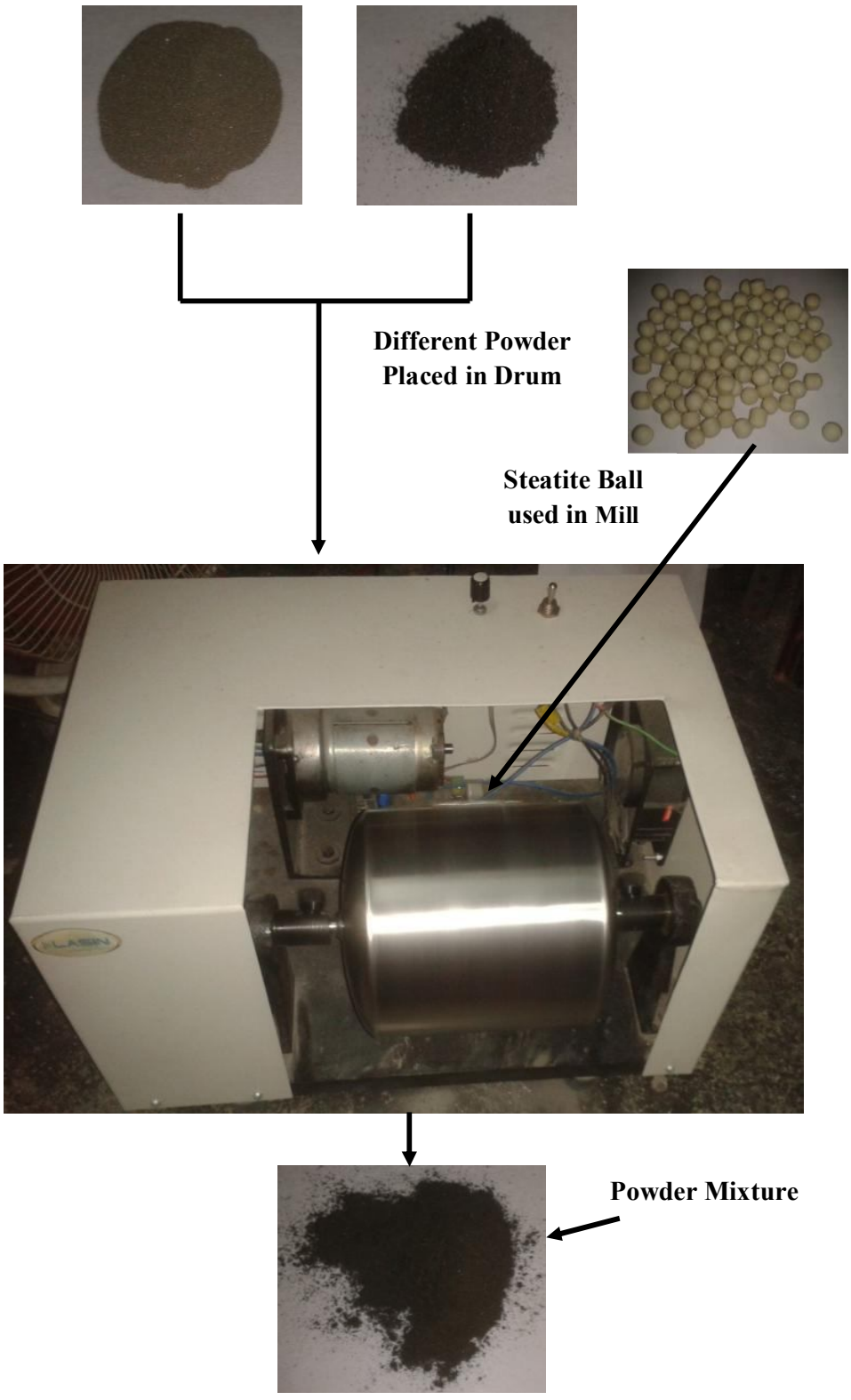

Figure 3.2 Process of Homogeneous Mixing

Max Pressure Holding Time	:	10 min at any one time
Maximum permissible Temperature	:	Room Temperature
Hydraulic Oil Capacity	:	400 ml.
Grade of Hydraulic Oil	:	Acantis HM-68 of ELF Lubricants
Maximum size of Die	:	Maximum out diameter 80mm or 50mm
Square		
		Maximum Height 90mm

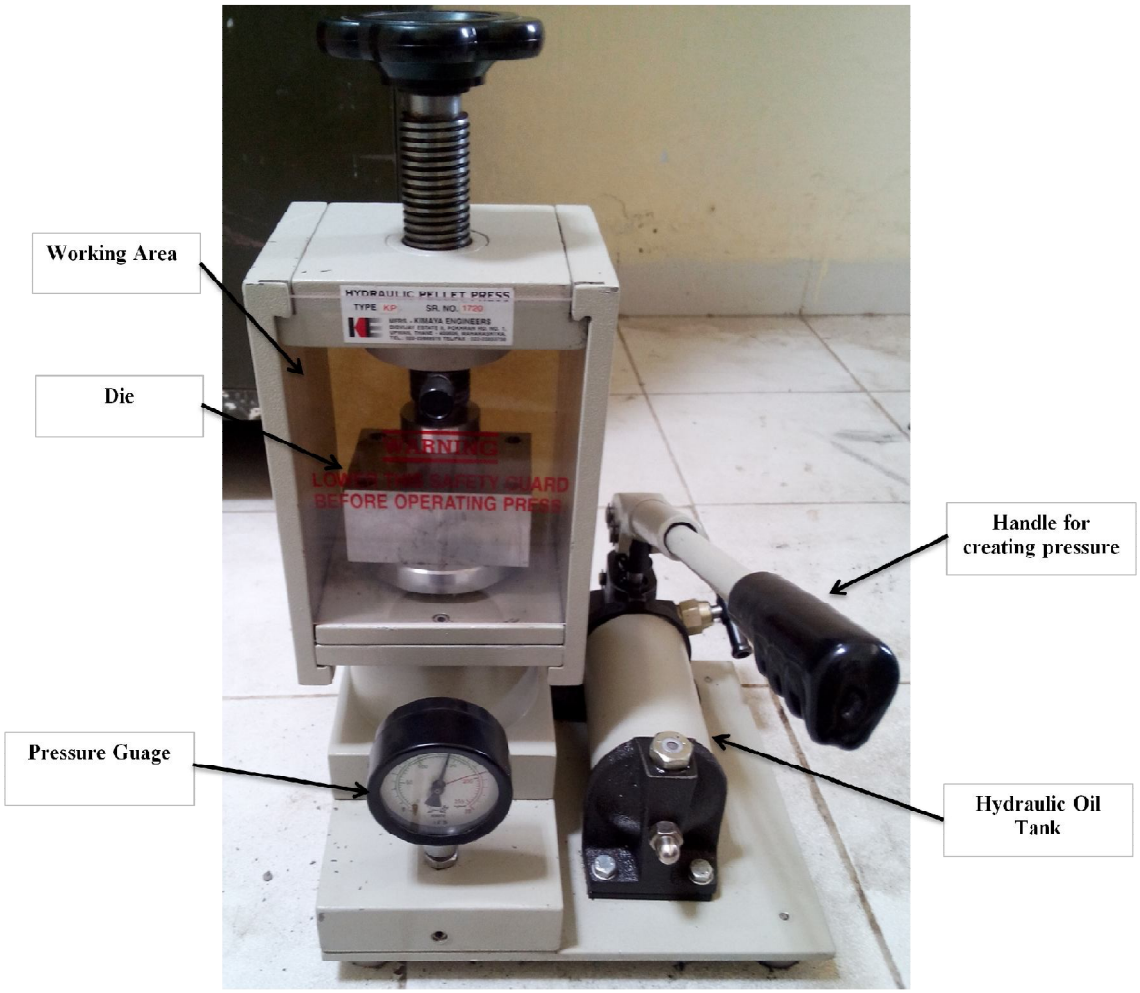

Figure 3.3 Powder Compaction Press

3.1.4 Furnace with Argon Gas Arrangement for Sintering

After the compaction, the green compact comes out from the die. It is then sintered for the diffusion and other atomic transport mechanism of powder particles. Sintering temperature is the ~60-70% melting temperature of material. Argon

atmosphere is mandatory to avoid the green compact from oxidation. So, to keep in mind these requirements the Ar cylinder is attached to the furnace (Figure 3.4) for the elimination of oxidation. A highly pure Ar (Purity > 99.999%) gas is used during sintering. The gauge fitting is used to regulate the pressure of Ar gas.

Figure 3.4: Furnace with Inert gas Arrangement

3.2 MEASUREMENT OF OUTPUT PARAMETERS

3.2.1 Strength and Young's Modulus

Solid cylindrical specimens were fabricated by powders of length 12 mm and diameter 6mm (using ASTM-E9-09; L/D= 2). Strength and young's modulus of specimen were measured using universal testing machine at a constant rate of 0.05mm/min and room temperature. Strength and Young's modulus are measured in 'MPa' and 'GPa' respectively.

Figure 3.5: Wear Test Rig (TR-20, Ducom, Bangalore)

Figure 3.6: Part A of Wear Test Rig

3.2.2 Wear Characteristics

Wear test was performed on friction and wear monitor **(Figure 3.5 and 3.6)** (TR-20, Ducom, Bangalore) at different temperatures from 37°C to 250°C. Normally EN 32 (HRC 65) was used for experimentations, but due to the nickel and titanium composition tungsten carbide disk (HRC 83) was used during this research work. The fixed parameters of wear test rig were sliding velocity (1.6m/s) and sliding distance (3000m) while load varied from 10N to 40N.

The test specimen and disc were cleaned ultrasonically with acetone to remove any dust particle or impurity from the surface. The test rig gives value of wear in µm (i.e. height of sample diminished) by linear variable displacement transducer and this value further converted into wear rate using equation 3.1 as:

$$Wear\ rate\ (mm^3/m) = \frac{height\ change\ of\ pin(mm) \times pin\ area\ (mm^2)}{Sliding\ Distance\ (m)} \qquad (3.1)$$

3.2.3 Micro-Hardness

Micro-hardness was calculated by Mitutoyo (Japan) make micro-hardness tester as shown in Figure 3.7 at 100kgf with 10s dwell time. Five different readings were taken on a sample and average of them is used in this research work.

Figure 3.7: Micro-hardness Tester

3.2.3 Corrosion Resistance

Corrosion resistance of fabricated material was checked using potentiostat (Metrohm Autolab, the Netherlands make). The electrolyte used for the research work is artificial Saliva (Wet Mouth- ICPA Health Product Make). The composition of artificial saliva consists of NaCl (400 mg/l), KCl (400 mg/l), $CaCl_2.2H_2O$ (795mg/l), NaH_2PO_4. H_2O (690 mg/l), KSCN (300 mg/l),Na_2S. $9H_2O$ (5mg/l),urea (1000 mg/l). In order to simulate the conditions of the human body, the artificial Saliva was maintained at a temperature of 37 ± 1˚C and at pH of 7.4. The $1cm^2$ area of sample

was exposed to the electrolyte. After 3 hours of immersion in artificial saliva, potentio-dynamic polarization curves were obtained at a scan rate of 0.001 Vs^{-1} from -0.1 V vs. versus the open-circuit potential (OCP) to the breakdown of passive region. The corrosion current densities and corrosion potentials of various specimens were determined from these curves by Tafel extrapolation methods. The mean value and standard deviation of the results were also calculated. The linear Tafel segments to the anodic and cathodic curves (-0.1 to + 0.1 V versus corrosion potential) were extrapolated to corrosion potential to obtain the corrosion current densities. The slope gives the Tafel slopes (b_a and b_c) and the intercept corresponds to corrosion current density i_{corr}. The i_{corr} (A/cm^2) was calculated using the Stern-Geary equation (**Stern, and Geary, 1957**);

$$i_{corr} = \frac{b_a . b_c}{2.3(R_P)(b_a + b_c)} \qquad \textbf{(3.2)}$$

Corrosion rate (*C.R*) in mm/year was calculated by using following relationship **(Spinks et al., 2002)** equation 3.3;

$$C.R = 3.268\times10^{3}\ \frac{i_{corr}}{\rho}\frac{MW}{z} \qquad \textbf{(3.3)}$$

Where *MW* is the molecular weight of the specimen (g/mole), ρ is density of the specimen (g/m3) and *z* is the number of electrons transferred in corrosion reactions.

3.2.4 Porosity

Porosity can easily be measured by weighing method, in which the weight of specimen is measured. Equation 3.4 is used

$$\mathrm{P} = 1 - \frac{d}{d_a} \qquad (\mathbf{3.4})$$

where d = mass of sample/ volume of sample

d_a - density of the alloy ($6.45 g/cm^2$)

With this method even the closed porosity will be taken into account.

3.2.5 Strain Recovery

Stress-Strain curve measures the stain recovery. Initially the material was loaded for 5% strain value and after that unloaded. It is measured that materials exhibit a closed loop or not. A closed loop represents a good stain recovery. It can be checked as from Figure 3.8.

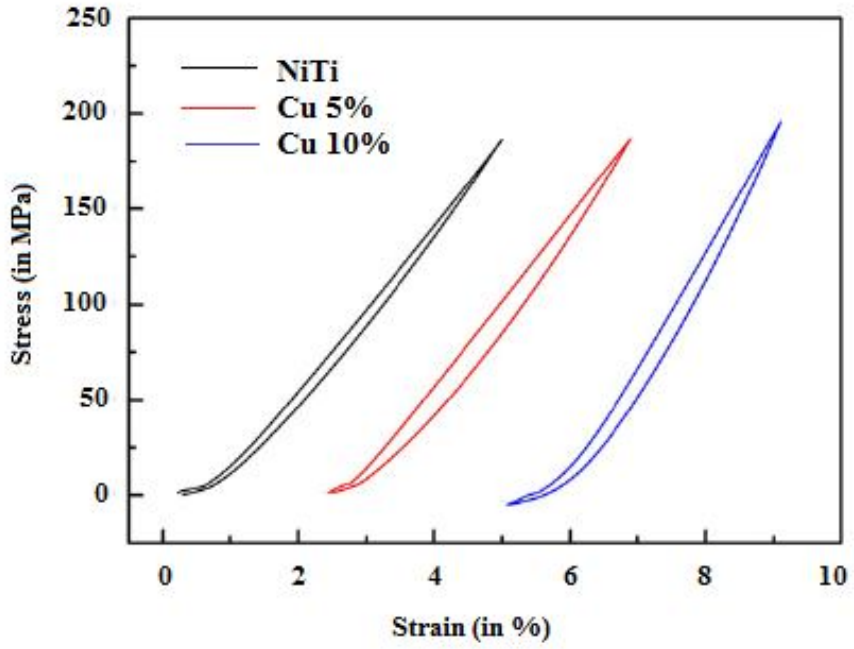

Figure 3.8: Strain recovery Measurement

3.2.6 Bio-compatibility

First of all samples were sterilized by conventional steam sterilization at 134°C for 30min. The *in- vitro* cytotoxicity test was performed by indirect Agar Diffusion method on strips (3mm x 4mm x 1mm) of $Ni_{50-x}Ti_{50}Cu_x$ (x=0, 5 and10) (as per ISO 10993-5) after 24 hours of contact. Modified Eagle Medium (MEM), supplemented with Foetal Bovine Serum as the culture medium and L929 mouse fibroblast cells were used. Test samples, positive controls (stabilized PVC Disc) and negative controls (High Density Poly Ethylene (USP)) in triplicate were placed on 1.5% agar overlayed on subconfluent monolayer of L-929 mouse fibroblasts.

Table 3.3: Cyto-toxicity Reactivity Grades

Grade	Reactivity	Description of Reactivity Zone
0	None	None detectable zone around or under specimen
1	Slight	Some malformed or degenerated cell under specimen
2	Mild	Zone limited to area under specimen
3	Moderate	Zone extending specimen size up to 0.33cm
4	Severe	Zone extending farther than 0.33 cm beyond specimen

Cells were incubated with test samples at 37 ± 1°C for 24 to 26 hours. The cultured cells were incubated with neutral red solution (50 mg% in saline). Microscopic examination of cytotoxicity was done to study the cellular response around and under the samples. The cytotoxicity reactivity are graded as 0, 1, 2, 3 and 4 on the basis of zone of analysis around and under the sample, general morphology and vacuolization as given above.

3.3 EXPERIMENTATION

The experimental procedure is as follows:

- Initially different powders were taken and weigh precisely.
- Homogeneous mixture of different powders was prepared by rotary ball mill.
- Experiments were performed on Kimaya Engineers make powder compaction press to make green compact (die is selected according to specimen required).
- Sintering was done in the presence of Argon gas environment to prevent oxidation of green compacts.
- After the fabrication of specimen the required testing is to be performed like strength, modulus of elasticity, corrosion behaviour etc.

3.4 PROCESS PARAMETERS

There are a number of process parameters affecting the nature of green compact and work-specimen. The different process parameters involved in powder metallurgy process can be:

3.4.1 Compaction Pressure

The compaction pressure is the pressure by which powder can be compacted in a die. The compaction press shows the load in 'kN' ranging from 1-20. There are two regions 1kN to 15kN falls in green region i.e. 'safe' region and from 15kN-20kN is red region means 'not-safe'. Any load from 1-15 can be applied considering the safe limit of die. Here in the present research work load varied only in safe region. Also to convert the compaction load into compaction pressure equation 3.5 is used as:

$$Compaction\ Pressure = \frac{Compaction\ Load}{Cross-sectional\ Area} \quad (3.5)$$

3.4.2 Blending/Mixing Time

Blending time or mixing time is the time for which powders can be mixed either with the use of rotary ball mill or manually, so that all the powder can be mixed homogeneously. In the present research work, powders were mixed from 4 hrs to 60 hrs and it is observed that 10 hrs of mixing is sufficient to make green compact.

3.4.3 Compaction Time

The homogeneous mixture is filled in die and finally die is placed in compaction press. Then the total time in which die remains in compressed condition with the help of powder compaction press is termed as compaction time. The maximum permissible compaction time is depends upon die and compaction press. Here in present research work, compaction press is designed for maximum 10min compaction time. If compaction time is more, then more time the powder particles will get to make bonds with each other.

3.4.4 Sintering Temperature

Normally sintering is to be carried at ~60-70% of melting temperature of alloys. Mostly researchers had worked on different temperatures ranging from 850°C to 1050°C **(Xu et al., 2014)**. So in the present work an attempt has been made to observe the effect of sintering temperature on fabricated material. Here sintering temperature varies from 950°C to 1150°C to investigate the effect of sintering temperature on the characteristics of NiTi alloys. The muffle furnace used in present work is shown in Figure 3.9.

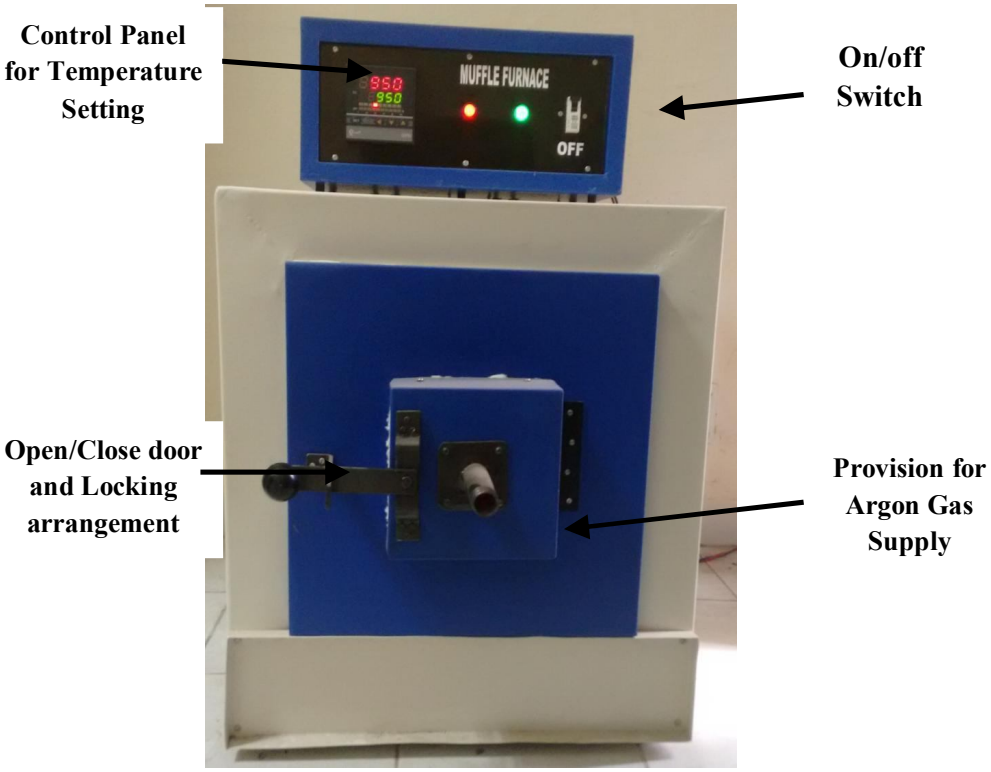

Figure 3.9: Muffle Furnace used for sintering

3.4.5 Sintering Time

It may be defined as the time for which green compact placed in furnace. The heat will reach upto the core of the specimen by passage of time. Sometimes if holding time is less, then the particle in the middle of specimen remains un-sintered. Also with the increase of sintering time the diffusion of particles and transport mechanism takes place uniformly, which results a higher strength. The effect of sintering temperature on the characteristics of NiTi alloy is measured in the present research work.

3.4.6 Concentration of alloying elements

The characteristics of the specimens depend upon its composition. NiTi alloys are very sensitive to composition; even a small change in the composition can vary its characteristics. Some additive can also be added to improve its strength, transformation temperature, porosity etc. In the present research work copper is mixed with Ni and Ti powders in 5% and 10% particles by weight percentage.

3.4.7 Temperature during Wear test

At different temperature conditions material shows different wear characteristics. In friction and wear monitor, a heater is equipped to change the temperature from room temperature to 400°C. In present work minimum temperature selected is 37°C to consider human body condition. After that wear test was performed from 50°C to 250°C. The selected levels for wear test are 37°C, 50°C, 100°C, 150°C, 200°C and 250°C. These wear tests were performed only on two specimens, one gives lower Young's modulus and another one is highest Young's modulus. Temperature indicator in friction and wear monitor is shown in Figure 3.10.

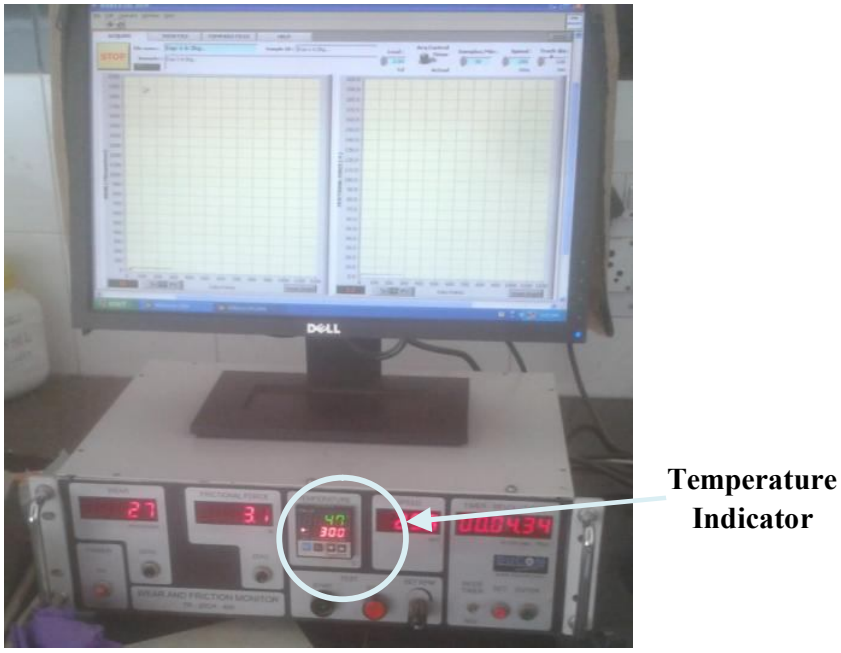

Figure 3.10: Temperature indicator in Friction and Wear Monitor

3.4.8 Load at wear test

Load during the wear test can vary from 0 kg to 6kg i.e. 0N to 60N (as per friction and wear monitor TR 20CH-400, DUCOM). In present work, load varies from 10N to 40N with minimum change of 10N in load. Larger load increases the wear rate due to increase of coefficient of friction between the pin and disk.

CHAPTER 4

EXPERIMENTAL DESIGN METHODOLOGY

4.1 INTRODUCTION

A scientific approach to plan the experiments is a necessity for efficient conduct of experiments. The process of planning the experiments is carried out by the statistical design of experiments, so that appropriate data will be collected and analyzed by statistical methods resulting in valid and objective conclusions. The statistical methodology is the only objective approach to analyze the problem that involves data that are subjected to experimental error. Thus, there are two aspects of an experimental problem: the design of the experiments and the statistical analysis of the data. These two points are closely related since the method of analysis depends directly on the design of experiments employed. The advantages of design of experiments are as follows:

- Numbers of trials is significantly reduced in comparison to full factorial experiments.
- Important decision variables which control and improve the performance of the product or the process can be identified.
- Optimal setting of the parameters can be found out.
- Qualitative as well as quantitative estimation of parameters can be made.
- Experimental error can be determined.
- Inference regarding the effect of parameters on the characteristics of the process can be made.

In the present work, the Taguchi's method has been used to plan the experiments and subsequent analysis of the data collected.

4.2 TAGUCHI EXPERIMENTAL DESIGN AND ANALYSIS

4.2.1 Taguchi's Philosophy

Taguchi's comprehensive system of quality engineering is one of the greatest engineering achievements of the 20th century. His methods focus on the effective application of engineering strategies rather than advanced statistical techniques. It includes both upstream and shop-floor quality engineering. Upstream methods efficiently

use small-scale experiments to reduce variability and remain cost-effective. Shop-floor techniques provide cost-based, real time methods for monitoring and maintaining quality in production. The farther upstream a quality method is applied, the greater leverage it produces on the improvement, and the more it reduces the cost and time. Taguchi's philosophy is founded on the following three very simple and fundamental concepts **(Ross, 1988; Roy, 1990):**

- Quality should be designed into the product and not inspected into it.
- Quality is best achieved by minimizing the deviations from the target. The product or process should be so designed that it is immune to uncontrollable environmental variables.
- The cost of quality should be measured as a function of deviation from the standard and the losses should be measured system-wide.

Taguchi proposes an "off-line" strategy for quality improvement as an alternative to an attempt to inspect quality into a product on the production line. He observes that poor quality cannot be improved by the process of inspection, screening and salvaging. No amount of inspection can put quality back into the product. Taguchi recommends a three-stage process for improving quality through offline quality control: system design, parameter design and tolerance design **(Ross, 1988, Roy, 1990)**. In the present work, Taguchi's parameter design approach is used to study the effect of process parameters on the various responses of the WEDM process.

4.2.2 Experimental Design Strategy

The array forces all experimenters to design almost identical experiments **(Roy, 1990).**

In the Taguchi method the results of the experiments are analyzed to achieve one or more of the following objectives **(Ross, 1988):**

- To establish the best or the optimum condition for a product or process
- To estimate the contribution of individual parameters and interactions
- To estimate the response under the optimum condition

The optimum condition is identified by studying the main effects of each of the parameters. The main effects indicate the general trends of influence of each parameter. The knowledge of contribution of individual parameters is a key in deciding the nature of control to be established on a production process. The analysis of variance (ANOVA) is the statistical treatment most commonly applied to the results of the experiments in determining the percent contribution of each parameter against a stated level of confidence. Study of ANOVA table for a given analysis helps to determine which of the parameters need control **(Ross, 1988).**

Taguchi suggests **(Roy, 1990)** two different routes to carry out the complete analysis. First, the standard approach, where the results of a single run or the average of repetitive runs are processed through main effects and ANOVA analysis (Raw data analysis). The second approach which Taguchi strongly recommends for multiple runs is to use signal- to- noise ratio (S/N) for the same steps in the analysis. The S/N ratio is a concurrent quality metric linked to the loss function **(Barker, 1990).** By maximizing the S/N ratio, the loss associated can be minimized. The S/N ratio determines the most robust set of operating conditions from variation within the results. The S/N ratio is treated as a response of the experiment. Taguchi recommends **(Ross, 1988)** the use of outer OA to force the noise variation into the experiment i.e. the noise is intentionally introduced into experiment. However, processes are often subject to many noise factors that in combination strongly influence the variation of the response. For extremely 'noisy' systems, it is not generally necessary to identify specific noise factors and to deliberately control them during experimentation. It is sufficient to generate repetitions at each experimental condition of the controllable parameters and analyze them using an appropriate S/N ratio **(Byrne and Taguchi, 1987).**

In the present investigation, the raw data analysis and S/N data analysis have been performed. The effects of the selected WEDM process parameters on the selected quality characteristics have been investigated through the plots of the main effects based on raw data. The optimum condition for each of the quality characteristics has been established through S/N data analysis aided by the raw data analysis. No outer array has been used and instead, experiments have been repeated three times at each experimental condition.

4.2.3 Loss Function

The heart of Taguchi method is the definition of the term 'quality' as the characteristic that avoids loss to the society from the time the product is shipped **(Barker, 1986).** Loss is measured in terms of monetary units and is related to quantifiable product characteristic.

Taguchi defines quality loss via his 'loss function'. He unites the financial loss with the functional specification through a quadratic relationship that comes from a Taylor series expansion. The quadratic function takes the form of a parabola. Taguchi defines the loss function as a quantity proportional to the deviation from the nominal quality characteristic **(Roy, 1990).** He found the following quadratic form to be a useful workable function (Roy, 1990):

$$L(y) = k\,(y-m)^2 \qquad (4.1)$$

Where,

L = Loss in monetary units

m = value at which the characteristic should be set

y = actual value of the characteristic

k = constant depending on the magnitude of the characteristic and the monetary unit involved

The loss function represented in Eq. 4.1 is graphically shown in Figure 4.1a. The characteristics of the loss function are **(Roy, 1990):**

- The farther the product's characteristic varies from the target value, the greater is the loss. The loss must be zero when the quality characteristic of a product meets its target value.
- The loss is a continuous function and not a sudden step as in the case of traditional (goal post) approach (Figure 4.1b). This consequence of the continuous loss function illustrates the point that merely producing a product within the specification limits does not necessarily mean that product is of good quality.

Average loss-function for product population

In a mass production process, the average loss per unit is expressed as **(Roy 1990):**

$$L(y)=\frac{1}{n}\left\{k\left(y_1-m\right)^2+k\left(y_2-m\right)^2+...+k\left(y_n-m\right)^2\right\} \quad (4.2)$$

Where,

y_1, $y_{2...}y_n$ = Actual value of the characteristic for unit 1, 2,…n respectively

n = Number of units in a given sample

k = Constant depending on the magnitude of the characteristic and the monetary unit involved

m = Target value at which the characteristic should be set

The Eq. 4.2 can be simplified as:

$$L(y)=k\left(MSD_{NB}\right) \quad (4.3)$$

Where,

MSD_{NB} = Mean squared deviation or the average of squares of all deviations from the target or nominal value

NB = "Nominal is Best"

Other loss functions

The loss-function can also be applied to product characteristics other than the situation where the nominal value is the best value (m).

The loss-function for a 'smaller is better' type of product characteristic (LB) is shown in Figure 4.2a. The loss function is identical to the 'nominal-is-best' type of situation when m=0, which is the best value for 'smaller is better' characteristic (no negative value). The loss function for a 'larger-is-better' type of product characteristic (HB) is also shown in Figure 4.2b, where also m=0.

4.2.4 Signal to Noise Ratio

The loss-function discussed above is an effective figure of merit for making engineering design decisions. However, to establish an appropriate loss-function with its

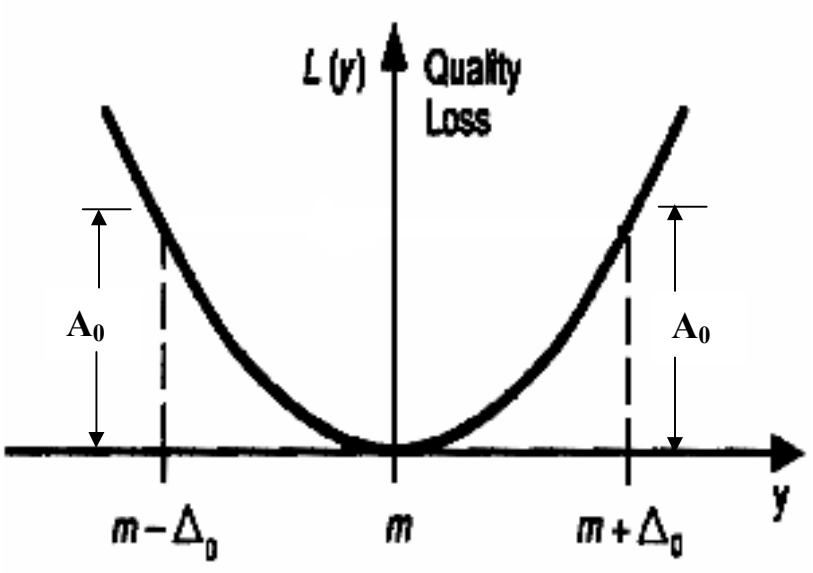

(a) Taguchi Loss Function

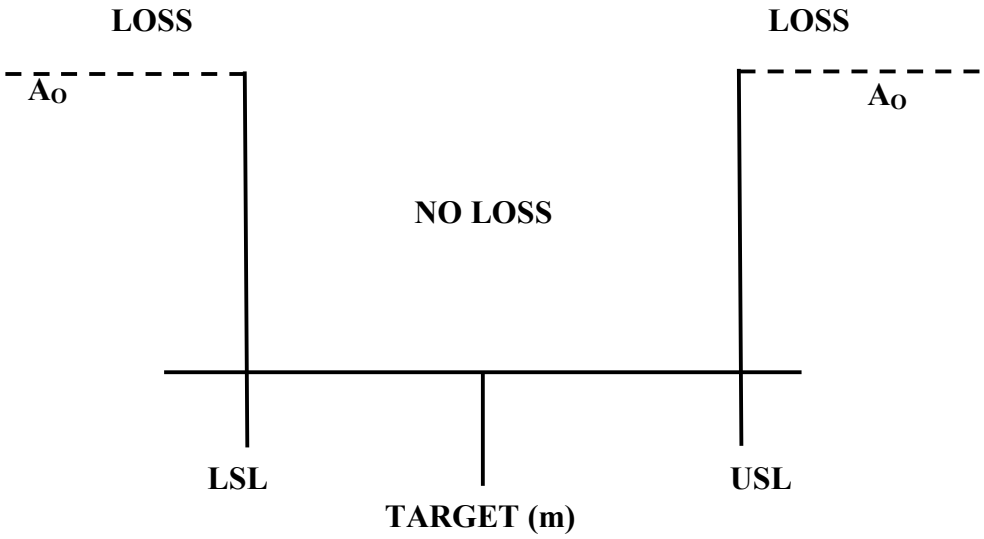

(b) Traditional (Goal-Post) Approach

Figure 4.1(a, b): The Taguchi Loss-Function and The Traditional Approach (Ross, 1988)

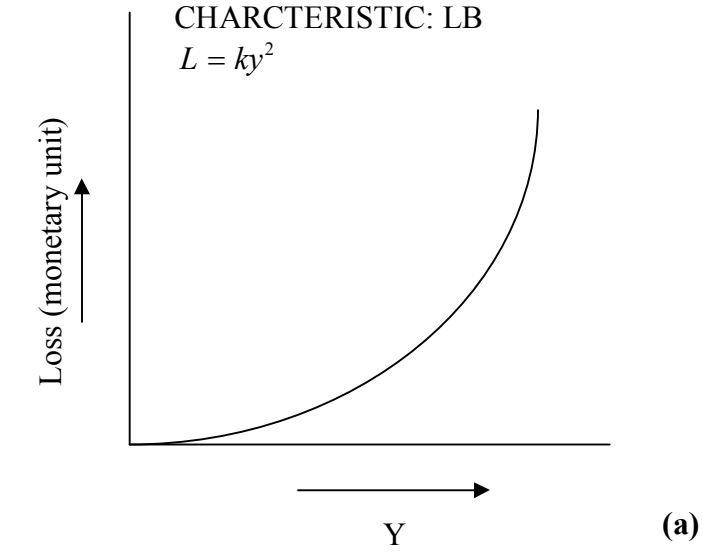

(a)

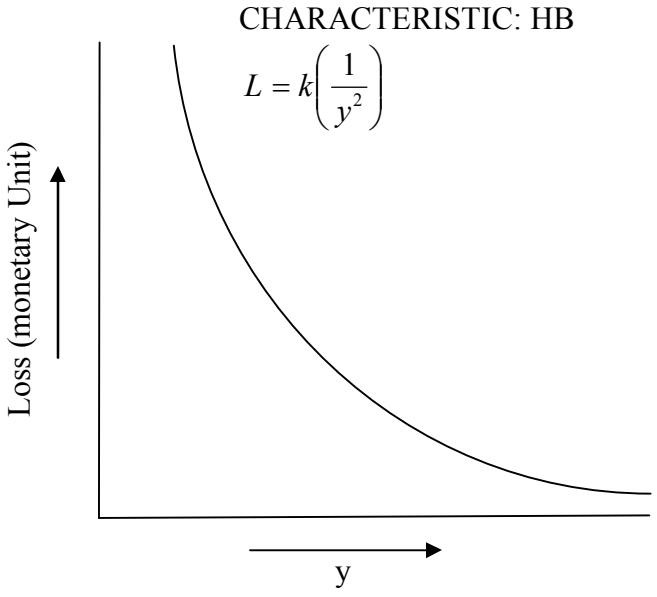

(b)

Figure 4.2(a, b): The Taguchi Loss-Function for LB and HB Characteristics (Barker, 1990)

k value to use as a figure of merit is not always cost-effective and easy. Recognizing the dilemma, Taguchi created a transform function for the loss-function which is named as signal -to-noise (S/N) ratio **(Barker, 1990).**

The S/N ratio is a concurrent statistic which is able to look at two characteristics of a distribution and roll them into a single number or figure of merit. The S/N ratio combines both the parameters (the mean level of the quality characteristic and variance around this mean) into a single metric **(Barker, 1990).**

A high value of S/N implies that signal is much higher than the random effects of noise factors. Process operation consistent with highest S/N always yields optimum quality with minimum variation **(Barker, 1990).**

The S/N ratio consolidates several repetitions (at least two data points are required) into one value. The equations for calculating S/N ratios for 'smaller is better' (LB), 'larger is better' (HB) and 'nominal is best' (NB) types of characteristics are as follows **(Ross, 1988):**

1. Larger the Better:

$$\left(S/N\right)_{HB} = -10 \log\left(MSD_{HB}\right) \tag{4.4}$$

Where,

$$MSD_{HB} = \frac{1}{R}\sum_{j=1}^{R}(1/y_j^2)$$

2. Smaller the Better:

$$\left(S/N\right)_{LB} = -10 \log\left(MSD_{LB}\right) \tag{4.5}$$

Where,

$$MSD_{LB} = \frac{1}{R}\sum_{j=1}^{R}(y_j^2)$$

3. Nominal the Best

$$\left(S/N\right)_{NB} = -10 \log\left(MSD_{NB}\right) \tag{4.6}$$

Where,

$$MSD_{NB} = \frac{1}{R}\sum_{j=1}^{R}(y_j - y_o)^2$$

R = Number of repetitions

The mean squared deviation (MSD) is a statistical quantity that reflects the deviation from the target value. The expressions for MSD are different for different quality characteristics. For the 'nominal is best' characteristic, the standard definition of MSD is used. For the other two characteristics the definition is slightly modified. For 'smaller is better', the unstated target value is zero. For 'larger is better', the inverse of each large value becomes a small value and again, the unstated target value is zero. Thus for all three expressions, the smallest magnitude of MSD is being sought.

4.2.5 Relation between S/N Ratio and Loss Function

Figure 4.2a shows a single sided quadratic loss function with minimum loss at the zero value of the desired characteristic. As the value of y increases, the loss grows. Since loss is to be minimized the target in this situation for y is zero.

The basic loss function (Eq. 4.1) is:

$L(y) = k\,(y-m)^2$

If $m = 0$

$L(y) = k\,(y^2)$

The loss may be generalized by using k=1 and the expected value of loss may be found by summing all the losses for a population and dividing by the number of samples R taken from this population. This in turn gives the following expression (Barker, 1990):

$$EL = \text{Expected loss} = (\Sigma y^2/R) \qquad (4.7)$$

The above expression is a figure of demerit. The negative of this demerit expression produces a positive quality function. This is the thought process that goes into the creation of S/N ratio from the basic quadratic loss function. Taguchi adds the final touch to this transformed loss-function by taking the log (base 10) of the negative expected loss and then he multiplies by 10 to put the metric into the decibel terminology **(Barker, 1990).**

4.2.6 Steps in Experimental Design and Analysis

The Taguchi experimental design and analysis flow diagram is shown in Figure 4.3. The important steps are discussed below.

Selection of orthogonal array (OA)

In selecting an appropriate OA, the pre-requisites are **(Ross, 1988; Roy, 1990):**

- Selection of process parameters and/or interactions to be evaluated
- Selection of number of levels for the selected parameters

The selection of parameters for investigation depends upon the product or process performance characteristics or responses of interest **(Ross, 1988).** Several methods are suggested by Taguchi for determining which parameters to include in an experiment. These are (Ross, 1988):

a) Brainstorming
b) Flow charting
c) Cause-Effect diagrams

The total Degrees of Freedom (DOF) of an experiment is a direct function of total number of trials. If the number of levels of a parameter increases, the DOF of the parameter also increases because the DOF of a parameter is the number of levels minus one. Thus, increasing the number of levels for a parameter increases the total degrees of freedom in the experiment which in turn increases the total number of trials. Thus, two levels for each parameter are recommended to minimize the size of the experiment **(Ross, 1988).** If curved or higher order polynomial relationship between the parameters under study and the response is expected, at least three levels for each parameter should be considered **(Barker, 1990).**

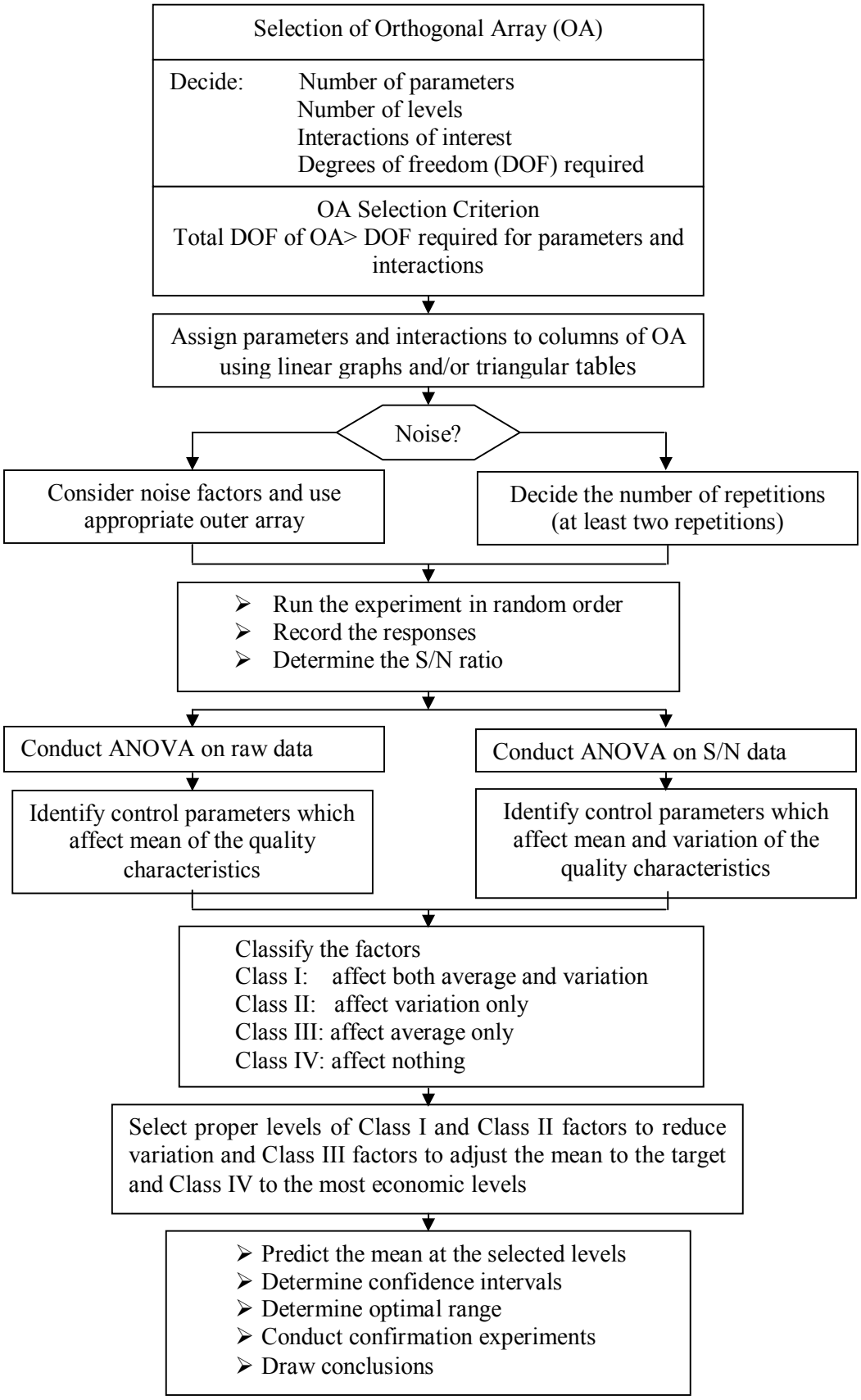

Figure 4.3: Taguchi Experimental Design and Analysis Flow Diagram

When a particular OA is selected for an experiment, the following inequality must be satisfied (Ross, 1988):

Total DOF of an OA ≥ Total DOF required for parameters and interactions (4.8)

Depending on the number of levels of the parameters and total DOF required for the experiment, a suitable OA is selected.

Assignment of parameters and interaction to the OA

The OAs have several columns available for assignment of parameters and some columns subsequently can estimate the effect of interactions of these parameters. Taguchi has provided two tools to aid in the assignment of parameters and interactions to arrays **(Ross, 1988; Roy, 1990):**

1. Linear graphs
2. Triangular tables

Each OA has a particular set of linear graphs and a triangular table associated with it. The linear graphs indicate various columns to which parameters may be assigned and the columns subsequently evaluate the interaction of these parameters. The triangular tables contain all the possible interactions between parameters (columns). Using the linear graphs and /or the triangular table of the selected OA, the parameters and interactions are assigned to the columns of the OA. The linear graph of L_{27} OA is given in Figure A.1 (Appendix A).

Selection of outer array

Taguchi separates factors into two main groups: controllable factors and uncontrollable factors (noise factors). Controllable factors are factors that can easily be controlled. Noise factors, on the other hand, are nuisance variables that are difficult, impossible, or expensive to control **(Byrne and Taguchi, 1987).** The noise factors are responsible for the performance variation of a process. Taguchi recommends the use of outer array for the noise factors and inner arrays for controllable factors. If an outer array is used, the noise variation is forced into the experiment. However, experiments against the trial conditions of the inner array (the OA used for the controllable factors) may be repeated and in this case the noise variation is unforced into the experiment **(Byrne and**

Taguchi, 1987). The outer array, if used, will have same assignment considerations. However, the outer array should not be as complex as the inner array because the outer array is noise only which is controlled only in the experiment **(Ross, 1988)**. An example of inner and outer array combination is shown in Table A.2 (Appendix A).

Experimentation and data collection

The experiment is performed against each of the trial conditions of the inner array. Each experiment at a trial condition is repeated simply (if outer array is not used), or according to the outer array (if used). Randomization should be done to reduce bias in the experiment.

The data (raw data) are recorded against each trial condition and S/N ratio of the repeated data points is calculated and recorded against each trial condition.

Data analysis

A number of methods have been suggested by Taguchi for analyzing the data: observation method, ranking method, column effect method, ANOVA, S/N ANOVA, plot of average response curves, interaction graphs etc. **(Ross, 1988).** However, in the present investigation the following methods have been used:

- Plot of average response curves
- ANOVA for raw data
- ANOVA for S/N data
- S/N response graphs
- Interaction graphs
- Residual graphs

The plot of average responses at each level of a parameter indicates the trend. It is a pictorial representation of the effect of parameter on the response. The change in the response characteristic with the change in levels of a parameter can easily be visualized from these curves. Typically, ANOVA for OAs are conducted in the same manner as the other structured experiments **(Ross, 1988).**

The S/N ratio is treated as a response of the experiment, which is a measure of the variation within a trial when noise factors are present. A standard ANOVA can be conducted on S/N ratio which will identify the significant parameters (mean and variation). Interaction graphs are used to select the best combination of interactive parameters **(Peace, 1993)**. Residual plots are used to check the accuracy.

Parameters design strategy

Parameter classification and selection of optimal levels

When the ANOVA on the raw data (identifying control parameters which affect average) and S/N data (identifying control parameters which affect variation) are completed, the control parameters may be put into four classes (Ross1988):

Class I : Parameters which affect both average and variation
(Significant in both i.e. raw data ANOVA and S/N ANOVA)

Class II : Parameters which affect variation only
(Significant in S/N ANOVA only)

Class III : Parameters which affect average only
(Significant in raw data ANOVA only)

Class IV : Parameters which affect nothing
(Not significant in both ANOVAs)

The parameters design strategy is to select the proper levels of class I and class II parameters to reduce variation and class III parameters to adjust the average to the target value. Class IV parameters may be set at the most economical levels since nothing is affected.

Prediction of the mean

After determination of the optimum condition, the mean of the response (μ) at the optimum condition is predicted. The mean is estimated only from the significant parameters. The ANOVA identifies the significant parameters. Suppose, parameters A and B are significant and A_2B_2 (second level of $A=A_2$, second level of $B=B_2$) is the

optimal treatment condition. Then, the mean at the optimal condition (optimal value of the response characteristic) is estimated as **(Ross, 1988):**

$$\mu = \overline{T} + \left(\overline{A}_2 - \overline{T}\right) + \left(\overline{B}_2 - \overline{T}\right)$$
$$= \overline{A}_2 + \overline{B}_2 - \overline{T}$$

Where

$\overline{T}$ = Overall mean of the response

$\overline{A}_2, \overline{B}_2$ = Average values of response at the second levels of parameters A and B respectively

Determination of confidence interval

The estimate of the mean (μ) is only a point estimate based on the average of results obtained from the experiment. Statistically this provides a 50% chance of the true average being greater than μ. It is therefore customary to represent the value of a statistical parameter as a range within which it is likely to fall, for a given level of confidence **(Ross, 1988).** This range is termed as the confidence interval (CI). In other words, the confidence interval envisages maximum and minimum values between which the true average should fall at some stated percentage of confidence **(Ross, 1988).**

The following two types of confidence interval are suggested by Taguchi for estimating mean of the optimal treatment condition **(Ross, 1988).**

1. Around the estimated average of a treatment condition predicted from the experiment, this type of confidence interval is designated as CI_{POP} (confidence interval for the population).
2. Around the estimated average of a treatment condition used in a confirmation experiment to verify predictions, this type of confidence interval is designated as CI_{CE} (confidence interval for a sample group).

CI_{POP} is for the entire population i.e., all parts ever made under the specified conditions, and CI_{CE} is for only a sample group made under the specified conditions. Because of the smaller size in confirmation experiments relative to entire population, CI_{CE} must slightly be wider. The expressions for computing the confidence intervals are given below **(Ross, 1988; Roy, 1990)**

$$CI_{POP} = \sqrt{\frac{F_\alpha(1, f_e) V_e}{n_{eff}}} \tag{4.9}$$

$$CI_{CE} = \sqrt{F_\alpha(1, f_e) V_e \left[\frac{1}{n_{eff}} + \frac{1}{R}\right]} \tag{4.10}$$

Where, $F_\alpha(1, f_e)$ = The F ratio at a confidence level of (1-α) against DOF 1, and error degree of freedom f_e.

$$n_{eff} = \frac{N}{1 + [\text{Total DOF associated in the estimate of the mean}]}$$

N = Total number of results

R = Sample size for confirmation experiment

In Eq. 4.10, as R approaches infinity, i.e., the entire population, the value 1/R approaches zero and $CI_{CE} = CI_{POP}$. As R approaches 1, the CI_{CE} becomes wider.

Confirmation experiment

The confirmation experiment is a final step in verifying the conclusions from the previous round of experimentation. The optimum conditions are set for the significant parameters (the insignificant parameters are set at economic levels) and a selected number of tests are run under specified conditions. The average of the confirmation experiment results is compared with the anticipated average based on the parameters and levels tested. The confirmation experiment is a crucial step and is highly recommended to verify the experimental conclusion **(Ross, 1988).**

CHAPTER – 5
METAL POWDER CHARACTERIZATION AND SELECTION OF PROCESS PARAMETERS

5.1 INTRODUCTION

The present chapter gives the details of powder preparation and investigation of the range of process parameters using one factor at a time approach (OFAT). The mechanism of powder mixing is also discussed in this section.

5.2 POWDER PREPARATION

Elemental powders were milled for different milling times (i.e. 4, 8, 30, 40, 50, and 60 h) and some powder was extracted for the scanning electron microscopy at every time interval. X-ray diffraction technique was used for the structural evaluation. In present research, Xpert Philips diffractometer was used for the structural evaluation after 4h and 60h respectively using Cu radiation (λ=0.15406 nm) at 40kV and 30mA. Jeol Make scanning electron microscopy (SEM) was used for the investigation of particle size and microstructure at 20kV. The surface integrity of steatite ceramic ball and hardened steel ball were also measured before and after experimentations by SEM. Powder and steatite balls sample were prepared by gold coating due to conductivity.

Initially both Ni and Ti had the different crystallite size, but with the increase milling time it becomes difficult to distinguish between Ni and Ti. Increase in milling results into the decrease in the crystallite size as in Figure 5.1. The probable reason for this is the collision in between the balls and vial. The powder in between the ball and vial deforms into smaller particles. Another reason for this reduction in crystallite size may be the increase in the chance of nucleation sites due to larger defect densities **(Suryanarayana, 2004)**. Structural instability and elastic energy utilized to enhance the free energy, which results the crystallite to amorphous transition and acts as another driving force for the reduction of crystallite size upto 31.03nm **(Sadrnezhaad et al.,**

2006). It is evident from Figure 5.1 that at large value of milling duration the crystallite size remains constant, this is due to the fact that a balance has been set between the rate of fracturing and the rate of cold welding of elemental powder particles.

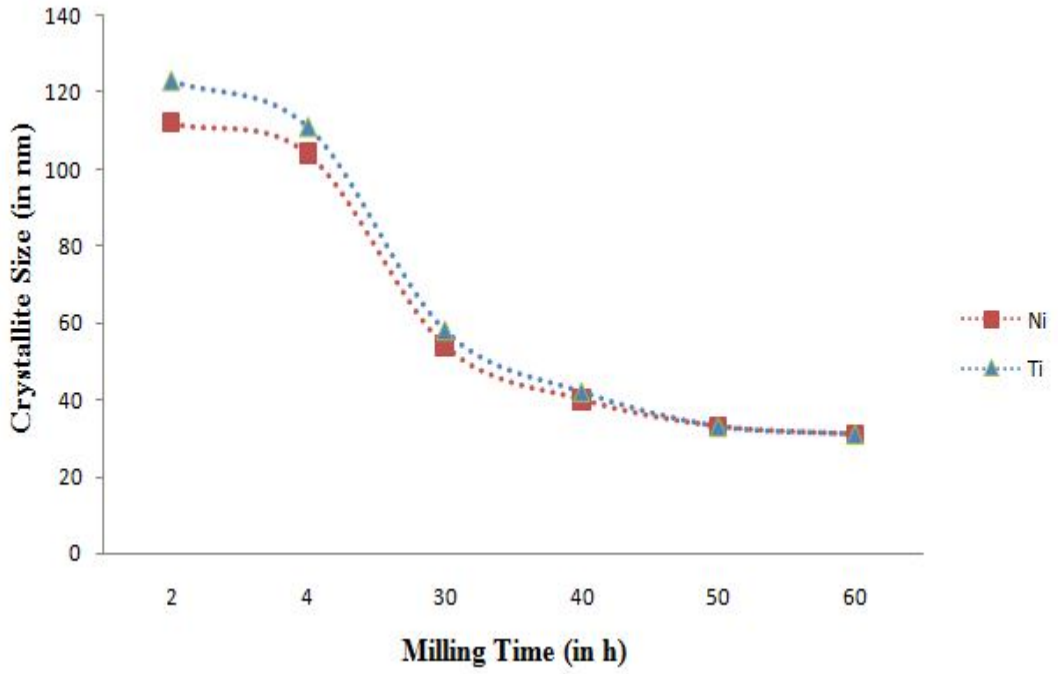

Figure 5.1: Variation of crystallite size after different milling time

5.2.1 SEM observation of Powder

Figure 5.2 (a) -5.2 (f) shows the morphology of alloyed powder sample at different milling times. In Figure 5.2 (a) the structure of elemental powder is found to be lamellar. This is due to the uninterrupted cold welding of ductile particle during high-energy ball mill operation. The space between these lamellae at this condition was found to be high, but with the increase in the duration of milling time (Figure 5.2 b – 5.2d) the laminated structure becomes sporadic with a decrement in the layer thickness.

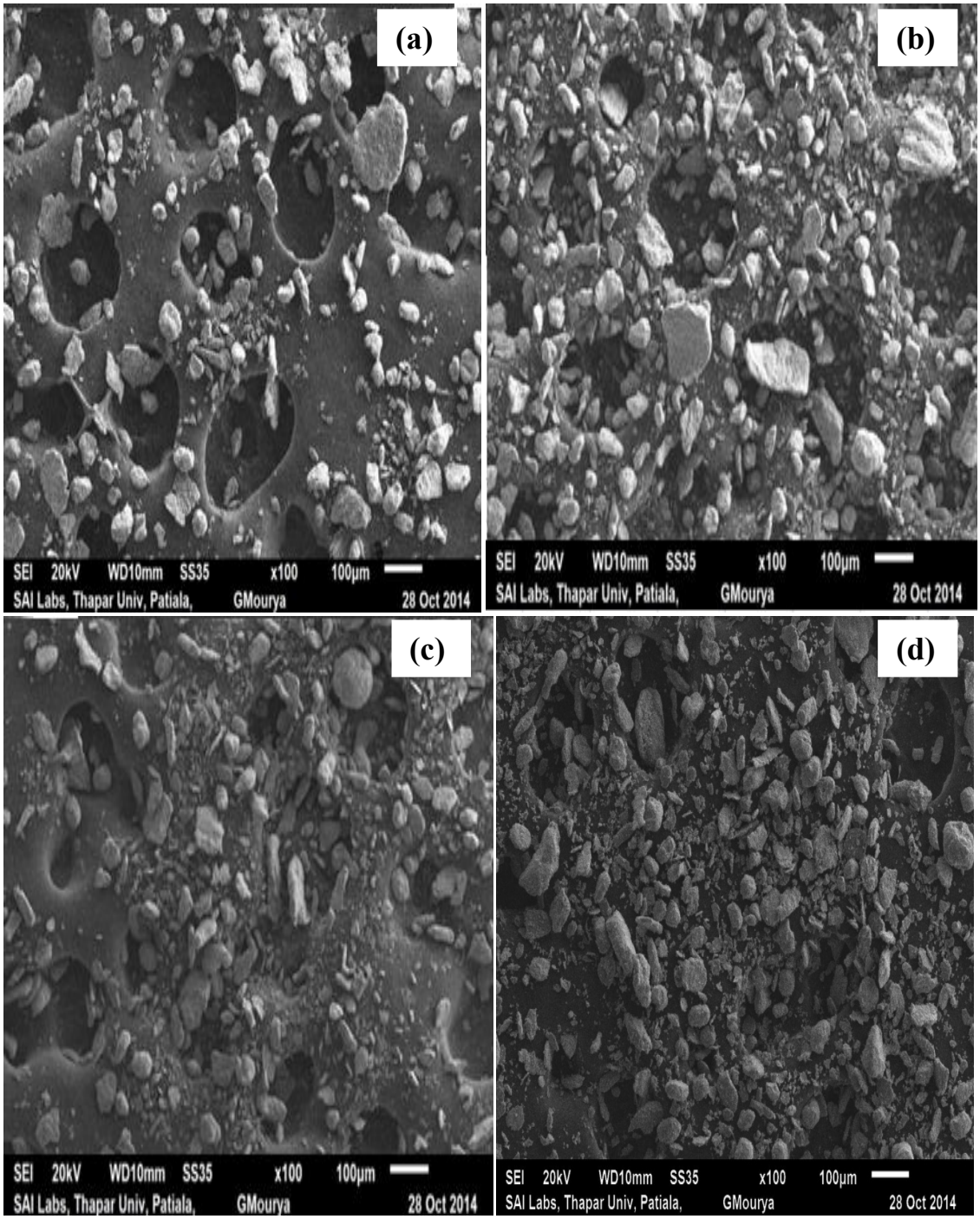
(a)
SEI 20kV WD10mm SS35 x100 100µm
SAI Labs, Thapar Univ, Patiala, GMourya 28 Oct 2014
(b)
SEI 20kV WD10mm SS35 x100 100µm
SAI Labs, Thapar Univ, Patiala, GMourya 28 Oct 2014
(c)
SEI 20kV WD10mm SS35 x100 100µm
SAI Labs, Thapar Univ, Patiala, GMourya 28 Oct 2014
(d)
SEI 20kV WD10mm SS35 x100 100µm
SAI Labs, Thapar Univ, Patiala, GMourya 28 Oct 2014

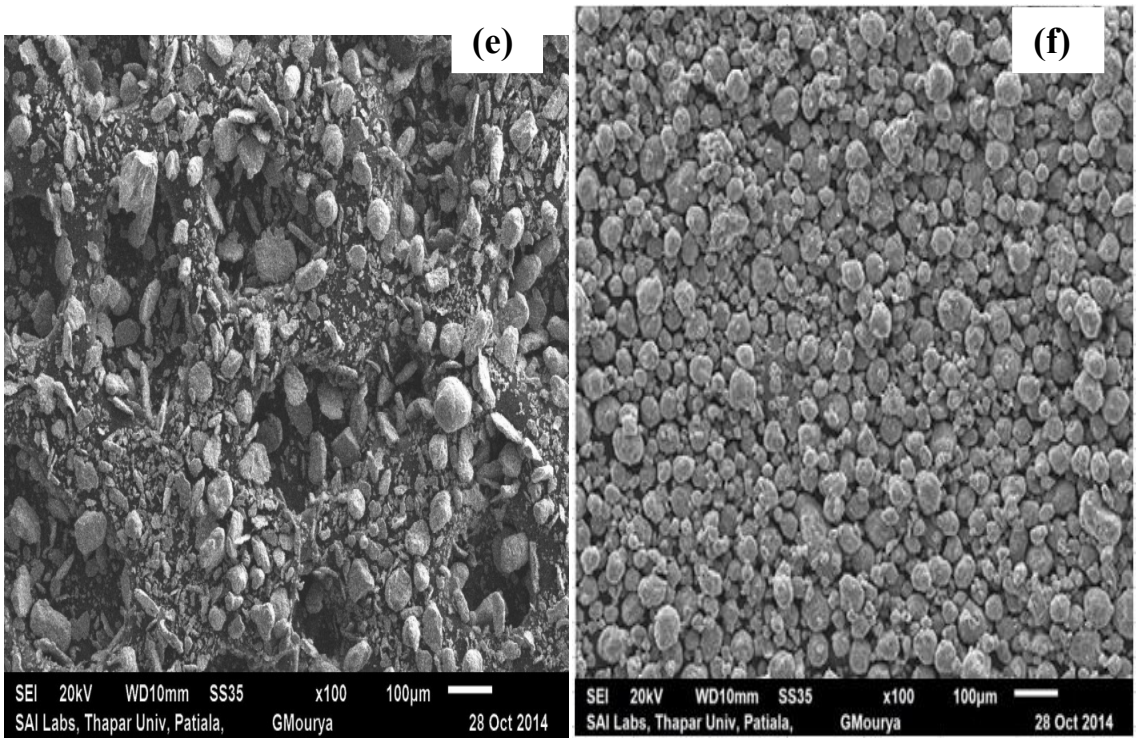

Figure 5.2: Scanning electron micro-graph of elemental powders at milling times (a) 4h; (b) 8h; (c) 30h; (d) 40h; (e) 50h; (f) 60h.

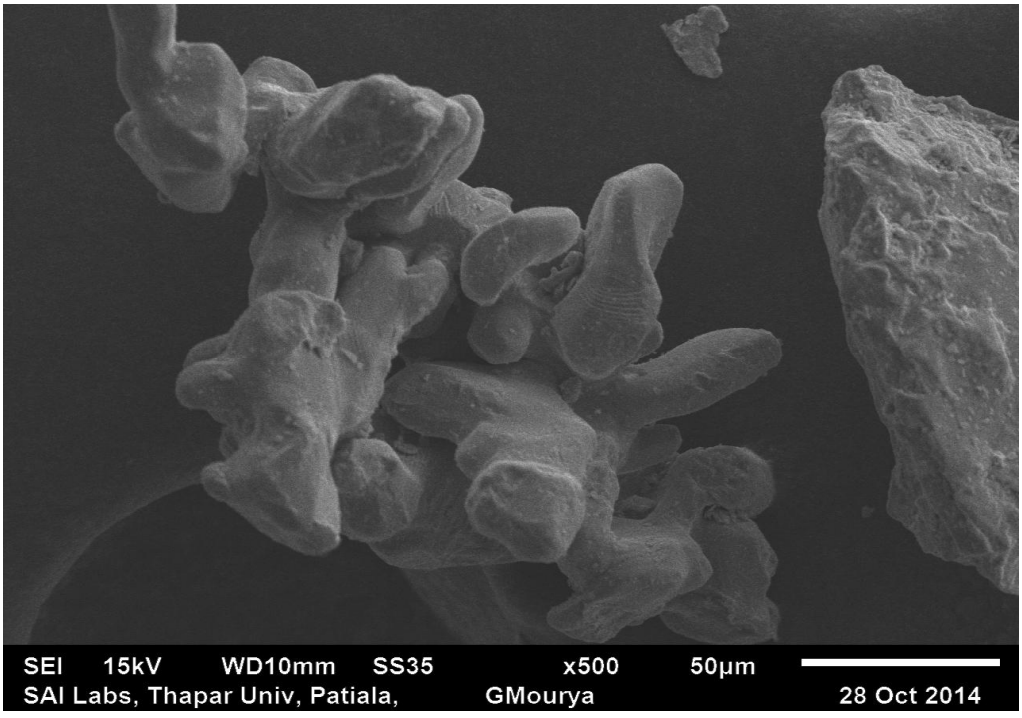

Figure 5.3: Scanning electron micro-graph presenting cold welded compound

Figure 5.2 (e) shows the formation of granular shape at most of the parts. The reason behind this is that with the increase of mill time, cold welding occurs again and again, which increases the brittleness of the particle and finally results into smaller particle with granular shape. At last in Figure 5.2 (f) all the Ni and Ti particle becomes homogeneous due to the repeated fracturing and cold welding, which again results into the generation of agglomeration, contain Ti and Ni particles. To understand the phenomena more acutely, Figure 5.3 has been added, where a compound of particles has been formed due to cold welding.

5.2.2 SEM observation of Balls

Figure 5.4 (a) presents the morphology of the unused steatite ceramic ball. The surface of ball was not so much smooth and contains some crater marks. Figure 5.4 (b) present the morphology of steatite ceramic ball after 60h of milling the nickel and titanium powder in high-energy ball mill. It has been found from these results that the surface is not so much affected after its operation. Figure 5.4 (c) presents an unused hardened steel ball surface. The SEM was taken after surface preparation (i.e. cleaning with HNO_3 and then dry) and a smooth surface has been observed. But with the passage of time in the ball mill (i.e. 60h) a rough surface in Figure 5.4 (d) has been observed. Pit marks along with the craters were observed. So from this it has been found that the steatite is more wear resistant as compared to hardened steel balls and also to resist the impurity addition into the powder due to disintegration of surface particles of steel balls.

5.2.3 X-Ray Diffraction Analysis

With the increase of milling time a decrement is observed in the diffraction peak along with broadening in the face-centered cubic (FCC) Ni and hexagonal closed pack (HCP) Ti. After 50h of milling time the formation of NiTi is observed and the Ni and Ti peaks are observed to be disappeared as in Figure 5.5. Lattice parameters of Ni atoms observed to be enhanced with the passage of time due to diffusion of Ti into Ni matrix. It was the body-centered cubic structure of NiTi after 60h milling.

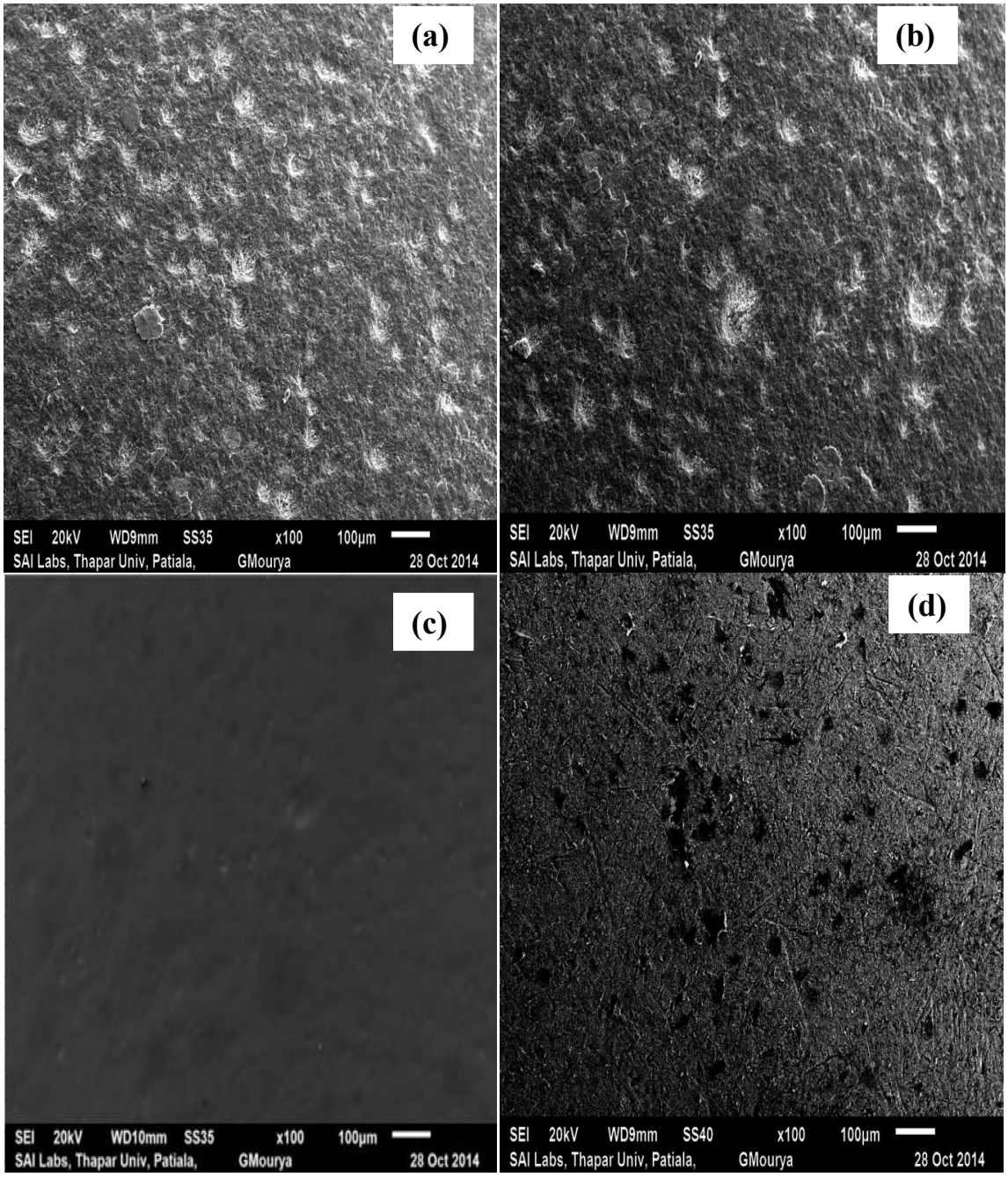

Figure 5.4: Scanning electron micro-graph of balls (a) Steatite at 0h (b) Steatite at 60h (c) Steel at 0h (d) Steel at 60h

Refinement in the crystalline size was assumed the main reason for broadening the peaks. Williamson-Hall formula **(Nazanin-Samani et al., 2010)** as in equation 5.1 was used to find out the crystallite size of compound.

$$\sqrt{\left(B_i^2 - B_o^2\right)}Cos\theta = 0.89\frac{\lambda}{d} + 2eSin\theta \tag{5.1}$$

Where B_i – XRD pattern's peak full width when maximum intensity is half,

B_o – Instrument broadening correction factor,

θ – Bragg angle,

e – Lattice strain

λ – wave-length of X-ray,

d – Crystallite size.

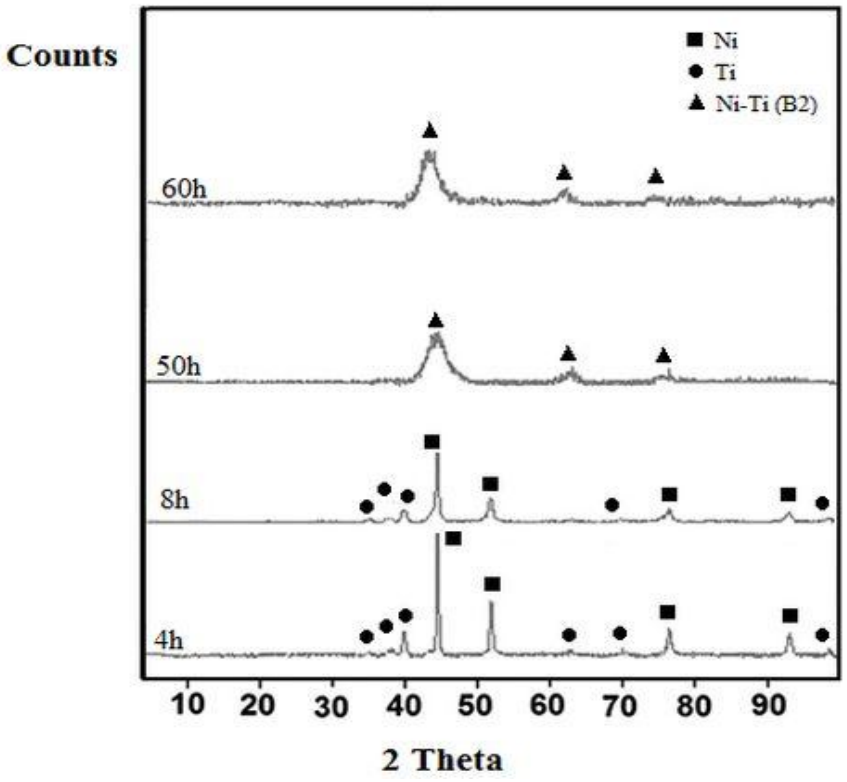

Figure 5.5: XRD pattern of powder after different milling time

5.3 SELECTION OF RANGE OF PARAMETERS (OFAT APPROACH)

The process parameters and their ranges were selected by literature review and preliminary study. In preliminary study, all factors remain constant at some central value,

while one factor varies from minimum to maximum value. The corresponding response was measured and a significant range of respective process parameter is observed. **Xu et al. (2014)** worked on the characteristics investigation after change in the sintering temperature and sintering time. Every time researchers defined a particular value of compaction pressure for fabricating NiTi alloys. Material scientist also studied the effect of additives on the properties of shape memory alloys. Although NiTi alloys show a good corrosion resistance, wear resistance, shape recovery and bio-compatibility. As porous structure favours bio-compatibility and tissue growth, but decreases the corrosion resistance and wear resistance, so copper is used as an additive and study its influences on characteristics of NiTi alloys. Powder compaction press of Kimaya Engineers (Mumbai) make of 15 kN was used in present work. Apart from the parameters which are to be investigated, the following parameters were kept constant during the experiments:

- Work-Material : Ni, Ti and Cu Powders
- Compaction Press Capacity : 15kN
- Compaction Time : 10min
- Work-piece height : 12mm
- Work-piece diameter : 6mm
- Blending time : 10hrs
- Ball mill rotation Speed : 300R.P.M.

5.3.1 Effect of Compaction Pressure on Response Variables

The Compaction Pressure is varied from 60MPa to 180MPa in steps of 20MPa. The values of the other process parameters are given as Sintering Temperature = 1050°C and Sintering time =45 min.

Table 5.1: Variation of Compressive strength and Porosity with Compaction Pressure

Sr. No.	Compaction Pressure (MPa)	Compressive Strength (MPa)	Porosity (%)
1	60	Powder	Powder
2	80	110	51
3	100	213.5	47
4	120	321.7	36
5	140	367.2	32
6	160	571.8	29
7	180 (Die-Limit)	634.6	26

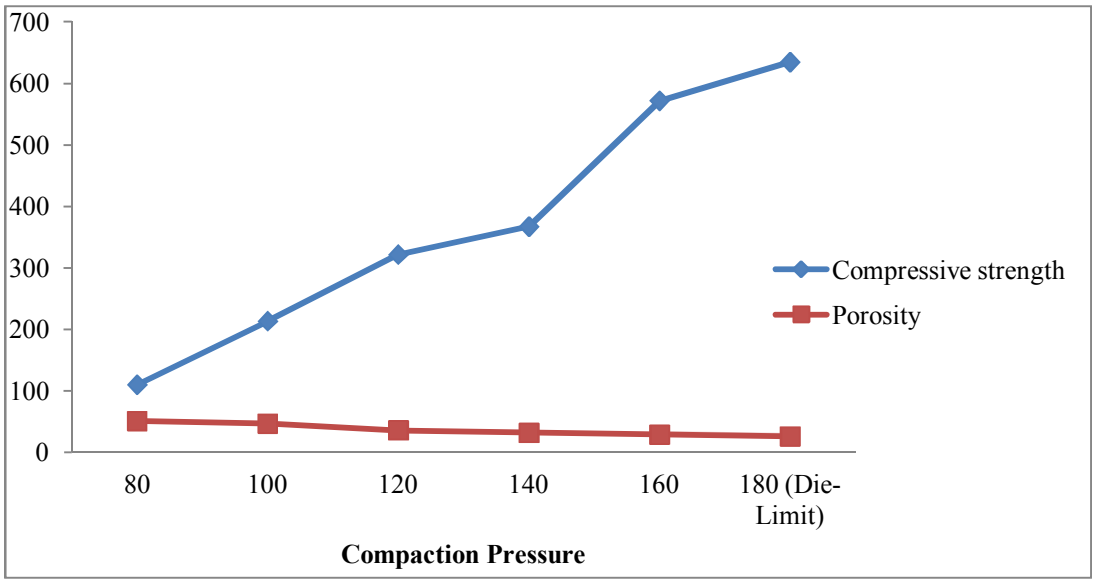

Figure 5.6: Scatter Plot of Compaction Pressure versus Response Variable

The experimentally observed values of the response variables for different values of compaction pressure are given in Table 5.1. The scatter plots of compaction pressure versus response variables are shown in Figure 5.6. The compressive strength increases while porosity decreases with the increase of compaction pressure.

Table 5.2: Variation of Compressive strength and Porosity with Sintering Temperature

Sr. No.	Sintering Temperature (°C)	Compressive Strength (MPa)	Porosity (%)
1	750	70	54
2	850	180.5	41
3	950	796.2	26
4	1050	474.3	30
5	1150 (Furnace)	365.8	32

5.3.2 Effect of Sintering Temperature on Response Variables

The sintering temperature is varied from 750°C to 1150°C in steps of 100°C. The values of the other process parameters are given as compaction pressure = 140MPa and Sintering time =45 min. The experimentally observed values of the response variables for different values of sintering temperature are given in Table 5.2. The scatter plots of sintering temperature versus response variables are shown in Figure 5.7. The compressive strength increases and then decreases while porosity first decreases and then increases with the increase of sintering temperature.

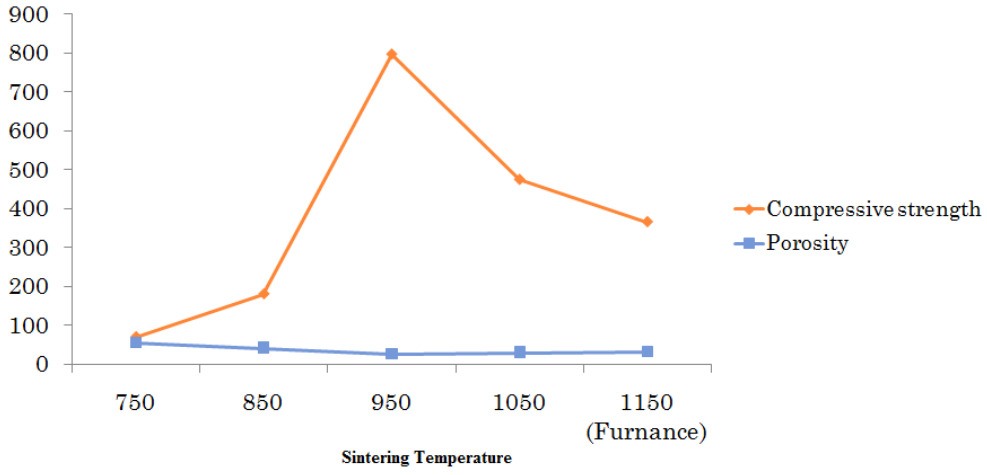

Figure 5.7: Scatter Plot of Sintering Temperature versus Response Variable

5.3.3 Effect of Sintering Time on Response Variables

The sintering time is varied from 10min to 60min in steps of 10min. The values of the other process parameters are given as compaction pressure = 140MPa and Sintering temperature =1050°C.

Table 5.3: Variation of Compressive strength and Porosity with Sintering Temperature

Sr. No.	Sintering Time (min)	Compressive Strength (MPa)	Porosity (%)
1	10	132.1	21
2	20	679.2	23
3	30	552.9	27
4	40	487.4	33
5	50	423.6	37
6	60	325.2	41

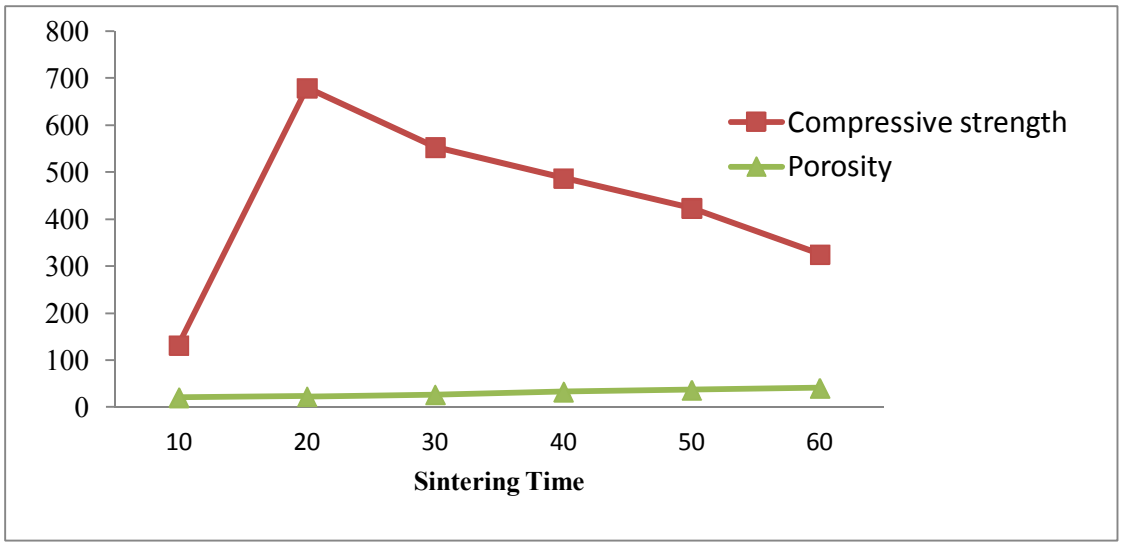

Figure 5.8: Scatter Plot of Sintering Temperature versus Response Variable

The experimentally observed values of the response variables for different values of sintering time are given in Table 5.3. The scatter plots of sintering time versus response variables are shown in Figure 5.8. The compressive strength first increases and then decreases while porosity increases with the increase of sintering time. This is due to fact that with the increase of sintering time, the diffusion between the nickel and titanium powder particles increases, which increases the bonding strength of the particles initially. So, the compressive strength increases. Also the porosity increases with the increase of sintering time. This is due to the continuum effect, which states that increase in the sintering time evaporate the binder from the green compact. Considering this, the range of process parameters selected is given in Table 5.4.

Table 5.4: Range of Process Parameters

Sr. No	Process Parameters	Symbol	(units)	Range
1.	Compaction Pressure	A	MPa	107 – 177
2.	Sintering Temperature	B	°C	950 – 1150
3.	Sintering Time	C	min	20 – 60

CHAPTER – 6
MECHANICAL CHARACTERIZATION

6.1 INTRODUCTION

The experiments were conducted according to the selected scheme of Taguchi's L_9 orthogonal array to investigate the effect of process parameters on the response variables e.g. compressive strength, young's modulus and porosity. At the optimal settings suggested by Taguchi experimental design, other testing will be performed. The other testing includes wear test, evaluation of micro-hardness and shape recovery etc. The experimental results are discussed subsequently in the following sections.

6.2 SELECTION OF ORTHOGONAL ARRAY

A set of three levels assigned to each process parameter has two degrees of freedom (DOF) according to Taguchi experimental design philosophy, so this gives a total of 6 DOF for three process parameters selected in this work. As in the present research work, L_9 orthogonal array is selected, so degree of freedom will be one value less i.e. equal to 8 **(Ross 1988)**.

Table 6.1: Process Parameters and their Levels

Factors	Parameters	Units	Levels		
			L1	L2	L3
A	Compaction Pressure	MPa	107	141	177
B	Sintering Temperature	°C	950	1050	1150
C	Sintering Time	Min	20	40	60

Table 6.2: Planning of Experiments According to L_9 OA

Sr. No.	Compaction Pressure (MPa)	Sintering Temp (°C)	Time (min)
1	107	950	20
2	107	1050	40
3	107	1150	60
4	141	950	40
5	141	1050	60
6	141	1150	20
7	177	950	60
8	177	1050	20
9	177	1150	40

For each trial in the L_9 array, the levels of the process parameters are indicated in Table 6.1. Design matrix of L_9 OA given in Table 6.2, according to which all experiments will be performed.

6.3 EXPERIMENTAL RESULTS

Table 6.2 represents the design matrix to perform the experimentations according to L_9 orthogonal array (OA). A total of 9 experiments were performed after varying the copper contents. The results of compressive strength (in MPa), elastic modulus (in GPa) and porosity (%) are given in Table 6.3-Table 6.5. The experiments were conducted to study the effect of process parameters on the response variables. The experimental results for different composition of copper are given in Tables 6.3-6.5. According to the experimental design selected, 9 experiments were conducted. The experiments were performed after varying the copper content into NiTi alloy from 0%, 5% and 10% at the cost of Ni element and the results were compared to see the effect of these contents on the characteristics of NiTi alloy.

Table 6.3: Porosity, Compressive Strength and Modulus of Elasticity of $Ni_{50}Ti_{50}$ according to L_9 Design Matrix

Sr. No.	Porosity (%)		Compressive Strength (MPa)		Young's Modulus (GPa)	
	Raw Data Mean	S/N ratio	Raw Data Mean	S/N ratio	Raw Data Mean	S/N ratio
1	21	26.444	841.3	58.499	6.3	-15.987
2	43	32.669	301.8	49.594	2.9	-9.248
3	56	34.964	82.6	38.340	1.4	-2.923
4	25	27.959	803.5	58.100	5.4	-14.648
5	41	32.256	327.6	50.307	2.5	-7.959
6	34	30.630	525.4	54.410	3.2	-10.103
7	28	28.943	769.2	57.721	5	-13.979
8	24	27.604	812.1	58.192	5.6	-14.964
9	34	30.630	518.7	54.298	3.4	-10.630

Table 6.4: Porosity, Compressive Strength and Modulus of Elasticity of $Ni_{45}Ti_{50}Cu_5$ according to L_9 Design Matrix

Sr. No.	Porosity (%)		Compressive Strength (MPa)		Young's Modulus (GPa)	
	Raw Data Mean	S/N ratio	Raw Data Mean	S/N ratio	Raw Data Mean	S/N ratio
1	23	27.235	859.3	58.683	6.6	-16.391
2	42	32.465	309.2	49.805	3.5	-10.881
3	51	34.151	77.4	37.775	2	-6.021
4	24	27.604	814.9	58.222	5.5	-14.807
5	40	32.041	351.6	50.921	2.7	-8.627
6	32	30.103	531.8	54.515	3.6	-11.126
7	27	28.627	783.5	57.881	5.2	-14.320
8	23	27.235	812.3	58.194	5.8	-15.269
9	33	30.370	526.7	54.431	3.6	-11.126

Table 6.5: Compressive Strength, Modulus of Elasticity and Porosity of $Ni_{40}Ti_{50}Cu_{10}$ according to L_9 Design Matrix

Sr. No.	Porosity (%)		Compressive Strength (MPa)		Young's Modulus (GPa)	
	Raw Data Mean	S/N ratio	Raw Data Mean	S/N ratio	Raw Data Mean	S/N ratio
1	28	28.943	871.4	58.804	7.1	-17.025
2	46	33.255	320.3	50.111	3.8	-11.596
3	53	34.486	88.1	38.900	2.3	-7.235
4	37	31.364	823.7	58.315	5.8	-15.269
5	45	33.064	363.8	51.217	3.1	-9.827
6	39	31.821	542.6	54.690	3.8	-11.596
7	29	29.248	791.4	57.968	5.4	-14.648
8	27	28.627	822.3	58.301	5.9	-15.417
9	37	31.364	535.9	54.582	3.8	-11.596

The collected data after experimentation were analysed through the application of Taguchi methods to ascertain the significant factors and their contribution for the variability of response quality characteristics. In the present study all the designs, plots and analysis have been carried out using Minitab statistical software (Minitab 16).

6.4 ANOVA for $Ni_{50}Ti_{50}$

6.4.1 ANOVA for Porosity of $Ni_{50}Ti_{50}$

Tables 6.6 and 6.7 give the ANOVA of raw data and S/N data for porosity in case of $Ni_{50}Ti_{50}$ alloy. P-value in case of sintering temperature and sintering time is less than 0.05, which indicates that these parameters play a significant role in the investigation of porosity. Compaction pressure represents a P-value equal to 0.085 and contributes 19.46% in porosity. According to P-value this factor comes under the category of non-significant terms, but it gives ~20% contribution into the process, so considered in Table 6.6. For the investigation of optimal setting, further analysis is carried for predicted values.

Table 6.6: Analysis of Variance for Means (Porosity)

Source	DF	SS	MS	F	P	p (%)
Compaction Pressure	2	194.67	97.333	10.81	0.085	19.46
Sintering Temperature	2	434.67	217.333	24.15	0.040	43.46
Sintering Time	2	352.67	176.333	19.59	0.049	35.26
Residual Error	2	18.00	9.000			1.8
Total	8	1000.00	**S = 3; R-Sq = 98.2%; R-Sq(adj) = 92.8%**			

DF - degrees of freedom, SS - sum of squares, MS - mean squares (variance), F-ratio (variance of a source to variance of error), $P < 0.05$ - determines significance of a factor` at 95% confidence level, p - % contribution.

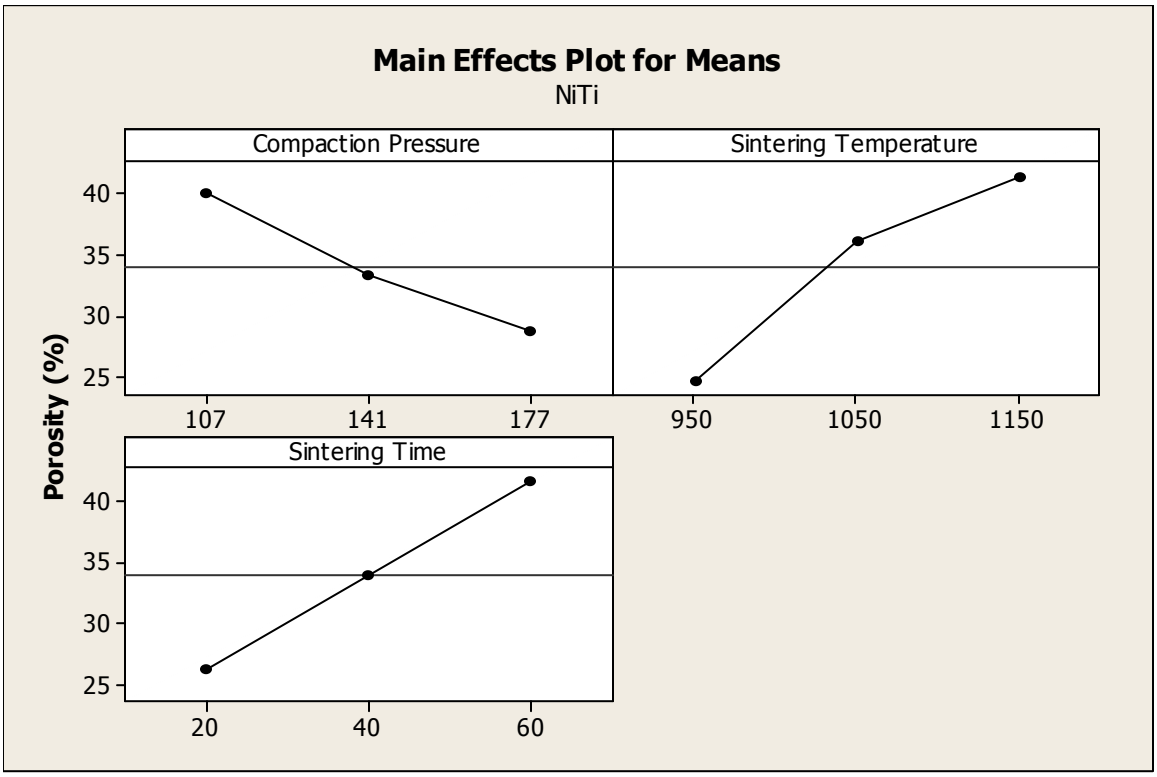

Figure 6.1: Variation of Porosity with Process parameters ($Ni_{50}Ti_{50}$)

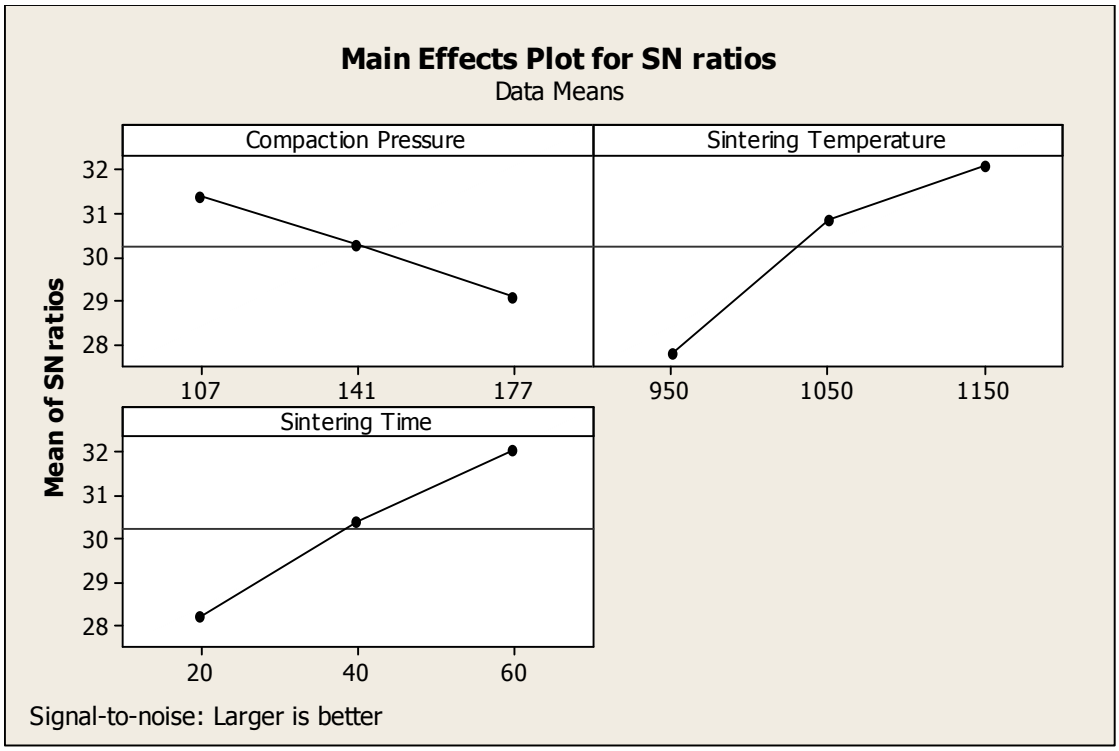

Figure 6.2: Variation of S/N values for Porosity ($Ni_{50}Ti_{50}$)

Table 6.7: Analysis of Variance for S/N ratios (Porosity)

Source	DF	SS	MS	F	P	p (%)
Compaction Pressure	2	7.947	3.9734	5.56	0.152	13.06
Sintering Temperature	2	29.308	14.6542	20.51	0.046	48.18
Sintering Time	2	22.138	11.0689	15.50	0.061	36.39
Residual Error	2	1.429	0.7143			2.35
Total	8	60.821	**S = 0.8452; R-Sq = 97.7%; R-Sq(adj) = 90.6%**			

Sintering temperature plays a major contribution of 43.36% followed by sintering time of 35.26% according to raw data from Table 6.6. S/N value follows the same pattern of percentage contribution. In Table 6.6 and 6.7, the R-square and adjusted R-square values are greater than 90% show a good variability explanations and lower S-values

represent a low value of errors. Figure 6.1 and 6.2 show the variation of porosity mean values and S/N values with process parameters

Porosity decreases with increase of compaction pressure as shown in Figure 6.1. This is due to the fact that with the increase of compaction pressures the voids in between the powder particles decrease. The voids in the material are decreased at the cost of porosity. Sintering temperature favours the porosity i.e. with the increase of sintering temperature porosity increases. The main reason behind this is the heating of material. With the increase of sintering temperature and sintering time, the organic binder particles present in the core of material evaporate, which increases porosity. Figure 6.2 follows the same pattern as explained in Figure 6.1.

Table 6.8: Response Table for Means (Porosity)

Level	Compaction Pressure	Sintering Temperature	Sintering Time
1	40.00	24.67	26.33
2	33.33	36.00	34.00
3	28.67	41.33	41.67
Delta	11.33	16.67	15.33
Rank	3	1	2

Table 6.9: Response Table for Signal to Noise Ratios (Porosity)

Level	Compaction Pressure	Sintering Temperature	Sintering Time
1	31.36	27.78	28.23
2	30.28	30.84	30.42
3	29.06	32.07	32.05
Delta	2.30	4.29	3.83
Rank	3	1	2

Table 6.10: Pooled ANOVA for Means (Porosity)

Source	DF	SS	MS	F	P	p (%)
Sintering Temperature	2	434.7	217.33	4.09	0.108	43.47
Sintering Time	2	352.7	176.33	3.32	0.142	35.37
Residual Error	4	212.7	53.17			21.27
Total	8	1000.0				

Table 6.11: Response Table after pooling for Means (Porosity)

Level	Sintering Temperature	Sintering Time
1	24.67	26.33
2	36.00	34.00
3	**41.33**	**41.67**
Delta	16.67	15.33
Rank	1	2

Table 6.8 and 6.9 give the response table for mean and S/N value of porosity in case of $Ni_{50}Ti_{50}$. Larger value of porosity will be beneficial for preventing stress shielding. Both Tables (Table 6.8 and 6.9) suggest the same optimal values of process parameters for porosity. Sintering temperature is affecting the porosity most followed by sintering time and compaction pressure.

Table 6.10 show the ANOVA after extracting compaction pressure as insignificant term from Table 6.6. Response table after pooling the insignificant term is given in Table 6.11. Figure 6.3 represent the variation of porosity with the change of significant process parameters. Figure 6.4 reveals the residual plots for porosity, which verifies ANOVA with the help of different test. Normality test, residual versus fitted, histogram test and variance test are verified. As all these tests represent the same order as required and indicate a sign of good ANOVA.

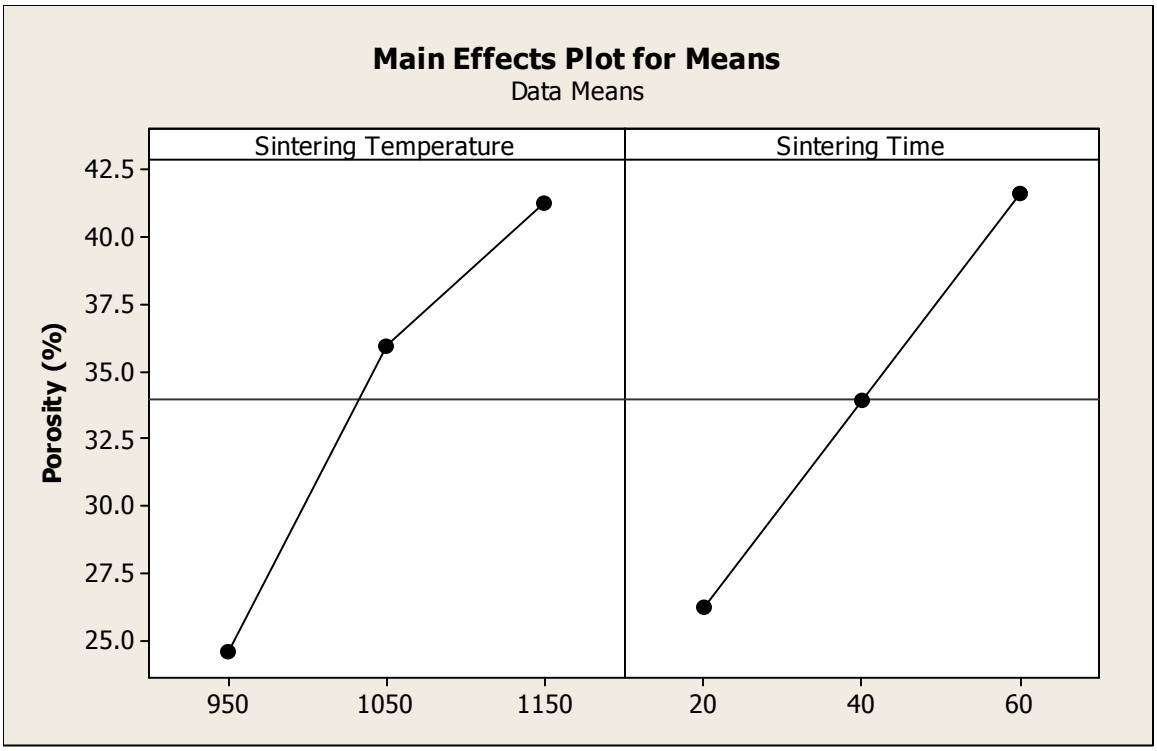

Figure 6.3: Variation of Porosity with Process parameters ($Ni_{50}Ti_{50}$)

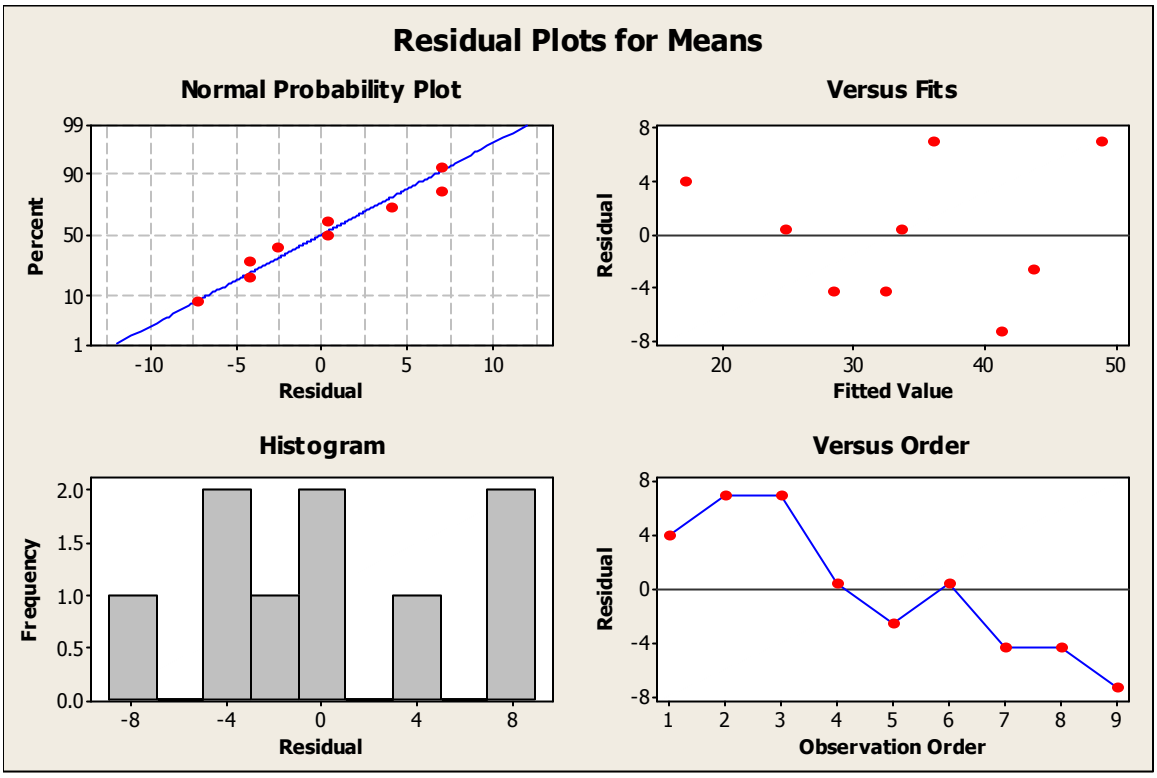

Figure 6.4: Residual plots for Porosity ($Ni_{50}Ti_{50}$)

Optimal Setting for Porosity (NiTi)

The optimum value of porosity is predicted at the selected levels of significant variable Sintering temperature (B_3), and sintering time (C_3) (Table 6.11). The estimated mean of the response characteristic can be determined as:

$$\overline{\mu_\sigma} = \overline{B_3} + \overline{C_3} - \overline{T} \qquad (5.6)$$

Where, $\overline{T}$ = overall mean of Porosity = ($\sum$R)/9 = 34

R values are taken from the Table 6.3 and the values of $\overline{B}_3$ and $(\overline{C_3})$ are estimated from the experimental data reported in the Table 6.11.

$\overline{B}_3$ = average value of porosity at the third level of sintering temperature =41.33

$(\overline{C_3})$= average value of porosity at the third level of sintering time =41.67

Substituting the values of various terms in the above equation,

$\mu_{porosity}$ = 41.67+41.33- (34) = 49

The 95 % confidence intervals of confirmation experiments (CI_{CE}) and population (CI_{POP}) are calculated as:

$$CI_{CE} = \sqrt{F_\alpha\,(1, f_e)\, V_e \left[\frac{1}{n_{eff}} + \frac{1}{R}\right]} \qquad \text{and} \qquad CI_{POP} = \sqrt{\frac{F_\alpha\,(1, f_e)\, V_e}{n_{eff}}}$$

Where, $F_\alpha\,(1, f_e)$ = The F ratio at the confidence level of (1-α) against DOF 1 and error degree of freedom f_e.

$$n_{eff} = \frac{N}{1 + [\text{DOF associated in the estimate of mean response}]} = 27 / (1+4) = 5.4$$

N = Total number of results = 9 x 3 =9, R = Sample size for confirmation experiments = 3

V_e = Error variance = 53.17; f_e = error DOF = 4 (Table 6.10)

$F_{0.05}\,(1, 4)$ = 7.71 (Tabulated F value (Ross, 1996))

So, CI_{CE} = ± 14.57 and CI_{POP} = ± 8.71

Therefore, the predicted confidence interval for confirmation experiments is:

$\mu_{porosity} - CI_{CE} < \mu_{porosity} < \mu_{porosity} + CI_{CE}$ i.e. $34.43 < \mu_{porosity} < 63.57$

The 95% confidence interval of the population is:

$\mu_{porosity} - CI_{POP} < \mu_{porosity} < \mu_{porosity} + CI_{POP}$ i.e. $40.29 < \mu_{porosity} < 57.71$

The optimal values of process variables at their selected levels are as follows:

(B_3) : 1150°C; C_3 : 60 min.

6.4.2 Compressive Strength of $Ni_{50}Ti_{50}$

Table 6.12 shows the analysis of variance (ANOVA) of compressive strength for 0% Cu contents. From Table 6.12, it is clear that sintering temperature plays a major role in the compressive strength. P-value of all process parameters is < 0.05, shows that all three parameters are significant.

Table 6.12: Analysis of Variance for Means ($Ni_{50}Ti_{50}$-Compressive Strength)

Source	DF	SS	MS	F	P-value	p (%)
Compaction Pressure	2	127409	63705	61.02	0.016	21.34
Sintering Temperature	2	300222	150111	143.78	0.007	50.32
Sintering Time	2	167141	83571	80.04	0.012	28.0
Residual Error	2	2088	1044			0.34
Total	8	596860	**S-32.3; R-Sq = 99.7% ; R-Sq(adj) = 98.6%**			

Table 6.13: Analysis of Variance for SN ratios (Compressive Strength)

Source	DF	SS	MS	F	P	p (%)
Compaction Pressure	2	98.72	49.362	7.17	0.122	28.85
Sintering Temperature	2	125.45	62.725	9.10	0.099	36.66
Sintering Time	2	104.32	52.159	7.57	0.117	30.47
Residual Error	2	13.78	6.889			4.02
Total	8	342.27	**S = 2.625; R-Sq = 96.0% ; R-Sq(adj) = 83.9%**			

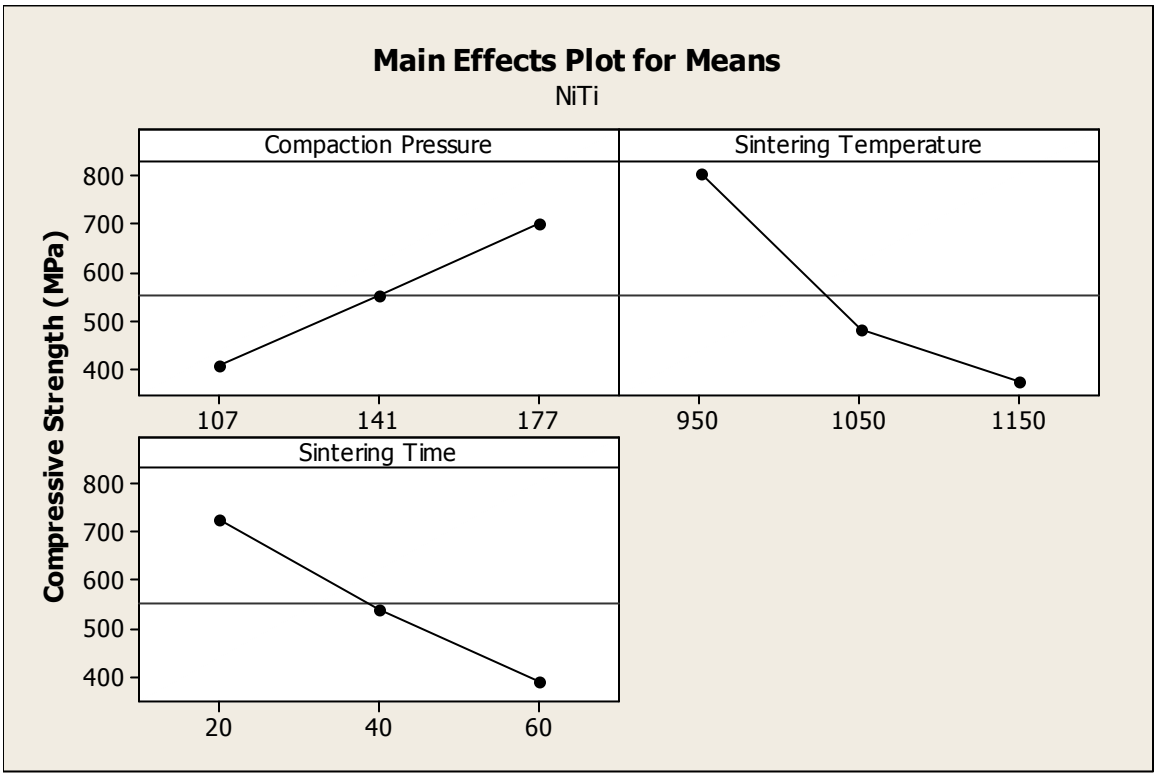

Figure 6.5: Variation of Compressive Strength with Process parameters ($Ni_{50}Ti_{50}$)

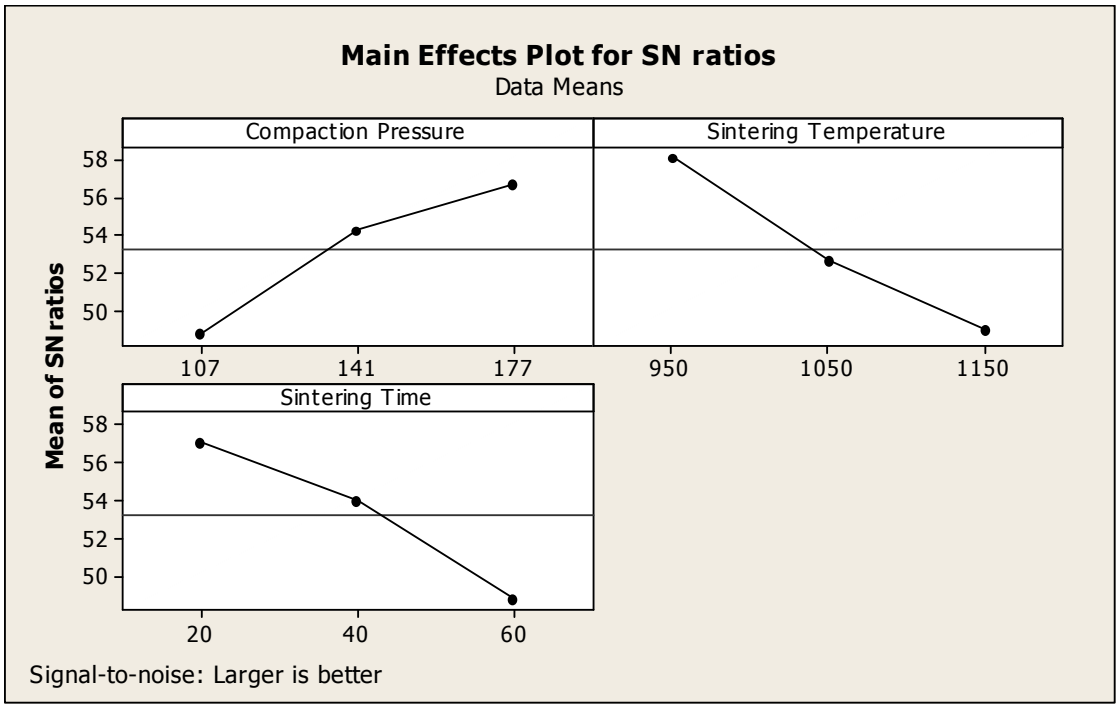

Figure 6.6: Variation of Compressive Strength (S/N ratio) with Process parameters ($Ni_{50}Ti_{50}$)

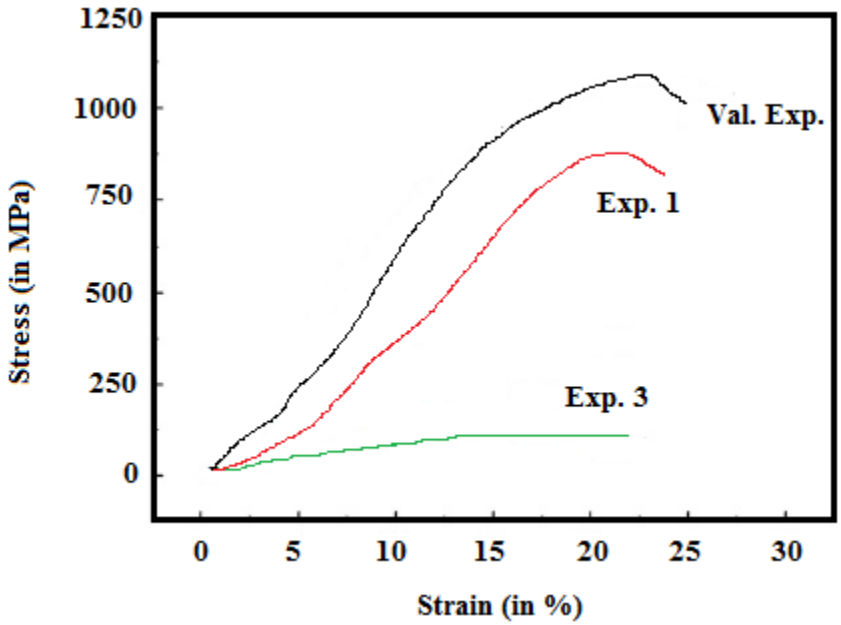

Figure 6.7: Stress-strain curve of NiTi for lowest, highest and validation Experiments

The value of R^2 is 99.7 % confirm that 99.7% of variability around the mean can be explained with these experiments due to significant and non-significant terms. While adjusted R^2 reveal that 98.6% variability can be explained due to significant terms only. The most significant parameter is sintering temperature. The percentage contribution of sintering temperature is 50.3% into the process followed by sintering time (28%) and compaction pressure 21.34%. Table 6.13 gives the ANOVA for S/N ratio of compressive strength. Figure 6.5 and 6.6 shows the variation of compressive strength mean values and S/N values with the process parameters. It is revealed that with the increase of compaction pressure, compressive strength found to be increase. This is due to the fact that with the increase of compaction pressure, the particle of powders gets attached together and forms a firm bonding, which can be assumed probable reason of higher compressive strength.

The increase of sintering temperature and time decrease the strength of material due to evaporation of the binder particles between the powder particle, so the porous structure has been formed. With the increase of time the evaporation takes place from the core of the green compact and decrement in compressive strength has been observed. Figure 6.7 shows compressive stress-strain variation for the selected experiments only.

Here the selected experiments are experiment 1 (highest compressive stress), experiment 3 (lowest compressive stress) and validation experiment (at optimized setting) compressive stress. Except for the initial stages in the compression test, it is categorized into three stages **(Gao et al., 2012)**. First stage is elastic deformation stage; in this the slope is assumed to be equal to the young's modulus. Second stage is the plastic stage, here a maximum value of stress occurs and known as compressive strength of the specimen. Last stage is the failure/rupture stage of specimen. In this it is clear that the young's modulus of porous NiTi varies from 1.4GPa to 6.3GPa, which is nearby the young's modulus **(Hench, 1998)** of bone (0.05–0.5 GPa and 3–20 GPa for cancellous bone and cortical bone respectively).

Table 6.14: Response Table for Means (Compressive Strength)

Level	Compaction Pressure	Sintering Temperature	Sintering Time
1	408.6	804.7	726.3
2	552.2	480.5	541.3
3	700.0	375.6	393.1
Delta	291.4	429.1	333.1
Rank	3	1	2

Table 6.15: Response Table for Signal to Noise Ratios (Compressive Strength)

Level	Compaction Pressure	Sintering Temperature	Sintering Time
1	48.81	58.11	57.03
2	54.27	52.70	54.00
3	56.74	49.02	48.79
Delta	7.93	9.09	8.24
Rank	3	1	2

Table 6.14 and 6.15 gives the response table for raw data and S/N values according to compressive strength. Delta represents the difference between maximum and minimum value, while rank gives the order of process parameters affecting the

response in a process. From both of these tables it has been found that sintering temperature affecting the process most followed by sintering time and compaction pressure.

Optimal Setting for Compressive strength (NiTi)

The optimum value of σ is predicted at the selected levels of significant variable compaction pressure (A_3), Sintering temperature (B_1), and sintering time (C_1) (Table 6.14). The estimated mean of the response characteristic can be determined as:

$$\overline{\mu_\sigma} = \overline{A_3} + \overline{B_1} + \overline{C_1} - 2\overline{T} \qquad (6.6)$$

Where, $\overline{T}$ = overall mean of compressive strength = (∑R)/9 = 553.57 MPa

R values are taken from the Table 6.3, and the values of $\overline{A}_3$, $\overline{B}_1$ and $\left(\overline{C_1}\right)$ are estimated from the experimental data reported in the Table 6.14.

$\overline{A}_3$ = average value of σ at the third level of compaction pressure = 700MPa

$\overline{B}_1$ = average value of σ at the first level of sintering temperature =804.7 MPa

$\left(\overline{C_1}\right)$= average value of σ at the first level of sintering time =726.3 MPa

Substituting the values of various terms in the above equation,

μ_σ = 700+804.7+726.3-2 (553.57) = 1123.86MPa

The optimal values of process variables at their selected levels are as follows:

(A_3) : 177MPa;

(B_1) : 950°C;

C_1 : 20 min.

6.4.3 Young's Modulus of $Ni_{50}Ti_{50}$

Table 6.16 shows the ANOVA (means) for young's modulus of NiTi alloy i.e. 0% Cu content. From Table 6.16 it is evident that the p-value for compaction pressure is

greater than 0.05 i.e. this process parameter is non-significant. Also p-value < 0.05 for sintering temperature and sintering time, shows that these parameters are significant. Sintering temperature gave a major contribution into the process with 59.12%, while sintering time contribution into the process is 29.18% followed by compaction pressure 10.2%.

Table 6.16: Analysis of Variance for Means ($Ni_{50}Ti_{50}$-Young's Modulus)

Source	DF	SS	MS	F	P-value	p (%)
Compaction Pressure	2	2.2467	1.1233	6.88	0.127	10.2
Sintering Temperature	2	13.0200	6.5100	39.86	0.024	59.12
Sintering Time	2	6.4267	3.2133	19.67	0.048	29.18
Residual Error	2	0.3267	0.1633			1.48
Total	8	22.0200	R-Sq = 98.5%; R-Sq(adj) = 94.1%			

DF - degrees of freedom, SS - sum of squares, MS - mean squares (variance), F-ratio (variance of a source to variance of error), P < 0.05 - determines significance of a factor` at 95% confidence level, p - % contribution.

Table 6.17: Analysis of Variance for S/N ratios (Young's Modulus)

Source	DF	SS	MS	F	P	p (%)
Compaction Pressure	2	22.015	11.0076	31.21	0.031	15.61
Sintering Temperature	2	74.070	37.0351	105.00	0.009	52.51
Sintering Time	2	44.248	22.1239	62.72	0.016	31.37
Residual Error	2	0.705	0.3527			0.51
Total	8	141.039	S = 0.5939; R-Sq = 99.5% ; R-Sq(adj) = 98.0%			

Table 6.17 gives ANOVA (S/N values) of Young's modulus of $Ni_{50}Ti_{50}$. Mean square can be easily obtained by dividing sum of square to the degree of freedom value. Larger will be the value of F-ratio larger be the contribution of that parameter in the process. P-values for all three parameters are less than 0.05, which represent a significant contribution of all process parameters into the investigation of young's modulus.

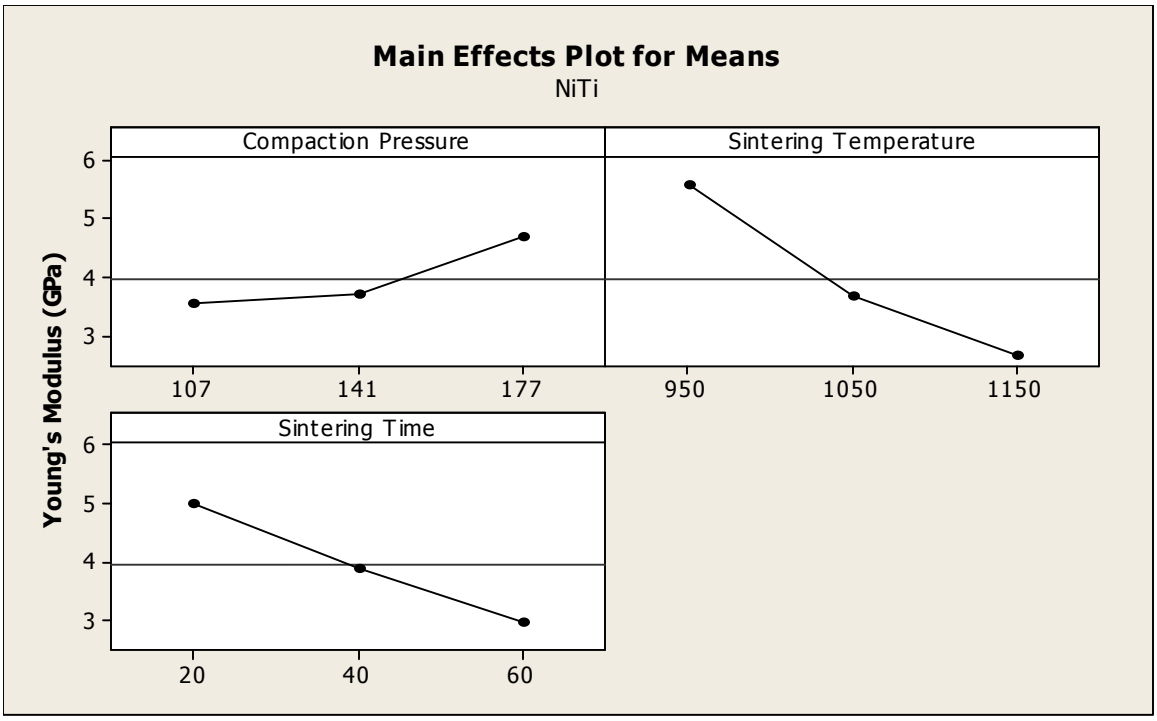

Figure 6.8: Variation of Young's Modulus with Process parameters ($Ni_{50}Ti_{50}$)

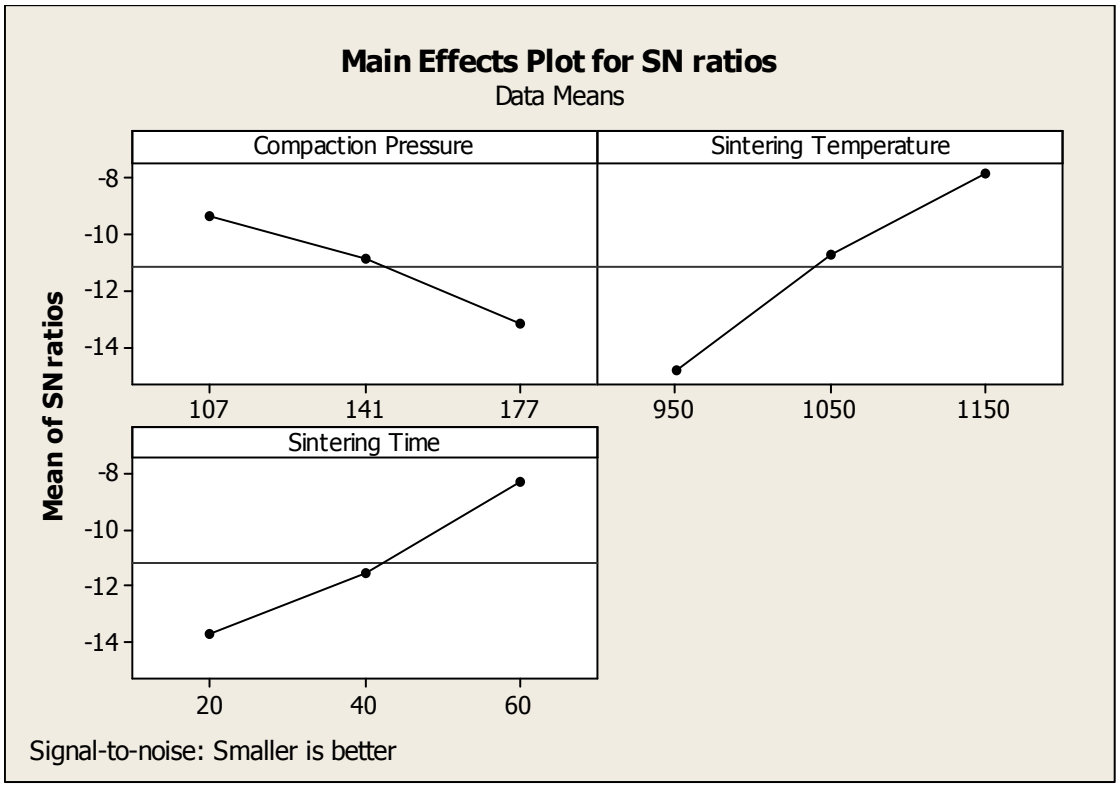

Figure 6.9: Variation of Young's Modulus (S/N ratio) ($Ni_{50}Ti_{50}$)

R-square gives the percentage of variability can be explained by this model (or value) due to significant and non-significant parameters. It is a statistical measure and is also known as coefficient of determination. Larger is value of R^2 will be considered in favorable side for the investigation of response. Adjusted R-square indicates the percentage variability explained by model due to significant terms only in a process. 'S' is termed as standard error of regression and indicates the average distance of observed value from the regression line. Lower value will be favorable, as the observed value will be near by the fitted line. Figure 6.8 represent that with the increase of compaction pressure the value of young's modulus found to be decrease. As lower value of young's modulus is required to match it with the moduli of bones **(Geetha et al., 2009)**.

Table 6.18: Response Table for Means (Young's Modulus)

Level	Compaction Pressure	Sintering Temperature	Sintering Time
1	**3.533**	5.567	5.033
2	3.700	3.667	3.900
3	4.667	**2.667**	**2.967**
Delta	1.133	2.900	2.067
Rank	3	1	2

Table 6.19: Response Table for S/N Ratio (Young's Modulus)

Level	Compaction Pressure	Sintering Temperature	Sintering Time
1	-9.386	-14.871	-13.685
2	-10.903	-10.724	-11.508
3	-13.191	-7.885	-8.287
Delta	3.805	6.986	5.398
Rank	3	1	2

Higher the value of compaction pressure, more closely the particles are bind together and hence a larger force is required to distort them, hence a larger value of

young's modulus. Increase in sintering temperature time decreases the modulus value as shown in Figure 6.8. The main reason behind this is the temperature removes the organic binder between the powders particles make it porous **(Christine et al., 1998)**. More time the green compact remains in the temperature, more number of binder particles assumed to be evaporate. Hence larger pores to be formed which decreases the young's modulus of NiTi. Figure 6.9 presents the variation of S/N values (young's modulus) with the change of process parameters in case of $Ni_{50}Ti_{50}$. Before going to start discussion on this it must be understood that either the response "Higher the better" or "Lower the best" type quality characteristics, but S/N values must be "Higher the better" type. The main reason behind this is that S/N value represents the signal to noise ratio or the ratio of significant factor to non-significant factor, which must be larger and shows that significant factor maximum contribution and non-significant factors minimum contribution. Here in Figure 6.9 represents the results, which are inline with the results obtained from Figure 6.8. As low value of compaction pressure and high value of sintering temperature and sintering time suggested by Figure 6.8 and Figure 6.9 both.

Table 6.18 and 6.19 reported the response table for mean value (raw data) and S/N values of young's modulus in case of $Ni_{50}Ti_{50}$ alloy. In Table 6.18, "lower is better" type characteristic consider while in Table 6.19 "higher the better" type quality characteristic is considered. After considering these conditions, Table 6.18 and Table 6.19 represent the same settings of process parameters for obtaining the lowest young's modulus. Also the order of process parameters (Rank) affecting response is same in both tables.

Table 6.20: Pooled ANOVA for Means (Young's Modulus)

Source	DF	SS	MS	F	P	p (%)
Sintering Temperature	2	13.020	6.5100	10.12	0.027	59.14
Sintering Time	2	6.427	3.2133	4.99	0.082	29.18
Residual Error	4	2.573	0.6433			11.68
Total	8	22.020				

Table 6.21: Response Table for Means (Young's Modulus)

Level	Sintering Temperature	Sintering Time
1	5.567	5.033
2	3.667	3.900
3	**2.667**	**2.967**
Delta	2.900	2.067
Rank	1	2

Table 6.20 gives the ANOVA for mean (Young's modulus) after pooling the compaction pressure from Table 6.16. The percentage contribution value of compaction pressure is added into the residual error. Table 6.21 reports the response table for mean values of Young's modulus after pooling.

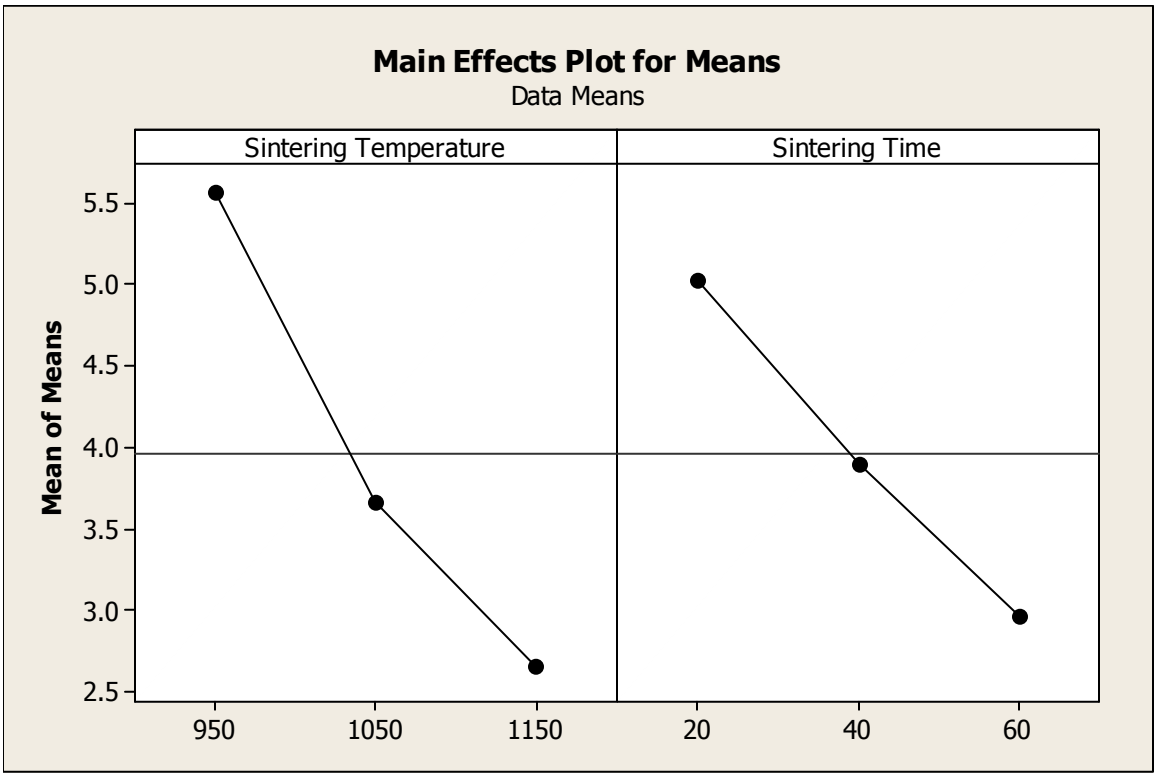

Figure 6.10: Variation of Young's Modulus with Process parameters ($Ni_{50}Ti_{50}$)

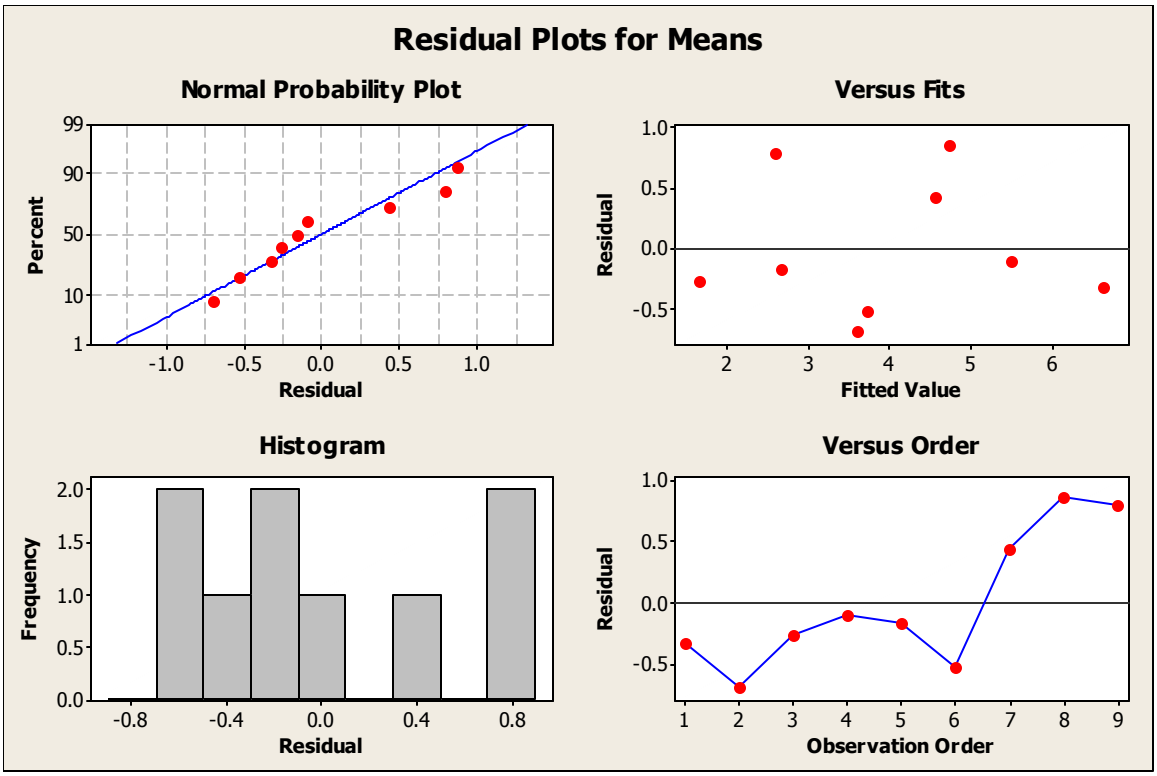

Figure 6.11: Residual Plot for Mean of Young's Modulus ($Ni_{50}Ti_{50}$)

Figure 6.10 represent the variation of Young's modulus after varying the remaining two process parameters i.e. sintering temperature and sintering time. Figure 6.11 gives the residual plots for young's modulus. It consists of some test for the verification of ANOVA. First test is normality test or normal distribution test, in which residuals fall on a straight line. This indicates that errors are normally distributed and verifies ANOVA. Another test is residual versus fitted value test, in which error must be randomly distributed. In Figure 6.11 all the errors are randomly distributed and ANOVA is good. Third Test is histogram and the last one is observation order or variance test. Both test indicates a good model and verifies ANOVA.

Optimal Setting for Young's Modulus (NiTi)

The optimum value of 'E' is predicted at the selected levels of significant variable Sintering temperature (B_3), and sintering time (C_3) (Table 6.21). The estimated mean of the response characteristic can be determined as:

$$\overline{\mu_E} = \overline{B_3} + \overline{C_3} - \overline{T} \qquad (5.6)$$

Where, $\overline{T}$ = overall mean of Young's Modulus = (∑R)/9 = 3.96 GPa

R values are taken from the Table 6.3 and the values of $\overline{B}_3$ and $(\overline{C}_3)$ are estimated from the experimental data reported in the Table 6.21.

$\overline{B}_3$ = average value of E at the third level of sintering temperature =2.667 GPa

$(\overline{C}_3)$= average value of σ at the third level of sintering time =2.967 GPa

Substituting the values of various terms in the above equation,

μ_E = 2.667+2.967- 3.96 = 1.674MPa

The 95 % confidence intervals of confirmation experiments (CI_{CE}) and population (CI_{POP}) are calculated as:

$$CI_{CE} = \sqrt{F_\alpha(1, f_e) V_e \left[\frac{1}{n_{eff}} + \frac{1}{R}\right]} \qquad \text{and} \qquad CI_{POP} = \sqrt{\frac{F_\alpha(1, f_e) V_e}{n_{eff}}}$$

Where, $F_\alpha(1, f_e)$ = The F ratio at the confidence level of (1-α) against DOF 1 and error degree of freedom f_e.

$$n_{eff} = \frac{N}{1 + [\text{DOF associated in the estimate of mean response}]} = 27 / (1+4) = 5.4$$

N = Total number of results = 27, R = Sample size for confirmation experiments = 3

V_e = Error variance = 0.6433; f_e = error DOF = 4 (Table 6.20)

$F_{0.05}(1, 4)$ = 7.71 (Tabulated F value (Ross, 1996))

So, CI_{CE} = ± 1.6 and CI_{POP} = ± 0.95

Therefore, the predicted confidence interval for confirmation experiments is:

$\mu_E - CI_{CE} < \mu_E < \mu_E + CI_{CE}$ i.e. $0.074 < \mu_E < 3.274$

The 95% confidence interval of the population is:

$\mu_E - CI_{POP} < \mu_E < \mu_E + CI_{POP}$ i.e. $0.724 < \mu_E < 2.624$

The optimal values of process variables at their selected levels are as follows:

(B_3) : 1150°C; C_3 : 60 min.

6.5 ANOVA for $Ni_{45}Ti_{50}Cu_5$

6.5.1 Analysis of Porosity in $Ni_{45}Ti_{50}Cu_5$

Table 6.22 and 6.23 give the ANOVA for raw data and S/N data of porosity. In both case the value of R-square and adjusted R-square is greater than 90%, which indicates that data retrieved from this analysis can explain greater than 90% variability. Standard error value is less as required for a good model. During the analysis (Table 6.22) it is found that sintering temperature had a major contribution of 40.98% preceded by sintering time (34.59%) and compaction pressure (23.87%). From Table 6.22 the effect of sintering temperature increased by ~ 4% upto 44.25%. Compaction pressure S/N value contribution remains constant at ~34%, while effect of compaction pressure in case of S/N value increased by ~13% and reached upto 23.87%.

Table 6.22: ANOVA for Means (Porosity)

Source	DF	SS	MS	F	P	p (%)
Compaction Pressure	2	184.222	92.111	43.63	0.022	23.87
Sintering Temperature	2	316.222	158.111	74.89	0.013	40.98
Sintering Time	2	266.889	133.444	63.21	0.016	34.59
Residual Error	2	4.222	2.111			0.55
Total	8	771.556	S = 1.453; R-Sq = 99.5%; R-Sq(adj) = 97.8%			

Table 6.23: Analysis of Variance for S/N ratios (Porosity)

Source	DF	SS	MS	F	P	p (%)
Compaction Pressure	2	9.6935	4.8468	11.34	0.081	10.17
Sintering Temperature	2	22.3669	11.1835	26.17	0.037	44.25
Sintering Time	2	17.6256	8.8128	20.62	0.046	34.87
Residual Error	2	0.8547	0.4274			1.69
Total	8	50.5408	S = 0.6537; R-Sq = 98.3%; R-Sq(adj) = 93.2%			

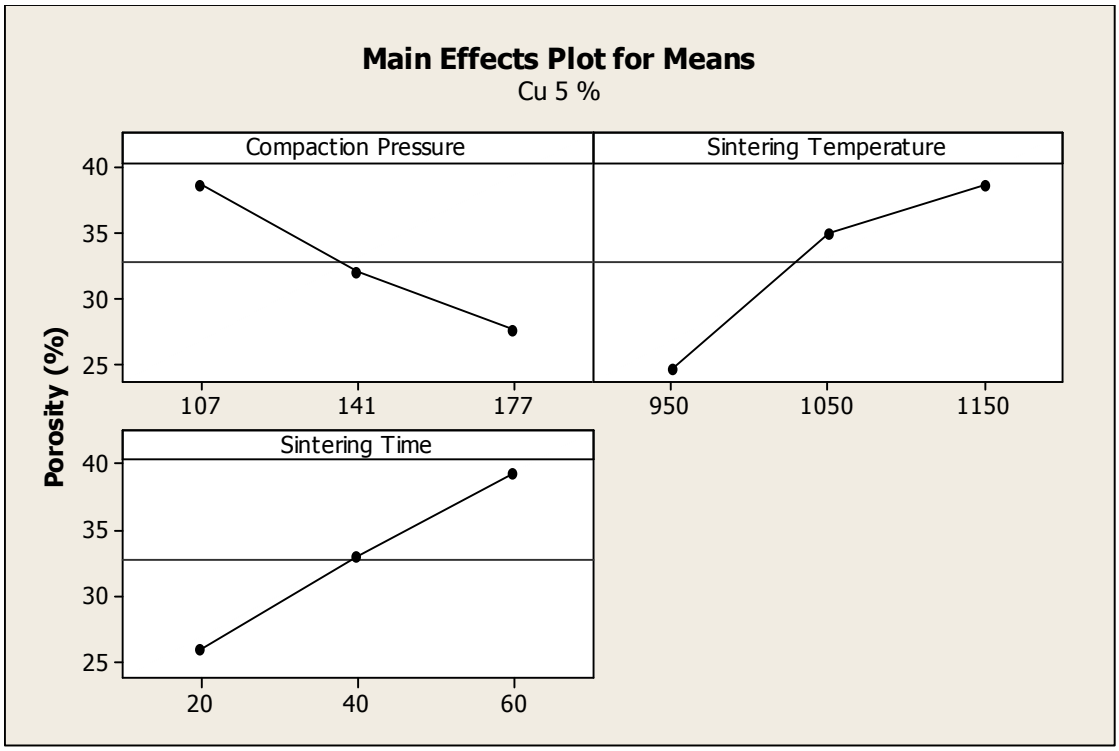

Figure 6.12: Variation of Porosity with Process Parameters ($Ni_{45}Ti_{50}Cu_5$)

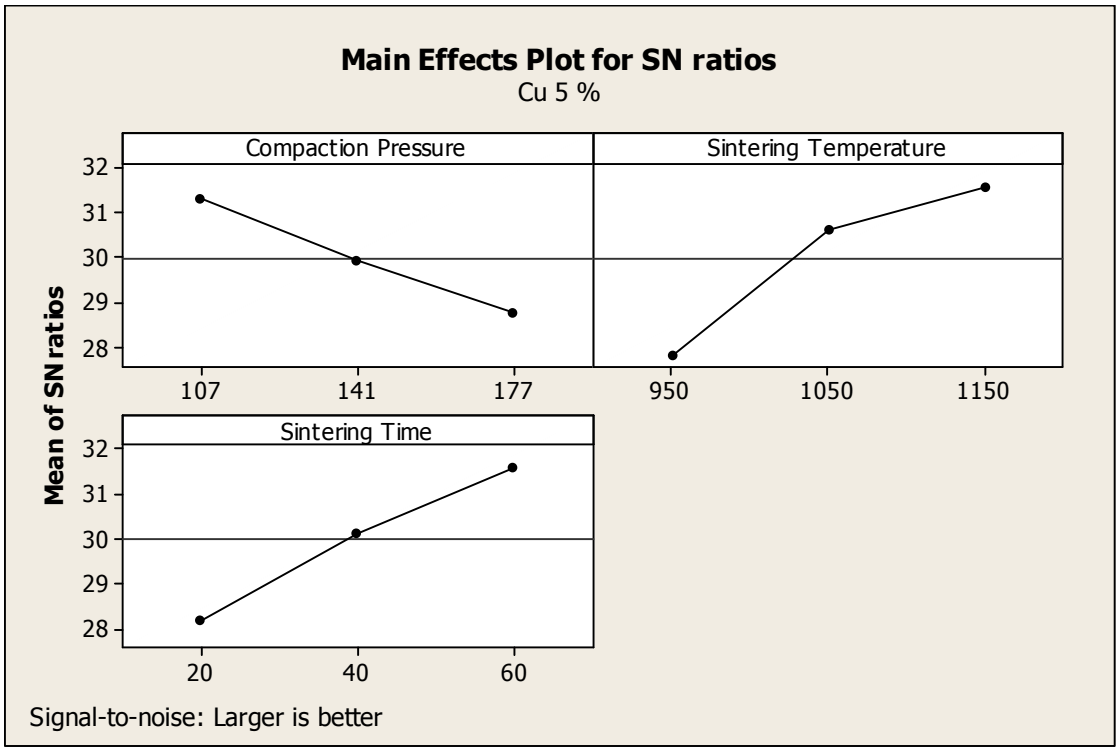

Figure 6.13: Variation of S/N ratio with Process Parameters ($Ni_{45}Ti_{50}Cu_5$)

Table 6.24: Response Table for Means (Porosity)

Level	Compaction Pressure	Sintering Temperature	Sintering Time
1	**38.67**	24.67	26.00
2	32.00	35.00	33.00
3	27.67	**38.67**	**39.33**
Delta	11.00	14.00	13.33
Rank	3	1	2

Table 6.25: Response Table for S/N Ratio (Porosity)

Level	Compaction Pressure	Sintering Temperature	Sintering Time
1	31.28	27.82	28.19
2	29.92	30.58	30.15
3	28.74	31.54	31.61
Delta	2.54	3.72	3.42
Rank	3	1	2

Figure 6.12 and 6.13 shows the variation of raw data and S/N data after 5% copper addition in NITi alloy at the cost of Ni element. In Figure 6.12, it is clear that with increase of compaction pressure, the porosity decrease from 38.67% to 27.67%. Porosity increased from 24.67% to 38.67% with the increase of Sintering temperature from level 1 (950°C) to level 3 (1150°C). Similarly porosity values enhanced from 26% to 39.33% with sintering time from level 1 (20min) to level 3 (60min). Same suggestions for optimum setting provided by Table 6.24 and 6.25.

Optimal Setting for Porosity ($Ni_{45}Ti_{50}Cu_5$)

The optimum value of porosity is predicted at the selected levels of significant variable compaction pressure (A_1), Sintering temperature (B_3), and sintering time (C_3) (Table 6.24). The estimated mean of the response characteristic can be determined as:

$$\overline{\mu_\sigma} = \overline{A_1} + \overline{B_3} + \overline{C_3} - 2\overline{T} \qquad (5.6)$$

Where, $\overline{T}$ = overall mean of Porosity = ($\sum$R)/9 = 32.77

R values are taken from the Table 6.4 and the values of $\overline{A_1}$, $\overline{B}_3$ and $\left(\overline{C_3}\right)$ are estimated from the experimental data reported in the Table 6.24.

$\overline{A}_1$ = average value of porosity at the first level of compaction pressure= 38.67

$\overline{B}_3$ = average value of porosity at the third level of sintering temperature =38.67

$\left(\overline{C_3}\right)$= average value of porosity at the third level of sintering time =39.33

Substituting the values of various terms in the above equation,

$\mu_{porosity}$ = 38.67+38.67+39.33- 2(32.77) = 51.13

The optimal values of process variables at their selected levels are as follows:

A_1 : 107MPa

(B_3) : 1150°C;

C_3 : 60 min.

6.5.2 Analysis of Compressive Strength in $Ni_{45}Ti_{50}Cu_5$

Table 6.26 shows ANOVA of compressive strength when 5% copper content is mixed with Ni and Ti in a rotary ball mill. It has been found from Table 6.26 that all three input process parameters play a significant role in the process i.e. P-value < 0.05 for all process parameters. The effect of compaction pressure increased and reaches upto 21.02%. Sintering temperature contains a major contribution (51.62%) followed by sintering time (26.98%) in the calculation of compressive strength. Table 6.27 gives the ANOVA for S/N values of $Ni_{45}Ti_{50}Cu_5$. It suggest that sintering temperature contains 36.39% contribution in the investigation of S/N values of compressive strength preceded by sintering temperature (29.27%) and compaction pressure (28.94%). In Table 6.26 and 6.27, value of R-square and adjusted R-square is greater than 75%, which indicates a good explanation of variability.

Table 6.26: ANOVA for Means (Compressive strength- $Ni_{45}Ti_{50}Cu_5$)

Source	DF	SS	MS	F	P	p (%)
Compaction Pressure	2	128115	64058	56.81	0.017	21.02
Sintering Temperature	2	314477	157239	139.45	0.007	51.62
Sintering Time	2	164373	82186	72.89	0.014	26.98
Residual Error	2	2255	1128			0.37
Total	8	609221	R-Sq = 99.6%; R-Sq(adj) = 98.5%			

Table 6.27: ANOVA for S/N ratios (Compressive strength- $Ni_{45}Ti_{50}Cu_5$)

Source	DF	SS	MS	F	P	p (%)
Compaction Pressure	2	104.14	52.071	5.70	0.149	28.94
Sintering Temperature	2	132.02	66.009	7.23	0.122	36.69
Sintering Time	2	105.32	52.659	5.76	0.148	29.27
Residual Error	2	18.27	9.134			5.07
Total	8	359.75	**S = 3.022; R-Sq = 94.9%; R-Sq(adj) = 79.7%**			

Figure 6.14 and 6.15 shows the variation of compressive strength and its S/N values with the process parameters i.e. compaction pressure, sintering temperature and sintering time. These follow the same pattern as follows in case of $Ni_{50}Ti_{50}$. Figure 6.16 shows the variation of compressive stress with the strain for experiment number 1 and 3 (i.e. maximum and minimum compressive stress). The validation experiment was also plotted on stress-stain diagram. Maximum compressive stress of 859.3 corresponds to 6.6GPa young's modulus, where 77.4MPa compressive stress obtained during third experimental run represent 2GPa young's modulus value.

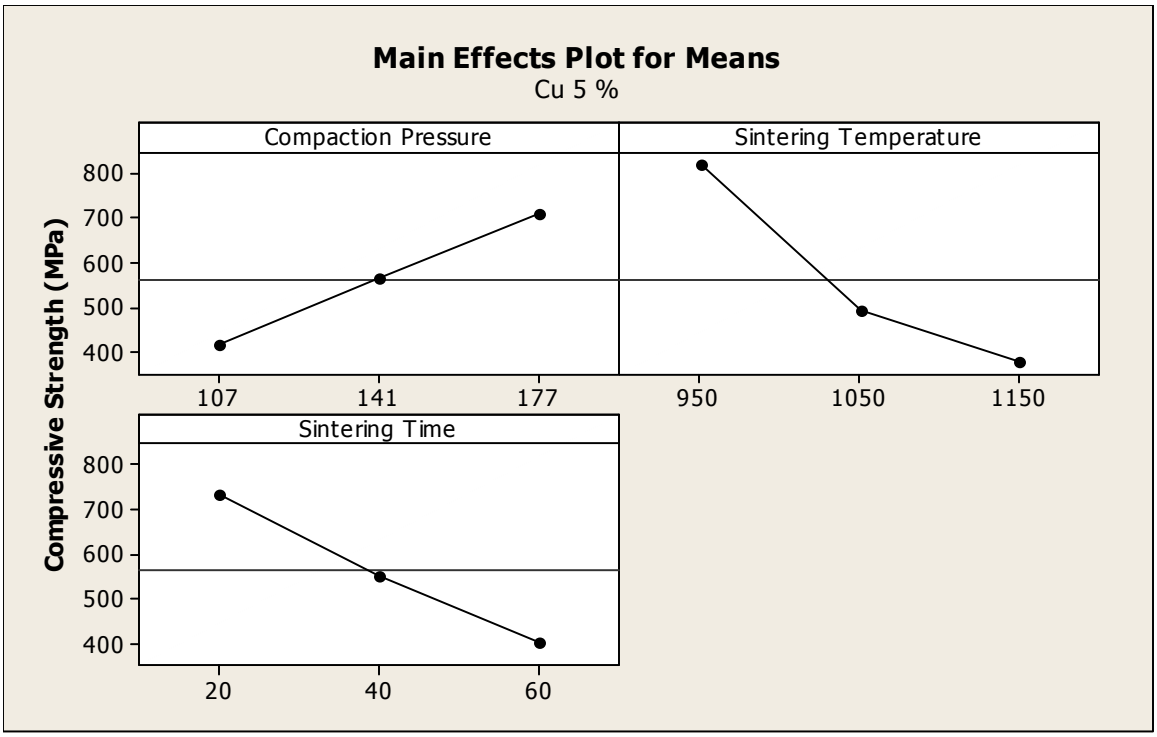

Figure 6.14: Variation of Compressive Strength ($Ni_{45}Ti_{50}Cu_5$)

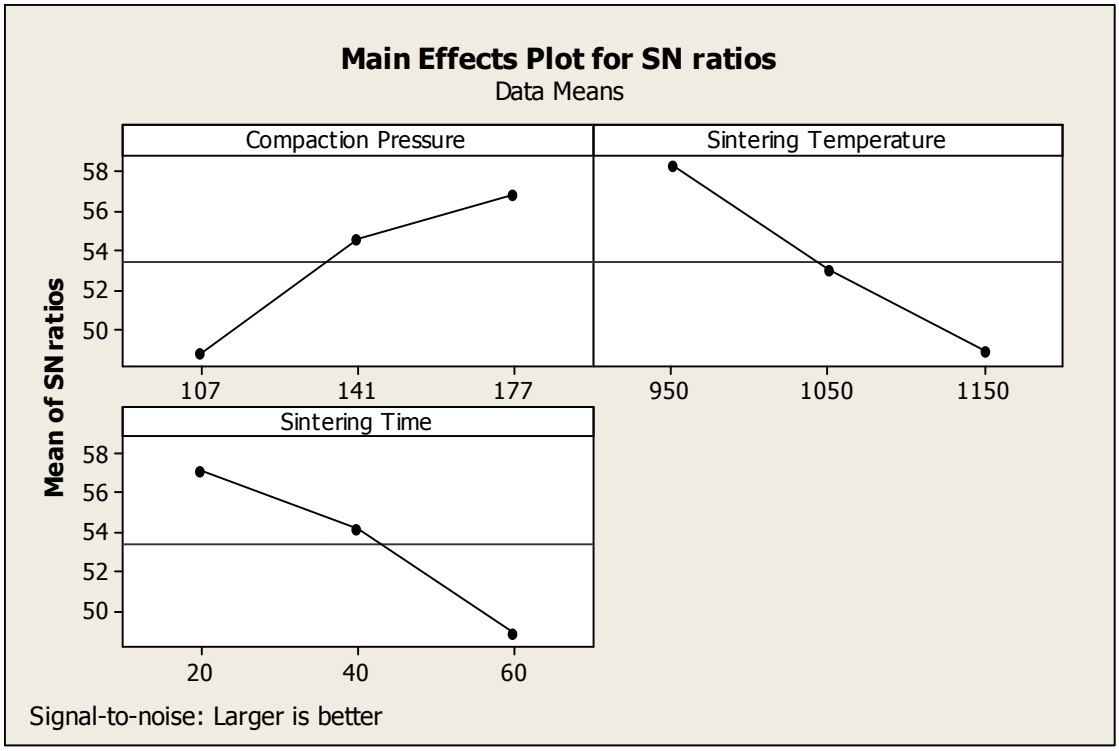

Figure 6.15: Variation of S/N ratio of Compressive Strength ($Ni_{45}Ti_{50}Cu_5$)

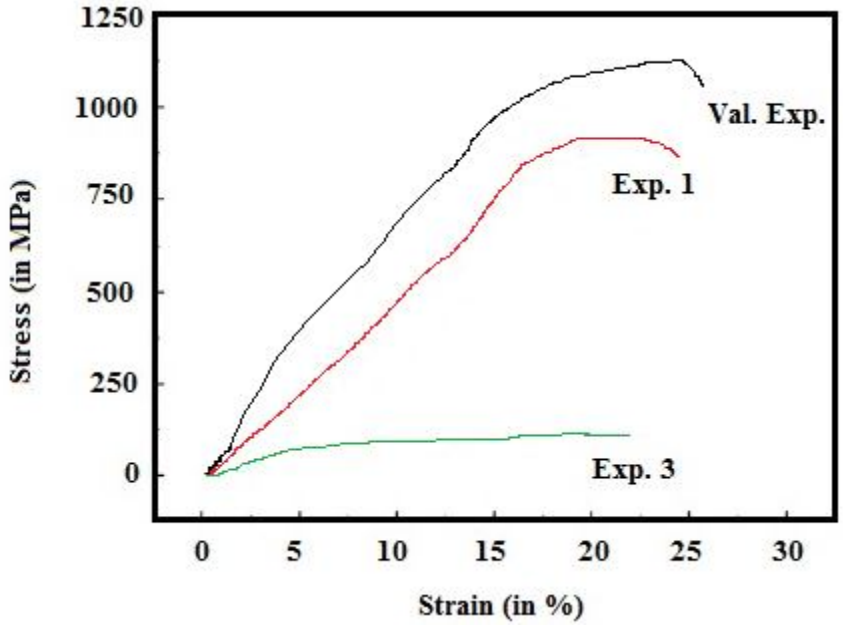

Figure 6.16: Stress-strain curve of $Ni_{45}Ti_{50}Cu_5$ for lowest, highest and validation Experiments

Table 6.28: Response Table for Means (Compressive strength- $Ni_{45}Ti_{50}Cu_5$)

Level	Compaction Pressure	Sintering Temperature	Sintering Time
1	415.3	**819.2**	**734.5**
2	566.1	491.0	550.3
3	**707.5**	378.6	404.2
Delta	292.2	440.6	330.3
Rank	3	1	2

Table 6.29: Response Table for S/N Ratios (Compressive strength- $Ni_{45}Ti_{50}Cu_5$)

Level	Compaction Pressure	Sintering Temperature	Sintering Time
1	48.75	58.26	57.13
2	54.55	52.97	54.15
3	56.84	48.91	48.86
Delta	8.08	9.35	8.27
Rank	3	1	2

Table 6.28 and 6.29 represent the response tables for mean values and S/N values of compressive strength in case of $Ni_{45}Ti_{50}Cu_5$. These Tables suggest the third level of compaction pressure, first level of sintering temperature and sintering time. Rank of process parameters are also same and are given in Table 6.28 and 6.29.

Optimal Setting for Compressive Strength ($Ni_{45}Ti_{50}Cu_5$)

The optimum value of 'E' is predicted at the selected levels of significant variable compaction pressure (A_1), Sintering temperature (B_1), and sintering time (C_1) (Table 6.28). The estimated mean of the response characteristic can be determined as:

$$\overline{\mu_\sigma} = \overline{A_3} + \overline{B_1} + \overline{C_1} - 2\overline{T} \qquad (5.6)$$

Where, $\overline{T}$ = overall mean of compressive strength = ($\sum$R)/9 = 562.96 MPa

R values are taken from the Table 6.4, and the values of $\overline{A}_3$, $\overline{B}_1$ and $\left(\overline{C_1}\right)$ are estimated from the experimental data reported in the Table 6.28.

$\overline{A}_3$ = average value of σ at the third level of compaction pressure = 707.5MPa

$\overline{B}_1$ = average value of σ at the first level of sintering temperature =819.2 MPa

$\left(\overline{C_1}\right)$= average value of σ at the first level of sintering time =734.5 MPa

Substituting the values of various terms in the above equation,

μ_σ = 707.5+819.2+734.5-2 (553.57) = 1135.28MPa

The optimal values of process variables at their selected levels are as follows:

(A_3) : 177MPa;

(B_1) : 950°C;

C_1 : 20 min.

6.5.3 Analysis of Young's Modulus in $Ni_{45}Ti_{50}Cu_5$

Table 6.30 gives the percentage contribution of input parameters for the investigation of young's modulus. The most significant process parameter is sintering temperature i.e. 58.59% preceding by sintering time (32.34%) and compaction pressure

(8.18%). Table 6.31 gives the ANOVA for S/N values of young's modulus in case of $Ni_{45}Ti_{50}Cu_5$. P-values for all process parameters are less than 0.05, which represent a significant contribution into the process. Sintering temperature play a major role (54.31%) followed by sintering time 34.38% and compaction pressure (11.28%). R-square and adjusted R-square also verified the test.

Table 6.30: ANOVA for Means (Young's Modulus- $Ni_{45}Ti_{50}Cu_5$)

Source	DF	SS	MS	F	P-value	p (%)
Compaction Pressure	2	1.5756	0.78778	9.33	0.097	8.18
Sintering Temperature	2	11.2822	5.64111	66.80	0.015	58.59
Sintering Time	2	6.2289	3.11444	36.88	0.026	32.34
Residual Error	2	0.1689	0.08444			0.87
Total	8	19.2556	R-Sq = 99.1%; R-Sq(adj) = 96.5%			

DF - degrees of freedom, SS - sum of squares, MS - mean squares (variance), F-ratio (variance of a source to variance of error), $P < 0.05$ - determines significance of a factor` at 95% confidence level, p - % contribution.

Table 6.31: Analysis of Variance for S/N ratio (Young's Modulus- $Ni_{45}Ti_{50}Cu_5$)

Source	DF	SS	MS	F	P	p (%)
Compaction Pressure	2	10.5071	5.2535	1059.37	0.001	11.28
Sintering Temperature	2	50.5650	25.2825	5098.20	0.000	54.31
Sintering Time	2	32.0163	16.0081	3228.03	0.000	34.38
Residual Error	2	0.0099	0.0050			0.01
Total	8	93.0983	S = 0.07042; R-Sq = 100.0%; R-Sq(adj) = 100.0%			

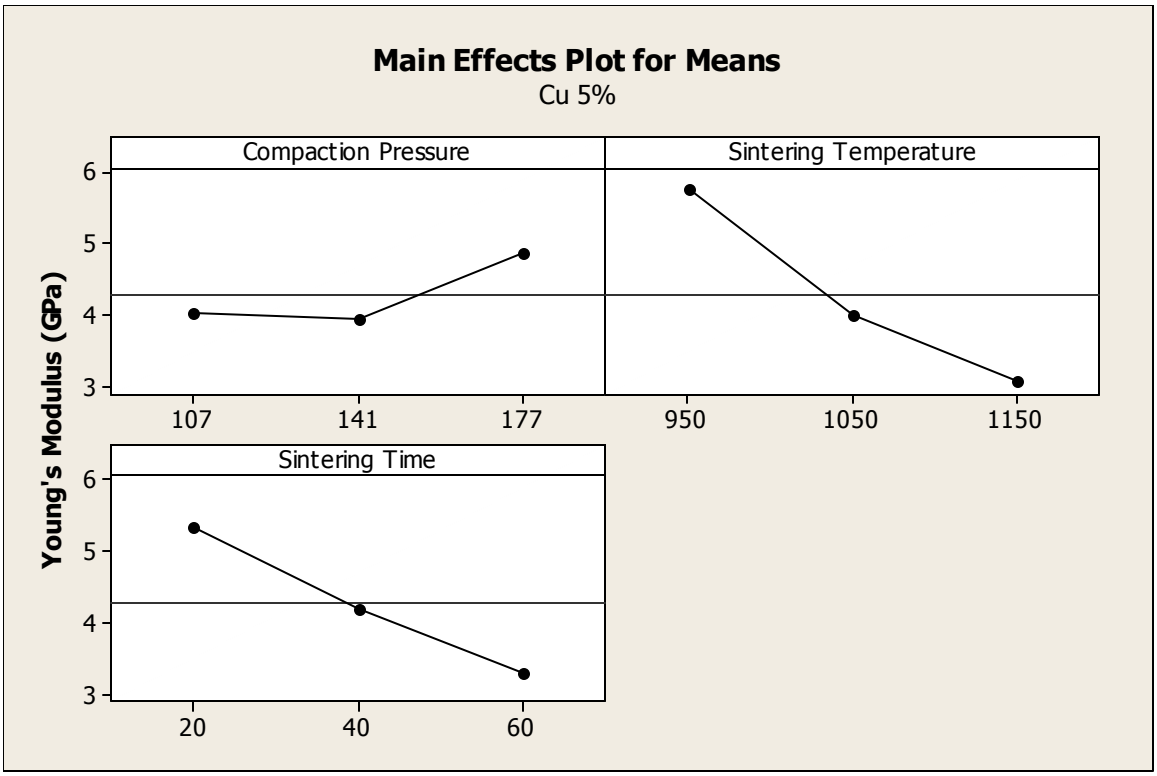

Figure 6.17: Variation of Young's Modulus with Process parameters ($Ni_{45}Ti_{50}Cu_5$)

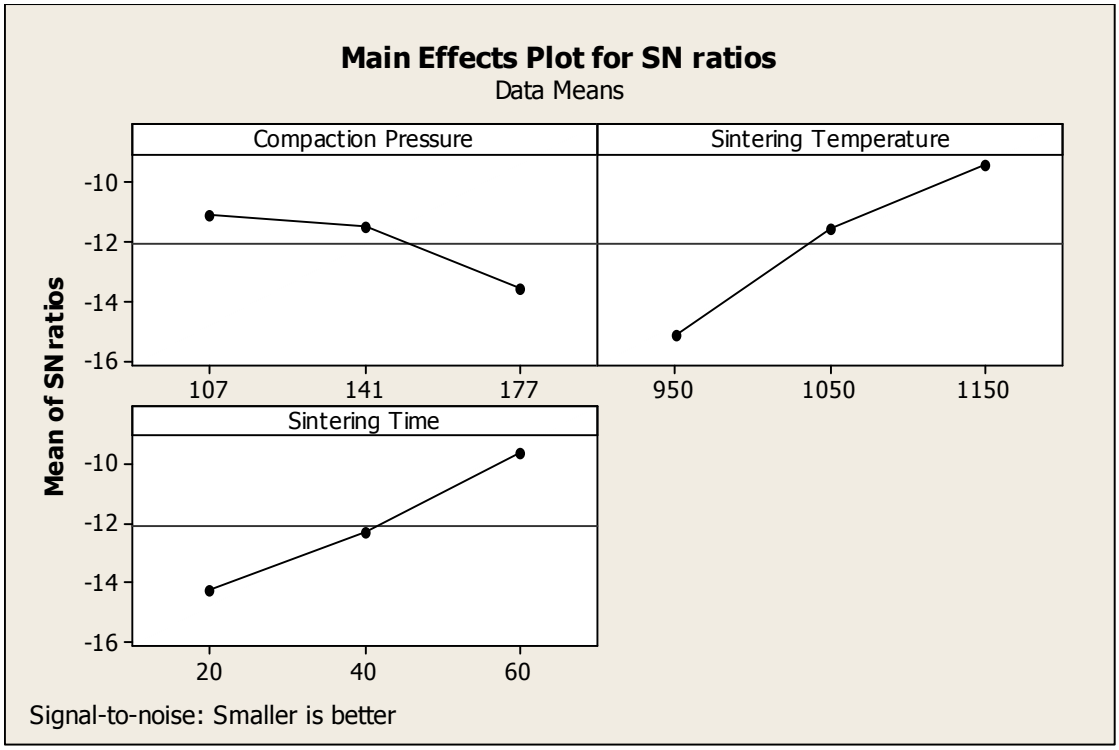

Figure 6.18: Variation of S/N ratio of Young's Modulus ($Ni_{45}Ti_{50}Cu_5$)

Figure 6.17 represent the variation young's modulus with the change of process parameters. It has been found that the young's modulus found to be decreased initially from 3kN to 4kN at an infinitesimal level (can be assumed constant) and then increased with the increase of compaction pressure from 4kN to 5kN. The probable reason for this is the adjustment of copper particle. In the initial stage copper particle comes as an ingredient in the material so young's modulus value found to be decrease from 4.033 GPa to 3.93GPa. But when compaction pressure further increase from 4kN to 5kN, then copper content sets in between the voids of NiTi particles and enhance the value of young's modulus from 3.067GPa to 4.867GPa. Higher value of sintering temperature (1150°C) favours the young's modulus (i.e. lowest young's modulus of 3.067GPa).Similarly larger sintering time (60min) favours to obtain smaller (i.e. 3.3 GPa) young's modulus. Figure 6.18 represent variations of S/N values with process parameters.

Table 6.32: Response Table for Means (Young's Modulus- $Ni_{45}Ti_{50}Cu_5$)

Level	Compaction Pressure	Sintering Temperature	Sintering Time
1	4.033	5.767	5.333
2	3.933	4.000	4.200
3	4.867	3.067	3.300
Delta	0.933	2.700	2.033
Rank	3	1	2

Table 6.33: Response Table for S/N Ratios (Young's Modulus- $Ni_{45}Ti_{50}Cu_5$)

Level	Compaction Pressure	Sintering Temperature	Sintering Time
1	-11.098	-15.173	-14.262
2	-11.520	-11.592	-12.272
3	-13.572	-9.424	-9.656
Delta	2.474	5.748	4.606
Rank	3	1	2

Table 6.32 and 6.33 represent the response table for mean values and S/N values. Both tables suggests the same ranking of process parameters i.e. sintering temperature affect the most for Young's modulus followed by sintering time and compaction pressure.

Table 6.34: Pooled ANOVA for Means (Young's Modulus)

Source	DF	SS	MS	F	P	p (%)
Sintering Temperature	2	11.282	5.6411	12.94	0.018	58.58
Sintering Time	2	6.229	3.1144	7.14	0.048	32.34
Residual Error	4	1.744	0.4361			9.05
Total	8	19.256				

Table 6.35: Response Table after pooling for Means

Level	Sintering Temperature	Sintering Time
1	5.767	5.333
2	4.000	4.200
3	**3.067**	**3.300**
Delta	2.700	2.033
Rank	1	2

Table 6.34 gives the pooled ANOVA for young's modulus after 5% copper addition in NiTi alloys. P-value in Table 6.34 is less than 0.05 and indicates that these parameters are significant at 95% confidence level. Table 6.35 gives response table after pooling the compaction pressure for the investigation of modulus value. Figure 6.19 represent the variation of modulus value with the change of significant process parameters. Figure 6.20 verifies ANOVA test viz. normal probability distribution, time-order study or variance test, histogram etc.

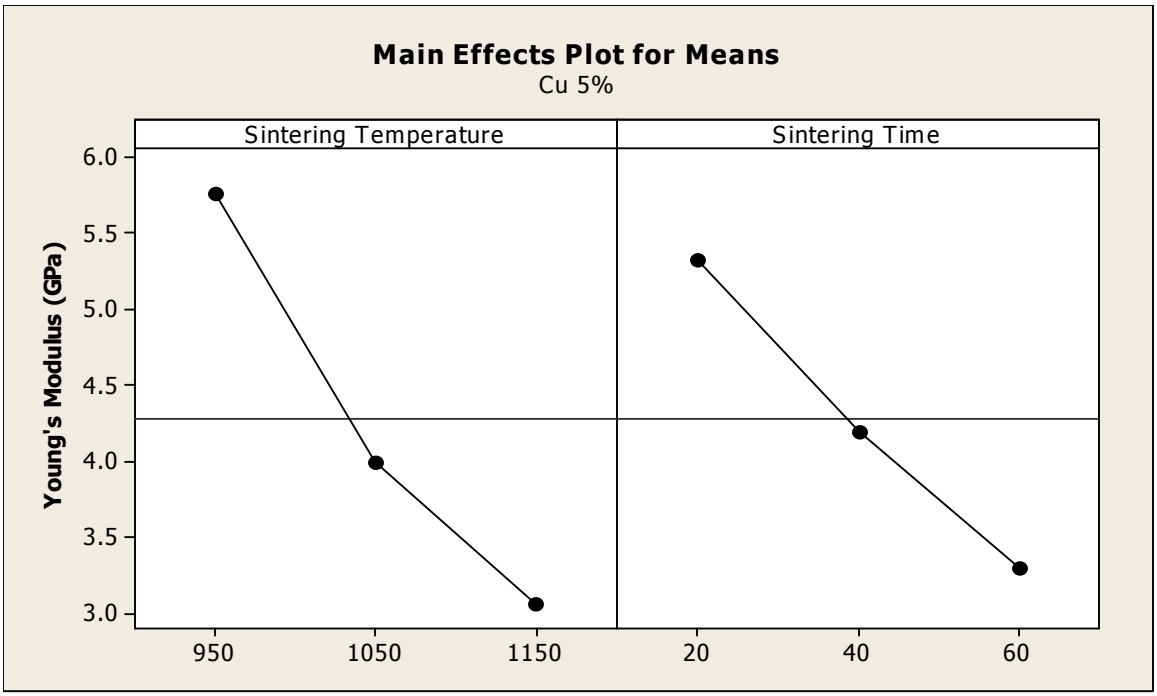

Figure 6.19: Variation of Young's Modulus with Process parameters ($Ni_{45}Ti_{50}Cu_5$)

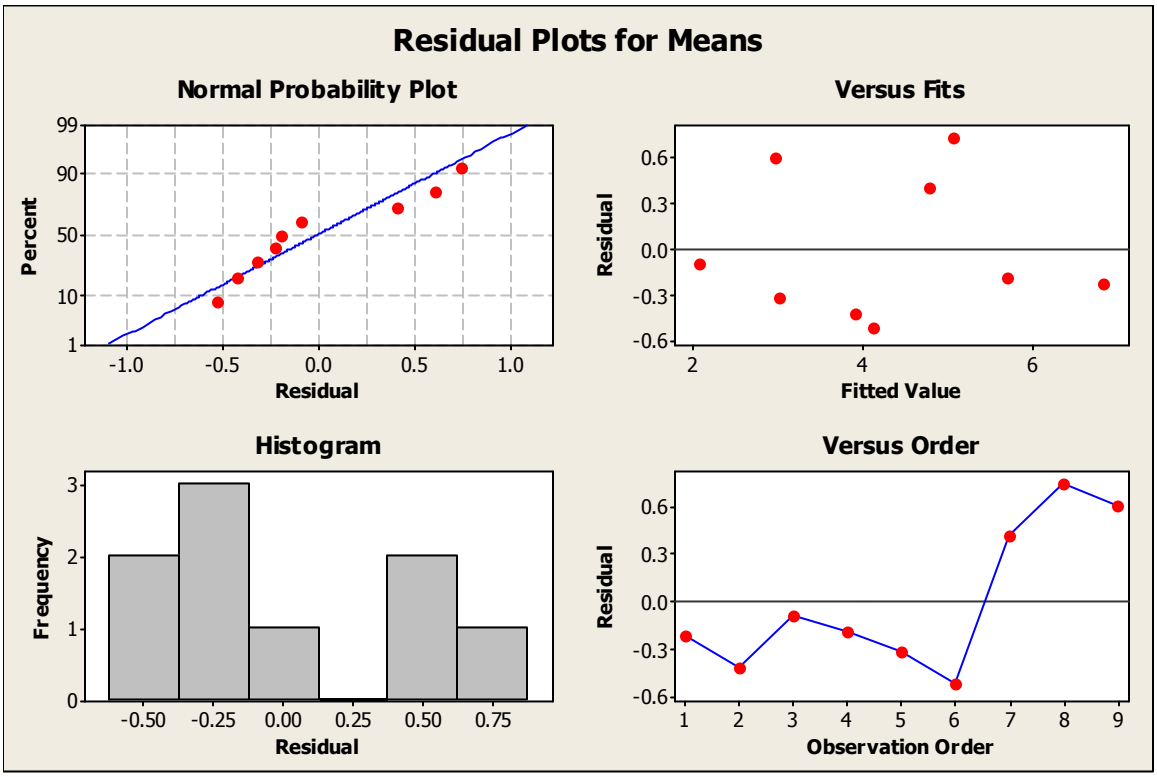

Figure 6.20: Residual Plots for Young's Modulus ($Ni_{45}Ti_{50}Cu_5$)

Optimal Setting for Young's Modulus ($Ni_{45}Ti_{50}Cu_5$)

The optimum value of 'E' is predicted at the selected levels of significant variable Sintering temperature (B_3), and sintering time (C_3) (Table 6.34). The estimated mean of the response characteristic can be determined as:

$$\overline{\mu_E} = \overline{B_3} + \overline{C_3} - \overline{T} \qquad (5.6)$$

Where, $\overline{T}$ = overall mean of Young's Modulus = ($\sum$R)/9 = 4.2 GPa

R values are taken from the Table 6.4 and the values of $\overline{B}_3$ and $(\overline{C_3})$ are estimated from the experimental data reported in the Table 6.34.

$\overline{B}_3$ = average value of E at the third level of sintering temperature =3.067 GPa

$(\overline{C_3})$= average value of σ at the third level of sintering time =3.300 GPa

Substituting the values of various terms in the above equation,

μ_E = 3.067+3.3- 4.2 = 2.167 GPa

The 95 % confidence intervals of confirmation experiments (CI_{CE}) and population (CI_{POP}) are calculated as:

$$CI_{CE} = \sqrt{F_\alpha(1, f_e) V_e \left[\frac{1}{n_{eff}} + \frac{1}{R}\right]} \qquad \text{and} \qquad CI_{POP} = \sqrt{\frac{F_\alpha(1, f_e) V_e}{n_{eff}}}$$

Where, $F_\alpha(1, f_e)$ = The F ratio at the confidence level of (1-α) against DOF 1 and error degree of freedom f_e.

$$n_{eff} = \frac{N}{1 + [\text{DOF associated in the estimate of mean response}]} = 27 / (1+4) = 5.4$$

N = Total number of results = 27, R = Sample size for confirmation experiments = 3

V_e = Error variance = 0.4361; f_e = error DOF = 4 (Table 6.34)

$F_{0.05}(1, 4)$ = 7.71 (Tabulated F value (Ross, 1996))

So, CI_{CE} = ± 1.32 and CI_{POP} = ± 0.78

Therefore, the predicted confidence interval for confirmation experiments is:

$\mu_E - CI_{CE} < \mu_E < \mu_E + CI_{CE}$ i.e. $0.847 < \mu_E < 3.487$

The 95% confidence interval of the population is:

$\mu_E - CI_{POP} < \mu_E < \mu_E + CI_{POP}$ i.e. $1.387 < \mu_E < 2.947$

The optimal values of process variables at their selected levels are as follows:

(B_3) : 1150°C;

C_3 : 60 min.

6.6 ANOVA FOR $Ni_{40}Ti_{50}Cu_{10}$

6.6.1 Analysis of Porosity in $Ni_{40}Ti_{50}Cu_{10}$

Table 6.36 and 6.37 reports the ANOVA for mean and S/N ratio of porosity for Ni.

Table 6.36: Analysis of Variance for Means (Porosity- $Ni_{40}Ti_{50}Cu_{10}$)

Source	DF	SS	MS	F	P	p (%)
Compaction Pressure	2	219.556	109.778	26.70	0.036	34.15
Sintering Temperature	2	213.556	106.778	25.97	0.037	33.21
Sintering Time	2	201.556	100.778	24.51	0.039	31.35
Residual Error	2	8.222	4.111			1.27
Total	8	642.889	**S = 2.028 R-Sq = 98.7% R-Sq(adj) = 94.9%**			

Table 6.37: Analysis of Variance for S/N ratios (Porosity- $Ni_{40}Ti_{50}Cu_{10}$)

Source	DF	SS	MS	F	P	p (%)
Compaction Pressure	2	11.6394	5.8197	48.65	0.020	33.98
Sintering Temperature	2	11.3727	5.6863	47.53	0.021	33.21
Sintering Time	2	10.9956	5.4978	45.96	0.021	32.11
Residual Error	2	0.2392	0.1196			0.7
Total	8	34.2469	**S = 0.3459; R-Sq = 99.3% ; R-Sq(adj) = 97.2%**			

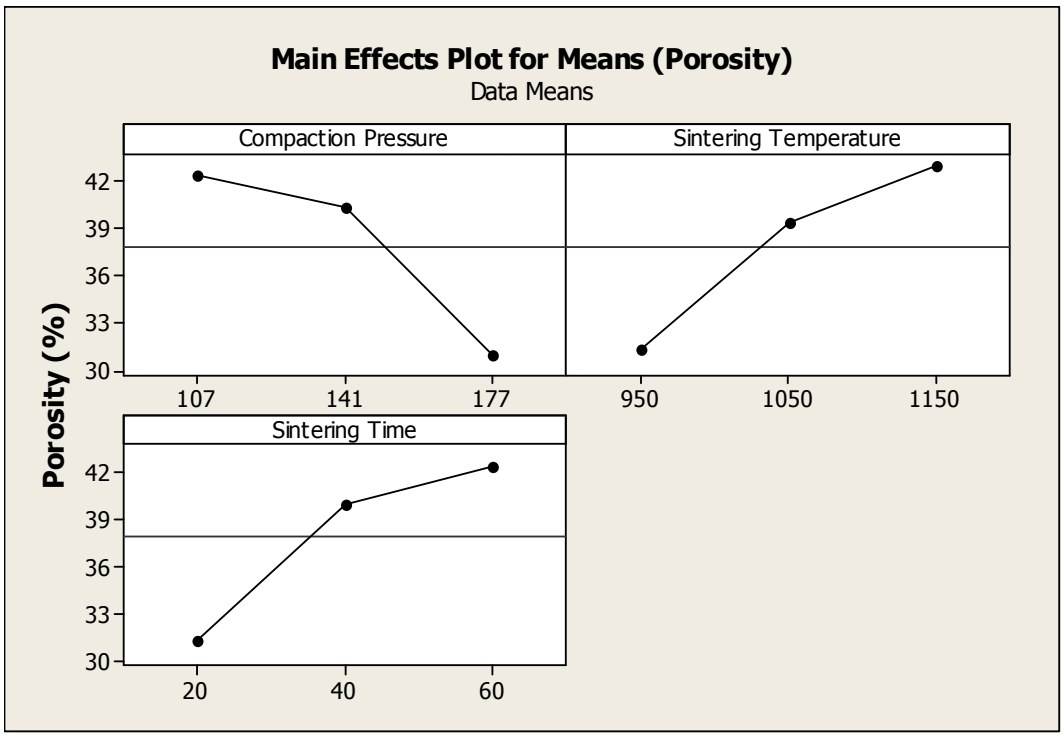

Figure 6.21: Variation of Means for Porosity ($Ni_{40}Ti_{50}Cu_{10}$)

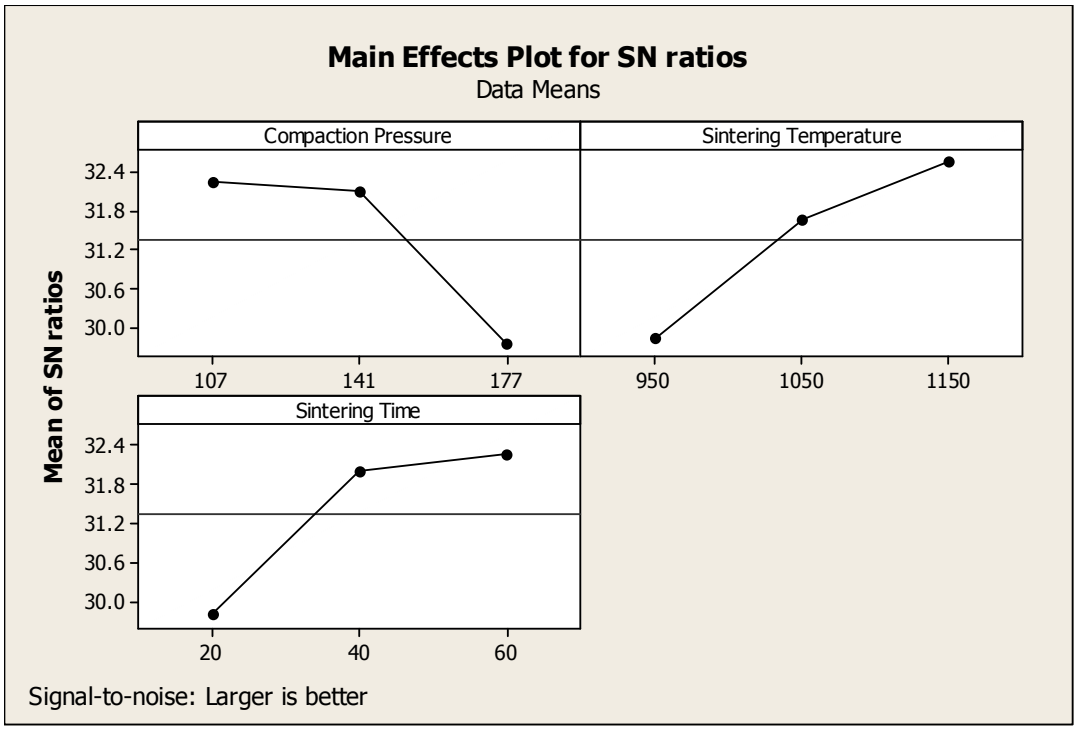

Figure 6.22: Variation of S/N ratio for Porosity ($Ni_{40}Ti_{50}Cu_{10}$)

Both of this analysis represent that all the process parameters had significant contribution in the investigation of porosity i.e. P-value is less than 0.05 in Table 6.36 and 6.37. All the parameters had approximately equal contribution (varies from 31% to 34%) in these analysis. Standard error is lower, while R-square and adjusted R-square is greater than 90%, which characterize a symbol of good results.

Figure 6.21 and 6.22 shows that lower value of compaction pressure, higher values of sintering temperature and sintering time favours a more porous structure. Increase in compaction pressure decreases the porosity due to removal of voids in powder particles. Results suggested by Figure 6.22 also aligned as obtained from Figure 6.21.

Table 6.38: Response Table for Means (Porosity- $Ni_{40}Ti_{50}Cu_{10}$)

Level	Compaction Pressure	Sintering Temperature	Sintering Time
1	**42.33**	31.33	31.33
2	40.33	39.33	40.00
3	31.00	**43.00**	**42.33**
Delta	11.33	11.67	11.00
Rank	2	1	3

Table 6.39: Response Table for Signal to Noise Ratios (Porosity- $Ni_{40}Ti_{50}Cu_{10}$)

Level	Compaction Pressure	Sintering Temperature	Sintering Time
1	32.23	29.85	29.80
2	32.08	31.65	31.99
3	29.75	32.56	32.27
Delta	2.48	2.71	2.47
Rank	2	1	3

Table 6.38 and 6.39 described the response table for mean values and S/N values of porosity in $Ni_{40}Ti_{50}Cu_{10}$. This states that at level 1 of compaction pressure porosity is

maximum (42.33%), which decreases with increasing compaction pressure at level 3 and becomes equal to 31%. At third level of sintering temperature porosity is maximum (43%), while at level 1 its value is 31.33%. Similarly level 1 of sintering time gives porosity equal to 31.33% and its value increases upto 42.33% at level 3.

Optimal Setting for Porosity ($Ni_{40}Ti_{50}Cu_{10}$)

The optimum value of porosity is predicted at the selected levels of significant variable compaction pressure (A_1), Sintering temperature (B_3), and sintering time (C_3) (Table 6.38). The estimated mean of the response characteristic can be determined as:

$$\overline{\mu_\sigma} = \overline{A_1} + \overline{B_3} + \overline{C_3} - 2\overline{T} \qquad (5.6)$$

Where, $\overline{T}$ = overall mean of Porosity = $(\sum R)/9 = 37.89$

R values are taken from the Table 6.5 and the values of $\overline{B}_3$ and $\left(\overline{C_3}\right)$ are estimated from the experimental data reported in the Table 6.38.

$\overline{A}_1$ = average value of porosity at the first level of compaction pressure = 42.33

$\overline{B}_3$ = average value of porosity at the third level of sintering temperature =43

$\left(\overline{C_3}\right)$= average value of porosity at the third level of sintering time =42.33

Substituting the values of various terms in the above equation,

$\mu_{porosity}$ = 42.33+43+42.33-2(37.89) = 51.88

The optimal values of process variables at their selected levels are as follows:

A_1 : 107MPa

(B_3) : 1150°C;

C_3 : 60 min.

6.6.2 Analysis of Compressive Strength in $Ni_{40}Ti_{50}Cu_{10}$

Table 6.40 gives ANOVA (mean values) of compressive strength for $Ni_{40}Ti_{50}Cu_{10}$. All three process parameter are significant as P-value is lower than 0.05.

Sintering temperature consist a significant contribution of 51.60% in compressive strength preceded by sintering time (27.21%) and compaction pressure (20.78%). Table 6.41 gives ANOVA for S/N values of compressive strength. This table gives the percentage contribution of process parameters into the investigation of S/N values for compressive strength and follows the patterns as sintering temperature – 37.34%; sintering time – 29.33% and compaction pressure 29.70%. R-square, adjusted R-square and standard error in Table 5.30 and 5.31 gives a sign of good model or data.

Table 6.40: ANOVA for Means (Compressive Strength- $Ni_{40}Ti_{50}Cu_{10}$)

Source	DF	SS	MS	F	P	p (%)
Compaction Pressure	2	126145	63072	53.10	0.018	20.78
Sintering Temperature	2	313133	156566	131.82	0.008	51.60
Sintering Time	2	165139	82569	69.52	0.014	27.21
Residual Error	2	2375	1188			0.39
Total	8	606792	**R-Sq = 99.6% ; R-Sq(adj) = 98.4%**			

DF - degrees of freedom, SS - sum of squares, MS - mean squares (variance), F-ratio (variance of a source to variance of error), $P < 0.05$ - determines significance of a factor` at 95% confidence level, p - % contribution.

Table 6.41: Analysis of Variance for S/N ratio (Compressive Strength- $Ni_{40}Ti_{50}Cu_{10}$)

Source	DF	SS	MS	F	P	p (%)
Compaction Pressure	2	93.75	46.875	6.09	0.141	28.70
Sintering Temperature	2	121.64	60.821	7.90	0.112	37.34
Sintering Time	2	95.79	47.893	6.22	0.138	29.33
Residual Error	2	15.40	7.698			4.7
Total	8	326.57	**S = 2.775; R-Sq = 95.3%; R-Sq(adj) = 81.1%**			

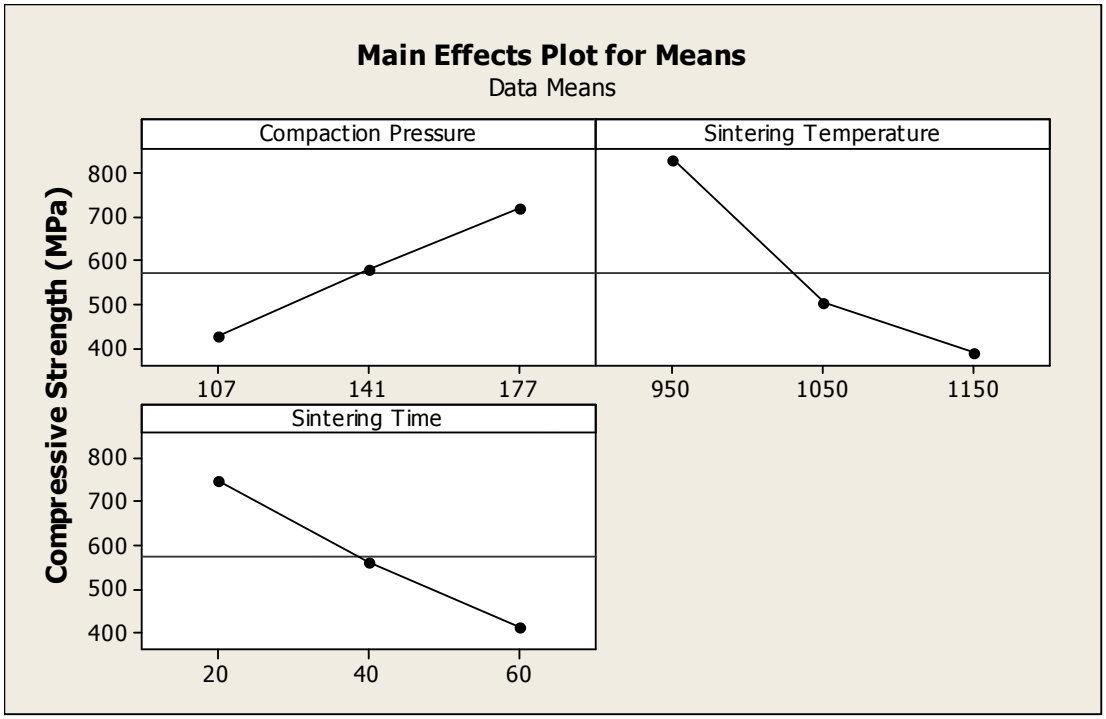

Figure 6.23: Variation of Compressive Strength ($Ni_{40}Ti_{50}Cu_{10}$)

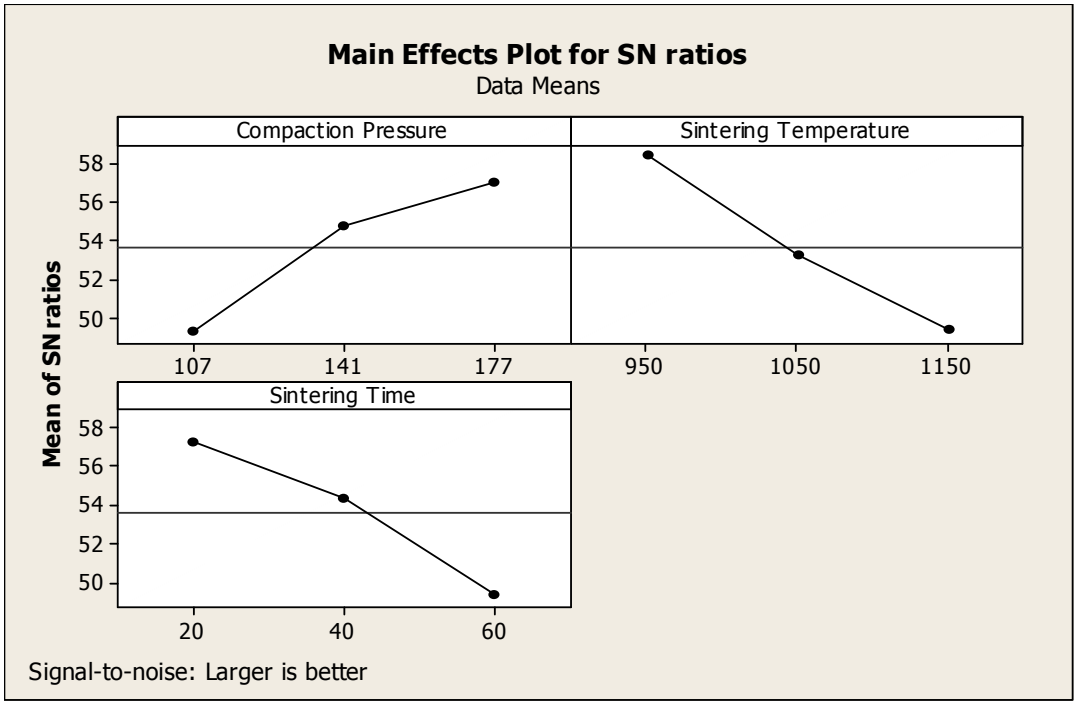

Figure 6.24: Variation of S/N ratio of Compressive Strength ($Ni_{40}Ti_{50}Cu_{10}$)

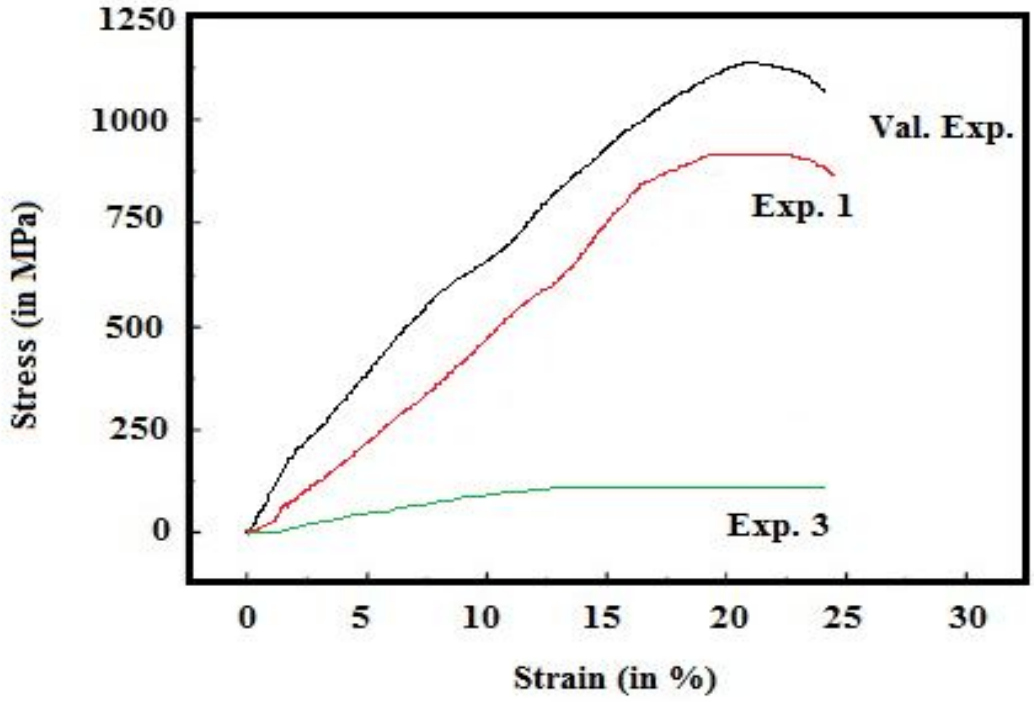

Figure 6.25: Stress-strain curve of $NiTiCu_{10}$ for lowest, highest and validation Experiments

Figure 6.23 shows that compressive strength of green compact increases 426.6MPa to 716.5MPa with the increase of compaction pressure from 107MPa to 177MPa. The main factor behind this increment is the bonding of particle with each-other by the increase of the load during compacting. Similarly higher sintering temperature and higher sintering time favours the compressive strength. Figure 6.24 represent the variation of parameter with the S/N value of compressive strength. Figure 6.25 shows the stress-strain graph for $Ni_{50}Ti_{40}Cu_{10}$. At different settings of process parameters along with the optimized setting for maximum compressive stress. It has been found that the addition of copper enhance the compressive strength of NiTi shape memory alloys.

Response table of mean data and S/N values (in Table 6.42 and 6.43) for compressive strength are reported for "Larger the better" type quality characteristics. Both tables suggest the same optimal setting for highest value of compressive strength.

The order of process parameters affecting the process response suggested by Table 6.42 and 6.43 is same as suggested by ANOVA Tables 6.40 and 6.41.

Table 6.42: Response Table for Means (Compressive Strength- $Ni_{40}Ti_{50}Cu_{10}$)

Level	Compaction Pressure	Sintering Temperature	Sintering Time
1	426.6	**828.8**	**745.4**
2	576.7	502.1	560.0
3	**716.5**	388.9	414.4
Delta	289.9	440.0	331.0
Rank	3	1	2

Table 6.43: Response Table for S/N Ratios (Compressive Strength- $Ni_{40}Ti_{50}Cu_{10}$)

Level	Compaction Pressure	Sintering Temperature	Sintering Time
1	49.27	58.36	57.26
2	54.74	53.21	54.34
3	56.95	49.39	49.36
Delta	7.68	8.97	7.90
Rank	3	1	2

Optimal Setting for Compressive Strength ($Ni_{40}Ti_{50}Cu_{10}$)

The optimum value of 'σ' is predicted at the selected levels of significant variable compaction pressure (A_1), Sintering temperature (B_1), and sintering time (C_1) (Table 6.42). The estimated mean of the response characteristic can be determined as:

$$\overline{\mu_\sigma} = \overline{A_3} + \overline{B_1} + \overline{C_1} - 2\overline{T} \qquad (5.6)$$

Where, $\overline{T}$ = overall mean of compressive strength = (∑R)/9 = 573.27 MPa

R values are taken from the Table 6.5, and the values of $\overline{A}_3$, $\overline{B}_1$ and $\left(\overline{C_1}\right)$ are estimated from the experimental data reported in the Table 6.42.

$\overline{A}_3$ = average value of σ at the third level of compaction pressure = 716.5MPa

$\overline{B}_1$ = average value of σ at the first level of sintering temperature =828.8 MPa

$\left(\overline{C}_1\right)$= average value of σ at the first level of sintering time =745.4 MPa

Substituting the values of various terms in the above equation,

μ_σ = 716.5+828.8+745.4-2 (573.27) = 1144.16MPa

The optimal values of process variables at their selected levels are as follows:

(A_3) : 177MPa;

(B_1) : 950°C;

C_1 : 20 min.

6.6.3 Analysis of Young's Modulus in $Ni_{40}Ti_{50}Cu_{10}$

Table 6.44 and 6.45 gives analysis of variance for mean values and S/N values of young's modulus after 10% copper addition into NiTi alloy. Sintering temperature had a major role (62.35%) in young's modulus investigation followed by sintering time (31.01%) and compaction pressure (5.49%). Also P-value in compaction pressure is greater than 0.05, which indicates that compaction pressure is a non-significant term for $Ni_{40}Ti_{50}Cu_{10}$. Table 6.45 is ANOVA table for S/N value. This Table suggests that all parameter are significant with P-value less than 0.05. R-square, adjusted R-square and 'S' represent a good sign of results.

Table 6.44: ANOVA for Means (Young's Modulus- $Ni_{40}Ti_{50}Cu_{10}$)

Source	DF	SS	MS	F	P	p (%)
Compaction Pressure	2	1.0689	0.5344	4.81	0.172	5.49
Sintering Temperature	2	12.1356	6.0678	54.61	0.018	62.35
Sintering Time	2	6.0356	3.0178	27.16	0.036	31.01
Residual Error	2	0.2222	0.1111			1.14
Total	8	19.4622	R-Sq = 98.9% ; R-Sq(adj) = 95.4%			

Table 6.45: ANOVA for S/N ratios (Young's Modulus- $Ni_{40}Ti_{50}Cu_{10}$)

Source	DF	SS	MS	F	P	p (%)
Compaction Pressure	2	6.5657	3.2829	90.09	0.011	8.38
Sintering Temperature	2	46.2169	23.1084	634.12	0.002	59.05
Sintering Time	2	25.4072	12.7036	348.60	0.003	32.46
Residual Error	2	0.0729	0.0364			0.09
Total	8	78.2626	S = 0.1909; R-Sq = 99.9%; R-Sq(adj) = 99.6%			

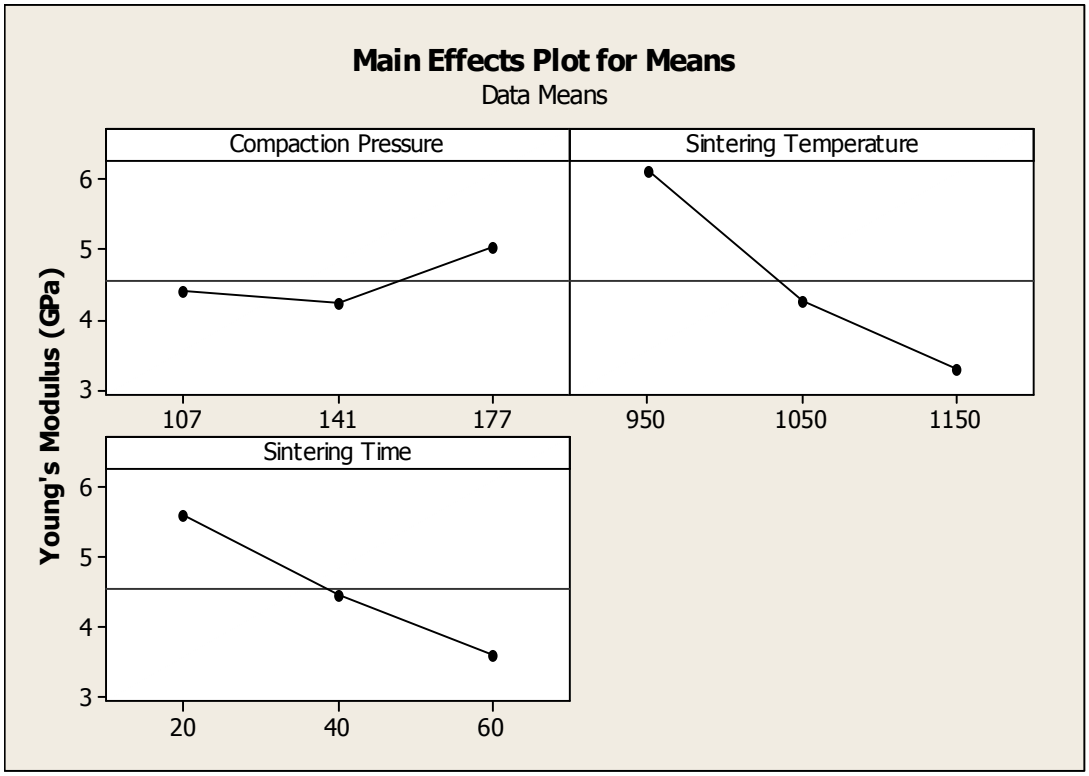

Figure 6.26: Variation of Young's Modulus with Process parameters ($Ni_{40}Ti_{50}Cu_{10}$)

Figure 6.26 and 6.27 represents the variation of young's modulus with the variation of process parameters for 10% of copper content. Young's modulus first decreases slightly from 4.4GPa to 4.2GPa and then increases upto 5.03GPa with the increase of compaction pressure. The favorable conditions for the lower value of young's modulus are higher sintering temperature and time. The reasons of these variations are already cited in the previous text.

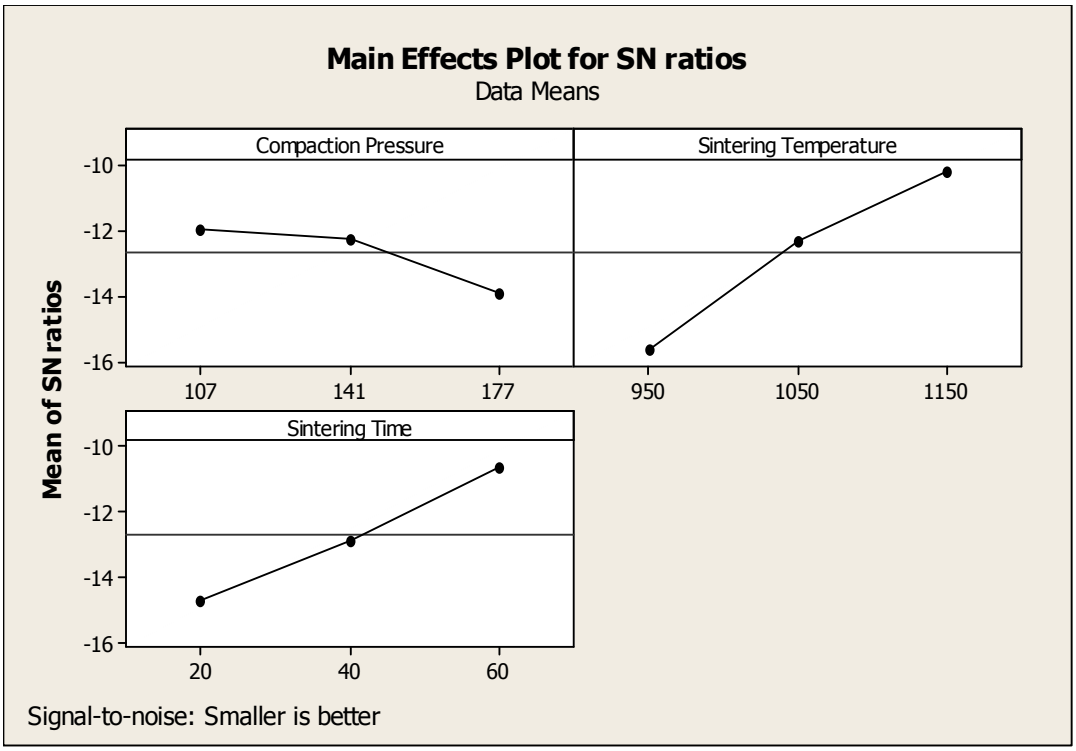

Figure 6.27: Variation of S/N ratio of Young's Modulus ($Ni_{40}Ti_{50}Cu_{10}$)

Table 6.46: Response Table for Means (Young's Modulus- $Ni_{40}Ti_{50}Cu_{10}$)

Level	Compaction Pressure	Sintering Temperature	Sintering Time
1	4.400	6.100	5.600
2	4.233	4.267	4.467
3	5.033	3.300	3.600
Delta	0.800	2.800	2.000
Rank	3	1	2

Table 6.46 and 6.47 reported the response values of mean and S/N data for young's modulus after 10% copper addition in NiTi alloy i.e. $Ni_{40}Ti_{50}Cu_{10}$. During S/N values evaluation, always "larger the better" type quality characteristics is considered whether the response is either "larger the better" or "lower the best" type quality characteristics. Both tables results the same settings of process parameters to gain the optimum (lower) value of Young's modulus.

Table 6.47: Response Table for S/N Ratio (Young's Modulus- $Ni_{40}Ti_{50}Cu_{10}$)

Level	Compaction Pressure	Sintering Temperature	Sintering Time
1	-11.95	-15.65	-14.68
2	-12.23	-12.28	-12.82
3	-13.89	-10.14	-10.57
Delta	1.94	5.51	4.11
Rank	3	1	2

Table 6.48: Pooled ANOVA for Means (Young's Modulus- $Ni_{40}Ti_{50}Cu_{10}$)

Source	**DF**	**SS**	**MS**	**F**	**P**	**p (%)**
Sintering Temperature	2	12.136	6.0678	18.80	0.009	62.35
Sintering Time	2	6.036	3.0178	9.35	0.031	31.01
Residual Error	4	1.291	0.3228			6.63
Total	8	19.462				

Table 6.49: Response Table for Means (Young's Modulus- $Ni_{40}Ti_{50}Cu_{10}$)

Levels	**Sintering Temperature**	**Sintering Time**
1	6.100	5.600
2	4.267	4.467
3	**3.300**	**3.600**
Delta	2.800	2.000
Rank	1	2

Table 6.48 reports the pooled ANOVA for young's modulus in case of $Ni_{40}Ti_{50}Cu_{10}$. P-value in Table 6.48 is less than 0.05 and indicates that these parameters are significant at 95% confidence level. Table 6.49 gives response table after pooling the compaction pressure for the investigation of modulus value. Figure 6.28 represent the variation of modulus value with the change of sintering temperature and time. Figure 6.29 verifies ANOVA by normal probability distribution test, time-order study or variance test, histogram test and residual versus fitted value test.

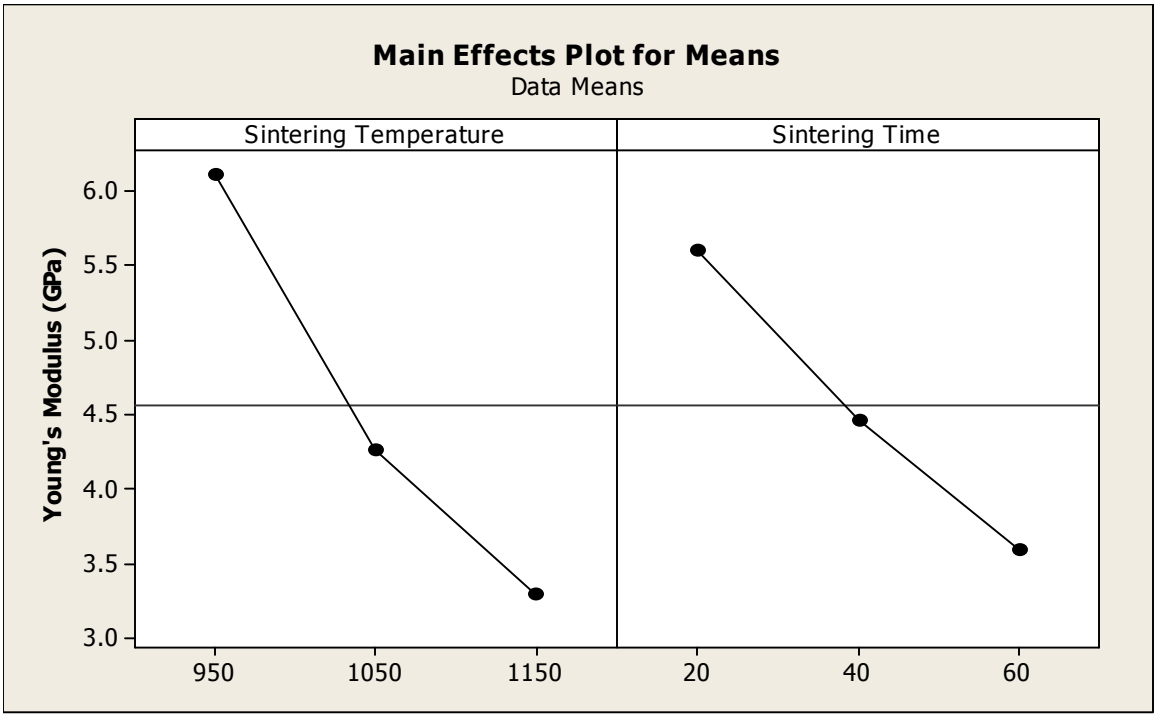

Figure 6.28: Variation of Young's Modulus with Process parameters ($Ni_{40}Ti_{50}Cu_{10}$)

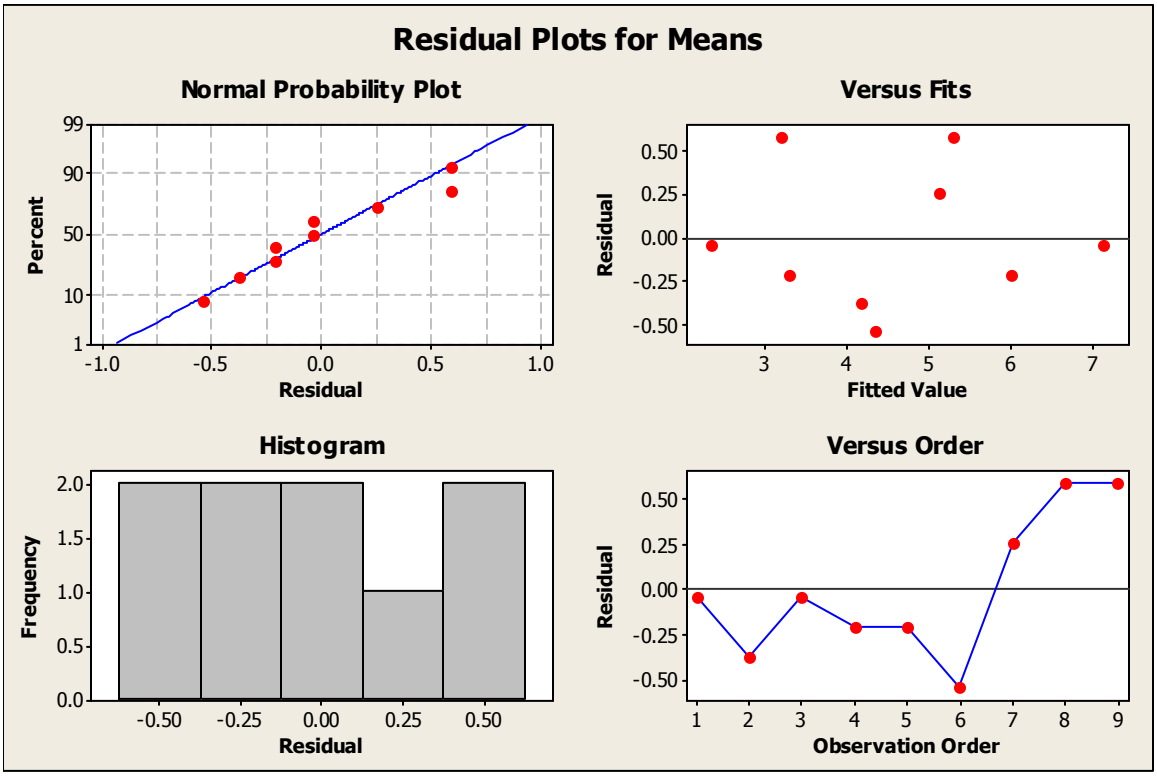

Figure 6.29: Residual Plots for Young's Modulus ($Ni_{40}Ti_{50}Cu_{10}$)

Optimal Setting for Young's Modulus ($Ni_{40}Ti_{50}Cu_{10}$)

The optimum value of 'E' is predicted at the selected levels of significant variable Sintering temperature (B_3), and sintering time (C_3) (Table 6.49). The estimated mean of the response characteristic can be determined as:

$$\overline{\mu_E} = \overline{B_3} + \overline{C_3} - \overline{T} \qquad (5.6)$$

Where, $\overline{T}$ = overall mean of Young's Modulus = ($\sum$R)/9 = 4.5 GPa

R values are taken from the Table 6.5 and the values of $\overline{B}_3$ and $(\overline{C_3})$ are estimated from the experimental data reported in the Table 6.49.

$\overline{B}_3$ = average value of E at the third level of sintering temperature =3.3 GPa

$(\overline{C_3})$= average value of σ at the third level of sintering time =3.6 GPa

Substituting the values of various terms in the above equation,

μ_E = 3.3+3.9 - 4.5 = 2.4MPa

The 95 % confidence intervals of confirmation experiments (CI_{CE}) and population (CI_{POP}) are calculated as:

$$CI_{CE} = \sqrt{F_\alpha\,(1, f_e)\, V_e \left[\frac{1}{n_{eff}} + \frac{1}{R}\right]} \qquad \text{and} \qquad CI_{POP} = \sqrt{\frac{F_\alpha\,(1, f_e)\, V_e}{n_{eff}}}$$

Where, $F_\alpha\,(1, f_e)$ = The F ratio at the confidence level of (1-α) against DOF 1 and error degree of freedom f_e.

$$n_{eff} = \frac{N}{1 + [\text{DOF associated in the estimate of mean response}]} = 27 / (1+4) = 5.4$$

N = Total number of results = 27, R = Sample size for confirmation experiments = 3

V_e = Error variance = 0.3228; f_e = error DOF = 4 (Table 6.48)

$F_{0.05}\,(1, 4)$ = 7.71 (Tabulated F value (Ross, 1996))

So, CI_{CE} = ± 1.13 and CI_{POP} = ± 0.678

Therefore, the predicted confidence interval for confirmation experiments is:

$\mu_E - CI_{CE} < \mu_E < \mu_E + CI_{CE}$ i.e. $1.27 < \mu_E < 3.53$

The 95% confidence interval of the population is:

$\mu_E - CI_{POP} < \mu_E < \mu_E + CI_{POP}$ i.e. $1.722 < \mu_E < 3.078$

The optimal values of process variables at their selected levels are as follows:

(B_3) : 1150°C;

C_3 : 60 min.

The optimized settings given by analysis carried from section 6.4 to section 6.6 are shown in Table 6.50. At the optimal settings of process parameters experiments are carried to validate the setting. In each experiment a predicted and experimental values denote a close tolerance. So, it represents good results reproducibility.

Table 6.50: Predicted and experimental Values

Sr. No.	Material	Response (Units)	Optimal Setting	Pred. Value	CI_{CE} and CI_{POP} (if any)	Exp. value
1	$Ni_{50}Ti_{50}$	**Por. (%)**	B_3C_3	49	**CI_{CE}: 34.43 < μ_{por}<63.57; CI_{POP}: 40.29 < μ_{por} < 57.71**	54
2		**σ (MPa)**	$A_3B_1C_1$	1123.86	----	1116.72
3		**E(GPa)**	B_3C_3	1.674	**CI_{CE}: 0.074 < μ_E <3.274; CI_{POP}: 0.724 < μ_E < 2.624**	1.7
4	$Ni_{45}Ti_{50}Cu_5$	**Por. (%)**	$A_1B_3C_3$	51.13	----	54.17
5		**σ (MPa)**	$A_3B_1C_1$	1135.28	----	1124.53
6		**E(GPa)**	B_3C_3	2.167	**CI_{CE}: 0.847 < μ_E <3.487; CI_{POP}: 1.387 < μ_E < 2.947**	1.9
7	$Ni_{40}Ti_{50}Cu_{10}$	**Por. (%)**	$A_1B_3C_3$	51.88	----	53
8		**σ (MPa)**	$A_3B_1C_1$	1144.16	----	1132.74
9		**E(GPa)**	B_3C_3	2.4	**CI_{CE}: 1.27 < μ_E <3.53; CI_{POP}: 1.722 < μ_E < 3.078**	2.2

6.7 STRAIN RECOVERY AND SUPER-ELASTICITY OF $NI_{50-X}TI_{50}CU_X$ (X=0, 5 AND10)

Figure 6.30 shows the stress-strain graph for loading-unloading of $Ni_{50-x}Ti_{50}Cu_x$ (x=0, 5 and10). Initially the material was loaded for 5% strain value and after that unloaded. It is apparent from the graph that all three materials exhibit a closed loop, which shows a good shape recovery even after the addition of copper contents into the NiTi shape memory alloy. After the calculation shape recovery and super-elasticity was given in Table 6.51.

Table 6.51: Super-elasticity and strain recovery of porous $Ni_{50-x}Ti_{50}Cu_x$ (x=0, 5 and10)

Material	Super-elasticity (%)	Shape recovery (%)
$Ni_{50}Ti_{50}$	4.01	69.8
$Ni_{45}Ti_{50}Cu_5$	3.92	66.7
$Ni_{40}Ti_{50}Cu_{10}$	3.82	62.1

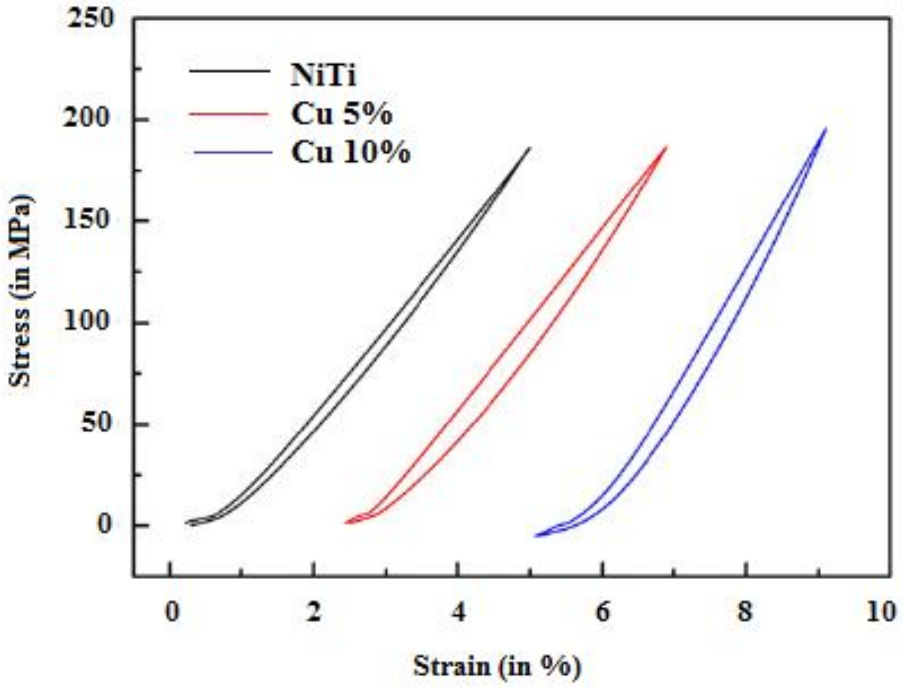

Figure 6.30: Stress-strain Graph of Loading-unloading at 5% pre-stain value for different Material

After the increase in the copper content into porous NiTi alloy, super-elasticity of porous alloy decreases as 4.01% to 3.82%. These results are inline with the previous findings of **(Xiong et al., 2008; Aydogmus and Bor, 2012)**. The shape-recovery also decreases from ~ 70% to ~62% with the increase of copper contents. The porous structure cannot show super-elasticity and shape memory characteristics in the range of 95% due to the presence of Ni_3Ti and Ti_2Ni phase **(Elahinia et al., 2012)**.

After the addition of copper, super-elasticity of the product still in the range of ~4%, this is very much close to the super-elasticity of natural bone consisting 2% recoverable strain **(Mour et al., 2010).**

CHAPTER – 7
TRIBOLOGICAL CHARACTERIZATION

7.1 MEASUREMENT OF MICRO-HARDNESS

Micro-hardness was calculated by Mitutoyo (Japan) make micro-hardness tester as shown in Figure 3.7 at 100kgf with 10s dwell time. Five different readings were taken on a sample and average of them is used in this research work. Table 7.1 gives the micro-hardness value in Vicker's hardness (HV) and in GPa. The value of Vicker hardness can be computed by equation 7.1.

$$HV = \frac{1.854F}{d^2} \qquad 7.1$$

Where F- Force Applied

d- Indentation depth; to convert HV into GPa simply multiply HV value to 0.009807.

Table 7.1: Samples and corresponding values of Young's Modulus and Microhardness

Sr. No	Material	Sample	Young's Modulus (GPa)	Microhardness (HV)	Microhardness (GPa)
1.	$Ni_{50}Ti_{50}$	Sample 1	7.3	364	3.57
2.		Sample 2	1.23	232	2.27
3.	$Ni_{45}Ti_{50}Cu_5$	Sample 1	7.4	397	3.89
4.		Sample 2	1.74	257	2.52
5.	$Ni_{40}Ti_{50}Cu_{10}$	Sample 1	7.62	437	4.28
6.		Sample 2	2.02	289	2.83

Micro-hardness depends upon the micro-structure of the fabricated material especially on which area indentation has been made. With the increase of copper

contents into NiTi alloy the hardness for sample 1 increases due to fill up the voids between the nickel and titanium. Similarly sample 2 exhibits the same pattern, but starting at a smaller value, due to lower young's modulus or process parameters selected for the fabrication of this sample.

7.2 WEAR TEST

The specimens for wear test were prepared according to the setting suggested by Table 7.2. There are two samples, which were selected one depending upon their Young's modulus and compressive strength.

Table 7.3 gives the wear rate (mm^3/m) of NiTi alloy at different values of load and temperature. It is found from the results that with the increase of load from 10N to 40N, the wear rate increases. This is due to the increase in the contact area of sample. An increase in the wear rate is observed with the increase in temperature. But a sudden decrement in the wear rate is observed after 150**°C.** This may be due to the formation of oxides and tribo layer. Debris produced from the depleted surfaces form tribo-layer due to the load and temperature action.

Table 7.2: Setting of Process Parameters for Wear Test Specimen preparation

Sr. No	Material	Sample	Compaction Pressure (MPa)	Sintering Temperature (°C)	Sintering Time (min)
1.	$Ni_{50}Ti_{50}$	Sample 1	177	950	20
2.		Sample 2	107	1150	60
3.	$Ni_{45}Ti_{50}Cu_5$	Sample 1	177	950	20
4.		Sample 2	141	1150	60
5.	$Ni_{40}Ti_{50}Cu_{10}$	Sample 1	177	950	20
6.		Sample 2	141	1150	60

Table 7.3: Wear rate of $Ni_{50}Ti_{50}$ at different temperatures and load

Load	Sample	Wear rate (mm^3/m) at Temperature Conditions ($Ni_{50}Ti_{50}$)					
		37°C	50°C	100°C	150°C	200°C	250°C
10N	Sample 1 (High σ)	1.42	1.78	1.93	2.04	1.92	2.21
20N		1.65	1.82	2.01	2.15	2.02	2.29
30N		1.81	1.98	2.19	2.31	2.14	2.38
40 N		2.9	3.14	3.28	3.67	3.73	3.82
10N	Sample 2 (Low E)	1.91	2.2	2.64	2.87	2.69	3.79
20N		2.24	2.38	2.83	3.2	2.98	3.96
30N		2.58	2.89	3.16	3.94	3.64	4.87
40 N		2.72	3.23	3.76	4.39	4.18	5.01

This layer contains oxides of material and transforms a layered arrangement termed as mechanically mixed layer (MML) investigated by **Yang et al. (2010)**. This layer shows a high hardness value as compared to base material on the sliding surface, which declines the wear rate at this point.

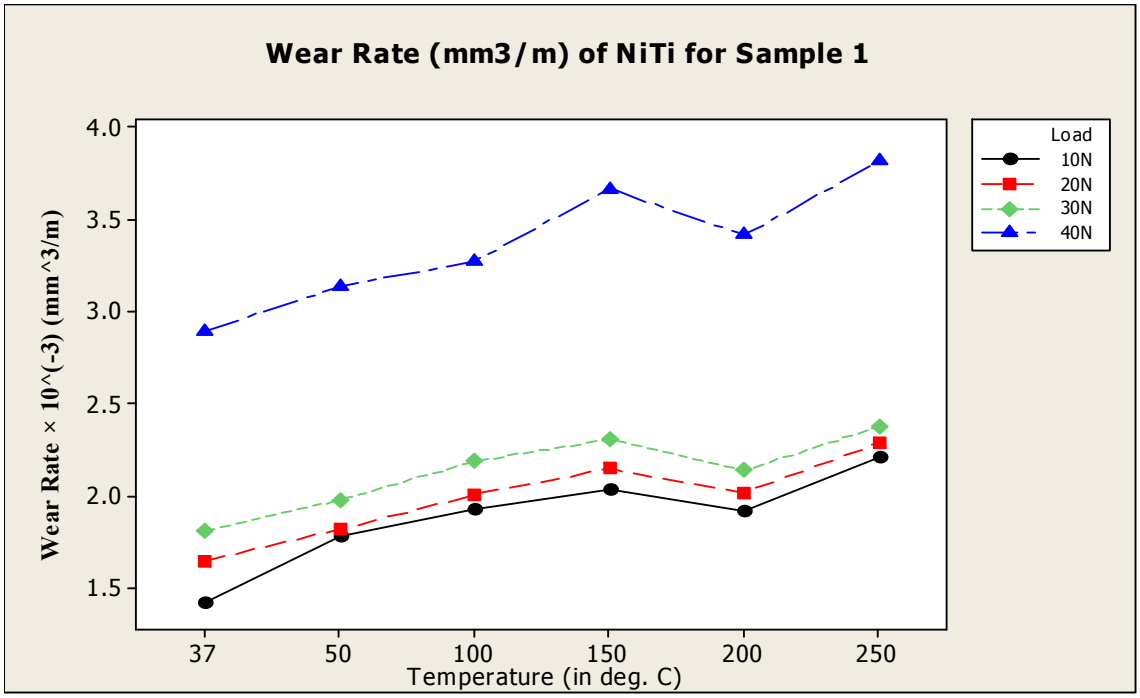

Figure 7.1: Wear Rate (mm^3/m) of $Ni_{50}Ti_{50}$ alloy for sample 1

Further when the temperature increase from 200°C, this layer shredded and new surface area comes into contact and wear rate increases as shown in Figure 7.1.

Wear rate of sample 2 is larger than the wear rate of sample 1 due to their Young's modulus value, which is larger in case of sample 1. Larger value of applied load (40N) and larger temperature (250°C) shows a maximum wear rate of 5.01mm^3/m, while at 37°C of temperature and 10N of load exhibit a wear rate of 1.91mm^3/m.

An increase in the wear was observed with temperature increase, but a steep transition found after 150°C due to formation of oxide layer. But when temperature further increased from 200°C, wear rate again increases due to removal of oxide layer (Figure 7.2).

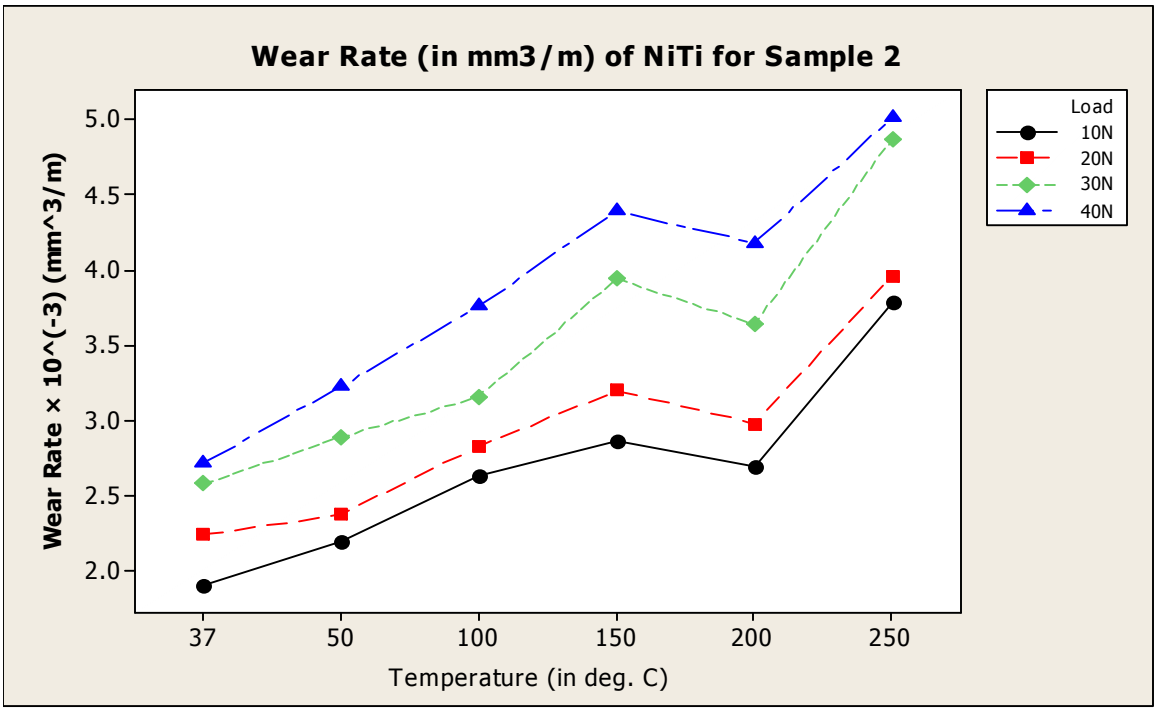

Figure 7.2: Wear Rate (mm^3/m) of $Ni_{50}Ti_{50}$ alloy for sample 2

Table 7.4 gives the wear rate in mm^3/m of $Ni_{45}Ti_{50}Cu_5$ (i.e. 5% copper addition) with the variation of temperature and load values. It has been observed from the Table 7.4 that with the addition of copper the wear rate is decreased as compared to $Ni_{50}Ti_{50}$. The reason for this wear reduction is the hardness of material. It is found that after addition of copper the hardness of material increases from 364Hv to 397Hv.

Table 7.4: Wear rate of $Ni_{45}Ti_{50}Cu_5$ at different temperatures and load

Load	Sample	Wear rate (mm^3/m) at Temperature Conditions ($Ni_{45}Ti_{50}Cu_5$)					
		37°C	50°C	100°C	150°C	200°C	250°C
10N	Sample 1	1.18	1.23	1.41	1.69	1.57	1.95
20N		1.26	1.31	1.47	1.78	1.64	2.06
30N		1.41	1.56	1.64	1.87	1.73	2.13
40 N		1.54	1.67	1.79	1.92	1.85	2.26
10N	Sample 2	1.42	1.63	1.74	1.88	1.57	2.17
20N		1.53	1.68	1.75	1.87	1.71	2.29
30N		1.74	1.82	1.9	1.98	1.82	2.35
40 N		1.83	1.94	2.07	2.17	2.01	2.48

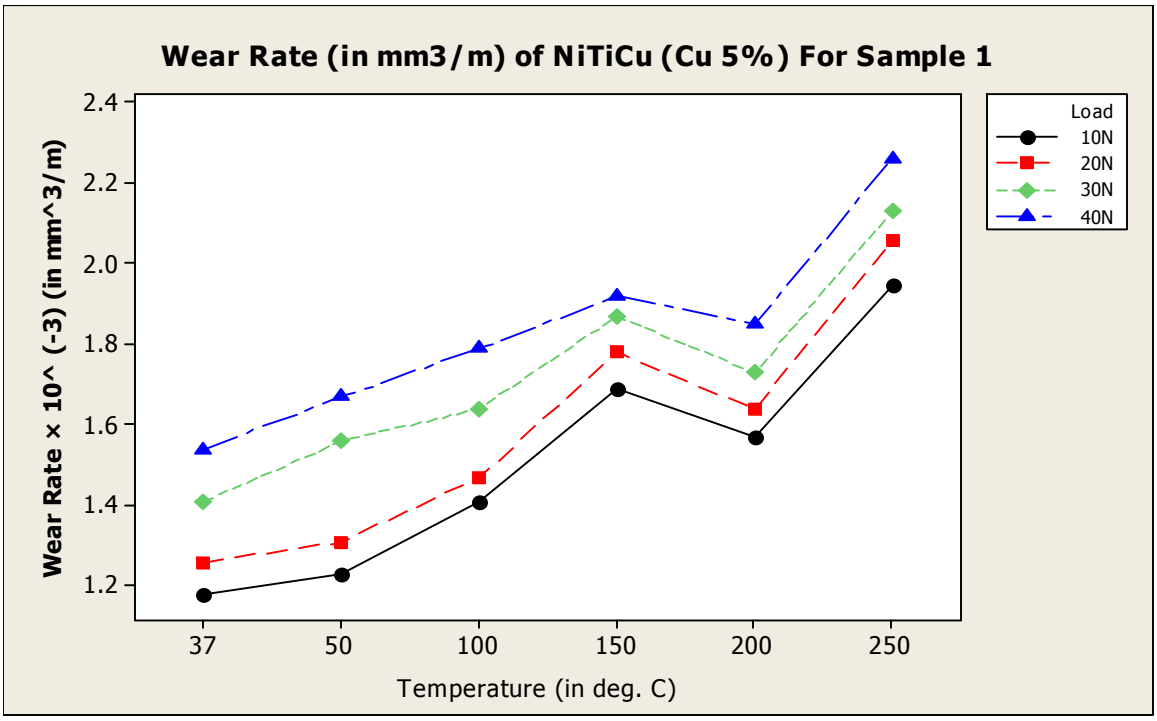

Figure 7.3: Wear Rate (mm^3/m) of $Ni_{45}Ti_{50}Cu_5$ alloy for sample 1

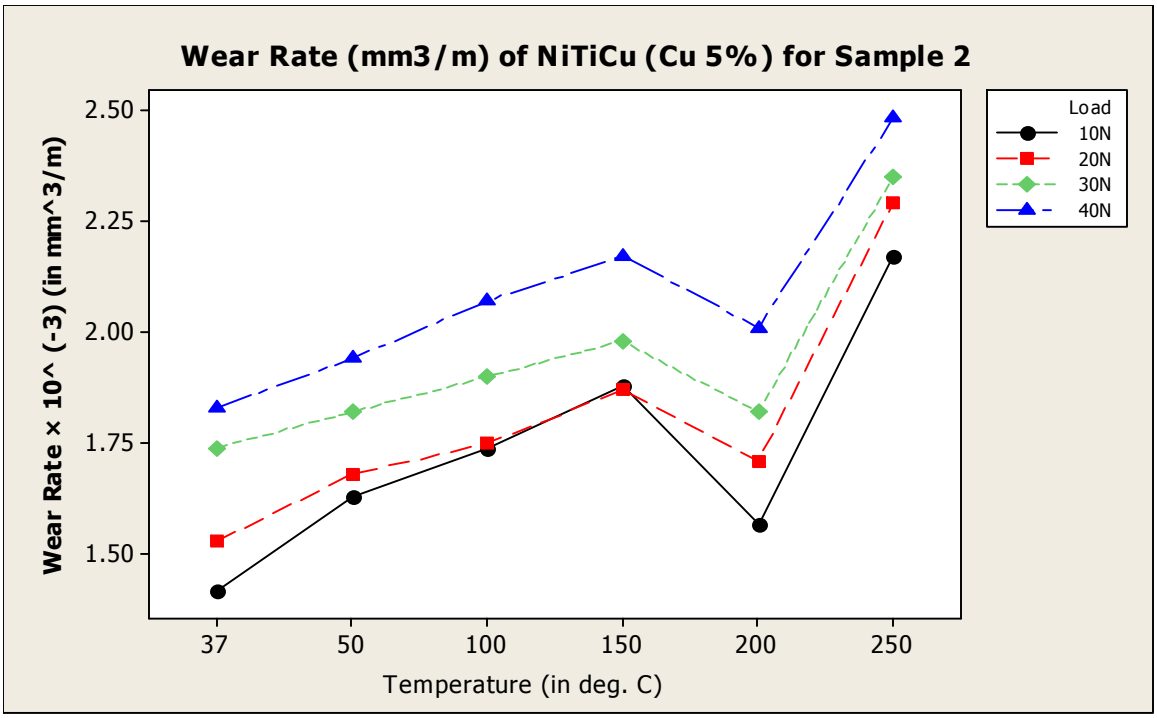

Figure 7.4: Wear Rate (mm^3/m) of $Ni_{45}Ti_{50}Cu_5$ alloy for sample 2

Table 7.5: Wear rate of $Ni_{40}Ti_{50}Cu_{10}$ at different temperatures and load

Load	Sample	Wear rate (mm^3/m) at Temperature Conditions ($Ni_{40}Ti_{50}Cu_{10}$)					
		37°C	50°C	100°C	150°C	200°C	250°C
10N	Sample 1	0.92	1.12	1.25	1.3	1.21	1.51
20N		1.03	1.11	1.23	1.48	1.32	1.67
30N		1.19	1.32	1.36	1.46	1.32	1.81
40 N		1.25	1.43	1.52	1.59	1.43	1.92
10N	Sample 2	1.2	1.32	1.45	1.53	1.42	1.89
20N		1.36	1.54	1.73	1.84	1.75	2.01
30N		1.42	1.57	1.88	2.01	2.93	2.25
40 N		1.48	1.64	1.96	2.14	2.02	2.34

As the copper particles were smaller in size, so these particles fill the voids between the nickel and titanium and make the material more wear resistant. Wear rate varies normally i.e. with a uniform manner it increases with load and temperature. But at 150 °C its value decreases due to MML formation, after that an increase in the slope

value of wear rate versus temperature graph (Figure 7.3) observed. Figure 7.4 shows the wear rate variation for sample 2 (lower young's modulus) after 5% copper addition. As sample 2 gives a lower Young's modulus due to which it shows a lower hardness value, so larger wear rate as compared to sample 1. The variation of wear rate is still the same i.e. wear rate increases with the load.

Wear rate decreases after 150°C and increases after 200°C. Some unexpected increases in wear rate after 100°C at 10N was observed. The probable reason may be the porosity of the material.

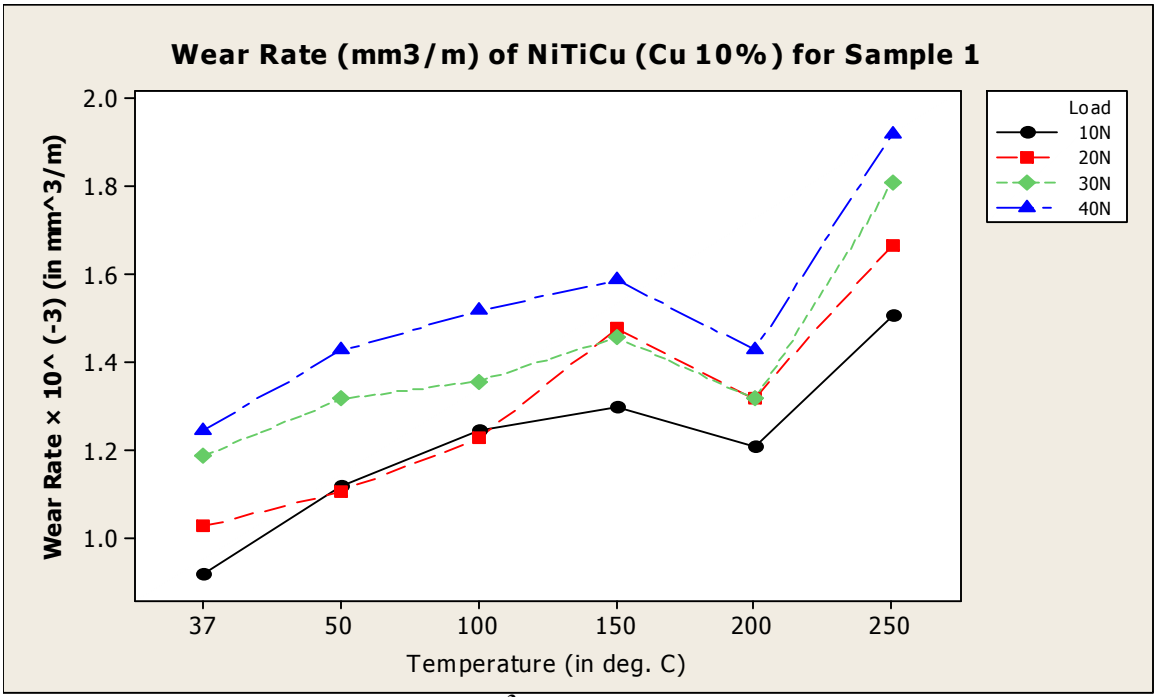

Figure 7.5: Wear Rate (mm^3/m) of $Ni_{40}Ti_{50}Cu_{10}$ alloy for sample 1

Wear rate (in mm^3/m) of $Ni_{40}Ti_{50}Cu_{10}$ at various values of load (from 10N to 40N) and temperature (37°C to 250°C) is given by Table 7.4. It was observed from the results that a wear rate further decreases after increasing the copper contents from 5% to 10% for sample 1 and sample 2 both. Figure 7.5 and Figure 7.6 present this wear rate according to load and temperature settings. It has been found from figures that wear rate follows same pattern as observed in the above text, but some non-uniformity in the results were found i.e. steep transition from higher to lower and lower to higher values.

These changes occur due to more number of copper particles in between the matrix, when these particles come into contact with WC, the wear rate found to be increased. But when nickel/titanium particle comes with WC disk contact then wear rate observed to be decreased.

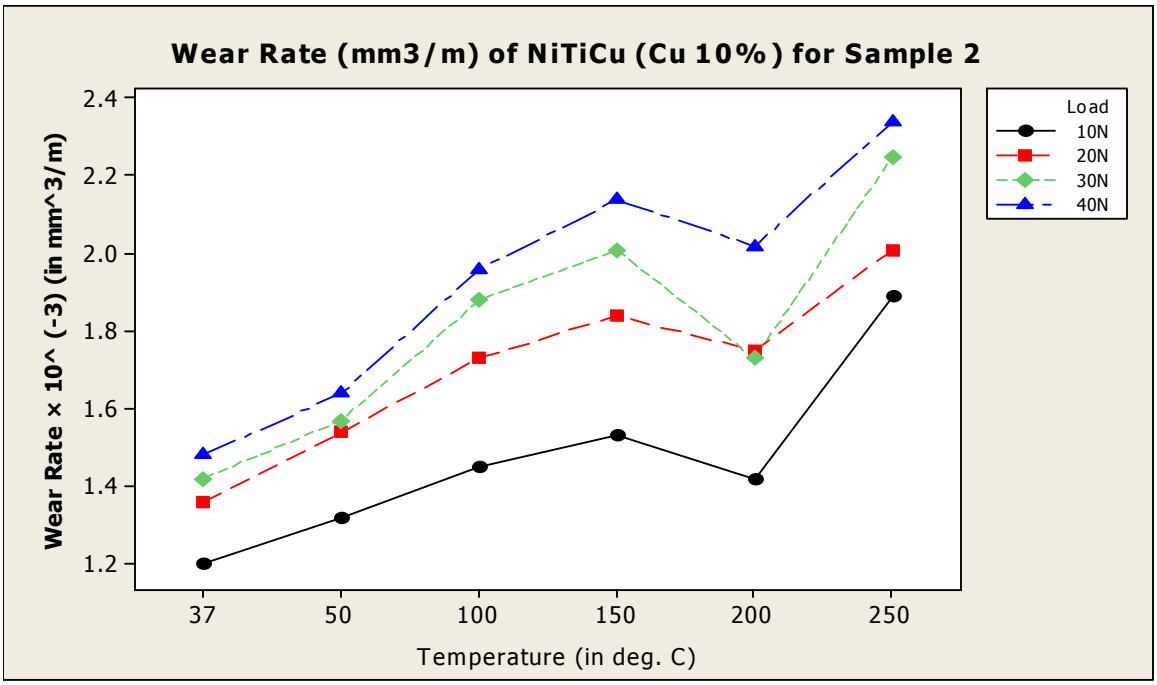

Figure 7.6: Wear Rate (mm^3/m) of $Ni_{40}Ti_{50}Cu_{10}$ alloy for sample 2

7.3 SURFACE PREPARATION AND MICRO-STRUCTURAL INVESTIGATION

Figure 7.7 shows the wear behavior of NiTi alloys and Figure 7.8 shows the debris of wear particles. Wear marks on the specimens were found. It has been found that the cracks and patches were also observed against the tungsten carbide disk. The close view of patches is shown in Figure 7.8. Figure 7.9 and Figure 7.10 represent the wear behavior of $Ni_{45}Ti_{50}Cu_5$ and $Ni_{40}Ti_{50}Cu_{10}$. Only small running marks were obtained on the pin fabricated by $Ni_{45}Ti_{50}Cu_5$ and $Ni_{40}Ti_{50}Cu_{10}$.

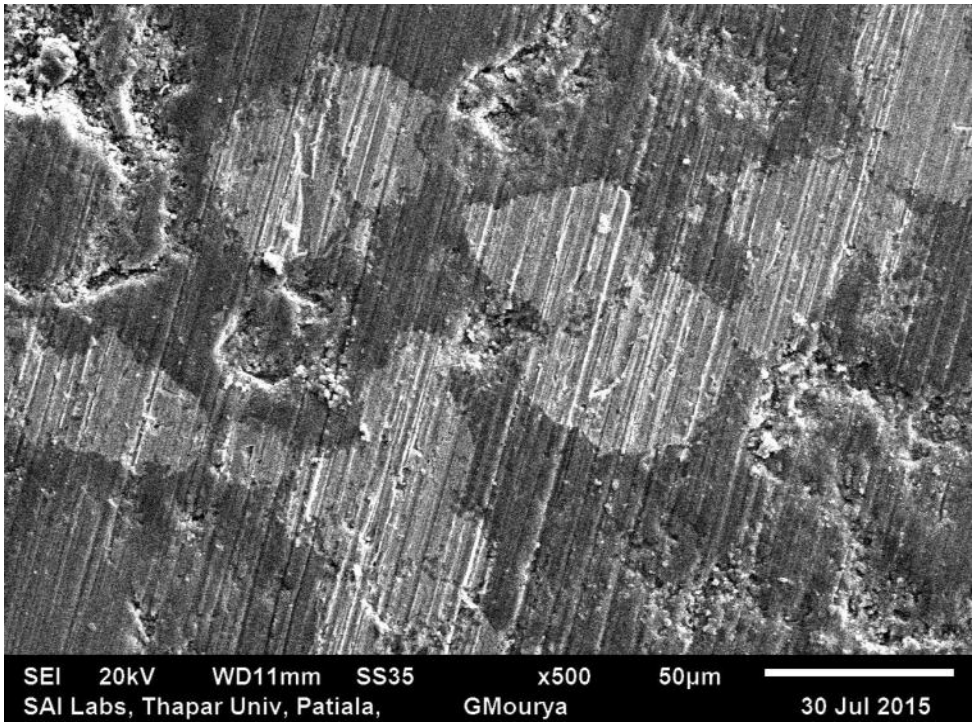

Figure 7.7: Wear Marks on Specimen

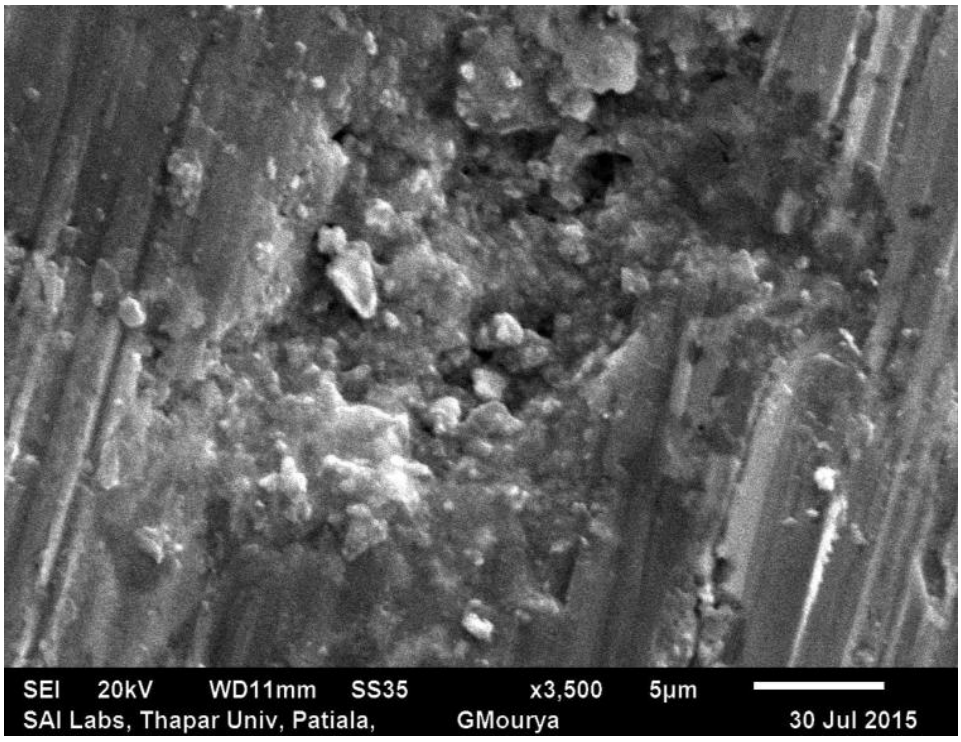

Figure 7.8: Wear Debris

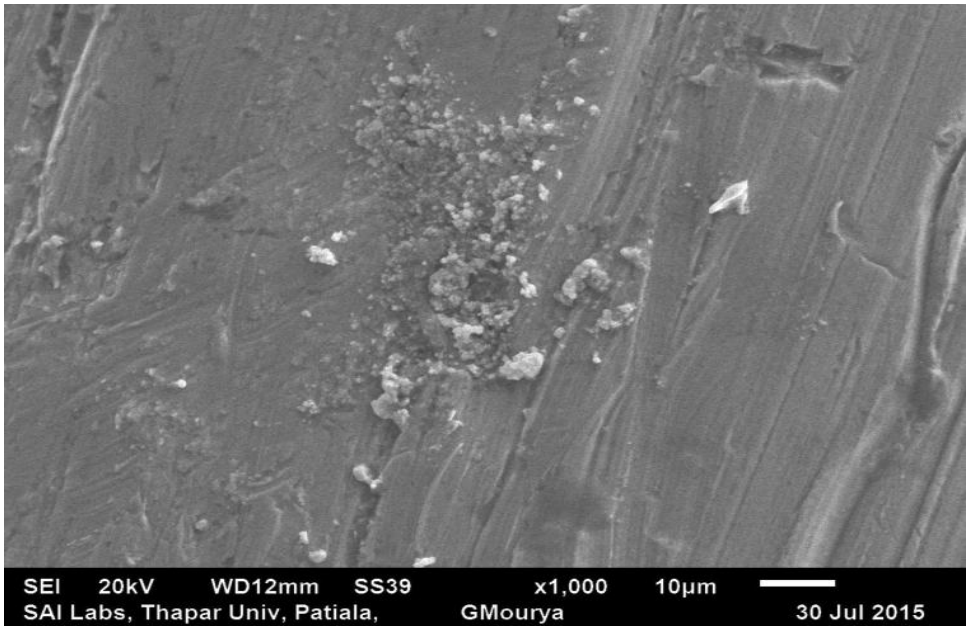

Figure 7.9: Wear Behavior ($Ni_{45}Ti_{50}Cu_5$)

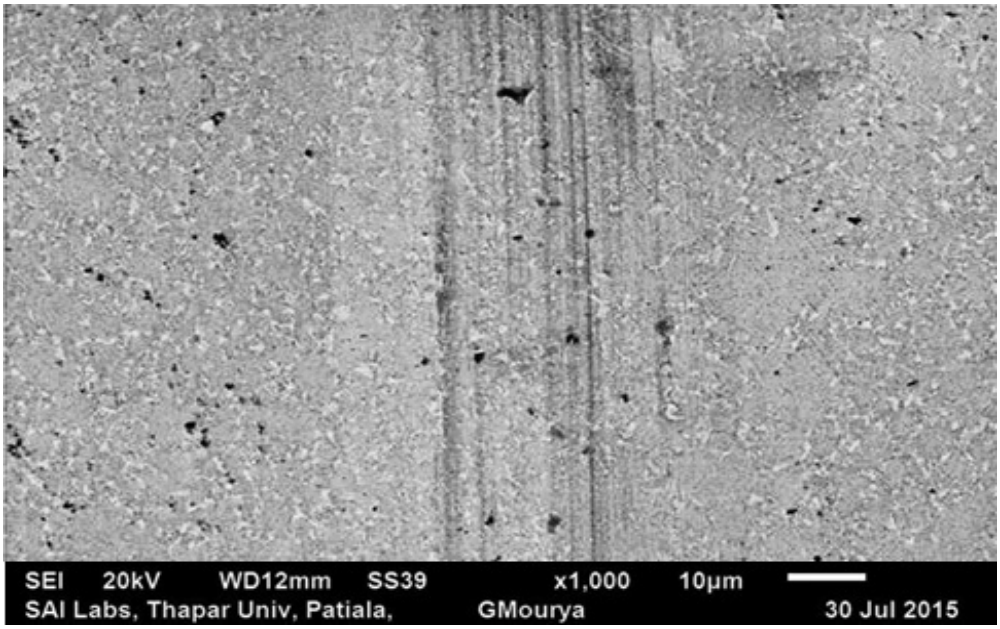

Figure 7.10: Wear Behavior ($Ni_{40}Ti_{50}Cu_{10}$)

When the 5% of copper is added, wear rate decreases reasonably. Increasing the copper contents upto 10%, wear rate again decreases as shown in Figure 7.10. Also the wear debris is found on the surface due to adhesive wear between the material and the disk.

CHAPTER 8

IN-VITRO TESTINGS

8.1 CORROSION TEST

In vitro testing of NiTi alloy for corrosion behavior was performed in the presence of artificial saliva at pH value 7.4 and temperature 37±1°C. Initially specimen surface were prepared using 400, 800 and 1200 grit size SiC abrasive papers. After that specimen were prepared by 1µm diamond paste to generate mirror finish. Then specimens were ultrasonically cleaned with the help of acetone for 10min to remove any dust and grease particles. This was followed by rinsing in de-ionized water. Figure 8.1 shows the potentiodynamic polarization curve for NiTi alloy (Experiment 3- Young's Modulus: 82GPa).

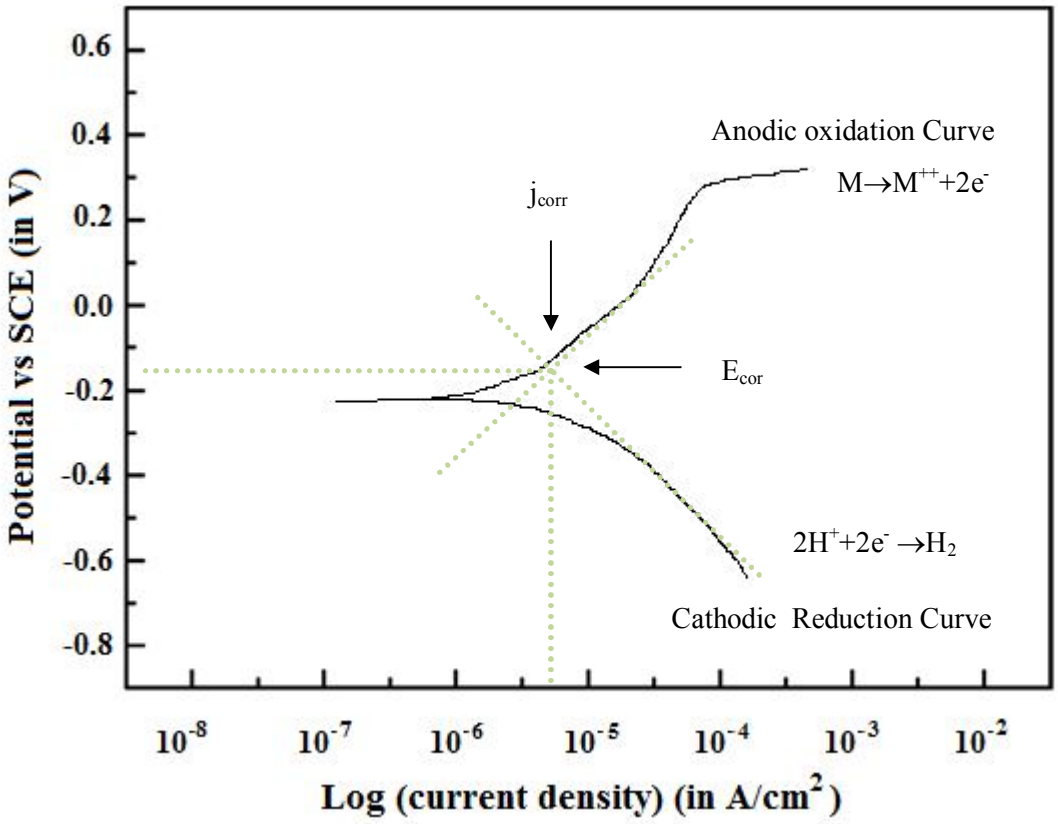

Figure 8.1: Potentiodynamic Polarization Curve (NiTi)

At the anodic oxidation curve reaction is

$M \rightarrow M^{++} + 2e^-$

At cathodic reduction curve the reaction is

$2H^+ + 2e^- \rightarrow H_2$

The open voltage potential (E_{corr}) and current density (I_{corr}) can be measured by plotting the slopes on cathodic and anodic curve as shown in Figure 8.1. The corrosion current density (i_{corr}) of specimen can be calculated by equation 8.1. The slope gives the Tafel slopes (b_a and b_c) and the intercept corresponds to corrosion current density i_{corr}. The i_{corr} (Acm^{-2}) was calculated using the Stern-Geary equation;

$$i_{corr} = \frac{b_a b_c}{2.3\ (R_P)(b_a + b_c)} \qquad (8.1)$$

Corrosion rate was investigated by following relationship as equation 8.2:

$$Corrosion\ Rate = 3.268 \times 10^{-3} \frac{i_{corr}}{\rho} \frac{MW}{z} \qquad (8.2)$$

MW- molecular weight of sample in g/mole,

ρ- Density of sample in g/m^3,

z- Number of electrons transfer in corrosion reaction.

Figure 8.2 and Figure 8.3 represent the potentiodynamic linear polarization curves for porous $Ni_{45}Ti_{50}Cu_5$ and $Ni_{40}Ti_{50}Cu_{10}$. It is observed from the Figures that the curve is shifting slightly towards the right with increasing copper contents. The current density increases by increasing the copper contents and the results were given by Table 8.1, while open voltage potential did not affect so much.

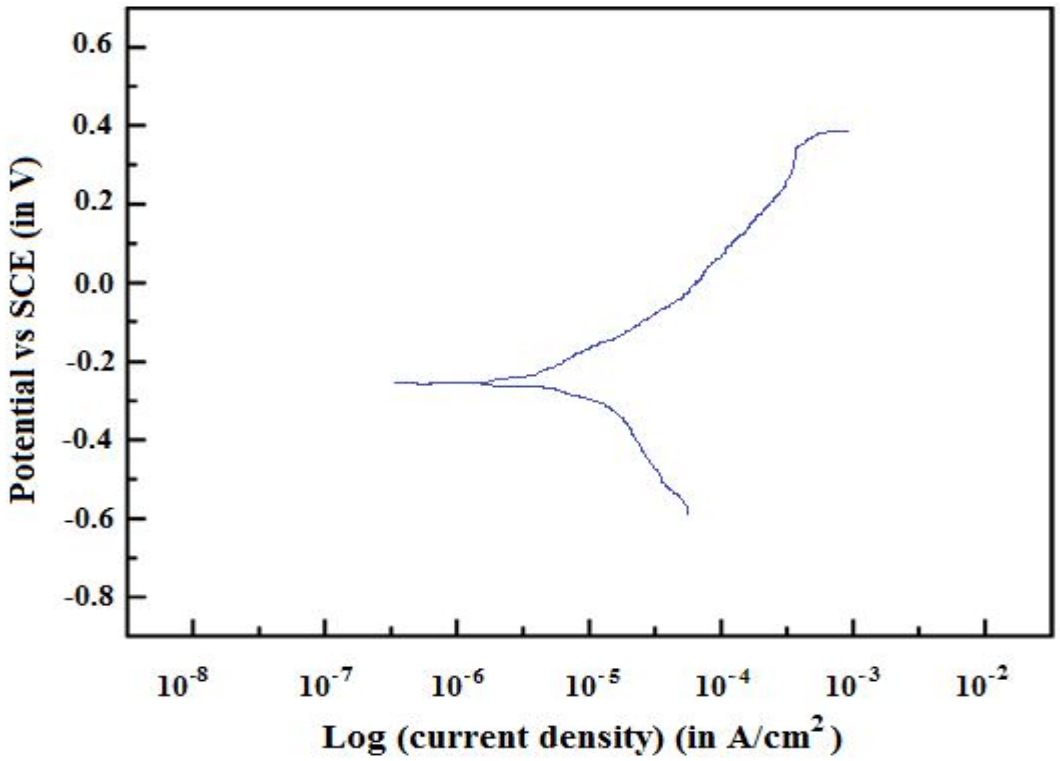

Figure 8.2 Potentiodynamic Polarization Curve ($Ni_{45}Ti_{50}Cu_5$)

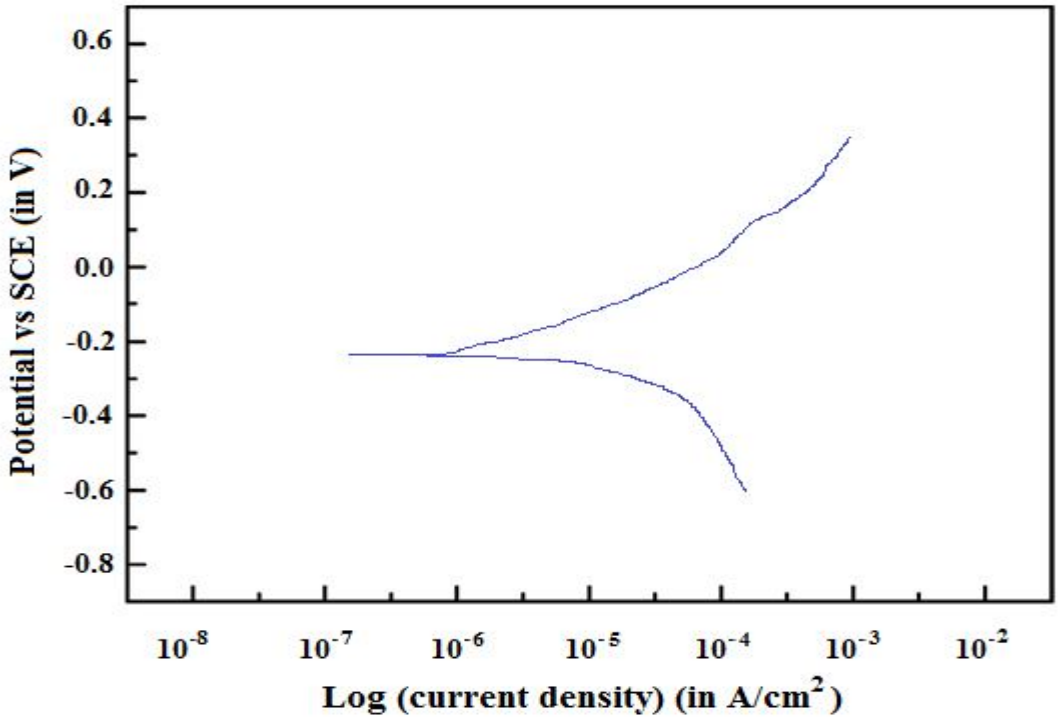

Figure 8.3: Potentiodynamic Polarization Curve ($Ni_{40}Ti_{50}Cu_{10}$)

Open current potential (OCP) denotes the corrosion tendency and a thermo-dynamic concept while current density describes a dynamic concept of corrosion rate of material. Porous material represents corrosion resistance slightly lower than the dense material **(Xu et al., 2014).** There are many reasons for lower corrosion resistance of porous material. First, the porous structure was very prone to producing cleft corrosion and speed up the corrosion process. Second, the real surface area of porous structure is more in artificial saliva. Finally, the cavitation corrosion would occur around the secondary Ni_3Ti and Ti_2Ni phases **(Bertheville, 2006)**. Corrosion behavior of material depends upon product composition, its structure and mechanical properties. The ideal bone implant materials should have the porosity in the range of 30–90% **(Barrabes et al., 2008)**.

Table 8.1: Open Current Potential and Current density of Material

Materials	Open Current Potential (E_{corr})	Current density (j_{corr})
NiTi	-0.175	6×10^{-6}
$Ni_{45}Ti_{50}Cu_5$	-0.25	0.8×10^{-5}
$Ni_{40}Ti_{50}Cu_{10}$	-0.11	4×10^{-5}

8.2 BIO-ACTIVITY OF MATERIAL

Figure 8.4, 8.5 and 8.6 represent the materials bio-activity in the presence of stimulated body fluid (SBF) for 14 days. The formation of calcium (Ca) and phosphorous (P) precipitates on the surface was investigated to confirm the bio-activity of $Ni_{50-x}Ti_{50}Cu_x$ (x=0, 5 and10). Formation of Ca and P precipitates has been observed on the surface of NiTi from Figure 8.4.

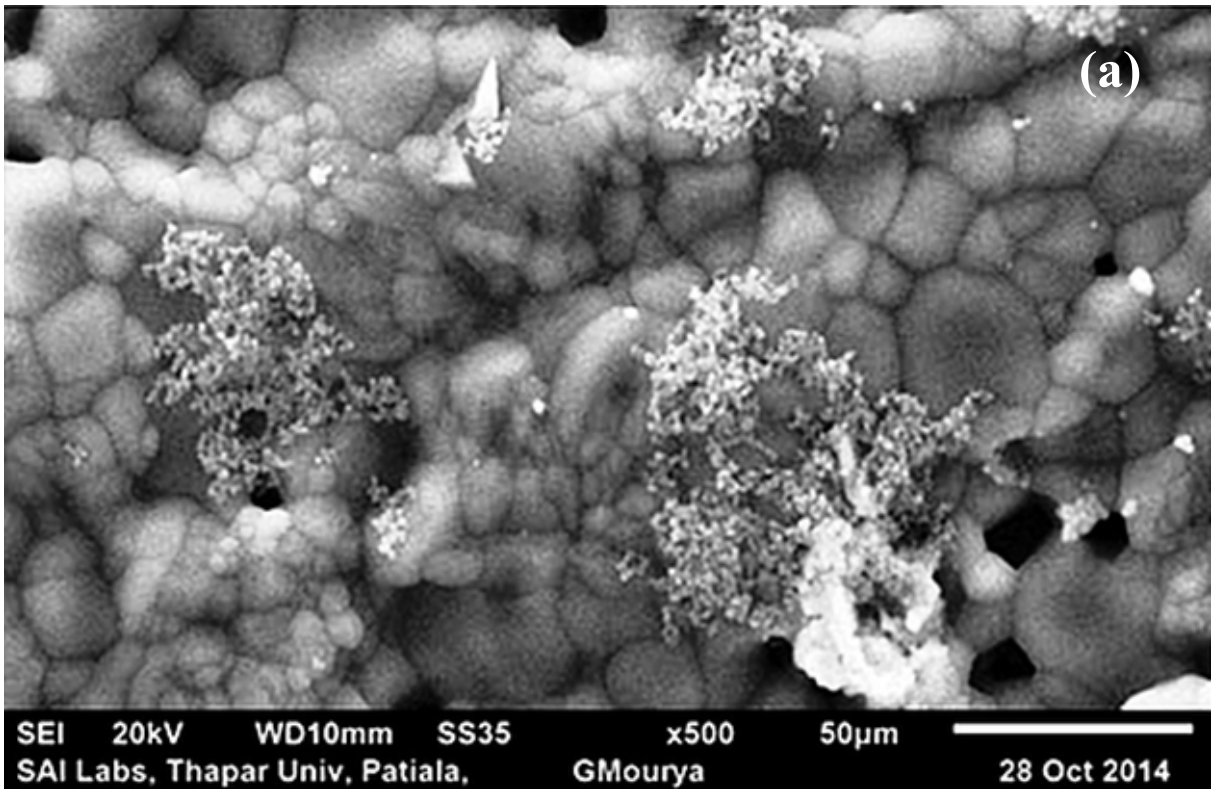

Figure 8.4: Bio-activity of $Ni_{50}Ti_{50}$ in the presence of SBF for 14 Days

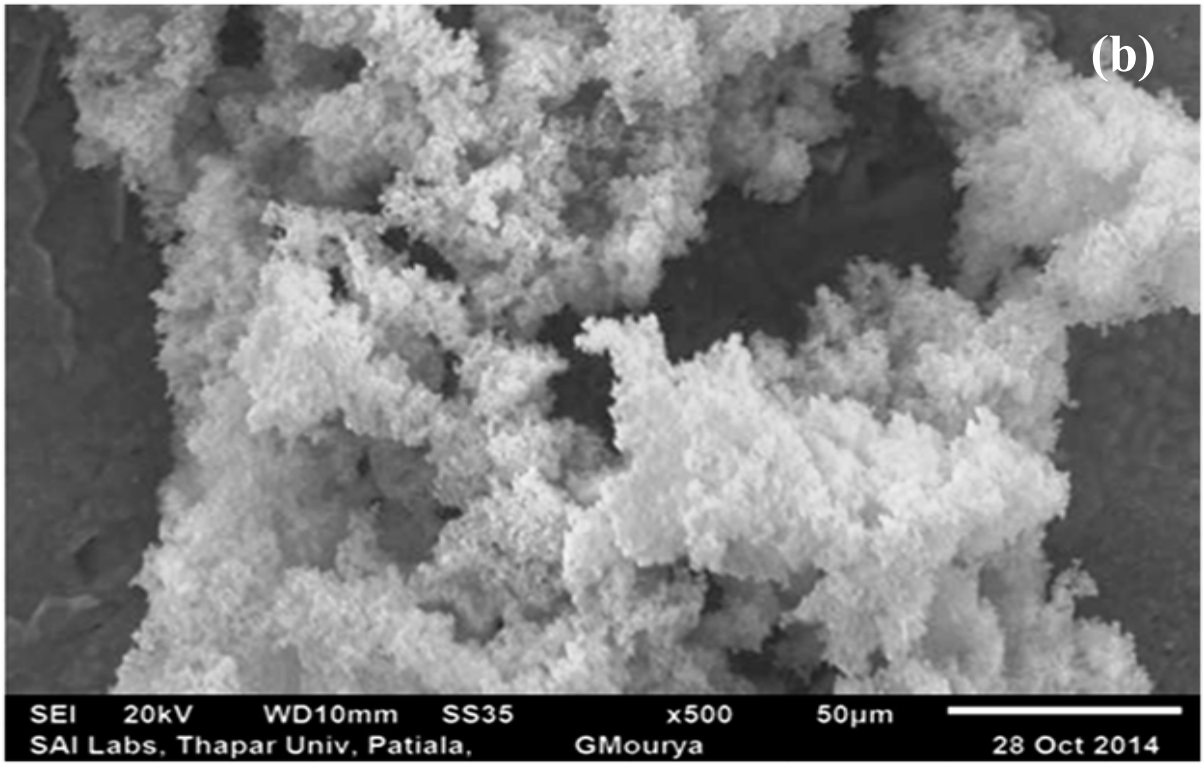

Figure 8.5: Bio-activity of $Ni_{45}Ti_{50}Cu_5$ in the presence of SBF for 14 Days

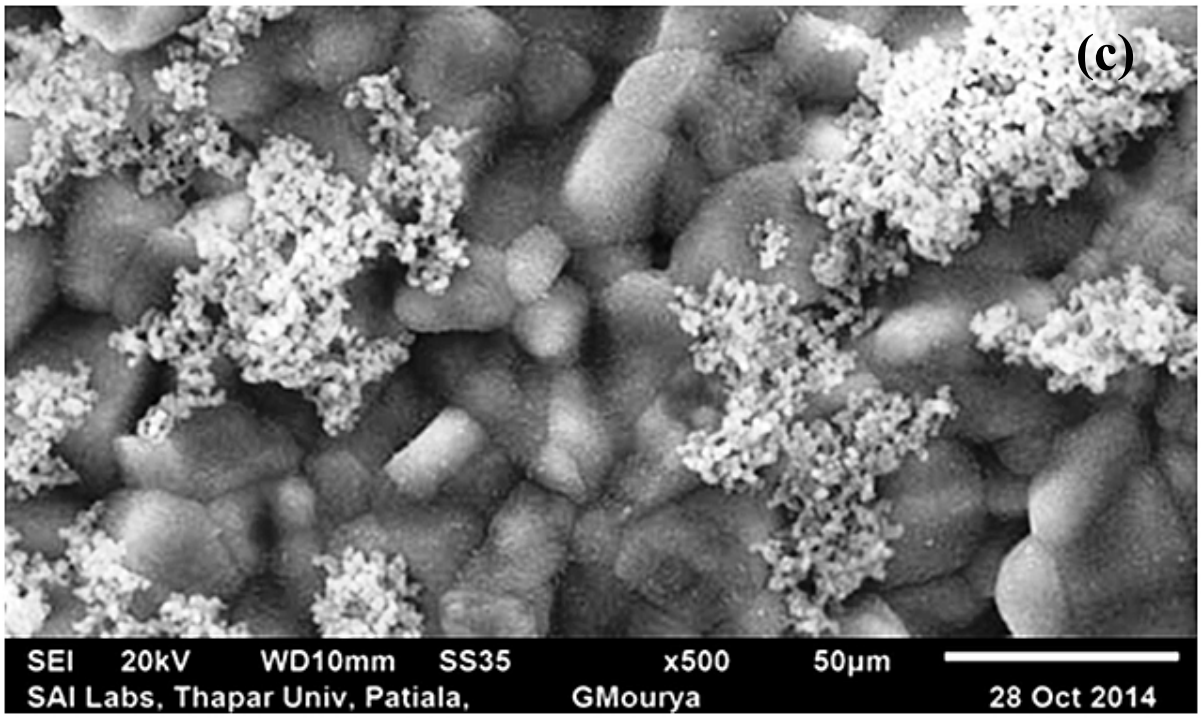

Figure 8.6: Bio-activity of $Ni_{40}Ti_{50}Cu_{10}$ in the presence of SBF for 14 Days

These Ca and P formation occurs mostly in the area of porous structure. So from this study it can easily be said that porous structure favors the cell-growth as compared to dense NiTi. Figure 8.5 represents a large number of Ca and P precipitation, much higher than the NiTi. So a limited amount (~5%) of copper addition in NiTi alloys enhances its bio-activity. But further increase in the copper content decreases the bio-activity i.e. formation of Ca and P precipitate formation decreases (Figure 8.6). The probable reason of this may be if copper contents increases from a certain amount then it may cause to fill the voids in the NiTi materials and a descending rate of bio-activity has been observed.

8.3 BIO-COMPATIBILITY TEST

In-vitro bio-compatibility test was performed on NiTi alloy in the presence of living cells (L929 mouse fibroblast). Figure 8.7 shows the microscopic image after incubation of cells at specified conditions (37±1°C for 24-26hrs). Figure 8.8 and 8.9 show the images of L929 around $Ni_{45}Ti_{50}Cu_5$ and $Ni_{40}Ti_{50}Cu_{10}$ respectively. From Figures 8.8 and 8.9, it is clear that there is no adverse effect of copper addition in NiTi alloy. All the images show the existence of L929 mouse fibroblast cell around the NiTi alloys.

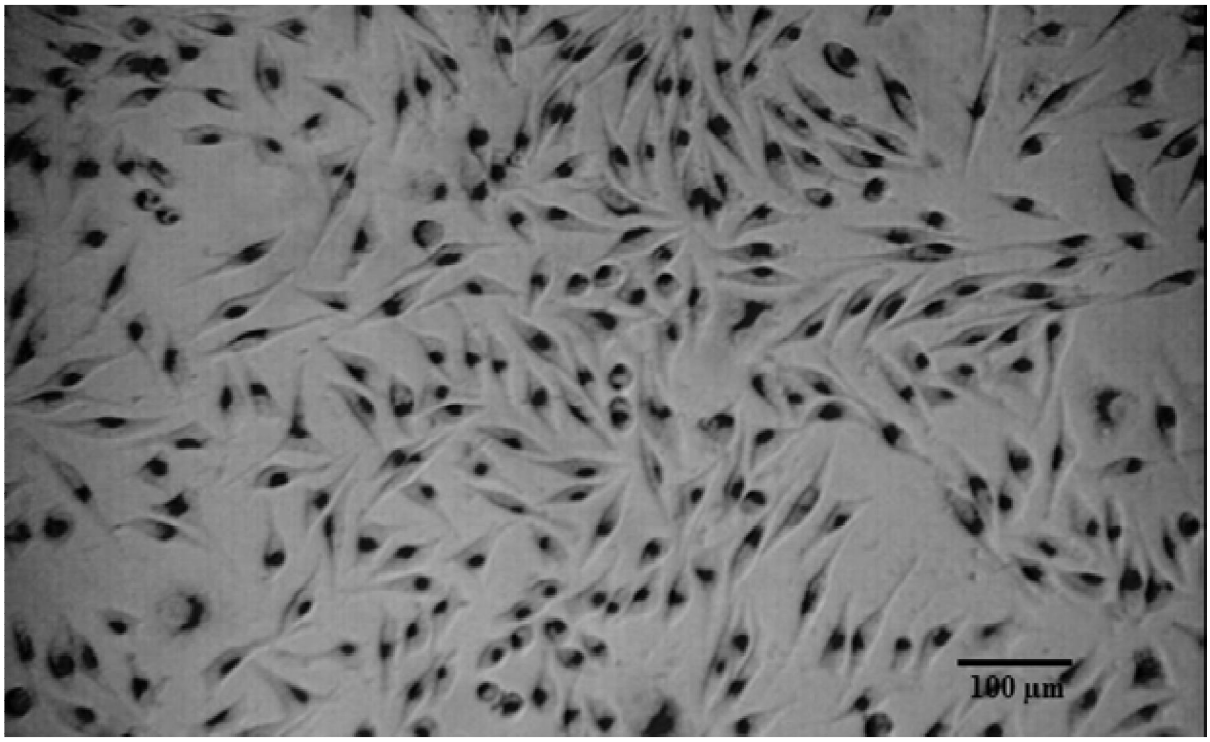

Figure 8.7: L929 mouse fibroblast cells around $Ni_{50}Ti_{50}$

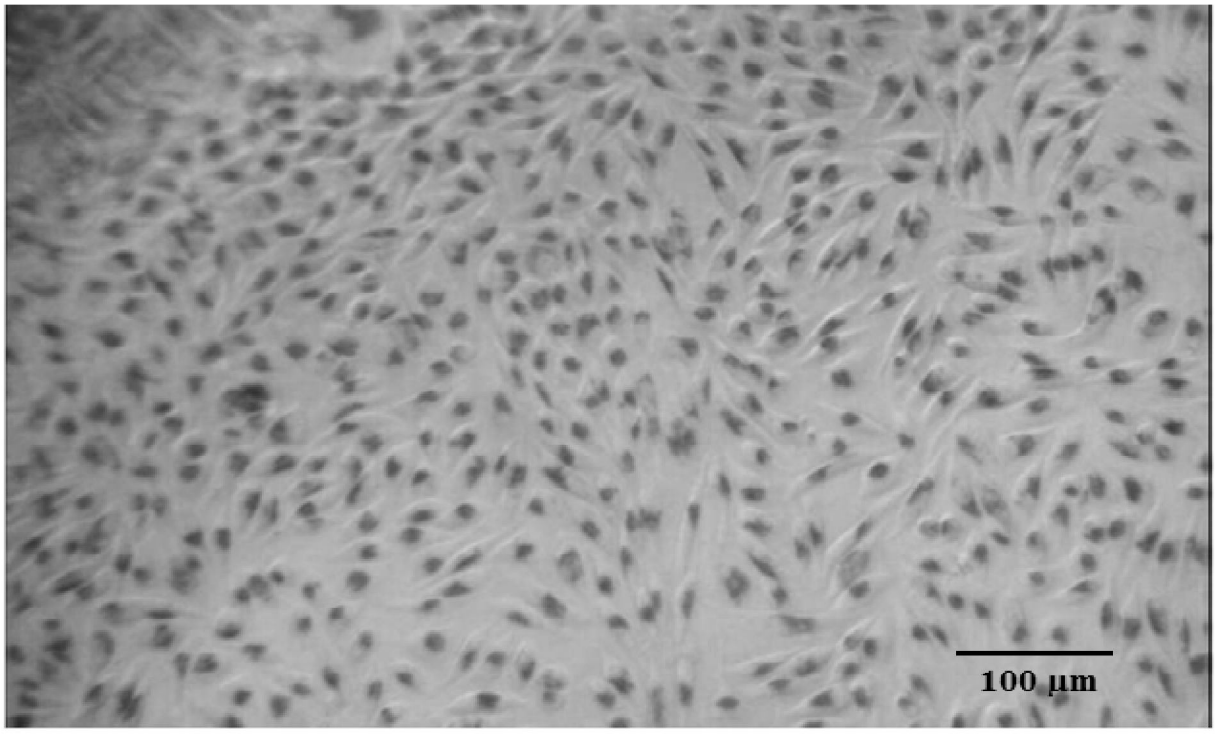

Figure 8.8: L929 mouse fibroblast cells around $Ni_{45}Ti_{50}Cu_5$

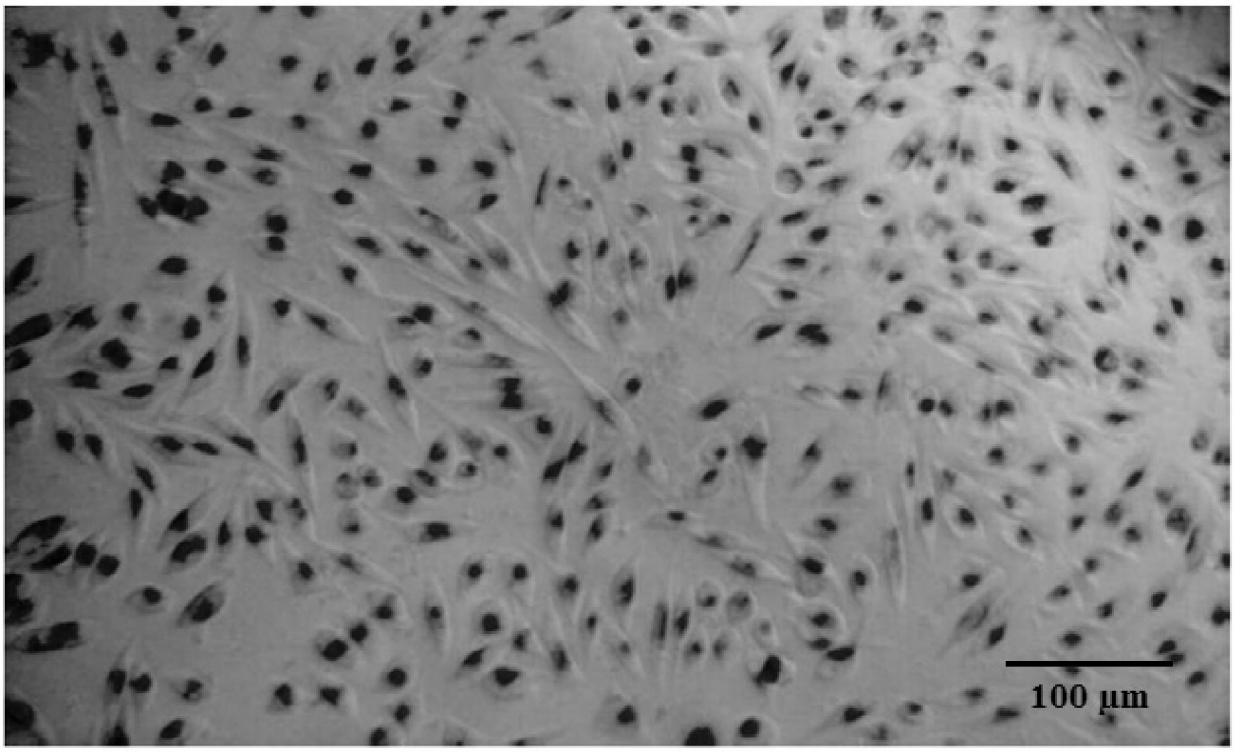

Figure 8.9: L929 mouse fibroblast living cells around $Ni_{40}Ti_{50}Cu_{10}$

It is also observed that L292 cells around the NiTi alloys increases after copper addition, so a large number of cells found on $Ni_{45}Ti_{50}Cu_5$ and $Ni_{40}Ti_{50}Cu_{10}$. The images show the presence of L929 cells around all these samples, which signify non-toxicity of materials. The qualitative analysis carried by microscopic evaluation is shown in Table 8.2 according to standards mentioned in Table 3.3 (Section 3.3.6).

Table 8.2: Qualitative Analysis of Cyto-toxicity Results

Sr. No.	Material	Grade	Reactivity
1.	Negative Control	0	Non-Toxic
2.	Positive Control	4	Severe Toxic
3.	$Ni_{50}Ti_{50}$	0	Non-Toxic
4.	$Ni_{45}Ti_{50}Cu_5$	0	Non-Toxic
5.	$Ni_{40}Ti_{50}Cu_{10}$	0	Non-Toxic

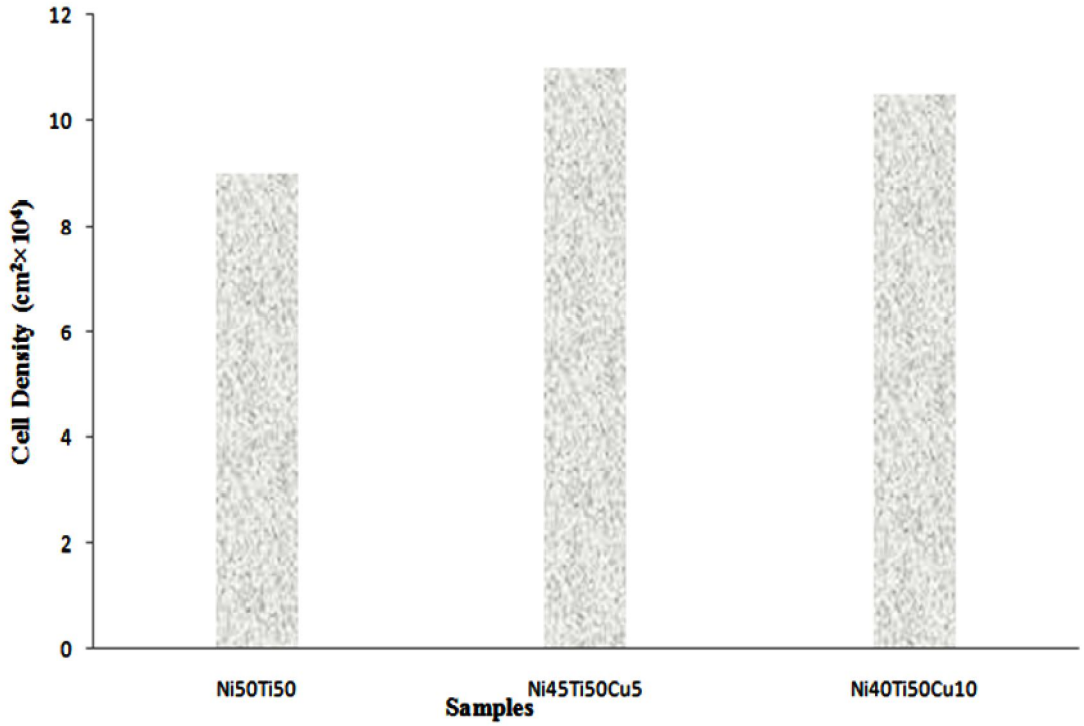

Figure 8.10: Cell density of $Ni_{50}Ti_{50}$, $Ni_{45}Ti_{50}Cu_5$ and $Ni_{40}Ti_{50}Cu_{10}$ after 26hrs of Cell culture

The quantitative analysis is demonstrated in Figure 8.10 by counting the cell density of living cells on NiTi alloys. The unit of measurement is number of live cells per unit area of specimen. Material physical and mechanical properties, composition, structure and porosity play a significant role in cell proliferation **(Anselme, 2000; Okumura et al., 2001)**. In present research work, $Ni_{45}Ti_{50}Cu_5$ represents best cell density of 11×10^4 cm^2, while after increasing copper contents the cell density decreases and gives a value of 10.5×10^4 cm^2 after 26hrs of cell culture. So, cyto-toxicity of material increases upto a certain level of copper addition and after that it decreases. These results are also according to the bio-activity of material. As explained earlier in section 8.2 that $Ni_{45}Ti_{50}Cu_5$ is most bio-active than $Ni_{40}Ti_{50}Cu_{10}$ and $Ni_{50}Ti_{50}$ is least bio-active due to the porosity of material.

CHAPTER 9

CONCLUSIONS AND FUTURE SCOPE OF RESEARCH

In the previous chapters, $Ni_{50-x}Ti_{50}Cu_x$ (x=0, 5 and10) alloys have been prepared by powder metallurgy process. The effect of process parameters on response variables viz. compressive strength, young's modulus and porosity has been discussed. An optimal setting of process parameters that yields the optimum quality features to green compact has also been obtained. The wear characteristics, micro-hardness, corrosion behavior, shape recovery and bio-compatibility of $Ni_{50-x}Ti_{50}Cu_x$ (x=0, 5 and10) alloys also investigated. The following sections give the conclusions as obtained from the present research work:

9.1 CONCLUSIONS

1. Ranges of powder metallurgy process parameters have been established based on review of literature as under in Table 9.1:

Table 9.1: Range of Process Parameters

Sr. No	Process Parameters	Symbol	(units)	Range	Levels		
					I	II	III
1.	Compaction Pressure	A	MPa	107 – 177	107	141	177
2.	Sintering Temperature	B	°C	950–1150	950	1050	1150
3.	Sintering Time	C	min	20-60	20	40	60

2. The summary results of predicted optimal values of the responses and their confidence intervals (both for confirmation experiment and population) are given in Table 9.2 as :

Table 9.2: Predicted and Experimental Values

Sr. No.	Material	Response (Units)	Optimal Setting	Pred. Value	CI_{CE} and CI_{POP} (if any)	Exp. value
1	$Ni_{50}Ti_{50}$	σ (MPa)	$A_3B_1C_1$	1123.86	----	1116.72
2		E(GPa)	B_3C_3	1.674	CI_{CE}: $0.074 < \mu_E < 3.274$; CI_{POP}: $0.724 < \mu_E < 2.624$	1.7
3		Por. (%)	B_3C_3	49	CI_{CE}: $34.43 < \mu_{por} < 63.57$; CI_{POP}: $40.29 < \mu_{por} < 57.71$	54
4	$Ni_{45}Ti_{50}Cu_5$	σ (MPa)	$A_3B_1C_1$	1135.28	----	1124.53
5		E(GPa)	B_3C_3	2.167	CI_{CE}: $0.847 < \mu_E < 3.487$; CI_{POP}: $1.387 < \mu_E < 2.947$	1.9
6		Por. (%)	$A_1B_3C_3$	51.13	----	54.17
7	$Ni_{40}Ti_{50}Cu_{10}$	σ (MPa)	$A_3B_1C_1$	1144.16	----	1132.74
8		E(GPa)	B_3C_3	2.4	CI_{CE}: $1.27 < \mu_E < 3.53$; CI_{POP}: $1.722 < \mu_E < 3.078$	2.2
9		Por. (%)	$A_1B_3C_3$	51.88	----	53

3. The most significant parameters with percent contribution in the analysis of porosity for $Ni_{50-x}Ti_{50}Cu_x$ (x=0, 5 and10) alloys are shown in Table 9.3.

Table 9.3: Percent Contribution of the Process Parameters on Porosity

Material	Compaction Pressure (A)	Sintering Temperature (B)	Sintering Time (C)	Residual error
$Ni_{50}Ti_{50}$	19.46	43.46	35.26	1.8
$Ni_{45}Ti_{50}Cu_5$	21.02	51.62	26.98	0.37
$Ni_{40}Ti_{50}Cu_{10}$	23.87	40.98	34.59	0.55

4. The most significant parameters with percent contribution in the analysis of compressive strength for $Ni_{50-x}Ti_{50}Cu_x$ (x=0, 5 and10) alloys are shown in Table 9.4.

Table 9.4: Percent Contribution of the Process Parameters on Compressive Strength

Material	Compaction Pressure (A)	Sintering Temperature (B)	Sintering Time (C)	Residual error
$Ni_{50}Ti_{50}$	21.34	50.3	28.0	0.34
$Ni_{45}Ti_{50}Cu_5$	21.02	51.62	26.98	0.37
$Ni_{40}Ti_{50}Cu_{10}$	20.78	51.60	27.21	0.39

5. The most significant parameters with percent contribution in the analysis of Young's Modulus for $Ni_{50-x}Ti_{50}Cu_x$ (x=0, 5 and10) alloys are shown in Table 9.5.

Table 9.5: Percent Contribution of the Process Parameters on Young's Modulus

Material	Compaction Pressure (A)	Sintering Temperature (B)	Sintering Time (C)	Residual error
$Ni_{50}Ti_{50}$	10.2	59.12	29.18	1.48
$Ni_{45}Ti_{50}Cu_5$	8.18	58.59	32.34	0.87
$Ni_{40}Ti_{50}Cu_{10}$	5.49	62.35	31.01	1.14

6. Wear Rate of $Ni_{50-x}Ti_{50}Cu_x$ (x=0, 5 and10) alloys have been evaluated by varying the load and temperature condition and is shown in Table 9.6 to 9.8 as:

Table 9.6: Wear rate of $Ni_{50}Ti_{50}$ at different temperatures and load

Load	Sample	Wear rate (mm^3/m) at Temperature Conditions ($Ni_{50}Ti_{50}$)					
		37°C	50°C	100°C	150°C	200°C	250°C
10N	Sample 1 (High σ)	1.42	1.78	1.93	2.04	1.92	2.21
20N		1.65	1.82	2.01	2.15	2.02	2.29
30N		1.81	1.98	2.19	2.31	2.14	2.38
40 N		2.9	3.14	3.28	3.67	3.73	3.82
10N	Sample 2 (Low E)	1.91	2.2	2.64	2.87	2.69	3.79
20N		2.24	2.38	2.83	3.2	2.98	3.96
30N		2.58	2.89	3.16	3.94	3.64	4.87
40 N		2.72	3.23	3.76	4.39	4.18	5.01

Table 9.7: Wear rate of $Ni_{45}Ti_{50}Cu_5$ at different temperatures and load

Load	Sample	Wear rate (mm^3/m) at Temperature Conditions ($Ni_{45}Ti_{50}Cu_5$)					
		37°C	50°C	100°C	150°C	200°C	250°C
10N	Sample 1 (High σ)	1.18	1.23	1.41	1.69	1.57	1.95
20N		1.26	1.31	1.47	1.78	1.64	2.06
30N		1.41	1.56	1.64	1.87	1.73	2.13
40 N		1.54	1.67	1.79	1.92	1.85	2.26
10N	Sample 2 (Low E)	1.42	1.63	1.74	1.88	1.57	2.17
20N		1.53	1.68	1.75	1.87	1.71	2.29
30N		1.74	1.82	1.9	1.98	1.82	2.35
40 N		1.83	1.94	2.07	2.17	2.01	2.48

Table 9.8: Wear rate of $Ni_{40}Ti_{50}Cu_{10}$ at different temperatures and load

Load	Sample	Wear rate (mm^3/m) at Temperature Conditions ($Ni_{40}Ti_{50}Cu_{10}$)					
		37°C	50°C	100°C	150°C	200°C	250°C
10N	Sample 1 (High σ)	0.92	1.12	1.25	1.3	1.21	1.51
20N		1.03	1.11	1.23	1.48	1.32	1.67
30N		1.19	1.32	1.36	1.46	1.32	1.81
40 N		1.25	1.43	1.52	1.59	1.43	1.92
10N	Sample 2 (Low E)	1.2	1.32	1.45	1.53	1.42	1.89
20N		1.36	1.54	1.73	1.84	1.75	2.01
30N		1.42	1.57	1.88	2.01	2.93	2.25
40 N		1.48	1.64	1.96	2.14	2.02	2.34

Table 9.9: Samples and corresponding values of Microhardness

Sr. No	Material	Sample	Micro-hardness (HV)	Micro-hardness(GPa)
1.	$Ni_{50}Ti_{50}$	S-1, (High σ)	364	3.57
2.		S- 2, (Low E)	232	2.27
3.	$Ni_{45}Ti_{50}Cu_5$	S- 1, (High σ)	397	3.89
4.		S- 2, (Low E)	257	2.52
5.	$Ni_{40}Ti_{50}Cu_{10}$	S- 1 (High σ)	437	4.28
6.		S- 2 (Low E)	289	2.83

7. Micro-hardness of $Ni_{50-x}Ti_{50}Cu_x$ (x=0, 5 and10) alloys have been evaluated in

terms of Vicker's hardness and given in Table 9.9.

8. Copper particles in NiTi alloys decrease the shape recovery while Super-elasticity remains approximately constant and reported results given in Table 9.10

Table 9.10: Strain recovery of porous $Ni_{50-x}Ti_{50}Cu_x$ (x=0, 5 and 10)

Material	Super-elasticity (%)
$Ni_{50}Ti_{50}$	4.01
$Ni_{45}Ti_{50}Cu_5$	3.92
$Ni_{40}Ti_{50}Cu_{10}$	3.82

9. Current density increases after addition of copper particle as in Table 9.11, which increases the corrosion rate

Table 9.11: Open Current Potential and Current density of Material

Materials	Open Current Potential (E_{corr})	Current density (j_{corr})
NiTi	-0.175	6×10^{-6}
$Ni_{45}Ti_{50}Cu_5$	-0.25	0.8×10^{-5}
$Ni_{40}Ti_{50}Cu_{10}$	-0.11	4×10^{-5}

10. In-vitro cyto-toxicity test was performed on NiTi alloys to investigate the qualitative and quantitative analysis of bio-compatibility test. The results are given as in Table 9.12.

Table 9.12: Qualitative and quantitative Analysis of Cyto-toxicity Results

Sr. No.	Material	Grade	Reactivity	Cell-density
1.	Negative Control	0	Non-Toxic	-----
2.	Positive Control	4	Severe Toxic	-----
3.	$Ni_{50}Ti_{50}$	0	Non-Toxic	9×10^4 cm^2
4.	$Ni_{45}Ti_{50}Cu_5$	0	Non-Toxic	11×10^4 cm^2
5.	$Ni_{40}Ti_{50}Cu_{10}$	0	Non-Toxic	10.5×10^4 cm^2

9.2 FUTURE SCOPE OF RESEARCH

- In the present research work response quality characteristics viz. compressive strength, Young's modulus, porosity, wear and bio-compatibility are considered. Other responses like tensile strength, machinability, transformation behavior etc. can also be measured.
- Taguchi Technique is applied for planning of experiment and optimization of process parameters. Multi-performance quality characteristics optimization with artificial intelligence techniques like genetic algorithm, fuzzy logic and neural network can also be used for optimization.
- The effect of other additives like La, B, Y etc. can be investigated. Effect of two or more additive on the characteristics of NiTi alloy can also be a future interest.
- Effect of other binders like PVC, poly-styrene etc. with varying composition on characteristics of NiTi SMA can be considered in future.
- Effect of machining and heat treatment on the shape memory and surface characteristics can be investigated in future.
- Coating of this SMA on steel and aluminum alloys can be another thrust area for researcher in near future.
- NiTi composites (with soft metals and alloys) can be considered for future investigation.
- Reaction time of SMA alloys and coated alloys can be future research interest.

REFERENCES

[1] Abedini , M., Ghasemi, H. M. and Ahmadabadi, M. N. (2012) " Effect of Normal Load and Sliding Distance on the Wear Behavior of NiTi Alloy," *Tribology Transactions*, 55:5, 677-684, DOI: 10.1080/10402004.2012.688166.

[2] Anselme, K. (2000) "Osteoblast adhesion on biomaterials: review," *Biomaterials*, Vol. 21, pp. 667-681.

[3] Asadi, H., Bodaghi, M., Shakeri M. and Aghdam, M. M. (2013) "An analytical approach for nonlinear vibration and thermal stability of Shape Memory Alloy hybrid laminated composite beams," *European Journal of Mechanics - A/Solid,* Vol. 42, pp 454-468.

[4] ASTM standard specification F2063-00. American society for testing and materials, 2000.

[5] Aust, E., Limberg, W., Gerling, R., Oger B. and T. Ebel T. (2006) "Advanced $TiAl_6Nb_7$ bone screw implant fabricated by metal injection moulding," *Advanced Engineering Materials* Vol. 8, pp. 365-370.

[6] Aydogmus T. and Bor S. (2012) "Superelasticity and compression behaviour of Porous TiNi alloys produced using Mg Spacers," *Journal of the mechanical Behavior of Bio-medical Materials,* Vol. 15, pp. 59-69.

[7] Balta, J., Simpson, J., Michaud, V., Manson J. and Schrooten J. (2001) "Embedded shape memory alloys confer aerodynamic profile adaptivity," *Smart Materials Bulletin*, Vol. 12, pp. 8–12. doi:10.1016/S1471-3918(01)80094-0

[8] Banhart, J. (2000) "Properties and applications of cast aluminum sponges," *Advanced Engineering Materials,* Vol. 2, pp. 188–191.

[9] Banhart, J. (2001) "Manufacture, characterisation and application of cellular metals and metal foams," *Progress in Material Science,* Vol. 46, pp. 559–632.

[10] Bansiddhi, A., Sargeant, T. D., Stupp S. I. and Dunand, D. C. (2008) "Porous NiTi for Bone Implant: A review," *Acta Biomateriala,* Vol. 4, pp. 773-782.

[11] Barker, T. B. (1990) "Engineering quality by design", Marcel Dekker, Inc., New York.

[12] Barker, T. B. (1986) "Quality engineering by design: Taguchi"s Philosophy", *Quality Progress*, December, pp. 33-42.

[13] Barrabes, M., Sevilla, P., Planell, J. A. and Gil, F. J. (2008) "Mechanical properties of nickel–titanium foams for reconstructive orthopaedics," *Material Science and Engineering C*, Vol. 28, pp. 23–27.

[14] Bashir, S., Shariat, Liu, Y. and Rio, G. (2013) "Hystoelastic deformation behaviour of geometrically graded NiTi shape memory alloys." *Materials and Design,* Vol. 50, pp. 879–885.

[15] Benafan, O., Garg, A., Noebe, R. D., Bigelow, G. S., Padula II, S. A., Gaydosh, D. J., Vaidyanathan, R., Clausen, B. and Vogel, S. (2015) "Thermomechanical behavior and microstructural evolution of a Ni-rich $Ni_{24.3}Ti_{49.7}Pd_{26}$ high temperature shape memory alloy," *Journal of Alloy and Compounds,* doi:10.1016/j.jallcom.2015.04.081.

[16] Bertheville, B. (2006) "Porous single-phase NiTi processed under Ca reducing vapour for use as a bone graft substitute," *Biomaterials,* Vol. 27, pp. 1246-1250.

[17] Bernard, A., Taillandier, G. and Karunakaran, K. P. (2009) "Evolutions of rapid product development with rapid manufacturing: concepts and applications," *International Journal of Rapid Manufacturing,* Vol. 1, pp. 3-18.

[18] Bhagyaraj, J., Ramaiah, K. V., Saikrishna, C. N, Bhaumik, S. K. and Gouthama, (2013) "Behavior and effect of Ti_2Ni phase during processing of NiTi shape memory alloy wire from cast ingot," *Journal of Alloys and Compounds,* Vol. 581, pp. 344–351.

[19] Birman, V. (1997) "Review of mechanics of shape memory alloy structures," *Applied Mechanics Reviews,* Vol. 50, pp- 629–645.

[20] Bormann, T. D., Schumacher, R., Muller, B., Mertmann, M. and Wil, M. (2012) "Tailoring Selective Laser Melting Process Parameters for NiTi Implants," *Journal of Materials Engineering and Performance,* Vol. 21, pp. 2519-2524.

[21] Bram, M., Ahmad-Khanloua, A., Heckmannb, A., Fuchsa, B., Buchkremera H. P. and Stovera, D. (2002) "Powder metallurgical fabrication processes for NiTi shape memory alloy parts," *Materials Science and Engineering A,* Vol.337, pp- 254-263.

[22] Bram, M. (2000) "High-porosity titanium, stainless steel, and superalloy parts," *Advanced Engineering Material,* Vol. 2, pp. 196–199.

[23] Bram, M., Bitzer, M., Buchkremer H. P. and Stover, D. (2012) "Reproducibility Study of NiTi Parts made by Metal Injection Molding," *Journal of Materials Engineering and Performance,* Vol. 21, pp. 2701-2712.

[24] Burton, D. S., Gao X. and Brinson, L. C. (2006) "Finite element simulation of a self-healing shape memory alloy composite,'' *Mechanics of Materials,* Vol. 38 (5-6), pp. 525-537.

[25] Busch, J. D. (1994) "The Frangibolt Flies: Using Shape Memory Alloy on the Spacecraft Clementine," *In: Proceedings of SMST-94*, Pacific Grove, California, 259.

[26] Byrne, D. M. and Taguchi, S. (1987) "The Taguchi approach to parameter design", *Quality Progress*, pp. 19-26.

[27] Castleman, L. S., Motzkin, S. M., Alicandri F. P. and Bonawit, V. L. (1976) "Biocompatibility of nitinol alloy as an implant material," *Journal of Biomedical and Material Research,* Vol. 10, pp.695-731.

[28] Catauro, M. Raucci, M. G. Continenza M. A. and Marotta, A. (2004) "Biocompatibility Tests with Fibroblasts of Cao Rich Calcium Silicate Glasses," *Journal of Materials Science* Vol. 39, pp. 373– 375.

[29] Christine, E., Corbin, S. F. J. Apte, S. P. (1998) "Porous metal structures and processes for their production," *US Patent*, 5846664 A.

[30] Dai, K. R., Hou, X. K., Sun, Y. H., Tang, R. G., Qiu S. J. and Ni, C. (1993) "Treatment of intra-articular fractures with shape memory compression staples," *Injury* Vol. 24, pp. 651–655.

[31] Damanpack, A. R., Bodaghi, M., Aghdam M. and Shakeri, M. (2014) "On the vibration control capability of shape memory alloy composite beams," *Composite Structures,* Vol. 110, pp. 325-334.

[32] Dieng, L., Helbert, G., Chirani, S. A., Lecompte, T. and Pilvin, P. (2013) "Use of Shape memory alloys damper device to mitigate vibration amplitudes of bridge cables," *Engineering Structures,* Vol. 56, 2013, pp. 1547-1556.

[33] Dixit, M., Newkirk J. W. and Mishra, R. S. (2007) "Properties of friction stir-processed Al 1100–NiTi composite," *Scripta Materialia,* Vol. 56, pp. 541–544.

[34] Duerig, T. W., Melton, K. N., Stockel D. and Wayma, C. M. (1990) "Engineering Aspects of Shape Memory Alloys," London: Butterworth-Heinemann.

[35] Duerig, T., Pelton A. and Stöckel, D. (1999) "An overview of nitinol medical applications," *Materials Science and Engineering: A* 273–275, pp. 149-160.

[36] Elahinia M. H. and Ahmadian, M. (2005) "An enhanced SMA phenomenological model. Part II. The experimental study," *Journal of Smart Material and Structure,* Vol. 14, pp. 1309-1319.

[37] Elahinia, M. H., Hashemi, M., Tabesh M. and Bhaduri, S. B. (2012) "Manufacturing and processing of NiTi implants: A review," *Progress in Materials Science,* Vol. 57, pp. 911-946.

[38] Es-Souni, M., Es-Souni M. and Brandies, H. F. (2005) "Assessing the Biocompatibility of NiTi shape memory alloys used for medical applications," *Analytical and Bioanalytical Chemistry,* Vol. 381, 2005, pp. 557-567.

[39] Farvizi, M., Ebadzadeh, T., Vaezi, M. R., Yoon, E. Y., Kim, Y. J., Kim, H. S. and Simchi, A. "Microstructural characterization of HIP consolidated NiTi–nano Al_2O_3 composites," *Journal of Alloys and Compounds* 04/2014; 606(C), pp. 21-26.

[40] Files, B. and Golson, G. B. (1997) "Terminator 3: Biomimetic self-healing alloy composite. In: SMST-97," in *Proceedings of the Second International Conference on Shape Memory and Superelastic Technologies*, California, pp. 281.

[41] Firstov, G. S., Van H. J. and KN, Y. U. (2004) "Comparison of high temperature shape memory behavior for ZrCu-based, Ti–Ni–Zr and Ti–Ni–Hf alloys," *Scripta Materialia,* Vol. 50, pp. 243–248.

[42] Firstov, G. S., Vitchev, R. G., Kumar, H., Blanpain, B. and Humbeeck, J. V. (2002) "Surface oxidation of NiTi shape memory alloy," *Biomaterials* Vol. 23, 2002, pp. 4863-4871.

[43] Freed, Y. and Aboudi, J. (2008) "Micromechanical investigation of plasticity-damage coupling of concrete reinforced by shape memory alloy fibers," *Smart Materials Structure,* Vol. 17, pp. 1-15.

[44] Frenzel, J., Zhang, Z. Neuking, K. and Eggeler, G. "High quality vacuum induction melting of small quantities of NiTi shape memory alloys in graphite crucibles," *Journal of Alloys and Compound,* Vol. 28, pp. 214-223.

[45] Frenzel, J., Zhang, Z., Somsen, C., Neukin, K. and Eggeler, G. (2007) "Influence of carbon on martensitic phase transformations in NiTi shape memory alloys," *Acta Materialia,* Vol. 55, pp. 1331-1341.

[46] Funakubo, H. (1987) Shape memory alloys. New York: Gordon and Breach Publishers.

[47] Furie, B. and B. C. (2008) "Furie Mechanisms of Thrombus Formation," *The New England Journal of Medicine,* Vol. 359, pp. 938-949.

[48] Gao, W., Meng, X., Cai W. and Zhao, L. (2015) "Effects of Co and Al addition on martensitic transformation and microstructure in ZrCu-based shape memory alloys," *Transactions of Nonferrous Metals Society of China,* Vol. 25, pp. 850-855.

[49] Gialanella, S., Ischia, G. and Straffelini, G. (2008) "Phase composition and wear behavior of NiTi alloys," *Journal of Material Science*, Vol. 43, 2008, pp. 1701–1710.

[50] Gibson, I., Rosen, D. W. and Stucker, B. (2010) "Additive manufacturing technology: rapid prototyping to direct digital manufacturing," in *Springer Science + Business Media. Inc*. 103.

[51] Godard, O., Lagoudas, M. and Lagoudas, D. (2003) "Design of space systems using shape memory alloys," *In: Proceedings of SPIE, Smart Structures and Materials*, 5056, San Diego, CA, pp. 545–558.

[52] Guo, W. and Kato, H. (2015) "Submicron-porous NiTi and NiTiNb shape memory alloys with high damping capacity fabricated by a new top-down process," *Materials and Design,* Vol. 78, pp. 74-79.

[53] Gao, Z., Li, Q., He, F., Huang, Y. and Wan, Y. (2012) "Mechanical modulation and bioactive surface modification of porous Ti–10Mo alloy for bone implants," *Materials and Design*, Vol. 42, pp. 13–20.

[54] Hadi, A., Yousefi-Koma, A., Moghadam, M., Elahinia, M. H. and Ghazavi, A. "Developing a novel SMA-actuated robotic module," *Sensors and Actuators A,* in Vol. 162, pp. 72-81.

[55] Hahnlen, R., Fox, G. and Dapino, M. (2012) "Ultrasonic Soldering Of Shape Memory NiTi To Aluminum 2024," *The Welding Journal,* Vol. 91, pp. 1s-7s.

[56] Hamada, K., Kawano, F. and Asaoka, K. (2003) "Shape recovery of shape memory alloy fiber embedded resin matrix smart composite after crack repair," *Dental Materials Journal* Vol. 22, pp. 160-167.

[57] Hao, L. and Harris, R. (2008) "Customised Implants for Bone Replacement and Growth," *In Bartolo P, Bidanda B, (Eds.) Bio-materials and Prototyping Applications in Medicine, Springer*.

[58] Hao, S., Cui, L., Jiang, D., Han, X., et al. (2013) "A Transforming Metal Nanocomposite with Large Elastic Strain, Low Modulus, and High Strength," Science, Vol. 339, pp. 1191-1194.

[59] Hoh, D. J., Hoh, B. L., Amar, A. P. and Wang, M. Y. (2009) "Shape memory alloys: metallurgy, biocompatibility, and biomechanics for neurosurgical applications," *Neurosurgery,* Vol. 64, pp. 199–214.

[60] Hosseini, S. A., Yazdani-Rad, R., Kazemzadeh, A. and Alizadeh, M. (2013) "Influence of Thermal Hydrogen Treatment of Titanium Particles on Powder Metallurgical Processing of NiTi-SMA," *Materials and Manufacturing Processes*, Vol. 28, pp. 1179-1183.

[61] Huang, H. H., Chiu, Y. H., Lee, T. H., Wu, S. C., Yang, H. W., Su, K. H., and C. C. Hsu, C. C. (2003) "Ion release from NiTi orthodontic wires in artificial saliva with various acidities," *Biomaterials*, Vol. 24, pp. 3585–3592.

[62] Huang, W. M., Ding, Z., Wang, C. C., Wei, J., Zhao, Y. and Purnawali, H. (2010) "Shape memory Materials," *Materials Today,* Vol. 13, pp. 54-61.

[63] Idelsohn, S., Pena, J., Lacroix, D., Planell, J. A., Gil, F. J. and Arcas, A. (2004) "Continuous mandibular distraction osteogenesis using superelastic shape memory alloy (SMA)," *Journal of Materials Science,* Vol. 15, pp. 541–546.

[64] Isalgue, A., Fernandez, J., Torra, V. and Lovey, F. C. (2006) "Conditioning treatments of Cu-Al-Be shape memory alloys for dampers," *Materials Science and*

Engineering A Structural Materials Properties Microstructure and Processing, Vol. 438, pp. 1085-1088.

[65] Janke, L., Czaderski, C., Motavalli, M. and Ruth, J. (2005) "Applications of shape memory alloys in civil engineering structures — overview, limits and new ideas," *Materials and Structures,* Vol. 38, pp. 578-592.

[66] Jani, J. M., Leary, J., Subic, A. and Gibson, M. A. (2014) "A review of shape memory alloy research, applications and opportunities," *Materials and Design,* Vol. 56, pp. 1078–1113.

[67] Jiang, J., Jiang, D., Hao, S., Yu, C., Zhang, J., Ren, Y., Lu, D., Xie, S. and Cui, L. (2015) "A nano lamella NbTi–NiTi composite with high strength," *Materials Science & Engineering A,* Vol. 633, pp. 121–124.

[68] Jiang, H., Ke, C., Cao, S., MA, X. and Zhang, X. (2013) "Phase transformation and damping behavior of light-weight porous TiNiCu alloys fabricated by powder metallurgy process," *Transactions of Nonferrous Metal Society of China,* Vol. 23, pp. 2029−2036.

[69] Jiang, S., Zhang, Y., Zhao, L. and Zheng, Y. (2013a) "Influence of annealing on NiTi shape memory alloy subjected to severe plastic deformation," *Intermetallics,* Vol. 32, pp. 344-351.

[70] Jiang, S., Zhang, Y. and Zhao, Y. (2013b) "Dynamic recovery and dynamic recrystallization of NiTi shape memory alloy under hot compression deformation," *Transactions of Nonferrous Metal Society of China,* Vol. 23, pp. 140−147.

[71] Jiang, S. Y. and Zhang, Y. Q. (2012) "Microstructure evolution and deformation behavior of as-cast NiTi shape memory alloy under compression," *Transaction of Nonferrous Metal Society of China,* Vol. 22, pp. 90-96.

[72] Johnson, A. D. and Martynov, V. V. (1997) "Applications of Shape-memory alloy thin film," *In: Proceedings of SMST-97*, Pacific Grove, California, 149.

[73] Kabiri, Y., Kermanpur, A. and Foroozmehr, A. (2012) "Comparative study on microstructure and homogeneity of NiTi shape memory alloy produced by copper boat induction melting and conventional vacuum arc melting," *Vacuum,* Vol. 86, pp. 1073-1077.

[74] Kaieda, Y. (2003) "Fabrication of composition-controlled TiNi shape memory wire using combustion synthesis process and the influence of Ni content on phase transformation behavior," *Science and Technology of Advanced Materials,* Vol. 4, pp. 239–246.

[75] Kang, S., Lee, Y., Lim, Y., Nam, J., Nam, T. and Kim, Y. (2008) "Relationship between grain size and martensitic transformation start temperature in a Ti-30Ni-20Cu alloy ribbon," *Scripta Materialia,* Vol. 59, pp. 1186-1189.

[76] Karaca, H. E., Saghaian, S. M., Basaran, B., Bigelow, G. S., Noebe, R. D. and Chumlyakov, Y. I. (2011) "Compressive response of nickel-rich NiTiHf high-temperature shape memory single crystals along the [1 1 1] orientation," *Scripta Materialia* Vol. 65, pp. 577–580.

[77] Kirkby, E. L., Rule, J. D., Michaud, V. L., Sottos, N. R., White, S. R. and Manson, J. A. (2008) "Embedded shape-memory alloy wires for improved performance of self-healing polymers," *Advanced Functional Materials,* Vol. 18, pp. 2253-2260.

[78] Koike, M., Martinez, K., Guo, L., Chahine, G., Kovacevic, R. and Okabe, T. (2011) "Evaluation of Titanium Alloy Fabricated Using Electron Beam Melting System for Dental Applications," *Journal of Materials Processing Technology,* Vol. 211, pp. 1400–1408.

[79] Kourambas, J., Delvecchio, F. C., Munver, R. and Preminger, G. M. (2000) "Nitinol stone retrieval-assisted ureteroscopic management of lower pole renal calculi," *Urology,* Vol. 56, pp. 935–939.

[80] Krishna, B. V., Bose, S. and Bandyopadhyay, A. (2007) "Laser processing of net-shape NiTi shape memory alloy," in *Metallurgical and Materials Transactions,* Vol. A 38, pp. 1096-1103.

[81] Krishna, B. V., Bose, S. and Bandyopadhyay, A. (2009) "Fabrication of porous NiTi shape memory alloy structures using laser engineered net shaping," *Journal of Biomedical Material Resseach B: Appl Biomater,* Vol. 89B, pp. 481-490.

[82] Krone, L., Schuller, E., Bram, M., Hamed, O., Buchkremer, H. and Stover, D. (2004) "Mechanical behaviour of NiTi parts prepared by powder metallurgical methods," *Materials Science and Engineering A,* Vol. 378, pp. 185–190.

[83] Kucharski , S., Levintant-Zayonts, N. and Luckner, J. (2014) "Mechanical response of nitrogen ion implanted NiTi shape memory alloy," *Materials and Design*. Vol. 56, 2014, pp. 671–679.

[84] Kudva, J. (2004) "Overview of the DARPA smart wing project*," Journal of Intelligent Material Systems and Structures,* Vol. 15, pp. 261–267.

[85] Kumar, A., Singh, D. and Kaur, D. "Variation in phase transformation paths of NiTi films as a function of film thickness," *Sensors and Actuators A* Vol. 178, 201, pp. 57– 63.

[86] Lagoudas, D. C. Rediniotis, O. K. and Khan, M. M. (1999) "Applications of shape memory alloys to bioengineering and biomedical Technology," In: *Proceedings of the 4th International Workshop on Mathematical Methods in Scattering Theory and Biomedical Technology*, Perdika, Greece, October 8-10.

[87] Lagoudas, D. C. and Vandygriff, E. L. (2002) "Processing and Characterization of NiTi Porous SMA by Elevated Pressure Sintering," *Journal of Intelligent Material Systems and Structures,* Vol. 13, pp. 837-850.

[88] Larry, L. and Hench. (1998) "Bioceramic," *Journal of American Ceramic Society*, Vol. 81, pp. 1705–1728.

[89] Li, B., Rong, L., Li, Y. and Gjunter, V. E. (2000b) "A recent development in producing porous Ni–Ti shape memory alloys," *Intermetallics,* Vol. 8, pp. 881-884.

[90] Li, B. Y., Rong, L. J., Li, Y. Y. and Gjunter, V. E. (2000a) "Synthesis of porous Ni–Ti shape-memory alloys by self-propagating high-temperature synthesis: reaction mechanism and anisotropy in pore structure," *Acta Materialia,* Vol. 48, pp. 3895-3904.

[91] Li, H. X., Mao, S. C., Zang, K. T., Liu, Y., Guo, Z. X., Wang, S. B., Zhang, Y. F. and Yin, X. Q. (2014) "An in situ TEM study of the size effect on the thermally induced martensitic transformation in nanoscale NiTi shape memory alloy," *Journal of Alloys and Compounds,* Vol. 588, pp. 337–342.

[92] Lin, H. C., Lin, K. M. and Cheng, I. S. (2001) "The electro-discharge machining characteristics of NiTi shape memory alloys," *Journal of Material Science,* Vol. 36, pp. 399-404.

[93] Lin, H. C., Lin, K. M. and Chen, Y. C. (2000) "A study on the machining characteristics of TiNi shape memory alloys," *Journal of Materials Processing Technology,* Vol. 105, pp. 327-332.

[94] Lee, J., Hwang, J., Lee, D., Ryu, H. J. and Hong, S. H. (2014) "Enhanced mechanical properties of spark plasma sintered NiTi composites reinforced with carbon nanotubes," *Journal of Alloys and Compounds,* Vol. 617, pp. 505–510.

[95] Lee, K. S., Yang, D. Y., Park, S. H. and Kim, R. H. (2006) "Recent Developments in the Use of Two-photon Polymerization in Precise 2D and 3D Microfabrication," *Polymers for Advanced Technologies,* Vol. 17, pp. 72–82.

[96] Levi, N., Kusnezov and Carman, G. P. (2008) "Smart materials applications for pediatric cardiovascular devices," *Pediatric Research,* Vol. 63, pp. 552–558.

[97] Luo, W., Ishikawa, K. and Aoki, K. (2006) "High hydrogen permeability in the Nb-rich Nb–Ti–Ni alloy," *Journal of Alloys and Compounds,* Vol. 407, pp. 115–117.

[98] Mabe, J., Cabell, R. and Butler, G. (2005) "Design and control of a morphing chevron for takeoff and cruise noise reduction," *In: Proceedings of the 26th Annual AIAA Aeroacoustics Conference,* Monterey, CA, pp. 1–15.

[99] Mani, R., Lagoudas, D. and Rediniotis, O. (2003) "MEMS based active skin for turbulent drag reduction," *In: Proceedings of SPIE, Smart Structures and Materials*, 5056, San Diego, CA.

[100] Manjaiah, M., Narendranath, S., Basavarajappa, S. and Gaitonde, V. N. (2014a) "Wire electric discharge machining characteristics of titanium nickel shape memory alloy," *Transactions of Nonferrous Metals Society of China,* Vol. 24, pp. 3201-3209.

[101] Mantovani, D. (2000) "Shape memory alloys: Properties and biomedical applications," *Journal of the Minerals. Metals and Materials Society,* Vol. 52, pp. 36-44.

[102] Morakabati, M., Aboutalebi, M., Kheirandish, S., Taheri, K. A. and Abbasi, S. M. (2011) "Hot tensile properties and microstructural evolution of as cast NiTi and NiTiCu shape memory alloys," *Materials and Design,* Vol. 32, pp. 406–413.

[103] Morgan, N. B., and Broadley, M. (2003) "Taking the art out of smart—forming processes and durability issues for the application of NiTi shape memory alloys in

medical devices," *In: Shrivastava S, editor. Proceedings of the materials and processes for medical devices conference*. ASM International, pp. 247-252.

[104] Nam, T. H., Lee, J. H., Nam, J. M., Kim, K. W., Cho, G. B. and Kim, Y. W. (2008) "Microstructures and mechanical properties of Ti–45 at.%Ni–5 at.% Cu alloy ribbons containing Ti2Ni particles," *Materials Science and Engineering A,* Vol. 483–484, pp. 460–463.

[105] Nasser, N. S., Su, Y., Guo, W. G. and Isaacs, J. (2005) "Experimental characterization and micromechanical modeling of super-elastic response of a porous NiTi shape-memory alloy," *Journal of the Mechanics and Physics of Solids,* Vol. 53, pp. 2320-2346.

[106] Nazanin-Samani, M., Kamali, A. R., Mobarra, R. and Nazarian-Samani, M. (2010) "Phase transformation of Ni–15 wt. % B powders during mechanical alloying and annealing," *Materials Letters,* Vol. 64, pp. 309–312. doi: 10.1016/j.matlet.2009.10.070

[107] Nikolay, Z., Vladimir, M. and Eric, J. (2014) "Mittemeijer, Evaluation of kinetic equations describing the martensite–austenite phase transformation in NiTi shape memory alloys," *Journal of Alloys and Compounds,* Vol. 616, pp. 385–393.

[108] Noort, R. V. (2012) "The Future of Dental Devices in Digital," *Dental Materials*, Vol. 28, pp. 3–12.

[109] Okumura, A., Goto, M., Goto, T., Yoshinara, M., Masuko, S., Katsuki, T. and Tanaka, T. (2001) "Substrate affects the initial attachment and subsequent behaviour of human oestoblastic cells (Saos-2)," *Biomaterials*, Vol. 22, pp. 2263-2271.

[110] Otubo, J., Rigo, O. D., Neto, C. D. M., Kaufman, M. J. and Mei, P. R. (2003) "NiTi shape memory alloy ingot production by EBM," *Journal of Physics IV* , Vol. 112, pp. 813-820.

[111] Otsuka, K. and Ren, X. (2005) "Physical metallurgy of Ti–Ni-based shape memory alloys," *Progress in Material Science,* Vol. 50, pp. 511–678.

[112] Ovsianikov, A., Farsari, M. and Chichkov, B. N. (2011) "Photonic and Biomedical Applications of the Two-photon Polymerization Technique," *In Bartolo PJ, (Ed.)*

Stereolithographic Processes, Stereolithography: Materials, Processes, Applications, Springe.

[113] Ozbulut, O. E., Hurlebaus, S. and Desroches, R. (2011) "Seismic Response Control Using Shape Memory Alloys: A Review," *Journal of Intelligent Material Systems and Structures,* Vol. 22, pp. 1531-1549.

[114] Peffer, A., Denoyer, K., Fossness, E. and Sciulli, D. (2000) "Development and transition of low-shock spacecraft release devices," *In: Proceedings of IEEE Aerospace Conference*, Vol. 4, pp. 277–284.

[115] Petrini, L. and Migliavacca, F. (2011) "Biomedical Applications of Shape Memory Alloys," *Journal of Metallurgy* 2011: 1-15. *doi:10.1155/2011/501483.*

[116] Pieczyska, E. A., Gajewska, K. K., Maj, M., Staszczak, M. and Tobushi, H. (2011) "Thermomechanical investigation of TiNi shape memory alloy and PU shape memory polymer subjected to cyclic loading**,"** *Procedia Engineering,* Vol. 74, pp. 287 – 292.

[117] Pitt, D., Dunne, J., White, E. and Garcia, E. (2001) "SAMPSON smart inlet SMA powered adaptive lip design and static test," *In: Proceedings of the 42nd AIAA Structures, Structrual Dynamics, and Materials Conference*, Seattle, WA.

[118] Prahlad, H. and Chopra, I. (2001) "Design of a variable twist tiltrotor blade using shape memmory alloy (SMA) actuators," *In: Proceedings of SPIE, Smart Structures and Materials. 4327, Newport Beach*, CA, pp. 46–59.

[119] Radu, I. and Li, D. Y. (2007) "Effects of ZrW_2O_8 and tungsten additions on the temperature range in which a pseudoelastic TiNi alloy retains its maximum wear resistance," *Wear,* Vol. 263, pp. 858-865.

[120] Rajurkar, K. P., Levy, G., Malshe, A., Sundaram, M. M., McGeough, J., Hu, X., Resnick, R. and De Silva, A. (2006) "Micro and Nano Machining by Electro-Physical and Chemical Processes," *Annals of the CIRP,* Vol. 55, pp. 643-666.

[121] Reinoehl, M., Bradley, D., Bouthot, R. and Proft, J. (2000) "The influence of melt practice on final fatigue properties of superelastic NiTi Wires," *In: Proceedings of international conference on shape memory and superelasticity technologies*, Pacific Grove, California.

[122] Ross, P.J., (1996) "Taguchi Techniques for Quality Engineering: Loss Function, Orthogonal Experiments, Parameter and Tolerance Design - 2nd ed.", New York, NY: McGraw-Hill.

[123] Ross, P. J. (1998) “Taguchi techniques for quality engineering”, McGraw-Hill Book Company, New York.

[124] Roy, R. K. (1990) “A primer on Taguchi method”, Van Nostrand Reinhold, New York.

[125] Ryan, G., Pandit, A. and Apatsidis, D. P. (2006) “Fabrication methods of Porous metals for use in orthopaedic applications,” *Biomaterials,* Vol. 27, pp. 2651–2670.

[126] Ryhanen, J. (1999) “Biocompatibility evaluation of nickel-titanium shape memory metal alloy,” PhD Thesis, University of Oulu.

[127] Sadeghi, A., Babakhani, A., Zebarjad, S. M. and Hassan, M. (2014) “Use of grey relational analysis for multi-objective optimisation of NiTiCu shape memory alloy produced by powder metallurgy process,” *Journal of Intelligent Material Systems and Structures,* Vol. 25, pp. 2093–2101.

[128] Sadrnezhaad, S. K., Arami, H., Keivan, H. and Khalifehzadeh, R. (2006) “Powder Metallurgical Fabrication and Characterization of Nanostructured Porous NiTi Shape-Memory Alloy,” *Materials and Manufacturing Processes,* Vol. *21* (8), pp. 727-735.

[129] Salito, A., Van, O. K. U. and Breme, F. (1998) “Schonende Beschichtungstechnik,” *Sulzer Technical Review,* Vol. 1, pp. 34-37.

[130] Sankaranarayanan, S., Shankar, V. H., Jayalakshmi, S., Bau, N. Q. and Gupta, M. (2015) “Development of high performance magnesium composites using $Ni_{50}Ti_{50}$ metallic glass reinforcement and microwave sintering approach,” *Journal of Alloys and Compounds,* Vol. 627, pp. 192–199.

[131] Sanders, B., Crowe, R. and Garcia, E. (2004) “Defense advanced research projects agency – Smart materials and structures demonstration program overview,” *Journal of Intelligent Material Systems and Structures,* Vol.15, pp. 227–233.

[132] Sattapan, B., Palamara, J. E. and Messer, H. H. (2000) “Torque during canal instrumentation using rotary nickel-titanium files,” *Journal of Endodontics,* Vol. 26, pp. 156–160.

[133] Savi, M. A. De Paula, A. S. and Lagoudas, D. C. (2011) "Numerical investigation of an adaptive vibration absorber using shape memory alloys," *Journal of Intelligent Material Systems and Structures,* Vol. 22, pp. 67-80.

[134] Schetky L McD (1994) "The Application of Constrained Recovery Shape Memory Devices for Connectors, Sealing and Clamping," *In: Proceedings of SMST-94*, Pacific Grove, California, 239.

[135] Shahin, K., Zou, G. P. and Taheri, F. (2005) "Shape memory alloy wire reinforced composites for structural damage repairs," *Mechanics Advanced Materials Structures,* Vol. 12, pp. 425-435.

[136] Sharma, N., Raj, T., Jangra, K. K. (2016) "Micro-Structural Evaluation of Niti-Powder, Steatite and Steel Balls after Different Milling Conditions," *Material and Manufacturing Processes*, Vol. 31, pp. 28-32.

[137] Song, D., Kang, G., Kan, Q. and Yu, C. (2014) "Chuanzeng Zhang, Non-proportional multiaxial transformation ratcheting of super-elastic NiTi shape memory alloy: Experimental observations," *Mechanics of Materials,* Vol. 70, pp. 94–105.

[138] Song, X., Li, Y. and Zhang, F. (2014) "Microstructure and mechanical properties of Nb-and Mo-modified NiTi–Al-based intermetallics processed by isothermal forging," *Materials Science & Engineering A*, Vol. 594, pp. 229–234.

[139] Spinks, G. M., Dominis, A. J., Wallace, G. G. and Tallman, D. E. (2002) "Electroactive conducting polymers for corrosion control," *Journal of Solid State Electrochemistry*, Vol. 6, pp. 85.

[140] Stern, M. and Geary, A. (1957) "Electrochemical polarization: I. A theoretical analysis of the shape of polarization curves," *Journal of the Electrochemical Society*, Vol. 104, pp. 56.

[141] Sun, L., Huang, W. M., Ding, Z., Zhao, Y., Wang, C. C., Purnawali, H. and Tang, C. (2012) "Stimulus-responsive shape memory materials: A review," *Material and Design,* Vol. 33, pp. 577-640.

[142] Suryanarayana, C. (2004) *Mechanical alloying and milling*; Marcel Dekke: New York.

[143] Svetlana, A., Shabalovskaya, Tian, H., Anderegg, J. W., Schryvers, D.U., Carroll, W. U. and Humbeeck, J. V. (2009) "The influence of surface oxides on the distribution and release of nickel from Nitinol wires," *Biomaterials,* Vol. 30, pp. 468–477.

[144] Tan, L., Dodd, R. A. and Crone, W. C. (2003) "Corrosion and wear-corrosion behavior of NiTi modified by plasma source ion implantation," *Biomaterials*, Vol. 24, pp. 3931–3939.

[145] Tang, C. Y., Zhang, L. N., Wong, C. T., Chan, K. C. and Yue, T. M. (2011) "Fabrication and characteristics of porous NiTi shape memory alloy synthesized by microwave sintering," *Materials Science and Engineering A,* Vol. 528, pp. 6006–6011.

[146] Tawfik, M., Ro, J. and Mei, C. (2002) "Thermal post-buckling and aeroelastic behaviour of shape memory alloy reinforced plates," *Smart Materials and Structures.* Vol. 11, pp. 297–307.

[147] Thierry, B., Merhi, Y., Bilodeau, L., Trépanier, C. and Tabrizian, M. (2002) "Nitinol versus stainless steel stents: acute thrombogenicity study in an ex vivo porcine model," *Biomaterials,* Vol. 23, pp. 2997–3005.

[148] Thorsen, T., Maerkl, S. J. and Quake, S. R. (2002) "Microfluidic large-scale integration," *Science* Vol. 298, pp. 580.

[149] Toro, A., Zhou, F., Wu, W. M. H., Geertruyden, W. V. and Misiolek, W. Z. (2009) "Characterization of Non-Metallic Inclusions in Superelastic NiTi Tubes," *Journal of Material Engineering Performance,* Vol. 18, pp. 448–458.

[150] Torrisi, L. (1999) "The NiTi superelastic alloy application to the dentistry field," *Bio-Medical Materials and Engineering,* Vol. 9, pp. 39–47.

[151] Tosun, G. and Tosun, N. (2012) "Analysis of Process Parameters for Porosity in Porous NiTi Implants," *Materials and Manufacturing Processes,* Vol. 27, pp. 1184-1188.

[152] Treppanier, C. (1999) "Undergraduate Engineering Project", *Department of Materials Engineering, EcolePolytechnique of Montreal*.

[153] Tuchinskiy, L. and Loutfy, R. (2003) "Titanium foams for medical applications," in *ASM Conference on Materials and Processes for Medical Devices, Anaheim, CA.*

[154] Vermaut, P., Lity, S. L., Portier, R., Ochin, P. and Utkiewicz, J. (2003) "The microstructure of melt spun Ti–Ni–Cu–Zr shape memory alloys," *Materials Chemistry and Physics,* Vol. 81, pp. 380-382.

[155] Vu, V. H., McHugh, W. T., Blasi, J. A., Fontaine, L. P. and Pinault, R. J. (1999) "Current Interrupter for Electrochemical Cells," US patent number 5879832.

[156] Walker, J. and Elahinia, M. H. (2013) "An investigation of Process Parameters on Selective Laser Melting of Nitinol," *In: Proceeding of ASME 2013 Conference on Smart Materials, Adaptive Structures and Intelligent Systems*, Snowbird, USA.

[157] Wang, J. and Mak, C. (2014) "Adaptive-passive vibration isolation between non rigid machines and non rigid foundations using a dual-beam periodic structure with shape memory alloy transverse connection," *Journal of Sound and Vibration,* Vol. 333, pp. 6005-6023.

[158] Weinert, K. and Petzoldt, V. (2004) "Machining of NiTi based shape memory alloys," *Material Science Engineering A,* Vol. 378, pp. 180-184.

[159] Wei, Z. G., Sandstrom, R. and Miyazaki, S. (1998) "Shape-memory materials and hybrid composites for smart systems – part i shape-memory materials," *Journal of Material Science,* Vol. 33, pp. 3743-3762.

[160] Wen, C. E., Mabuchi, M., Yamanda, Y., Shimojima, K., Chino, Y. and Asahina, T. (2001a) "Processing of biocompatible porous Ti and Mg," *Scripta Materialla,* Vol. 45, pp. 1147–1153.

[161] Wen, C. E., Yamanda, Y., Shimojima, K., Chino, Y., Asahina, T. and Mabuchi, M. (2001b) "Fabrication and characterization of autogenous titanium foams*," Europeon Cells and Materials,* Vol. 1, pp. 61–622.

[162] Whitcher F. D., (1997) Simulation of in vivo loading conditions of nitinol vascular stent structures. *Computers and Structures* 64: 1005-1011.

[163] Williams, E., Shaw, G. and Elahinia, M. (2010) Control of an automotive shape memory alloy mirror actuator. *Mechatronics* 20: 527-534.

[164] Williams, K., Chiu, G. and Bernhard, R. (2000) "Controlled continuous tuning of an adaptively tunable vibration absorber incorporating shape memory alloys," *In: Proceedings of SPIE, Smart Structures and Materials, 3984, Newport Beach*, CA, pp. 564–575.

[165] Wu, M. H. and Ewing, W. A. (1994) "Pilot-Operated Anti-Scald Safety Valve: Design and Actuator Considerations," *In: Proceedings of SMST-94*, Pacific Grove, California, 311.

[166] Wu, M. H. and McD Schetky, L. (2000) "Industrial Applications for Shape Memory Alloys," *In: Proceedings of the International Conference on Shape Memory and Superelastic Technolgies*, Pacific Grove, California, pp. 171-182.

[167] Wu, T. and Wu, M. H. (2000) "NiTi-Nb plugs for sealing high pressure Fuel passages in fuel injector application," *In: Proceedings, SMST-2000*, Pacific Grove, California.

[168] Xiong, J. Y., Li, Y. C., Wang, X. J., Hodgson, P. D. and Wen, C. E. (2008) "Titanium — nickel shape memory alloy foams for bone tissue engineering," *Journal of the Mechanical Behavior of Biomedical Materials,* Vol. 1, pp. 269-273.

[169] Xu, J. L., Bao, L. Z., Liu, A. H., Jin, X. F., Luo, J. M., Zhong, Z. C. and Zheng, Y. F. (2015a) "Effect of pore sizes on the microstructure and properties of the biomedical porous NiTi alloys prepared by microwave sintering," *Journal of Alloys and Compounds,* Vol. 645, pp. 137–142.

[170] Xu, J. L., Bao, L. Z., LZ, A. H., Liu, A. H., Jin, X. J., Tong, Y. X., Luo, J. M., Zhong, Z. C. and Zheng, Y. F (2015b) "Microstructure, mechanical properties and superelasticity of biomedical porous NiTi alloy prepared by microwave sintering," *Materials Science and Engineering C,* Vol. 46, pp. 387–393.

[171] Xu, J. L., Jin, X. F., Luo, J. M. and Zhong, Z. C. (2014) "Fabrication and properties of porous NiTi alloys by microwave sintering for biomedical applications," *Materials Letters,* Vol. 124, pp.110–112.

[172] Yadroitsev, I., Thivillon, L., Bertrand, P. and Smurov, I. (2007) "Strategy of Manufacturing Components with Designed Internal Structure by Selective Laser Melting of Metallic Powder," *Applied Surface Science,* Vol. 254, pp. 980–983.

[173] Yan, L., Liu, Y. and Liu, E. (2013) "Wear behaviour of martensitic NiTi shape memory alloy under ball-on-disk sliding tests," *Tribology International*, Vol. 66, pp. 219–224.

[174] Yan, L. and Liu, Y. (2015) "Wear Behavior of Austenitic NiTi Shape Memory Alloy," *Shape Memory Superelasticity*, Vol. 1, pp. 58-68.

[175] Yan, L. and Liu, Y. (2015) "Effect of temperature on the wear behavior of NiTi shape memory alloy," *Journal of Material Research*, Vol. 30, No. 2, Jan 28, pp. 186-196.

[176] Yang, R., Cui, L. and Zheng, Y. (2006) "Synthesis of TiC/NiTi composite particles by chemical reaction in molten salts," *Materials Science and Engineering A,* Vol. 438–440, pp. 1133–1134.

[177] Yang, Z. R., Wang, S. Q., Zhao, Y. T. and Wei, M. X. (2010) "Evaluation of Wear Characteristics of Al_3Tip/Mg Composite," *Material Characterization*, Vol. 61, pp 554–563.

[178] Yea, C. L. and Sung, W. Y. (2004) "Synthesis of NiTi intermetallics by self-propagating combustion," *Journal of Alloys Compounds,* Vol. 376, pp. 79–88.

[179] Yeom, J. T., Kim, J. H., Hong, J. K., Kim, S. W., Park, C.H., Nam, T. H. and Lee, K. Y. (2014) " Hot forging design of as-cast NiTi shape memory alloy," *Materials Research Bulletin,* Vol. 58, pp. 234–238.

[180] Ying, Z., Minoru, T., Yansheng, K. and Akira, K. (2005) "Compression behavior of porous NiTi shape memory alloy," *Acta Materialia,* Vol. 53, pp. 337-343.

[181] Zhang, Y. P., Yuan, B., Zeng, M. Q., Chung, C. Y. and Zhang, X. P. (2007) "High porosity and large pore size shape memory alloys fabricated by using pore-forming agent (NH_4HCO_3) and capsule-free hot isostatic pressing," *Journal of Materials Processing Technology,* Vol. 192–193, pp. 439-442.

[182] Zider, R. B. and Krumme, J. F. (1990) "Eyeglass Frame including Shape Memory Elements," US patent number 4896955.

APPENDIX A

INNER / OUTER ORTHOGONAL ARRAY AND LINEAR GRAPH

A.1 LINEAR GRAPH OF L_{27} OA

The linear graph of L_{27} OA is shown in Fig A.1. The dot in the figure represents a column available for a three level factor which is allocated 2 degrees of freedom (DOF). The line represents two columns (as indicated) which will evaluate the interaction of the factors assigned to the respective dots. The two-factor interaction of 3 level factors is having 4 DOF. So, two columns have to be assigned for each two factor interaction.

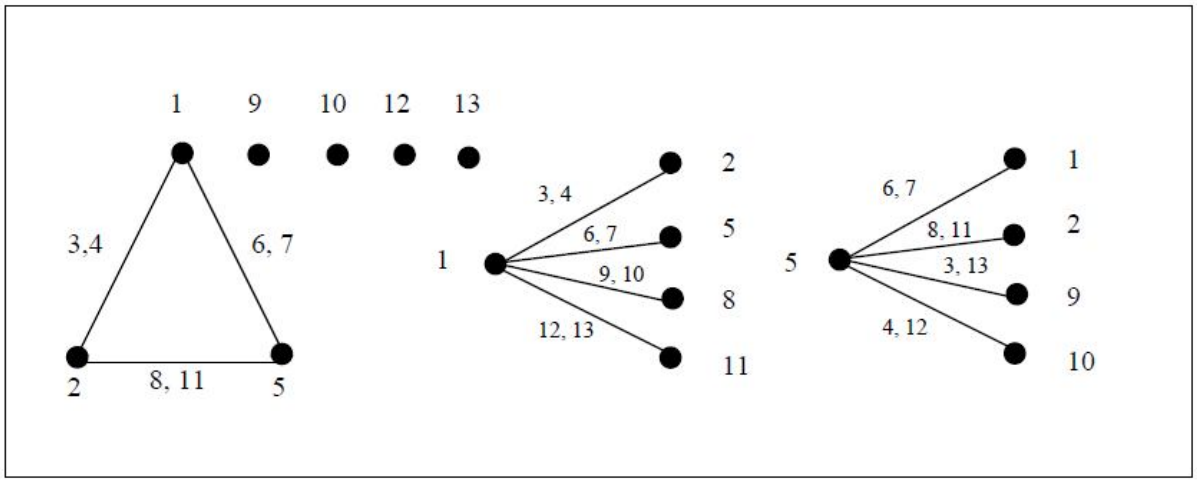

Figure: A.1 Linear Graph of L_{27} Orthogonal Array (Peace 1993)

A.2 INNER / OUTER ORTHOGONAL ARRAY

The Table A.1 represents a situation where outer array is used along with the inner array (a two level OA). The inner array is an L_8 OA, having seven columns and eight experiment runs. The associated outer array is an L_4 OA (2 – level OA) where at the most three noise factors can be assigned for each experimental condition of the inner array. The experiments are repeated four times with different noise conditions specified in the outer array. There will be 32 data points (under "Results" column) for such a design.

TABLE A.1: INNER / OUTER ORTHOGONAL ARRAY (ROY 1990)

OUTER ARRAY

Noise Factors	1	1	2	2
	1	2	1	2
	1	2	2	1
Columns	1	2	3	4

INNER ARRAY

CONTROL FACTORS								RESULTS		
Column No. / Exp. No	1	2	3	4	5	6	7	1	2	3
1	1	1	1	1	1	1	1	-	-	-
2	1	1	1	2	2	2	2	-	-	-
3	1	2	2	1	1	2	2	-	-	-
4	1	2	2	2	2	1	1	-	-	-
5	2	1	2	1	2	1	2	-	-	-
6	2	1	2	2	1	2	1	-	-	-
7	2	2	1	1	2	2	1	-	-	-
8	2	2	1	2	1	1	2	-	-	-

Brief Bio-data

I, Neeraj Sharma, am pursuing PhD in the field of Material Development and Characterization, from Faculty of Engineering and Technology, YMCA University of Science and Technology, Faridabad, Haryana, India. I did Master of Technology in Mechanical Engineering from M.M.E.C., Mullana, Bachelor of Engineering in Mechanical Engineering from Kurukshetra University, Kurukshetra. I have three years experience in reputed industries and six years teaching experience. Presently, I am working as Assistant Professor in Mechanical Engineering Department in D.A.V. University, Jalandhar. I published 15 SCI research papers in different Journals. My area of research interest is material development, characterization and its processing by traditional and non-traditional means.

LIST OF PUBLICATIONS OUT OF THESIS

List of Published Papers

Sr. No.	Title of the paper and Journal Details	Publisher	Impact factor	Whether referred or non referred	Whether you paid any money for publication	Remarks
1.	Microstructural Evaluation of NiTi-powder, Steatite, and Steel Balls After Different Milling Conditions, ***Materials and Manufacturing Processes***, Vol. 31, Issue 5, pp. 628-632.DOI: 10.1080/10426914.2015.1004710.	Taylor and Francis	1.419 (SCI)	Referred	-No-	Published
2.	Parameter optimization and experimental study on wire electrical discharge machining of porous Ni40Ti60 alloy, ***Proceedings of the Institution of Mechanical Engineers Part B: J Engineering Manufacture***, DOI: 10.1177/0954405415577710.	Sage Publication	0.978 (SCI)	Referred	-No-	Online First Published
3.	Fabrication of NiTi Alloy: A Review, ***Proceedings of the Institution of Mechanical Engineers Part L: J Materials: Design and Applications,*** doi: 10.1177/1464420715622494	Sage Publication	0.793 (SCI)	Referred	-No-	Online First Published

4.	Physical and Tribological Characteristics of Porous NiTi SMA Fabricated by Powder Metallurgy, **Particulate Science and Technology: An International Journal**, DOI: 10.1080/ 02726351.2016.1171814	Taylor and Francis Publication	0.707 (SCI)	Referred	-No-	Online First Published
5.	Porosity exploration of SMA by Taguchi, Regression Analysis and Genetic Programming, **Journal of Intelligent Manufacturing**, Doi: 10.1007/s10845-016-1236-8	Springer Publication	1.995 (SCI)	Referred	-No-	Online First Published
6.	Applications of Nickel-Titanium Alloy, **Journal of Engineering and Technology**, 2015, 5 (1), 1-7.	Medknow Kluwer (USA)	-No-	Referred	-No-	Published
7.	Morphological Characteristics Measurement of Nickel-Titanium Alloy by Scanning Electron Microscopy, **The IUP Journal of Mechanical Engineering**, 2013, VI (4), pp. 1-5.	IUP Online	-No-	Referred	-No-	Published
8.	Fabrication and Development of Die for Powder Compaction Press, Proceeding of National Conference on Advances in Engineering, Technology & Management (AETM 15) at M.M.U. Sadopur, Ambala on 4 April, 2015.	National Conference , M.M.U. Sadopur, Ambala, Haryana	-No-	Referred	Conference Registration Fee	Published
9.	Feasibility Study of $Ni_{50}Ti_{50}$ Compression Test Specimen Prepared By P/M Method, In: Proceeding of National Conference AFTME-2014 at PEC University of	National Conference PEC University of Tech., Chandigarh	-No-	Referred	Conference Registration Fee	Published

	Technology, Chandigarh on 17-18 October, 2014, pp. 59-63.					

List of Communicated Papers

Sr. No.	Title of the paper	Journal and Publisher	Impact Factor	Whether referred or non referred	Whether you paid any money for publication	Remarks
1	*Investigation of Mechanical characteristics, Shape recovery and Bioactivity of Porous $Ni_{50-x}Ti_{50}Cu_x$ (x=0, 5 and 10) prepared by P/M method.* Manuscript ID: JMDA-16-0030	Proceedings of the Institution of Mechanical Engineers Part L: J Materials: Design and Applications	0.793	Referred	-No-	Under Review
2	Dry Sliding Wear Behavior at Different temperatures of $Ni_{50-x}Ti_{50}Cu_X$ (x= 0, 5 and 10) alloy Prepared by P/M method. Manuscript ID: JAERO-16-0113	Proceedings of the Institution of Mechanical Engineers Part G: J of Aerospace Engineering	0.678	Referred	-No-	Under Review

List of Accepted Papers

1.	Transformation Temperature and Corrosion Behavior of Porous NiTi and NiTiCu Shape Memory Alloy,	Journal of Engineering and Technology (Medknow Kluwer (USA))	-No-	Referred	-No-	Accepted